Fabrication and characterization of microstructured scaffolds for complex 3D cell cultures

Dissertation zur Erlangung des akademischen Grades
Doktor der Naturwissenschaften (Dr. rer. nat.)

vorgelegt der Fakultät für Mathematik und Naturwissenschaften
der Technischen Universität Ilmenau

von Dipl.-Ing. Justyna Weronika Borowiec

1. Gutachter: Prof. Dr. Andreas Schober
2. Gutachter: Prof. Dr. Uwe Ritter
3. Gutachter: Prof. Dr. Aldo R. Boccaccini

Tag der Einreichung: 26.08.2020
Tag der wissenschaftlichen Aussprache: 23.06.2021

DOI: 10.22032/dbt.50717
URN: urn:nbn:de:gbv:ilm1-2021000418

Zusammenfassung

In einem natürlichen Gewebe wird das zelluläre Verhalten durch Stimuli der Mikroumgebung reguliert. Verschiedene chemische, mechanische und physikalische Reize befinden sich in einem lokalen Milieu und versorgen die Zellen mit einem biologischen Kontext. Im Vergleich zur *in vivo* Situation, zeigen Standard 2D *in vitro* Zellkulturmodelle viele Unterschiede in der zellulären Mikroumgebung und können infolgedessen eine Veränderung der Zellantwort verursachen. Die Schaffung einer physiologisch realistischeren Umgebung auf künstlichem Substrat ist ein Schlüsselfaktor für die Entwicklung zuverlässiger Plattformen, die es den kultivierten Zellen ermöglichen, sich natürlicher zu verhalten. Daher sind neuartige Substrate auf Biomaterialbasis mit maßgeschneiderten Eigenschaften sehr gefragt.

Die Mikrotechnik ist ein leistungsstarkes Werkzeug, das bei der Herstellung der Funktionsgerüste hilft, um verschiedene Eigenschaften der *in vivo* Umgebung zu reproduzieren und auf *in vitro* Bedingungen zu übertragen. Die Gerüstkonstruktionsparameter können manipuliert werden, um die für das jeweilige Gewebe spezifischen Anforderungen zu erfüllen. Eine der grundlegenden Einschränkungen bei aktuellen Herstellungsverfahren ist jedoch die Unfähigkeit, mehrere Gerüsteigenschaften auf vorgefertigte Weise in eine einzelne Gerüststruktur zu integrieren.

Diese Dissertation befasst sich mit Gerüstmikrofabrikations- und Oberflächenmodifikations-techniken, welche die Mikrostrukturierungstechnologie verwenden und die gleichzeitige Kontrolle über verschiedene Gerüsteigenschaften ermöglichen. Diese Ansätze bei der Mikrofabrikation von Polymergerüsten werden verwendet, um physikalische und chemische Eigenschaften bereitzustellen, die für die Leberzellkultur optimiert sind. Die physikochemischen Aspekte, die die zelluläre Mikroumgebung von Lebergewebe *in vivo* ausmachen, werden diskutiert und anschließend werden relevante Technologien vorgestellt, mit denen einige dieser Aspekte *in vitro* reguliert werden können.

Im ersten Teil dieser Arbeit wird ein neuartiges zweistufiges Verfahren zur Herstellung von Polymergerüsten mit mikroporöser Struktur und definierter Topographie gezeigt. Um 3D-Matrizen mit integrierter Porosität zu erhalten, wurde nach der Herstellung mikroporöser Folien ein Mikrostrukturierungsprozess unter Verwendung der Mehrschicht Polymer-Thermoformtechnologie durchgeführt. Diese Methoden wurden verwendet, um Substrate für die organotypische 3D-Hepatozytenkultivierung herzustellen. Poröse Gerüste mit Mikrokavitäten wurden aus lösungsmittelgegossenen und phasengetrennten Polymilchsäure (PLA) Folien gebildet. Die Proben wurden auf grundlegende mechanische und Oberflächenspezifische Eigenschaften sowie auf die Zellleistung untersucht. Um einen Bezugspunkt für die Bewertung der hergestellten Matrices bereitzustellen, wurden PLA-Gerüste mit zuvor beschriebenen Substraten auf Polycarbonat (PC)-Basis mit ähnlicher Geometrie verglichen. HepG2-Zellen, die in PLA-Gerüsten kultiviert wurden, zeigten eine gewebeartige 3D-Aggregation und eine erhöhte Sekretionsrate von

Albumin im Vergleich zu PC-Gerüsten. Anschließend wurde dieses zweistufige Herstellungsverfahren verwendet, um schnell abbaubare Gerüste für die gerüstfreie Zellblatttechnik herzustellen. Gerüste mit kontrollierter Porosität und Topographie, die die Schlüsselmerkmale von Lebersinusoiden nachahmen, wurden aus Poly(milch-co-glykolsäure) (PLGA)-Copolymer hergestellt und für den *in vitro* Abbau in Zellkultur charakterisiert. Um die Beziehung zwischen dem Abbau des Gerüsts und der Organisation der Zellen in der PLGA-Matrix aufzudecken, wurde die Lebensfähigkeit und Morphologie der kultivierten Zellen zusammen mit der Morphologie des Gerüsts untersucht.

Im zweiten Teil dieser Arbeit wurden verschiedene technische Lösungen für die gerichtete Strukturierung mikroporöser Polymergerüste bewertet und ihre Eignung zur Erzeugung einer benutzerdefinierten lebenswichtigen oligozellulären Morphologie auf künstlichem Substrat vorgestellt. Besonderes Augenmerk wurde auf das 3D-Mikrokontaktdruckverfahren (3DμCP) gelegt, das die Vorteile des Mikrothermoformens und des Mikrokontaktdrucks kombiniert und eine räumlich-zeitliche Kontrolle über morphologische und chemische Merkmale in einem einzigen Schritt ermöglicht. Um das Potenzial dieser Technik aufzuzeigen, wurden Gerüste mit bestimmten Mikrostrukturen wie Kanäle mit verschiedenen Tiefen und Breiten sowie komplexere Muster hergestellt und verschiedene ECM-Moleküle gleichzeitig in die vordefinierten Geometrien übertragen. Die Gültigkeit des 3DμCP-Prozesses wurde durch mikroskopische Messungen, Fluoreszenzfärbung und Testen der Substrate auf Zelladhäsionsantwort gezeigt.

Schließlich wird in dieser Arbeit die Herstellungsmethode zur Erzeugung komplexer Gerüste für die 3D- und gesteuerte Co-Kultivierung von Leberzellen vorgestellt. Polymermatrizen, die die grundlegende Leberarchitektur replizieren und somit eine gut organisierte Leberzellzusammensetzung ermöglichen, wurden erfolgreich unter Verwendung der 3DμCP-Methode hergestellt. Auf der Polycarbonatoberfläche wurden gleichzeitig chemische und topografische Leitfäden in Form sinusförmiger Strukturen strukturiert. Um die 3D-Gewebemikrostruktur zu replizieren, wurden EA.hy926- und HepG2-Zellen auf beiden Seiten des strukturierten porösen Gerüsts Co-kultiviert und anschließend einander gegenüber gestapelt, wodurch zugehörige Kanäle zur Bildung einer Kapillare führen. Das Potenzial unseres 3DμCP-strukturierten Gerüsts für die gerichtete Co-Kultivierung von Zellen wurde unter statischen Zellkulturbedingungen demonstriert. Am Ende wurden Gerüste für die weiteren Anwendungen im perfundierten Bioreaktorsystem angepasst.

Abstract

In a natural tissue, cellular behavior is regulated by microenvironmental stimuli. Different chemical, mechanical and physical cues reside in a local milieu and provide cells with a biological context. Compare to the *in vivo* situation, standard 2D *in vitro* cell culture models show many differences in the cellular microenvironment and as a consequence can cause alteration in cellular response. Creating physiologically more realistic environment on artificial substrate is a key factor for development of reliable platforms that enables the cultured cells to behave in a more natural manner. Therefore, novel biomaterial-based substrates with tailored properties are highly demanded.

Microtechnology is a powerful tool that helps in the production of the functional scaffolds for reproducing various characteristics of the *in vivo* environment and transfer them to *in vitro* conditions. Scaffold design parameters can be manipulated to meet the needs specific to given tissue. However, one of the fundamental limitations in current fabrication methods is the inability to integrate multiple scaffold characteristics within a single scaffold structure in a pre-designed manner.

This dissertation discusses scaffold microfabrication and surface modification techniques that use microstructuring technology and allows simultaneous control over various scaffold properties. These approaches in microfabricating polymeric scaffolds are used to provide physical and chemical characteristic those are more optimal for liver cell culture. The physiochemical aspects that constitute the *in vivo* cellular microenvironment of liver tissue are discussed and subsequently relevant technologies that can be used to regulate some of those aspects *in vitro* are presented.

In the first part this thesis demonstrates a novel two-step procedure for manufacturing polymeric scaffolds with microporous structure and defined topography. To achieve 3D matrixes with integrated porosity, fabrication of microporous foils was followed by microstructuring process using multilayer polymer thermoforming technology. These methods were used to produce substrates for organotypic 3D hepatocyte cultivation. Porous scaffolds with the structure of microcavities were formed from solvent casted and phase separated polylactic acid (PLA) foils. Samples were investigated for basic mechanical and surface properties as well as cellular performance. Moreover, to provide a reference point for the evaluation of produced matrixes, PLA scaffolds were compared to previously reported polycarbonate (PC) based substrates with similar geometry. HepG2 cells cultured within PLA scaffolds showed 3D tissue-like aggregation and enhanced secretion rate of albumin in comparison to PC scaffolds. Subsequently, this two-step fabrication method was used to produce fast degradable scaffolds for scaffold-free cell sheet engineering. Scaffolds with controlled porosity and topography mimicking the key features of liver sinusoids were produced from poly(lactic-*co*-glycolic acid) (PLGA) copolymer and characterized for *in vitro* degradation in cell culture. To reveal the relationship between

degradation of the scaffold and organization of the cells in PLGA matrix, viability and morphology of the cultured cells was examined along with scaffolds morphology.
In the second part of this work, various technical solutions for directed patterning of microporous polymer scaffolds were evaluated and their suitability for creating a user-defined vital oligocellular morphology on artificial substrate was presented. Special attention was given to the 3D microcontact printing (3DμCP) method that combines the advantages of microthermoforming and microcontact printing and provides spatiotemporal control over morphological and chemical feature in a single step. To show the potential of this technique, scaffolds with determined microstructures like channels with various depths and widths as well as more complex patterns were fabricated and different ECM molecules were simultaneously transferred inside the predesigned geometries. The validity of 3DμCP process has been demonstrated by microscopic measurements, fluorescence staining and testing the substrates to cell adhesion response.
Finally, this thesis presents fabrication method for manufacturing complex scaffolds for 3D and guided co-cultivation of liver cells. Polymer matrixes that replicate basic liver architecture and thus facilitate well-organized hepatic cell composition were successfully produced using the 3DμCP method. Chemical and topographical guidance cues in the form of sinusoidal structures were simultaneously patterned on the polycarbonate surface. To replicate 3D tissue microstructure, EA.hy926 and HepG2 cells were co-cultured on both sides of the patterned porous scaffold and subsequently stacked facing each other by virtue of which associated channels results in the formation of a capillary. The potential of our 3DμCP patterned scaffold for directed co-cultivation of cells was demonstrated under static cell culture conditions. At the end, scaffolds were adapted for the further applications in perfused bioreactor system.

Scope and outline of the thesis

The ultimate goal of this work is to integrate novel concepts of micromanufacturing along with polymer processing and modification methods to attain complex scaffolds with pre-designed architectures as well as tuned structural properties. Moreover, to provide more attractive microenvironment for cultured cells, distinct scaffolds characteristic are integrated within a single scaffold structure in a pre-designed manner. Evaluation of manufactured scaffolds is guided by an understanding of the behavior and responses of cells cultured on these scaffolds.

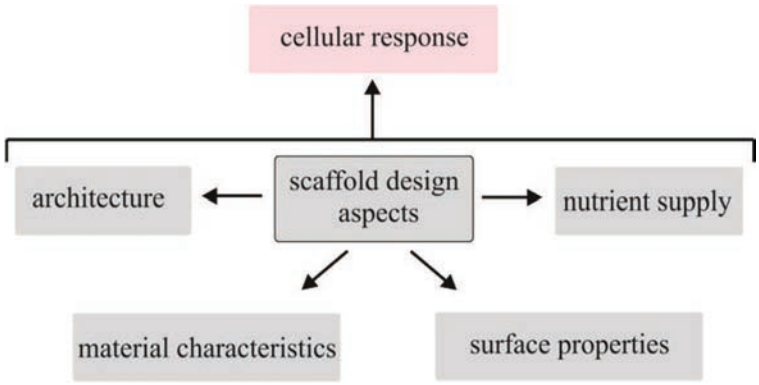

Figure 1: Main scaffold design categories, which could have impact on cellular response.

This thesis focuses on development of the scaffolds for various cell culture and tissue engineering applications with special regard to the parameters that allow reproduction of the liver tissue microenvironment. While creating novel strategies for functional scaffold development, the cell-scaffold interaction need to be considered at various levels and different design aspects must to be included (Fig. 1). Thus, many parameters, which mutually interact and affect the cell-scaffold interaction, are involved during the course of this work.

Main topics included in this dissertation are:

- Biomaterial engineering: selection of appropriate material and processing methods, evaluation of material properties
- Scaffold microarchitecture: formation of pre-designed topography and porosity
- Surface modification: alterations of scaffolds surface properties at micrometer scale, protein coating
- Going 3D: 3D material structuring, multi-layer stacking, up-scaling concepts
- Nutrients and oxygen delivery: preparation of the scaffolds applicable for medium transport through the single scaffold unit as well as complex tissue construct
- Cellular response: evaluation of the behavior and responses of cells cultured within the scaffolds.

The work is presented in 7 chapters; the empirical results are laid out in the chapters: 3, 4, 5 and 6. The structure of the work is as follows:

- First chapter presents literature overview of various aspects in liver tissue engineering (TE) and scaffold design for 3D cell culture. Topics discussed are: the general requirements for scaffold design, biomaterials applied in TE applications, scaffold fabrication techniques and polymer surface modification methods with special regard to materials and methods adopted in the different chapters of this thesis. Current *in vitro* strategies for improving culturing of liver cells are discussed as well. Subsequently, this chapter shows previous research of our group and introduce important theoretical context for this studies. Finally, overall description of our current *in vitro* liver model is given.

- Chapter 2 describes the main experimental techniques used for scaffold fabrication, cell culture and finally characterization and analysis of fabricated matrices and cultured cells.

- Chapter 3 and 4 deal with fabrication techniques for manufacturing 3D scaffolds with controllable porosity and topography. These chapters are describing the application of phase separation methods along with thermoforming techniques in scaffold fabrication and how to tune the morphology of the scaffolds by variation in processing parameters. In chapter 3 manufactured scaffolds are used for 3D hepatocyte cultivation, while chapter 4 explores the possibility of using our fabrication method to produce rapidly biodegradable substrates for scaffold-free cell sheet engineering applications. Moreover, these chapters relate to materials science and the corresponding cell-scaffold interaction. Comparing cell culture performance in scaffolds prepared from different materials, the role of material properties on cell behavior is discussed.

- Chapter 5 deals with directed modification of scaffolds surface to control arrangement of cells on 3D surface. Different methods for patterning of microporous polymer scaffolds at the microscale level are evaluated. Special attention is given to the 3D microcontact printing (3DμCP) method that combines the advantages of microthermoforming and microcontact printing. Evaluation of protein adsorption to 3D matrices and correlation to cell attachment, proliferation and cell morphology is described.

- Chapter 6 deals with complexity involved in liver tissue engineering and translating this complexity into scaffolds design mimicking tissue architecture. 3D architecture and up-scaling, multiple cell types and design mimicking *in vivo* environment are introduced in this study. Using the method described in chapter 5, polymer matrixes that replicate key structures of liver sinusoids and facilitate well-organized hepatic cell composition are produced. The potential of the scaffolds for guided 3D co-cultivation of hepatic cells is presented. Finally, evaluation of our system in the context of the currently available methods is given.

- Chapter 7 summarizes the main results and conclusions of this thesis. Further, it gives an outlook on a number of aspects that can be explored to improve and optimize scaffolds manufacturing as well as cell culturing methods proposed in this study in order to build optimal systems for complex liver cell cultures.

Table of contents

Abbreviations and acronyms

2D	two-dimensional
3D	three-dimensional
3DμCP	three-dimensional microcontact printing
μCP	microcontact printing
μFP	microfluidic printing
ATR-FTIR	attenuated total reflectance Fourier transform infrared spectroscopy
BSA	bovine serum albumin
CAD	computer-aided design
DAPI	4′,6-diamidino-2-phenylindole
DEP	dielectrophoresis
DMEM	Dulbecco's modified Eagle's medium
EA.hy926	immortal human umbilical vein cell line
EC	endothelial cells
ECM	extracellular matrix
ELISA	enzyme-linked immunosorbent assay
FCS	fetal calf serum
FDA	Food and Drug Administration
FEP	poly-(tetrafluoroethylene-co-hexafluoropropylene)
HEMA	2-hydroxyethyl methacrylate
HepG2	human hepatocyte carcinoma cell line
HF	hollow fiber
IP	immersion precipitation
L929	mouse fibroblast cell line
LSM	laser scanning digital microscope
M_w	molecular weight
ME	ß-mercaptoethanol
MEM	minimum essential medium
MTP	microtiter plate
NPCs	non-parenchymal cells
p	pressure

PBS	phosphate buffered saline
PC	polycarbonate
PEI	polyethyleneimine
PDLA	poly(D-lactic acid)
PDLLA	poly(D,L-lactic acid)
PDMS	polydimethylsiloxane
PE	polyethylene
PEI	polyethylenimine
PET	polyethylene terephthalate
PGA	poly(glycolic acid)
PLA	poly(lactic acid)
PLGA	poly(lactic-co-glycolic)
PLLA	poly(L-lactic acid)
PNIPAAm	poly(*N*-isopropylacrylamide)
R_a	surface roughness
rpm	revolutions per minute
RT	room temperature
SDS-PAGE	sodium dodecyl sulfate–polyacrylamide gel electrophoresis
SEM	scanning electron microscope
SFF	solid freeform fabrication
T	temperature
T_g	glass transition temperature
T_m	melting temperature
TE	tissue engineering
TIPS	thermally induces phase separation
UV	ultraviolet

1. Introduction

1.1 Cell culture systems and tissue engineering

1.1.1 Principles of tissue engineering

In the early 1990s tissue engineering (TE) has emerged as a new interdisciplinary field, which apply the principles of biology and engineering to provide solutions to the development of functional substitutes that restore, replace or regenerate defective tissues (1, 2). In the basic paradigm, tissue engineering technologies are based on three main components: cells, biomaterial scaffold and signals (Fig. 1.1). The cells could be stem cells, progenitor cells or fully differentiated cells (3). The scaffolds essentially act as a template for tissue formation and could be made of a synthetic biomaterial or be natural extracellular matrix. The third pillar of tissue engineering are signals, provided chemically by growth factors or physically by a microenvironment (4). Since TE attempts to mimic the structure and function of natural tissue, the natural environment of the specific tissue have to be fundamentally understood and many aspects and parameters must be preserved in the design and fabrication of well-functioning tissue engineering constructs.

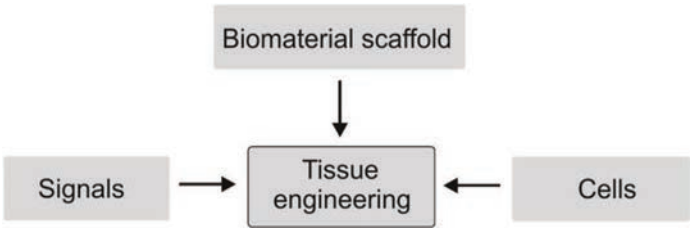

Figure 1.1: Tissue engineering triad.

1.1.2 Why do we need to engineer tissues?

Tissue engineering in the clinic

The initial aim of TE was to develop life-like replacement tissues and organs (5). TE originates from reconstructive surgery where transplanting tissues and organs from one individual into another is practiced to restore the function of damaged tissue (3). Transplantation, although very successful, have severe constrains. The major problem is insufficient donor organs and pathogen transmission. Difficulties with the immune system produce chronic rejection and destruction over time. Moreover, deficiency of donor organs is growing year by year as the population ages and new cases of organ failure emerge (3). Within this context TE can produce new solution to provide needed tissue that addresses most limitations of direct transplantation. Tissue or organ substitute containing patients own cells would eliminate dependency on donors, while preventing constrains concerning rejection and pathogen transmission (3). Despite limited success in production of complex organs, clinical applications of substitute tissues have been reported in literature. To date,

the most approved tissue-engineered constructs that have shown success in clinical trials are skin, cardiovascular, bone, cartilage and, most recently, bladder (6-10).

Tissue engineering for non-clinical applications

Over the last 30 years tissue engineering has evolved as a multidisciplinary field aiming to develop constructs that are not only considered as biological substitutes to replace defective tissues but also are highly desired to other fields of research (11, 12). Such systems are not meant as implantable structures but are frequently used as *ex vivo* complex tissue and organ models (13). Various field of research has been benefited from such non-clinical TE. Few are discussed below.

Fundamental biological research

Engineering human tissues in the laboratory has an important role to play in fundamental biological studies, creating multiple opportunities to advance research and discovery (13). TE models can improve our understanding of the nature of the human body at the tissue and cellular levels. Such systems can reproduce physiological microenvironments more realistic than traditional culture methods (14). This allows understanding how *in vivo* microenvironments are constructed and how cells interact with other cells and the surrounding environments (15). Therefore TE organ systems may provide relevant information regarding cellular basis for pathophysiology, growth, and homeostasis in different organs (14).

Screening systems

One of the most prominent directions of non-clinical tissue engineering is the development of TE-based screening systems that allow more thorough studies of toxicity, metabolism and life cycle of putative drugs and cosmetics (16). Despite of the progressing discovery of new compounds that are potentially candidates for pharmaceutical applications, the development of new drugs is a long and complex process with growing difficulty. Drug regulations are very tight and the number of compounds that progress successfully throughout clinical development is only about 8% (16). Currently, the standard procedure of screening new compounds starts with the preclinical testing on cell culture and animal models, followed by clinical trials. The costs of development increases exponentially along this pathway; therefore it is important that toxic or nonfunctional compounds are sieved out in preclinical test while promising candidates are prioritized. However, a lot of poor drug candidates are still not identified and fail first during clinical test (17, 18). Many of these failures are caused by the misleading data collected from the cell culture test in which the cellular response to drugs is altered mainly due to poorly reconstructed cellular microenvironments (19). On the other hand, data obtained using standard animal models can often be confounded or challenging to interpret. *In vivo* microenvironments of animals are slightly different from those of human beings and different species often respond differently to treatments or compounds (16). Animal model tests also cause ethical problems and the acceptance in the public of animal use in experiments for drug and cosmetic tests is decreasing. In European Union the 3Rs initiative (20) (Reduce, Refine and Replace animal experiments) has caused an official forbiddance on animal use for screening of cosmetic ingredients since 2009. Cosmetics containing components tested on

animals can no longer be marketed. For screening of therapeutics, animals may be used only with the implementation of rigorous reduction and refinement protocols (16). Therefore there is a great need for microtissue-based diagnostic and testing system of sufficient complexity that provide more informed results for a better prediction of drug candidate (21). In consequence, duration, cost failure rate and risk of clinical trials could be reduced (16).

Disease model

Other aim of non-clinical tissue engineering is to develop tissue substitutes, which can be used as disease models. Diseased human tissue can be utilized for therapeutic drug testing as well as for basic science studies to understand the onset and propagation of different medical conditions (13), with special regard to the cancer disease (22). Nowadays, advanced cancer models can provide information about cell movement in 3D environment, illustrate the invasive properties of the carcinoma, can be used to observe the feedback mechanism between tumor and stromal cells or monitor the interactions of cancer cells with different cytokines (13, 23). For even better understanding of complex cancer biology there is a growing need for TE-based model of healthy and disease tissue from the same cell source that could limit the variation of cancer cells from different patient and for personalized medicine (24).

1.1.3 Cell culture models – the way to improve the understanding of tissue physiology

Basic cell culture

Cell culturing process was started off as tissue culture in 1907, when R. G. Harrison was investigated the origin of nerve fibers, specifically, a small piece of tissue that was placed in a lymph (25). Hanging from a cover-slip, the lymph formed a drop, in which tissue was retained. Thus it was for the first time demonstrated that tissue could be maintained outside the body (25, 26). Further advances in tissue culture were made by A. Carel and C. Lindbergh, who grew tissue on glass plates and developed methods to keep cells continuously growing (27).

Since this time significant improvements have been made on the cell culture techniques. Nowadays, cells can be collected from a variety of sources, separated by trypsin and the cells growth and differentiation could be continually observed (28). In routine cell culture, cells are typically grown as a monolayer on a flat surfaces such as micro-well plates or Petri-dishes with synthetic medium as a source of nutrition. Such 2D cell culture systems are easy, cost-effective and maintain high cell viability, enabling the growth of cells to investigate a particular biological mechanism or process under specified test conditions. Thousands of research have relied on this format for the growth of cells, greatly improving the understanding of basic cell biology and creating the data for tissue engineering applications or for pharmaceutical assays (28). However the limitations of 2D cultures and how they represent the behavior of cells in authentic tissues plays a crucial role in the value of the data obtained from such conventional cultures (29).

Advanced cell culture - in vitro platforms for tissue engineering

In the real tissue, nearly all cells are surrounded by other cells and reside in an extracellular matrix (ECM), which provides a complex 3D microenvironment for the cell growth. ECM is a noncellular component, fundamentally composed of water, proteins and polysaccharides that serve essential physical scaffolding for the cellular constituents (30). 2D substrates used in conventional cell culture are not able to mimic this complex microenvironment and require a dramatic adaptation by culturing cells like cell flattening and remodeling of the internal cytoskeleton. As a consequence, tissue-specific architecture, mechanical and biochemical cues and cell–cell communication are lost (29). These drawbacks can alter gene expression, cell metabolism or functionality and thus influence the results of biological assays (22, 31). To reduce the gap between cell cultures and native tissues, various 3D cell culturing methods have been developed (32). 3D cell culture techniques enter the third dimension and enhance the spatial organization of the cells, allowing for:

- maintaining the normal 3D shape, structure and function of the cells
- greater cell-to-cell contact and increased intercellular signaling
- reduction of cellular stress and artificial responses caused by cell adaptation to 2D substrates
- enhanced creation of origin tissue architecture by providing a more natural environment for different cell types (33).

As a consequence, the 3D culture systems enhance the potential of the cultured cells to predict cellular responses of the real tissue and provide more reliable *in vitro* models (18, 34). 3D culture methods are adopted in different cell-based analysis, drug discovery, cancer cell biology, stem cell study as well as in engineered functional tissues for non-clinical applications or implantation (28). Moreover, the 3D cultures maintain an opportunity for adaptation of other strategies that more closely mimic the *in vivo* conditions and together have the potential to create an artificial systems mimicking the complete hierarchical, geometrical, and functional organization found in an actual tissue (21, 32). Such strategies for complex 3D cultivation of liver cells will be discussed in subsections 1.4.3 and 1.4.4.

3D cell culture methods can be widely categorized as scaffold-free and scaffold-based approaches (Fig. 1.2). Scaffolds-free systems are based on the natural tendency of many cell types to aggregate and form a multi-cellular aggregates, in which cells could create their own ECM components. Such cellular spheroids are simple models that can readily be imaged, therefore are the system of choice for many different therapeutically orientated biomedical studies (35). Spheroids can be produced in various ways, but it is beyond the scope of this thesis to discuss all methods in detail; however, a great review is given (17).

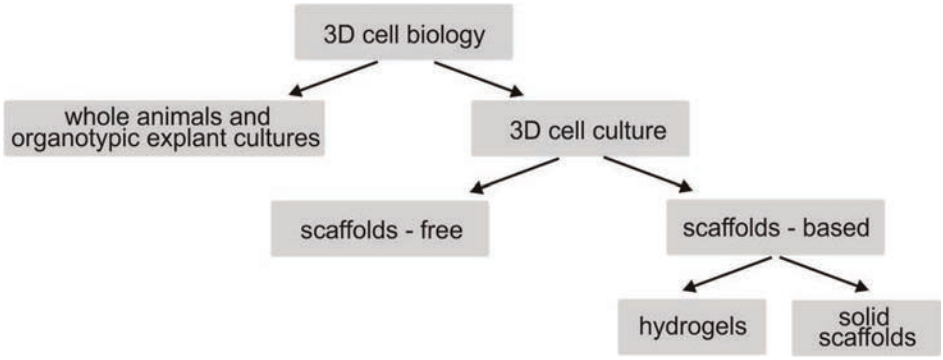

Figure 1.2: Different methods for 3D cell biology.

Nevertheless, as the capacity and complexity of the 3D model increases, the need for scaffold becomes noticeable. Large cellular aggregates do not provide any spatial control of the aggregated cells. Additionally, the lack of mass transfer may result in the deficiency of oxygen and nutrients as well as the accumulation of waste at the core of the spheroid. The use of highly porous scaffolds can provide a control of the gas exchange as well as the diffusion of soluble nutrients and chemical agents. Moreover, solid scaffolds provide space to support cultured cells and organize cellular distribution in a controllable and reproducible manner (33). In the next section the requirements of scaffold material for advanced cell culture and non-clinical tissue engineering applications will be discussed in details.

1.2 Scaffolds

1.2.1 Requirements

The scaffold attempts to mimic the function of the natural ECM, providing a temporary template for the growth of cultured cells (36). Scaffolds for TE applications have three primary roles:

- serve as an adhesion substrate for the cell
- define 3D space for the cultured cells and maintain mechanical support
- guide the development of new tissues with the appropriate function (36).

To serve their intendent function scaffolds should have appropriate properties. Following is a summation of the most important requirements of scaffolds for TE applications.

External geometry

To mimic the natural ECM in living tissue, the nano- to macroscale structural architecture of the scaffold should be controlled (37). The scaffold architecture would ideally offer 3 levels of control. On a scale of millimeters to centimeters, macroscopic shape and composition are essential. On a scale of hundreds of microns, the size and orientation of pores and channels are important to regulate. Finally, on a scale of tens of microns to submicrons, locally surface texture and porosity are crucial (37, 38).

Biocompatibility

Definition and requirement for biocompatibility can change depending on the specific application. Biocompatibility of a scaffold for a clinical TE product refers to the ability to perform as a substrate that will support the appropriate cellular activity, without eliciting any undesirable local or systemic responses in the eventual host. Biocompatibility of scaffolds for cell cultures can refer the lack of toxicity to the cultured cells (39). Many important factors like scaffolds chemistry, structure or morphology can determine their biocompatibility (39, 40).

Suitable degradation rates

Biodegradation stands for solid scaffolds which break down due to macromolecular degradation (41). It can occur through physical, chemical and/or biological process that are mediated by biological agents. The products of the degradation should be non-toxic and do not interfere with other tissues (37, 41). Most scaffolds used for therapeutic applications should degrade to allow cells to produce their own ECM and eventually replace the implanted scaffold (41). For TE applications that extend beyond therapeutic implants, biodegradable as well as biostable scaffolds are desired, depending on the intended use (42).

Mechanical properties

Scaffold should have the proper mechanical strength that will retain its primary structure after cell attachment and subsequent tissue formation. Mechanical properties should be designed to match the attribute of healthy tissue; therefore different properties like hardness or elasticity are required depending on the application (43).

Controllable porosity

Interconnected pore structure and high porosity are essential for cellular penetration and sufficient cell nutrition through easy diffusion of nutrients to and waste products from the scaffold (44). Moreover, by altering the pore size and porosity, the cell viability and proliferation can be enhanced. The mean pore size of the scaffolds varies from one cell type to another and must be designed and controlled depending on the envisioned application (44). Since the increased porosity can determine the final mechanical properties of the scaffold, it is often compromised as the result of the required mechanical strength.

Surface properties

Scaffolds surface is the initial site of the interactions with cells. Surface properties, which include both chemical and topographical characteristics, stiffens, charge or polarity, should promote cell attachment, spreading and proliferation. Surface of the scaffold greatly affects the cellularity, gene expression of cells and the overall tissue composition (45).

Easy sterilization

As with all materials in contact with cell culture or human body, scaffolds must be easy sterilizable to prevent contamination or infection (46).

Scalability for cost effective industrial production

To become clinically or commercially viable, scaffold should be cost effective and possible to produce in a scalable manufacturing process (47).

1.2.2 Materials

The choice of suitable material is the crucial criterion for scaffolds fabrication and should be considered together with the type of scaffolds that will be used and expected performance (42, 48). Potential materials with respective characteristics discussed in the preceding paragraph include natural polymers, synthetic polymers, metals, ceramics, glasses and composites of these materials (Fig. 1.3).

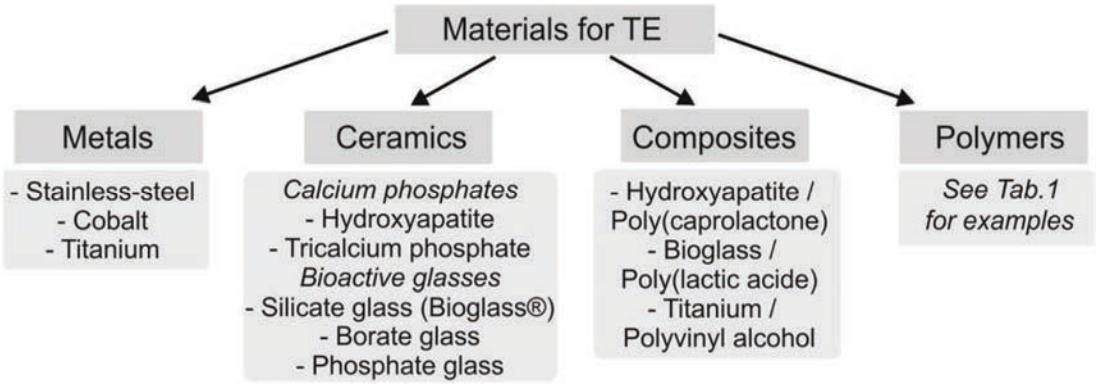

Figure 1.3: Classes of biomaterials applied in TE applications with examples of commonly used substances.

Rigid polymers, ceramics, metals and composites are not generally used for soft tissue regeneration, but there is a widespread use of these materials for hard TE products like bone tissue substitutes and implants (48-50). Although metal and ceramics have contributed to crucial advantages in orthopedic tissue substitutes, their significant disadvantages for other TE applications are limited processability, lack of biomechanical properties found in soft tissue and non-biodegrability (with the exception of biodegradable bioceramics) (51).

In contrast, polymeric materials have wide range of chemical, physical and mechanical properties that be tuned by varying the proper polymer itself (52) or can be achieve by additional polymer modification (53). Moreover, in comparison to metals or ceramics, polymeric scaffolds are easier to fabricate into desired shapes and generate lower cost (42). Based on origin, polymers for scaffold fabrication can be classified into natural or synthetic (Tab. 1.1).

Table 1.1: Polymers frequently applied in TE applications.

Natural polymers		Synthetic polymers	
Sub-classification	**Examples**	**Sub-classification**	**Examples**
Protein-origin polymers	Collagen Gelatin Fibrin Elastin	*Biodegradable*	
		Polyesters	Poly(lactic acide) PLA Poly(glycolic acid) PGA Poly(ε-caprolactone) PCL
Polysaccharidic polymers	Chitosan Starch Alginate Hyaluronan Agarose Cellulose	Polypropylene fumerates	Poly(propylene fumerate) PPF
		Biostable	
		Silicones	Polydimethylsiloxane PDMS
		Polystyrene	Polystyrene PS
		Polyacrylates	Poly(methyl mathacrylate) PMMA
Polyhydroxyalkanoates	Poly(β-hydroxybutyrate) PHB Poly(hydroxybutyrateco-valerate) PHBV	Polyolefins	Polypropylene PP Polyethylene PE
		Polyesters	Polycarbonate PC

Natural polymers are directly extracted from plants, animals or human tissues (54). Consequently, they provide compositional uniqueness, are biologically active and usually promote great cell adhesion and growth. Since their degradation products are the part of the body or body fluids, they tend to exhibit better biocompatible properties over synthetic materials. However, they generally show poor mechanical characteristics and are not convenient to produce a scaffold with homogenous and reproducible structure (55).

Synthetic polymers can be obtained by polymerization of different monomers and therefore wide range of physical and chemical properties can be tailored based on monomer units or polymerization reaction. Additionally, they have more predictable uniformity than materials from natural sources, can be produced in large uniform quantities and are often cheaper than natural polymers (54). However, they lack of biochemical stimuli like basic constituents of ECM occurring in natural polymers, and mostly require an additional coating with ECM proteins (53). In clinical TE synthetic materials can generate the risk of rejection due to reduced bioactivity (56). The desired longevity of the polymer dictates the use of biostable or biodegradable polymers. However, it should be noted that biostable polymers have been labeled “biostable” as compared with accepted biodegradable polymers, while in the human body environment any polymer will degrade after a certain time. Therefore the use of biostable polymers in TE can be viewed as degradable materials, which have much longer degradation time in comparison with accepted biodegradable polymers, but eventually will degrade in human body (42).

Since it is beyond the scope of this thesis to discuss all materials in detail, the next subsections focus only on the polymers used in this work.

Collagen

Protein-based polymers have the advantage of mimicking many features of ECM and thus they have found their way into extensive use in many TE applications (57). Collagen is an abundant structural protein found in all animals and the major protein component of the humans ECM. In *in vivo* environment, collagen interacts with cells and provides crucial signals for the regulation of cell attachment, migration, proliferation, differentiation, and survival (58).

The defining feature of collagen is a triple-helical structure (59). Each collagen molecule is composed of three polypeptide strands with the conformation of a left-handed helix. These three left-handed helices wind together to form into a right-handed triple helix, which is a single collagen molecule (Fig. 1.4). Collagen molecules have a length of about 300 nm and are stabilized by many hydrogen bonds. Under appropriate conditions, they can be further assembled by a parallel staggering into fibrils and subsequently in a complex, hierarchical manner that finally leads to the macroscopic fibers and networks (59). To date, 27 collagen types have been identified (57). The most abundant and usually considered for biomedical applications is the collagen type I. It is present in most soft and hard connective tissues such as bone, cartilage, tendon, cornea, blood vessels or skin, forming fibrillary constructs in ECM surrounding the cells (57).

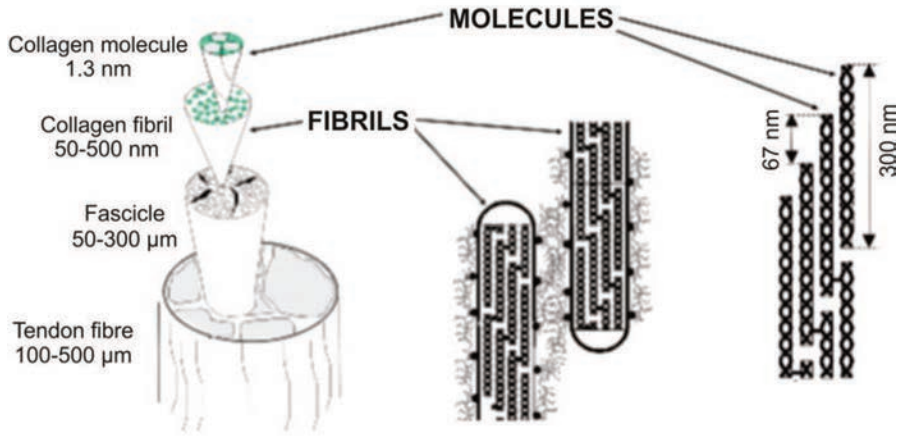

Figure 1.4: Sketch of the hierarchical structure of collagen. Figure replicated after (60).

The potential of collagen to interact with cells and to regulate cellular activities along with great biocompatibility makes this polymer especially attractive for use in TE (58). Collagen scaffolds have been shown to have high compatibility for supporting growth and function of many cell types (58, 61). However, collagen used in TE applications is mainly isolated from animal tissues, creating concerns related to the risk of transmission of infectious agents and precipitating immunological reactions (57). Additionally, this material is hard to process and its rate of degradability is difficult to control. In common with all natural polymers, collagen has relatively poor mechanical properties. However, the properties of collagen scaffolds can be improved by physical or chemical cross-linking methods or by introducing other biomaterials such as ceramic phase (57). This natural polymer offers also other perspectives for application in TE. Since

collagen has recognition signals and suitable mechanical properties to cells as well as shows good adsorption to many materials, it constitutes the ideal material to develop biointerfaces with promising functions. Therefore it is frequently used as coating material to control cell-material interactions and cell behavior on different surfaces (62).

Saturated aliphatic polyesters – PLA, PGA and copolymers

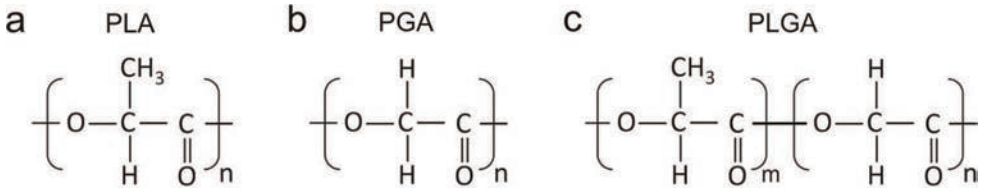

Figure 1.5: Molecular structure of (a) poly(lactic acid) (PLA), (b) poly(glycolic acid) (PGA) and (c) poly(lactic-co-glycolic) (PLGA).

Poly-α-hydroxy esters including poly(lactic acid) (PLA), poly(glycolic acid) (PGA) and their random block copolymers poly(lactic-co-glycolic) (PLGA) are the most applied synthetic polymers for scaffolds fabrication in TE (48). They own such popularity to their prominent advantages like adjustability of degradation rates, good mechanical properties and excellent processability (63). Degradation rate as well as physical and mechanical properties of aliphatic polyesters are adjustable by using polymers with various molecular weights and by changing the monomer ratios in lactide/glycolide copolymers (Tab. 1.2).

Table 1.2: Melting point (T_m), glass transition point (T_g), degradation time, modulus and elongation at a break of poly-α-hydroxy esters frequently applied as scaffold materials (48, 63-66)

Polymer	**T_m (°C)**	**T_g (°C)**	**Degradation (months)**	**Modulus (GPa)**	**Elongation (%)**
PGA	225-230	35-40	6-12	7.0	15-20
PLLA	173-178	60-65	12-18	2.7	5-10
PDLLA	Amorphous	55-60	11-15	1.9	3-10
PLGA (85/15)	Amorphous	50-55	5-6	1.4-2.8	3-10
PLGA (75/25)	Amorphous	50-55	4-5	1.4-2.8	3-10
PLGA (50/50)	Amorphous	45-50	1-2	1.4-2.8	3-10

On the other hand, solubility is determined by the degree of crystallinity, the molar mass and various comonomer units occurring in the polymer. Therefore good solvents must be selected individually for different polymers. Typical non-solvents are water, alcohols and unsubstituted hydrocarbons (63). The chemical properties of poly-α-hydroxy esters allow biodegradation due to simple hydrolysis of the ester backbone in the aqueous solution (67). Degradation products can ultimately by metabolized or eliminated by natural pathways in the body. However, these products

are simultaneously particularly acidic and lower the pH in the environment adjacent to the polymer. This local acidity can influence cellular viability or induce adverse tissue reaction (67).

PGA

PGA has the simplest chemical structure from all linear aliphatic polyesters (Fig. 1.5 (b)). Glycolide monomer is synthesized from the dimerization of glycolic acid. PGA has a high melting point as well as high degree of crystallinity. As a result, is insoluble in most organic solvents (68). Products from PGA exhibit high strength and modulus and are very stiff, what limit their application. To reduce the stiffness of the material glycolide can be copolymerized with other monomers. However, due to its hydrophilic nature, after implantation PGA is losing its mechanical strength rapidly. It can be completely degraded in 4-6 months and degradation products are converted to metabolites or eliminated by other mechanism (68, 69).

PLA

PLA can be prepared by ring opening polymerization or polycondensation from lactic acid, which can be found in many products of natural origin (63). PLA is structurally very similar to PGA (Fig. 1.5 (a)), but the presence of a pendant methyl group on the alpha carbon significantly affects its chemical, physical and mechanical properties (68). PLA is more hydrophobic and therefore degrades slower, however, in organic solvents dissolves much easier than PGA. Presence of the methyl group also causes chirality at the alpha carbon of PLA; and thus, semi-crystalline (L+) PLLA, semi-crystalline (D-) PDLA, and amorphous racemic (D,L) PDLLA isomers are possible. The stereochemistry influences the final properties (63, 64). PDLLA, due to the presence of both isomeric forms of lactic acid with random distribution is incapable to arrange into crystalline organized structure. In contrast, PLLA is semicrystalline and therefore relatively hard material with higher tensile strength and modulus (Tab. 1.2). Occurrence of crystalline regions in the structure of PLLA cause higher chemical stability and slower water uptake, therefore hydrolysis and consequent degradation of the PLLA is also slower than PLGA. Degradation products of all PLA isomers can be cleared through the tricarboxylic acid cycle (63).

PLGA

PLGA copolymer can be prepared at different ratios between its constituent lactic and glycolide monomers by a ring-opening co-polymerization. To synthesize PLGA of higher molecular weights, the same process with catalysts or cyclic dimers as a starting material can be used (70). In the composition of PLGA different PLA isomers can occur. Since the degradation rates are easily controlled for an amorphous polymer, the use of PDLLA isomer is preferred compared with PLLA. When PLLA isomer is applied, PLGA with a PGA percentage of 25–70% is amorphous. Using PDLLA isomer, this ratio extends to 0–70% PGA (65). By varying the ratio between the lactic and glycolide monomers, PLGA offers good control of mechanical and degradative properties. Higher glycolide content results in a decrease of T_g of PLGA and of the mechanical properties of corresponding material (70). PLGA with a higher content of glycolide is also more hydrophilic and degrade faster. An exception to this rule is copolymer 50:50 which exhibits the

faster degradation than copolymers with higher content of glycolide. The degradation rates can be also influenced by the molecular weight of the polymer, functionalization of the end group and the shape of the scaffold (71, 72).

Polycarbonate (PC)

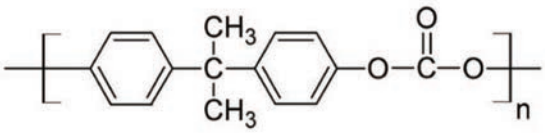

Figure 1.6: Molecular structure of polycarbonate (PC).

Polycarbonate (PC) is a synthetic and biostable polyester that can be produced by reaction of bisphenol-A and phosgene or phosgene equivalents (73). PC is mainly amorphous and thermoplastic, with a glass transition temperature of 147°C and melting point of 225°C. High heat resistance and good form stability make the material interesting for scaffold fabrication. Using PC, constructs with small dimensions in micrometer scale can be reproducibly produced with high aspect ratios (73). Moreover, unlike most thermoplastics, polycarbonate is not very brittle and therefore resistant to shocks and breaks. In the visible spectrum PC has very high optical transparency. Although great physical properties, PC is sensitive towards a broad range of organic and inorganic materials, mainly toward bases and organic solvents (73). It was also reported that utilization of PC under conditions such as increased temperature or neutral to alkaline pH may lead to release of Bisphenol-A (BPA), which is endocrine-disrupting chemical with weak estrogenic activity and is also suspected to be a carcinogen (74). However, there is currently no data available whether PC substrates for cell culture experiments may release BPA and therefore negatively affect the results. In addition, PC was proved to be biocompatible according to several test requirements of ISO 10993-1 (73) and ISO 10993-5 (75) and applicable for medical purposes. Polycarbonate has found widespread utility as material for medical applications (76) as well as for cell culture insert systems (77) and advanced *in vitro* models (78).

PDMS

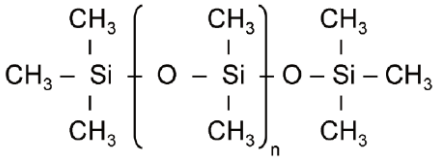

Figure 1.7: Molecular structure of polydimethylsiloxane (PDMS).

PDMS belongs to the group of silicone elastomers and is the most widely used silicon-based polymer (79). Silicones are a class of silicone compounds that possess at least one silicone-carbon bond and have siloxane linkage. Silicone products have unique properties, which are affected in large part by the exceptional mobility of the siloxane chains (79). The siloxane backbone is highly polar; however, it is effectively covered by non-polar side groups. For PDMS polymer this are

pendant methyl groups that only weakly interact with each other, shielding the main chain (Fig.1.7). As result, polysiloxanes have low intermolecular forces and the siloxane chain have extremely low rotation barriers (80). Therefore silicones show relatively poor mechanical properties, unusually high permeability to gases, very low glass transition temperatures and low polymer viscosities that change lightly with temperature (79, 80).
Silicone polymers can easily be transformed into a three-dimensional network using a crosslinking reaction that allows formation of chemical bonds between adjacent chains (80). Elastomers formed by crosslinking of PDMS are simple to handle and manipulate. They can be used to develop microstructures with submicron features, while retaining all the unique properties of silicones. Therefore PDMS is commonly used for soft lithographic replication and microfluidic (81). In addition, PDMS elastomers are transparent, non-fluorescent and demonstrated high degree of biocompatibility as well as biostability following clinical implantation (82). Since the final structural and surface properties of PDMS materials are relevant to the design, fabrication and development methods, they can be individually adjusted to the desired products (83, 84).

1.2.3 Fabrication and processing methods

The requirements of scaffolds for TE are complex and specific to the structure as well as function of the tissue of interest. Thus, the scaffold fabrication technique must be chosen accordingly to manufacture the constructs with desired characteristic (68). Typically, the selected fabrication process determines the choice of applicable materials and vice versa. Since the fabrication method can significantly alter the properties of the scaffold, the choice of the correct technique is critical (68). This section briefly describes frequently applied scaffold fabrication techniques, with the special attention to phase separation and microthermoforming as these are the main fabrication methods used in this thesis.

1.2.3.1 Approaches for controlled microporosity

A wide range of techniques have been employed to create biomaterials with controlled microporosity for engineered tissue structures. Following is a summation of the most commonly used methods.

Solvent casting and particulate leaching

Solvent casting is one of the oldest methods in polymer processing for producing thin polymeric films from solutions (69). This method is based on dissolving the polymer, casting the solutions onto an appropriate surface and evaporating the solvent. In combination with particulate leaching this technique can be also used to produce porous scaffolds (69). Calibrated mineral or organic particles like sodium chloride, ammonium bicarbonate or saccharose can be dispersed in a polymer solution and after evaporating the solvent, leached out from polymeric films by selective dissolution. Highly porous polymer matrix can be prepared using this method. The subsequent scaffolds porosity is controlled by amount of porogen added, while the pore size is determined by the size of the porogen particles (68, 69, 85). However, this method can be used

only to produce thin membranes up to 3 mm thick. Moreover, the use of organic solvents create the risk of remaining residues after processing. To exclude the use of organic solvent particulate leaching can be combined with other techniques like compression-molding (86) or foaming (87).

Gas foaming

Gas foaming method uses a soluble inert gases such as CO_2 or N_2 as a porogen to form porosity in polymer disc or films via pressure quenching (85). In brief, polymer samples are equilibrated with high pressure gas to form a polymer/gas solution and subsequently the gas pressure is decreased to generate thermodynamic instability. Gas molecules are clustering to minimize their free energy and consequently are forming nuclei (85, 88). This method eliminates the need of organic solvents, while the low processing temperatures prevent degradation of the polymer during foaming. However, since dissolved gas molecules diffuse to the pore nuclei, the macropores with a closed pore structure are mostly created (85). Open porous morphologies can be obtained only in particular cases (89).

Electrospinning

Electrospinning is the most popular process used for fabrication of scaffolds with nonwoven fibrous structure (90). The basic electrospinning setup usually consist of 3 major components: a high voltage power supply, a syringe pump and a collecting target (91). In brief, this method involves loading the polymer solution into a syringe, pumping it at a slow rate by a syringe pump, charging of solution using a high electrostatic force and then stretching of the viscoelastic material into fibers. As the stretched jet of liquid travels, the solvent evaporates and the polymer fiber is captured on the appropriate collector (90, 91). Fibrous electrospun scaffolds show high surface-to-volume ratio and are similar to the fiber network in natural ECM (91). Moreover, using multiple needles simultaneously during electrospinning process, different polymer solutions can be combined and multicomponent scaffolds can be produced (90). This technique allows for the production of polymer fibers with diameters varying from 3 nm to greater than 5 µm. However, despite the pore size can be also modulated, normally it does not extend 10 µm and therefore electrospun scaffolds can hinder cell infiltration (69).

Meltblowing

Meltblowing is a one-step and solvent-free process for producing nonwoven fabrics from thermoplastic polymers that was first patented in 1939 (92). Over the years, meltblowing products have been used in a wide range of applications (93). In this method, the polymer is melted and is then extruded through linear die heads. Subsequently, high-velocity hot air is utilized to draw the molten polymer fiber. This air is also used to stream convey the fibers on to a collector, where they are quenched and solidify in ambient air, forming a cohesive nonwoven web (93). This process hat the capability to handle various polymers or blends of polymers, while fiber diameter, alignment or density can be modified. In contrast to electrospinning, the melt blowing is a high throughput process; fabrics can be created at a rate up to 5000 m/min (92), making meltblown products promising candidates for commercialization of nonwoven scaffold

based tissue engineering. However, since there have been limited previous studies to evaluate meltblown scaffolds for TE applications, further research is needed to understand the interplay of fabric properties and their effects on cell behavior (94).

Phase separation

The phase separation techniques are based on preparation of homogeneous and uniform polymer-solvent solution and thermodynamic demixing of obtained solution into a polymer-rich and polymer-poor phase (95). Thus, this methods allow to produce highly porous scaffolds with wide range of pore size and interconnected structure through a simple fabrication process (96). Phase separation of polymer solutions can be induced in several ways. For the preparation of the polymeric scaffolds the main techniques are thermally induces phase separation and immersion precipitation.

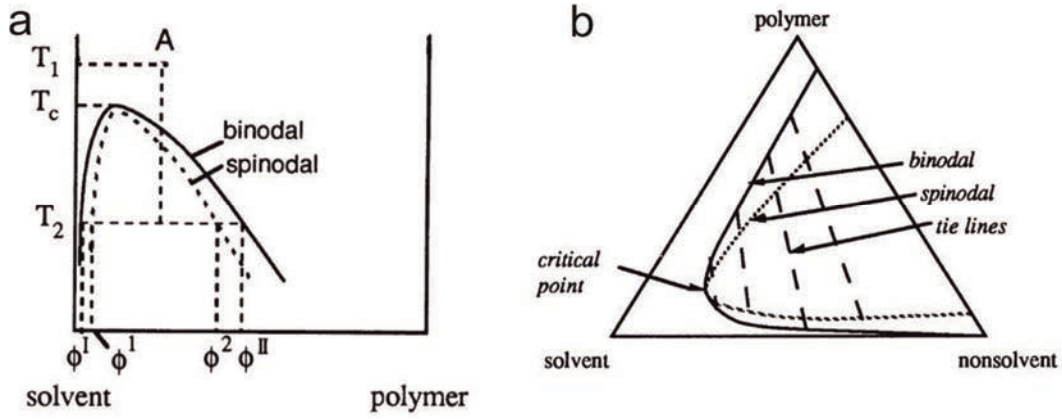

Figure 1.8: Schematic temperature – concentration phase diagram for TIPS process (a) and representation of a ternary system with a liquid-liquid demixing gap for IP process (b). Figures reproduced after (97).

Thermally induces phase separation (TIPS) uses the thermal energy as a driving force to induce phase separation by cooling the solution below its solubility temperature (95). As consequence, polymer-solution is separated into a polymer-rich and polymer-poor phase. The quenched polymer solution is subsequently freeze-dried to remove the solvent and produce scaffold with porous structure (95). Fig. 1.8 (a) shows a schematic temperature-concentration phase diagram for a polymer-solvent system. Above the bimodal curve the polymer solution is homogenous, while below this curve the two-phase region occur. Additionally, the two-phase region is divided by the spinodal curve into unstable and metastable zone. After quenching in the metastable region the phase separation is initiated by nucleation and growth. This leads to the formation of scaffolds with big pores and closed structure. In contrast, in the unstable region the phase separation is initiated by spinodal decomposition and leads to the formation of a bicontinous structure (97). Thus, the freezing under the spinodal curve results in formation of scaffolds with open microporous network and interconnected structure, which are preferable for TE applications. Additionally, the shape, size and the interconnectivity of the pores can be tuned with manipulating

the processing parameters such as polymer concentration, quenching temperature, type of solvents or additives (98).

Immersion precipitation (IP) process uses the changes in polymer-solvent composition brought about by the addition of a third component, which is a nonsolvent (99). To induce phase separation, a polymer – solvent solution is casted on a suitable support and immersed in a coagulation bath containing a nonsolvent. Precipitation occurs because of the exchange of solvent and nonsolvent (95). The solvent and nonsolvent must be miscible with each other. The solvent diffuses into the coagulation bath whereas the nonsolvent will diffuse into the cast film. Demixing takes place when the exchange of solvent and nonsolvent is proceeded so far that the solution becomes thermodynamically unstable. Finally a solid polymeric film is obtained with an asymmetric structure (95). Fig. 1.8 (b) shows a schematic isothermal phase diagram for mixtures of a polymer, solvent and a nonsolvent. The phase diagram is divided into a homogenous region and an area representing a liquid – liquid demixing gap. Demixing will occur by the addition of such an amount of nonsolvent that the solution becomes thermodynamically unstable (99). Analogously with temperature – concentration phase diagram for TIPS (Fig. 1.8 (a)), liquid-liquid demixing gap is also divided into metastable and unstable area. Therefore the phase separation proceeds in the same way as described for TIPS. Structure of the created scaffolds can be manipulated by changing many factors like choice of polymer, choice of solvent and nonsolvent, composition of casting solution, composition of coagulation bath, temperature of the casting solution or the evaporation time of the coagulation bath (95, 99).

1.2.3.2 Micromold based methods

Micromolding is a set of replication-based techniques for microstructuring of polymer materials by feature-transferring mechanisms using molds (generally known as masters or tools) (100). To create features on a polymer substrate the master pattern on a mold is replicated to a polymer material. All micromolding methods are based on four primary steps:

- microfabrication of the mold with a negative or inverse geometry of the desired pattern
- insertion of polymer substrate to the mold
- cooling or curing of the molded substrate
- detachment of the microstructured material from the mold (100).

Micromolding is a cost-effective way to produce structured polymer materials containing features with precisely controlled shape and size down to tens of nanometers (101). It is also robust and reproducible fabrication approach. Once mold insert is fabricated with a suitable pattern, it can be used multiple times; hence many parts with the same pattern can be molded with little exertion. Moreover, using micromolding methods a variety of different polymers can be processed, which allows one to find an appropriate material for different use (101).
Since the mold insert provides the primary microstructure that is replicated to the polymer material, it can be considered as the most important tool in micromolding process (102). There are various terms, which need to be completed by the molding tool depending on the type of

micromolding as well as type of the molded material. The microstructure created on the mold must always have smooth side walls, should be resistant to lateral and normal forces during injection and demolding as well as must remain intact over many molding cycles (102).
In respect of different tooling materials, micromolding techniques can be divided into two categories: hard mold processes and soft mold processes. Hard molds can be made of quartz, silicon or metals using different production methods like electroplating, mechanical micromachining, electric discharge machining, lithographic processes, wet etching or reactive ion etching (102). However, production of a metallic micromold with well-defined microstructures is expensive and demanding. Therefore very often for prototyping purposes silicon-based molds are used even though they are rather brittle (101). In contrast, soft molds are mainly made from PDMS and can be easy fabricated by casting the elastomeric polymer to prefabricated silicon wafers (8). Thus it is possible to generate a large variety of soft molds in a simple way.

There are different micromolding processes, which are designed for microstructuring of thermoplastic polymers applied for various engineering disciplines. The most common micromolding technique applied for scaffold fabrication is polymer casting. However, in recent years also micromolding technologies like hot embossing or microthermoforming have been translated from other engineering disciplines and utilized in creating microfeatures in engineered scaffolds in a controlled manner (102). This methods are described in the following subsections.

Replica molding

Replica molding technique is one of the most popular methods for generation of patterned cell-laden hydrogels for 3D tissue engineering constructs (103). This approach has become especially attractive for TE due to the possibility of application of soft molds, which can be easy fabricated. In a conventional micromolding by polymer casting the prepolymer solution is casted between a flat surface and a patterned mold. Subsequently, to lock the geometry and provide the solid material in the shape of the pattern used, the polymer of interest is cured by UV or temperature assisted crosslinking (103).

Hot embossing

Hot embossing is a microfabrication method that uses temperature, pressure and vacuum conditions to replicate a topographical pattern into a polymer substrate (104). Initially, the embossing tool and the planar polymer substrate are mounted on heating plates of the embossing machine. This machine mainly consists of a force frame which delivers the embossing force (105). The polymer and the molding tool are placed in contact and heated above glass transition temperature of the polymer. Subsequently, molding tool is pressed under vacuum into a polymer substrate softened by raising temperature, stamping of a pattern into a polymer. Finally, the molding tool and the polymer substrate are cooled below the glass transition temperature and de-embossed (104) .
With hot embossing fabrication technology high aspect ratio structures can be fabricated over large surface areas and the hot embossing products feature sizes of structures with notable

influence over cells (106). This approach is also a flexible, low-cost and high-throughput method with the potential to economically mass produce of cell culture substrates (105, 107).

Thermoforming

During the thermoforming process the heated polymeric substrates in the form of films or thin plates are subjected to pressures (32). As a consequence, they undergo 3D stretching into molds and become thin walled structures (108, 109). To stretch the polymeric substrate into desired microstructures without tearing it, the polymer must be heated to its entropy- or rubber elastic state (109). Thus, the thermoformed film must be above energy-elastic state, but below viscous state. Thermoforming temperature of substrates from amorphous thermoplastics is mostly slightly above T_g of their polymer. Substrates from semi-crystalline thermoplastics are microstructured between a temperature above T_g of their amorphous regions and a temperature slightly above the T_m of their crystalline regions (109).

The complete thermoforming process are based on the following sequence of phases:

(a) polymer substrate is inserted into microthermoforming machine and clamped at its edges or around the forming zone by tool closure,
(b) the film is heated and consequently softened, the microstructures of the moulding tool are evacuated and gas chamber is formed,
(c) the heated film is formed by high pressure intake that can be applied either to the upper face of the sheet by compressed air (pressure assisted forming) or by evacuation of the volume between the sheet and the mould (vacuum forming),
(d) the hot polymer comes into contact with the heated mould that subsequently is gradually cooled, which effectively freezes the newly formed microstructure and therefore the polymer substrate takes up the mould shape,
(e) the pressure is removed, the film is cooled down below its softening range,
(f) after tool opening the foil can be removed from the thermoforming machine and the microstructured part can be cut out of the surrounding film (73, 108).

Microthermoforming technology creates reproducible scaffolds with well-determined proprieties and high uniformity. Since this microstructuring process is a single-step operation, an effective production of scaffolds can be achieved through parallelization (73). However, the main disadvantage of this micromolding method in production of substrates for cell culture applications is the disability to form microporous materials. During the processing of the porous films pressure equalization occurs through the pores (73). Thus, to achieve microstructured and porous polymer substrates, postmodification methods must be applied (109).

1.2.3.3 Solid freeform fabrication (SFF) methods

SFF, also known as computer-assisted fabrication or rapid prototyping, is a common name for a group of techniques that can generate a physical model directly from computer-aided design data (110). 3D scaffolds can be fabricated through repetitious deposition and processing of material

layers using computer-controlled instruments (111). The SFF fabrication methods consist of 3 processes: collecting 2D image slices of a target specimen from commonly used medical imaging such as computer tomography, converting the obtained data into solid geometric models using CAD or other software and finally, fabrication of 3D scaffold using automated layer-by-layer manufacturing process (112). Based on the way materials are deposited, SFF systems may be categorized into laser-based, nozzle-based or printer-based (112). SFF methods allow for the fabrication of complex and patient specific scaffolds with controlled micro- and macro-architecture. Although those methods allow for a good control of geometry, the design/fabrication resolution is mostly limited. Currently it occurs at scale above 100 µm, while integration of micrometer features must be incorporated during post-processing steps (110, 111). Additionally, SFF methods are limited to specific materials, which are not suitable for mass production (110).

1.3 Polymer surface engineering

1.3.1 Why do we need to modify polymer surface?

In natural tissues contacts of cells with surrounding ECM and neighboring cells are mediated by cell adhesion receptors. In particular, integrin family comprises largest group and play a major role as anchorage molecules (113). Integrins create a mechanical link between the membrane and the ECM as well as between the ECM and the cytoskeleton (114). During the cell adhesion integrins are employed not only in physical anchoring process but also in signal transduction through the cell membrane. In most cell types, biochemical signals essential for cell survival, proliferation and function are triggered by integrins after attachment. Without attachment the cell undergoes programmed cell death, so-called apoptosis (114).
However, cell-surface interactions on synthetic polymers are limited. In contrast to natural polymers, synthetic materials lack of ECM constitutes. Additionally, they comprise no functional groups in the polymeric chains such as amine or thiol groups, that could be used to conjugate specific cell-recognizable signal molecules (53). Despite many anchorage-dependent cells secrete ECM and can adhere to unmodified polymer surfaces, they expend additional energy producing ECM. Moreover, smooth postfabrication surfaces and hydrophobicity of synthetic materials are additional factors that limit cell contact spreading prior to ECM development (53). Thus, to improve surface characteristic of polymeric substrates for tissue engineering applications, different modification approaches were developed.

1.3.2 Surface modifications techniques

There are two main approaches to modification of synthetic materials: bulk and surface modifications. Bulk modification changes the entire biomaterial, altering its structural and mechanical properties, and are not suitable for modification of the polymer scaffolds that are predesigned using microengineering approaches (115). Surface modification, by contrast, concentrate on changing only the scaffold surfaces, while preserving the integrity of the material's backbone (53). Surface treatment provides added functionality and is concentrated on the cell–

surface interface. Following is a summation of the major groups of surface modification approaches.

Surface coating

Coating of polymer surfaces with cell adhesive proteins like fibronectin, vitronectin, collagen or laminin has been one of the most common approaches that influences cell response to biomaterial surfaces (116). Proteins deposited on a biomaterial surface form noncovalent adsorption bonds, that are depending on forces such as electrostatic interactions, van der Waals forces, and ligand–receptor pairings (53). Protein adsorption depends on the properties of protein itself as well as on the properties of the material to which it adsorbs. It can be enhanced by changing the surface energy, polarity, charge or morphology of the polymer substrate (53). Generally, increased adsorption can be observed on hydrophobic surfaces, where proteins form an amphiphilic interface between the hydrophobic polymer surface and the aqueous solution (117).

Covalent immobilization of bioactive compounds

Covalent immobilization of bioactive molecules on polymer surfaces provide the most stable bond between the compound and the polymer surface (118). Biomolecules can be cross-linked to a surface covalently using a pendant functional group and mild chemical reactions that do not change relevant properties such as protein conformation (53). However, since surface of basic synthetic materials is functionally inactive, this modification method required functionalization of the polymer surface prior to cross-linking with certain biomolecule.

Functionalization involves the introduction of functional groups on the polymer surface. Created groups can provide direct bioactivity for cell binding or can be used to immobilize different bioactive molecules (53). Common functional groups in bioconjugation chemistry include thiols, aldehydes, carboxylic acids, hydroxyls, and primary amines (118). However, the specific group added to the inert surface should be compatible with the reactive sites on the biomolecule that is planned to be finally covalently immobilized on the functionalized biomaterial. Functional groups can be introduced to the biomaterial surface using different methods, including plasma deposition (119), wet chemical methods such as amylolysis (120) or physical entrapment of small functional molecules (121). Recently, our group has developed a mild and efficient method for the functionalization of polycarbonate using terminal diamines (122).

Topographical modification

Topographical modifications enhance cell attachment through changes in the geometry of biomaterial surface (53). In general, topographical alterations aim to increase the roughness of the biomaterial surface and thus enlarge the area available for cell interaction. Additionally, surface roughening increase hydrophilicity of the biomaterial. Adherent cells can recognize modifications restricted to low-micron and nanometer ranges (53). Topography of the biomaterials can be changed using different methods like plasma or chemical surface etching (123), grafting of different length polymer chains (124) or using micromolding methods such as hot embossing (125).

1.3.3. Micropatterning: principles and methods

Cellular architecture and organization are one of the factors that regulate the functions of various tissues. As a result, cells are very sensitive to geometrical constraints from their microenvironment. In this context, controlling cell adhesion to polymer substrates is one of the key issues in studying cell-cell interactions *in vitro* as well as in fabrication of tissue engineered constructs (126).

Despite first techniques for manipulating cell adhesion pattern have been developed more than 50 years ago, for many years they have not been commercially available or accessible to cell biology laboratories (127). Currently, common microengineering techniques provide various tools to restrict the location and shape of the surface area, in which cells can attach (128) . Thus, researches are able to organize the surface of the cell culture substrates and promote selective adhesion of one or more cell types to predetermined regions, so-called micropatterns (129).

Methods to create micropatterned cultures that control the cellular microenvironment can rely on physical localization of cells on chemically uniform surface (130), electrical stimulation (131), regional chemical (132) or topographical (133) modification of surface to promote cell adhesion or creation of localized nonadhesive domains (134).

Soft lithography

Among several approaches available for generating chemically patterned cell culture (135), soft lithographic techniques have especially emerged as simple and efficient manually operated methods to pattern different planar substrates with proteins or prepolymers. This set of techniques, developed by the Whitesides group (136), has a common characteristic that at some stage of the process a soft elastomeric stamp with a relief feature is used. The most widely used material to make a stamps for soft lithographic approaches is PDMS. This polymer has a number of properties which are very well suited for patterning applications (137). In particular, PDMS has adequate flexibility to make conformal contact even with rough surface, while its mechanical stiffness is sufficient to reproduce pattern in the micrometer range. PDMS stamps are usually prepared by pouring prepolimer mixture into a non-adhesive micropatterned master to display a faithful reproduction of the master pattern after curing (137).

The most common methods of soft lithographic family are microcontact printing (μCP) and microfluidic printing (μFP).

Microcontact printing (μCP)

Microcontact printing technique was originally devised as a method to pattern gold, however, its value in patterning surfaces for other applications quickly became apparent (138). This method offers great flexibility with regards to both the choice of substrate and the material to be transferred during printing.

Generally, μCP is based on the contact-transfer of ‘inked’ material from elastomeric stamp with bas relief features onto a substrate (139). Thus, only the areas with protrusions are able to contact the substrate and the ink is selectively transferred according of the pattern of the stamp

(Fig. 1.9 (a)). Inking of the stamp can be achieved either by immersion of the stamp in the ink solution or by placing a few droplets of the material of interest on the patterned side of the stamp. However, due to hydrophobic surface properties of the PDMS, water soluble inks such as protein solutions do not wet surface of the stamps. The easiest way to increase the hydrophilicity of PDMS is oxidation either by UV/ozone or by oxygen plasma treatment. The oxidation of the PDMS surface allows the printing of such polar inks owning to the oxygen rich surface layer formed upon oxidation (137). Increasing the hydrophilicity of the stamp may help to create an evenly dried, thick protein layer on PDMS surface.

Proteins can be transferred from inked PDMS stamp onto a variety of substrate materials with hydrophilic or hydrophobic surfaces. However, the mechanism of transferring of molecules from stamp to the surface is not yet entirely understood (132). Nevertheless, since virtually all surfaces in air are covered by thin molecular aqueous layer, water could be considered as the intermediary solvent that enable efficient transfer. Consequently, the transfer efficiency may be partially dependent on the ambient humidity (114).

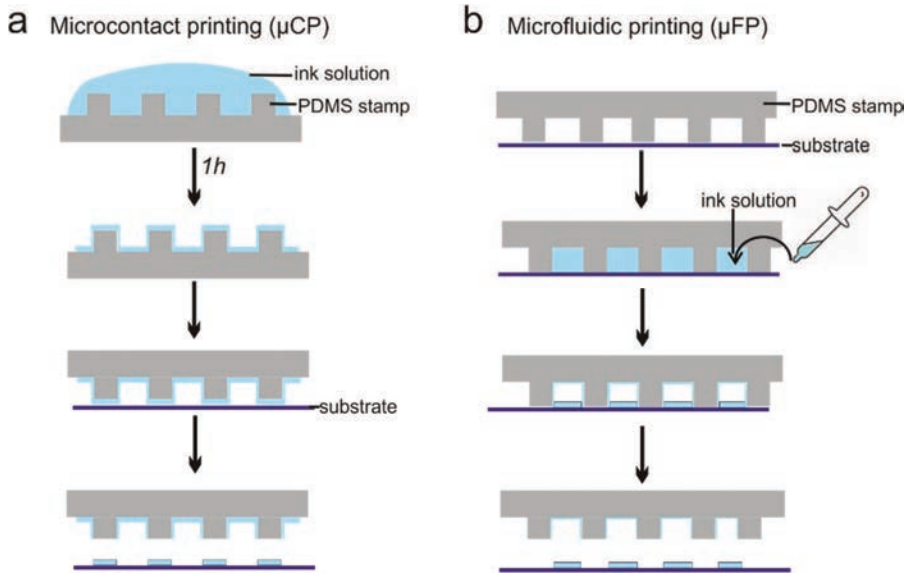

Figure 1.9: Scheme of microcontact printing (μCP) and microfluidic printing (μFP) methods.

Microfluidic printing (μFP)

In μFP technique the microchannels patterned on a PDMS stamp are used to deliver fluids to selective area of a surface (114). After placing the stamp on a substrate, stamp features and the surface of the substrate form a network of interconnected channels (Fig. 1.9 (b)). Filling the channels with ink solution is achieved by using capillary forces or pressure. In contrast to μCP method, ink is transferred to the sites where the PDMS does not come into contact with the surface. After the patterning material attached onto the surface of the substrate, stamp can be removed (140). PDMS stamp is able to block wetting of the substrate in the areas where the stamp contacts the surface due to a combination of its unique properties: elastomeric nature of the PDMS

material allow for a highly conformal contact with the surface, while the hydrophobicity of its surface impedes wetting of liquids at the PDMS-substrate interface (114).

1.3.4 Micropatterning of 3D scaffolds surface

Most of the current micropatterning methods are designed only for 2D constructs, despite the fact that cells naturally residue in 3D environment and may behave significantly different in 2D and 3D cell culture systems (128). Therefore, new techniques to control arrangement of cells within the 3D constructs are of high importance in modern biotechnology. It has been demonstrated that there is a synergistic effect of integrated chemical and topographical patterning for hosting single cells inside microwells and thus controlling their 3D shape (141), noninvasively controlling the shape of ECs (142) or for directing morphological maturity in neurons (143). Nevertheless, to create the combinatorial patterns for these research, multistep protocols and wet-printing techniques were utilized. Thus, the efficiency of this methods in terms of high throughput is limited. Furthermore, techniques applied in this studies are not well suited to the patterning of microporous materials.

On the other hand, recent work has demonstrated considerable progress in developing methods to independently engineer microtopography and patterned chemistry such that the topography neither determines nor limits the configuration of the chemical pattern. It was shown that microthermoforming process can be used to create patterned 3D substrates with randomly distributed biofunctional cues at microstructures (144). Sun et al. used “PoT” printing technique that enables the transfer of bioactive species inside of geometrically restricted sites by using specially designed soft stamp (145). In another study researches have used a crack-based approach to produce fiber-like patterns on microfabricated substrates (146). Despite a step forward, these techniques are restricted in terms of defining chemical patterns particularly in regard to geometrical patterning. Thus, how to engineer permeable 3D culture systems with integrated chemical and geometrical characteristics is a big challenge that need to be addressed.

Described techniques for scaffold fabrication and modification can be used to develop complex substrates for various non-clinical tissue engineering applications. In this thesis different approaches in microfabricating scaffolds are developed, with special regard to the parameters that allow reproduction of the liver tissue microenvironment, and thus provide more optimal systems for *in vitro* liver cell culture. Therefore, in the next section the physiochemical aspects that constitute the *in vivo* cellular microenvironment of liver tissue are introduced and subsequently currently available methods that can be used to regulate some of those aspects *in vitro* are discussed.

1.4. Artificial models of the liver

1.4.1 Need for liver tissue engineering

Liver carries out over 500 functions including complex metabolic, synthetic, immunologic and detoxification process (147). Because of its overall importance, liver disease and the following

loss of liver function is an enormous clinical challenge. Due to complications of cirrhosis, viral hepatitis and hepatocellular carcinoma, liver failure led to approximately 2 million deaths per year worldwide (148). Main determinants of liver failure are alcohol consumption, obesity and hepatitis B and C virus infections. Moreover, drug-induced liver injury continues to increase as a major cause of acute hepatitis. In Europe liver disease is a serious issue. Europe has the largest burden of liver disease in the world (149), with the burden expected to grow across many countries. The epidemiology of liver disease in Europe is diverse. Increasing cirrhosis and liver cancer may be linked to dramatic increases in harmful alcohol, while the rise of obesity across most European countries may cause an increase in non-alcoholic fatty liver disease in the future (149).

The most common treatment for patients with end-stage liver failure is organ transplantation. However, despite liver transplantation is the second most common solid organ transplantation, only less than 10% of global transplantation needs are met at current rates (148). Therefore, there is a urgent need for the development of a liver support technologies that could provide temporary function for patients with liver failure as well as for the development of more physiologically realistic *in vitro* liver models for drug screening and disease mechanisms studies (147).

1.4.2 Structure and cellular components of the liver

The liver is the largest solid organ in the body. The liver of adult humans weighs from 1300 to 1700 g. The topography of this organ is characterized by the smaller left lobe and about six times larger right lobe (150). From below two large vessels enter the liver: the hepatic artery and the portal vein. Hepatic blood flow amounts of 1200 to 1800 ml/min. Of this blood, 75% are supplied by the portal vein and 25% by the hepatic. Oxygen is provided from both sources. Of the top of the liver the central veins coalesce into a big vein called the inferior vena cava, which collects the blood leaving the liver (150).

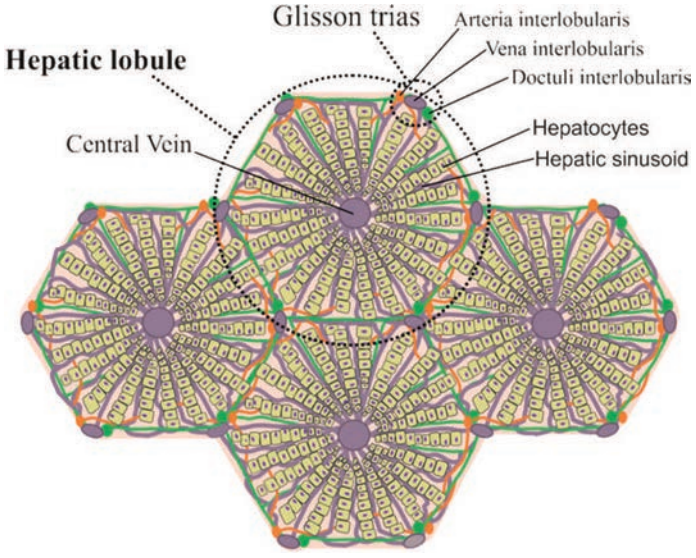

Figure 1.10: Basic structure of the liver tissue.

The smallest structural unit of the liver is the liver lobule (Fig. 1.10). Liver is built of approximately 1 million hepatic lobules, each of hexagonal shape with 1 mm diameter and the thickness of about 2 mm (150). The lobule consists of hepatocyte plates, which are the most numerous cells in the liver. Blood enters the lobules through branches of the portal vein and hepatic artery. At each of the 6 vertex of the lobule is a portal (Glisson's) triad. Each portal triad comprises an artery (*Arteria interlobularis)*, a vein (*Vena interlobularis)* and a bile duct (*Doctuli interlobularis).* Blood from the portal triad approaches all surface of the lobules through network of capillaries called sinusoids (150, 151). The sinusoids have an average diameter of approximetly 5-10 µm (151). Unlike capillaries elsewhere, liver sinusoids lack a basal membrane (151, 152) and are composed of fenestrated liver sinusoidal endothelial cells (LSEC) that are the largest groups of NPCs in the liver. LSECs are highly specialized cells and most permeable endothelial cells of the mammalian body (153). They have large pores (fenestrae) with a diameter of 0.1-0.3 µm that enable free flow of molecules from plasma to hepatocytes (154). Between the LSEC and hepatocytes is a 0.2 to 0.4 µm wide area called space of Disse. The sinusoidal surfaces of hepatocytes are amplified by numerous microvilli, which extend into the space of Disse and are therefore in direct contact with the blood. Remaining hepatocyte surface faces adjacent hepatocytes. A single hepatocyte has contact with six to ten other hepatocytes. The intracellular surface is mostly flat, except where microvilli form bile canaliculi to improve bile secretion (151).

Table 1.3: Cellular composition of the liver (151, 154).

Cell type	**No. of cells / percent of all liver cells**	**Location in the liver**	**Function**
Hepatocytes	$1*10^{11}$ (~60%)	Arranged in cords, sandwiched by ECM in the space of Disse, 50% of total hepatocyte surfaces face adjacent hepatocytes, 35% face sinusoids and 13% is infolded to form bile canaliculi.	Most of the metabolic and synthetic functions of the liver e.g.: -express majority plasma proteins such albumin, protease inhibitors, transporters, blood coagulation factors -control of the homeostatis of triglycerides, bile acids, glucose\glucogen, cholesterol, vitamins -metabolism of amino acids and metals -urea synthesis for ammonia detoxification and pH regulation.
Sinusoidal endothelial cells	$3x10^{10}$ (~19%)	Line the wall of the hepatic sinusoid, form a sinusoidal vessels, surround sheets of hepatocytes. Form a porous fenestrated barrier.	Form physical barrier for blood circulation, regulate substrate transfer between the blood and hepatocytes. Actively participate in inflammatory reactions, leukocyte recruitment, and host immune responses to pathogens.
Macrophages (Kupffer cells)	$2x10^{10}$ (15%)	Located within the lumens of sinusoids.	High endocytic and phagocytic activity.
Pit cells	$1*10^{10}$	Located along sinusoids and in portal tracts.	Liver-associated natural killer (NK) cells.
Stellate cells	6%	Located in the space of Disse between the hepatocytes and the sinusoids epithelium.	Store retinoids. Synthesize, secrete and degrade components of ECM.

1.4.3 *In vitro* strategies for improving hepatocyte viability and function

The main aim of *in vitro* liver tissue engineering is to sustain a functional liver cell population. Since hepatocyte metabolism plays a central role in liver function, most scientific efforts focus on preservation or improvement of hepatocyte function (155). However, maintaining fully functional hepatocytes *ex vivo* is a big challenge. The most important problem following hepatocyte isolation is the rapid loss of their differentiated structure and function (15). Despite isolated hepatocytes cultured under standard tissue culture conditions secrete albumin (a marker of liver protein synthesis), urea (a marker of nitrogen metabolism) and show cytochrome P450 activity, these liver-specific functions steadily decrease within the first week of culture, suggesting that important liver-specific microenvironmental cues are missing from this culture (155, 156).

Under physiological conditions multiple types of cells regulate specific liver function; all the cells form complex 3D microlevel structures and work together in a strictly defined mechanical and physical microenvironment along with biochemical factors (Fig. 1.11). Therefore, to provide more realistic environment for the cultured hepatocytes, different factors that constitute *in vivo* cellular environment of the liver tissue need to be included (32). In the following sections the main factors are discussed and examples of methods used to mimic those factors *in vitro* are given.

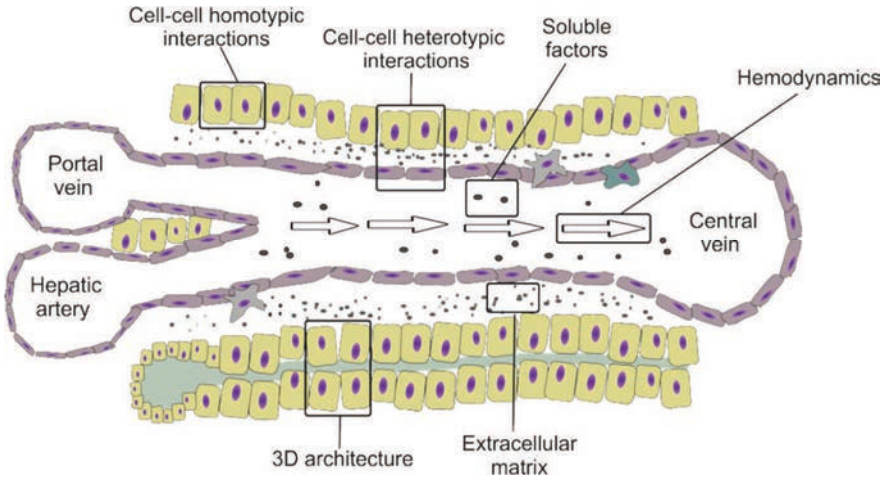

Figure 1.11: Different factors that constitute the *in vivo* cellular environment of the liver.

Extracellular matrix

The nature of cellular interactions with the surrounding ECM environment is one of the most important factors determining maintenance of normal hepatic functions *in vitro* (157). Composition and geometries of ECM may influence both cell shape and cytoarchitecture. As a consequence, the chemical composition and biophysical characteristics of materials used as cell culture substrates are able to significantly affect structural and functional properties of cultured hepatocytes (157). Thus, the choice of scaffold material and scaffold surface modification is crucial.

Immunochemical analysis of the space of Disse has shown that the basal surface of hepatocytes *in vivo* is in intimate contact with several ECM proteins such as collagen (types I-IV), laminin, fibronectin and heparin sulfate proteoglycans. The proportion of these components are changing across the liver acinus (157, 158). Since the main disadvantages of synthetic polymers is the lack of cell recognition moieties for specific cell adhesion (159), in cell cultures on synthetic scaffolds ECM molecules are mostly used to bring the desired cell type in contact with scaffold surface. Modification and functionalization scaffolds surface by the complexation of natural biomacromolecules such as collagen and gelatin is an effective method to improve their biocompatibility (160). Hepatocytes attach to the ECM *via* transmembrane integrin receptors. This connection allows adhesion and influence cell migration as well as phenotypic expression (161). The impact of ECM proteins on the differentiated functions of hepatocytes *in vitro* has been widely studied. It was shown that culturing cells with collagen or other ECM molecules may restore hepatocyte-ECM interactions and thus improve viability and hepatic function (161), while functionalization of microporous scaffolds with various ECM molecules was shown to play distinct roles in the phenotypic regulation of cells cultured in a 3D environment (162).

Three dimensional architecture

Hepatocytes are polygonal in shape and are multi- polarized with distinct apical (bile canalicular) and basal (sinusoidal) surfaces that serve different functions (163). Therefore cell polarity is essential to maintain liver structure and activity (164). However, since hepatocytes are adherent cells, the 2D substrate forces them to change their cytoskeleton toward a flattened morphology. As a result 2D cell cultures cause modifications in hepatocyte shape and form, as well as limit cell-cell and cell-matrix interactions. Cell polarization along with bile canaliculi formation is reduced and important signaling pathways necessary for normal hepatocyte function are lost (154).

In an attempt to mimic the hepatic microenvironment, various more complex culture systems have been developed (32). An established method that is known to improve the longevity of hepatocyte cultures is the addition of a second layer of collagen on top of the cultured hepatocytes (156, 164). Although such “collagen sandwich” systems do not represent a definitive 3D cellular organization, cell-matrix adhesion from above and below reduces cytoskeletal flattening and support cell-cell contact between neighboring hepatocytes (154). To establish more complex culture system with definitive 3D cellular organization and fully restored intercellular interactions, hepatocytes can be stabilized in 3D spheroids using different method (Fig. 1.12).

The easiest technique for placing hepatocytes into 3D organization is formation of hepatospheres (165). If adhesion to a substrate is prevented, hepatocytes can re-aggregate by cellular self-assembly. Thus, hepatospheres can spontaneously form on nonadhesive surfaces such as nontreated culture plates or plates coated with various polymers (165). In such spheroid culture hepatocytes with stable viability were maintained for longer periods of time (166). Still, the applicability of hepatospheres can be restricted by certain properties of this configuration. Since hepatospheres cultures are biomaterial-free approaches, they do not provide precise control over the spheroid structures. Lack of regulation over their size and fusion of small spheroids into larger structures causes variability in the transport of metabolites in and out of the aggregates and

formation of necrotic cores in the center of large hepatospheres (151, 155). Cell aggregates may form differently across wells and experiments, which consequently may generate large variations in downstream assays such as drug screening (167, 168).

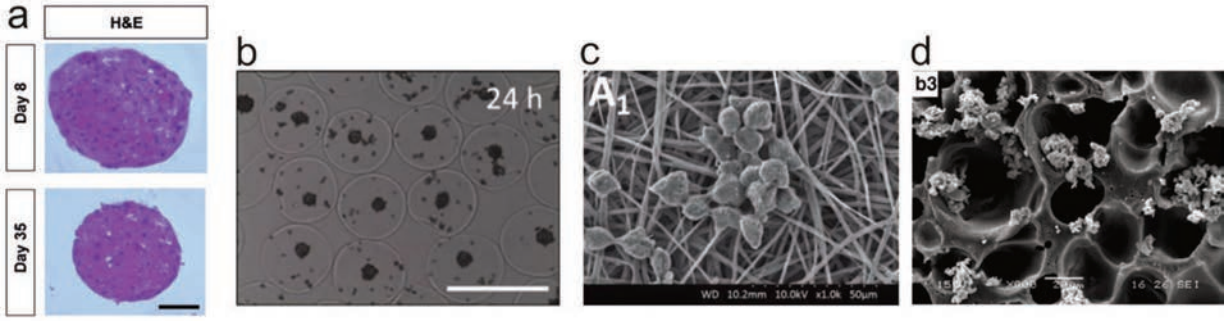

Figure 1.12: Various 3D hepatocyte culture systems: (a) spheroids formed by seeding of primary human hepatocytes into ultra-low attachment 96-well plates (165), (b) hepatocytes entrapped inside hydrogel microcapsules (169) and (c) hepatocytes cultured inside PLGA scaffolds with fibrous (170) and (d) sponges structure (171).

To enhance control over 3D hepatocyte culture cells can be embed into both hydrogels and synthetic scaffolds. Due to high water content and unique mechanical properties hydrogels have the ability to simulate the nature of most soft tissues (172). Substrates used for hepatic cell culture can be formed from a large array of natural and synthetic materials (173). A wide variety of studies using hydrogel matrices has been proven to enhance functionality of cultured hepatocytes significantly (154). On the other hand, hydrogel applications are limited by poor mass transfer of nutrient and xenobiotic, as well as due to difficulties in cell retrieval. In contrast, porous solid scaffolds favor diffusion of oxygen, nutrients and test compounds. Solid cell culture substrates provide a site of attachment for hepatocytes generating the physical and chemical instructive signals to the cells (174). The cultivation of hepatocytes on scaffolds from naturally derived materials has shown that these materials can significantly enhance hepatocyte function and support viability when fabricated into specific 3D geometries (175, 176). The hepatogenic differentiation of stem cells in natural matrix has also been widely reported (177). Naturally derived substrates are suitable for mimicking cell-matrix interaction, however, next to the previously mentioned drawbacks assigned to the natural scaffold materials (subsection 1.2.2), scaffolds fabricated purely from these molecules exhibit limited versatility in designing devices with particular biomechanical properties (178).

Some of the most successful scaffolds used to support 3D hepatocyte growth were fabricated from synthetic materials such as saturated aliphatic polyesters, poly(ε-caprolactone), polyvinyl alcohol or polystyrene (173, 179). Depending on the manufacturing process, synthetic polymer scaffolds are available in the form of membranes (180), sponges (181) or fibrous substrates (170), which are suitable for perfusion. Each type of the scaffold offers its own advantages and disadvantages in mimicking the organization of *in vivo* tissue structures (179). Hepatocytes cultivated within such porous synthetic scaffolds preserved hepatocyte-specific cytoskeleton (182), have shown

preservation of hepatocyte parameters, such as urea and albumin synthesis (182, 183), exhibited greater detoxification ability (171) and enzymatic expression (184) as well as exhibited differential expression of genes associated with drug metabolism (184).

Multiple cell types / co-culture

Hepatocytes activity is dependent on interaction between neighboring hepatocytes and between hepatocytes and ECM, but also on heterotypic interactions between hepatocytes and other cell types occurring in the liver (185-187). Non-parenchymal cells (NPCs) are secreting many diffusible factors which can affect the hepatocytes. Numerous studies originally initiated in 1983 by Guguen-Guillouzo et al. (187) have shown that in both 2D and 3D formats, co-cultivation of hepatocytes with other cells, including liver derived cells like liver biliary epithelial cells and NPCs as well as non–liver-derived cells, can support hepatocyte activity (188, 189).

The largest groups of NPCs in the liver are ECs. ECs in the liver are forming a vascular endothelium, which is not only a physical barrier, but also contributes to different physiological and pathological processes. The importance of the endothelial cells can be observed both in the liver growth and in the adult organ (153, 186, 190). Moreover, ECs are implicated in most liver diseases and are very interesting object for liver toxicity testing (191). In view of these facts, the presence of hepatocytes and ECs with their fenestrations is one of the main requirements for successful liver tissue engineering (192). Previous *in vitro* cell culture experiments have shown that co-culturing of hepatocytes with ECs can lead to stabilization of the hepatocyte phenotype and functions for extended periods of time (185, 192). Enhanced production of albumin and synthesis of urea (193-196) as well as improved drug biotransformation (193) were noted. Production of different cytochromes like CYP3A4 or CYP450 enzymes, that oxidize xenobiotics and pharmaceuticals was found to increase (197, 198). The enhanced ability of co-cultured hepatocytes to transcribe different liver specific genes was also clearly demonstrated (193, 199). Moreover, hepatocytes supported by endothelial cells maintained a differentiated shape (195) and established a functional apical and basal polarization (200). The functional structure of the bile canaliculi, expressed by claudin-3, a tight junction protein, was actively formed and maintained in the stratified co-culture (193). In contrast to other NPCs, ECs were also shown to induce the hepatic expression of low-density lipoprotein (LDL-R) and epidermal growth factor (EGF-R) receptors (201), which expression is one of a major function of hepatocytes *in vivo*.

In addition, the interaction between ECs and hepatocytes has been shown to be reciprocal in improving the survival and keeping of phenotype of the ECs. The co-cultured hepatocytes secrete growth-promoting substances that stimulate *in vitro* endothelial cell proliferation (202). Short-range soluble signals coming from a relatively stable hepatocellular model are able to prolong survival and the expression of LSEC phenotypic markers (203). Furthermore, recent studies have shown that addition of a third cell type, like mesenchymal cells or fibroblast can further stabilize hepatic and endothelial phenotypes *in vitro* (197, 204, 205).

Mimicking in vivo architectures

Despite simple co-cultures can perform better than monocultures, approaches based on randomly distributed various cell types do not represent the specific anatomical relationship between cells. Different parameters important for organotypic interactions, like neighborhood relations and corresponding distances between different cell types are not controlled in such random co-cultures (154). This can led to ineffective or abnormal cell interactions and consequently to unreliable functioning of the cells (154). However, much progress has been made in recent years on cell positioning techniques (please see section 1.3.3). Novel *in vitro* approaches allow for controlled modulation of homotypic and heterotypic cell-cell interactions resulting in enhanced culture systems with better predictive power (154).

To first micropattern liver cells Bhatia et al. adapted a technique from the semiconductor industry (206). Rat hepatocytes were localized on collagen-coated circular domains and then surrounded with 3T3-J2 murine embryonic fibroblasts. This technique, also known as micropatterned co-cultures (MPCCs) allowed tuning of homotypic and heterotypic interactions between cells while keeping cell numbers/ratios constant across the various patterned configurations (Fig. 1.13 (a)). Overall, several key findings regarding importance of both type of cell interactions in tissue function emerged from these pioneering studies (207). Later, human MPCCs were miniaturized into a multiwell format (208) and from this moment have exemplified utility in many applications. This platform has been used to study basic mechanisms underlying hepatocyte-stromal co-cultures, drug metabolism and toxicity, and most recently, the life cycle of HCV and human Plasmodium pathogens (167, 209). The MPCCS were also used to study the functionality of micropatterned co-culture of hepatocytes with liver NPCs (205, 210).

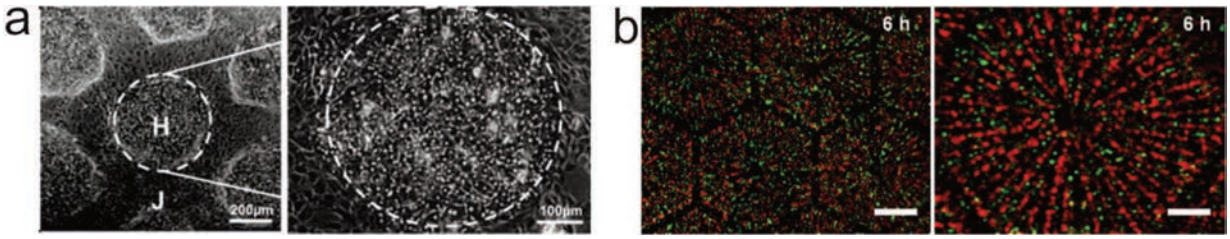

Figure 1.13: Micropatterned liver models: (a) primary human hepatocytes organized into 2D islands and surrounded by fibroblast using micropatterned co - culture (MPCC) technique (209) and hepatocytes (red) and endothelial cells (green) mimicking the morphology of liver lobule using dielectrophoresis (DEP)-based patterning method (131).

Micropatterned hepatocyte co-cultures were also successfully generated using many different methods like piezoelectric printing (211), patterning of synthetic polymers on polyelectrolyte multilayer surfaces (212), using PDMS membrane-based micropatterning technique (213), by application of photosensitive (214) and thermoresponsive polymers (215) or without scaffold surface patterning using dielectrophoresis (DEP)-based patterning method (216). Through DEP manipulation the original randomly distributed hepatic and endothelial cells were manipulated separately and aligned into the desired pattern (Fig. 1.13 (b)) that mimic the morphology of the

liver lobule (131, 217). However, this design enables only 2D structure, while organotypic perfusion is not feasible. Thus, more sophisticated method for mimicking *in vivo* tissue architectures are desirable. More recently, M. Busche et al. have developed HepaChip microplate, a microfluidic platform with continuous, unidirectional perfusion, where cells are selectively assembles into elongated micro-tissues using an automated DEP process (218). Despite a big step forward, one of the biggest inherent drawbacks of this method is requirement relating to the use of specialized equipment and devices during the preparation and application of this system.

Microfluidic

Basic cell cultures with monolayer designs offer benefits of relatively straightforward construction and control of mass transfer resistances. However, as the level of cell culture complexity increase, new requirements for maintenance of hepatic functionality occur (219).

Nutrient and oxygen supply in liver tissue with high cellular density is possible by the full vascularization of this organ (150). Molecules such as oxygen, nutrients or hormones are introduced and removed along with the flow of blood, which produce molecular gradients and modulate the hepatocyte phenotype in zones from the portal triad to the central vein. Besides, a network of sinusoidal capillaries transports blood to all surfaces of the lobules (150). Moreover, oxygen consumption in liver is notably high. Under normal physiologic conditions liver consumes 20–30% of total oxygen used by the body, while hepatocytes themselves consume oxygen at 10- to 100-fold the rates of most cells (219). Therefore, as hepatocytes are extremely metabolic and their functions are closely related to oxygen supply, there exists an enormous need to provide appropriate oxygen delivery in hepatocyte culture *in vitro* (219, 220). In cell culture medium, oxygen is depleted very quickly compared to other key nutrients. Thus, cells must be located within relatively short distance from an oxygen support source. Since for liver the oxygen gradient across a layer of 5 cell diameters (approximately 120 μm) ranges from normoxic to hypoxic (219), the appropriate oxygen tension in 3D cell culture is particularly significant. Therefore, to improve nutrients and oxygen delivery, while allowing dilution or removal of toxic metabolites, *in vitro* culture systems enabling continuous perfusion with culture medium were designed (219). Although so far no ideal microfluidic platform has been developed for fully mimicking hepatocyte microenvironment, perfused systems have proven advantageous over standard static hepatocyte culture (220, 221). Such systems are able to improve viability, live span and metabolic activity of cultured hepatocytes (154). Application of perfusion for hepatocyte cell culture can also improve control over cellular microenvironment and cell-cell communication. Since one of the important modes of intercellular communication is the release of soluble cyto- and chemo-kines, cell-cell communication in microfluidic environment can be regulated by physicochemical transport processes. In perfused cell culture signaling molecules can better diffuse through the surrounding medium before they bind to receptors (220).

1.4.4 Complex 3D liver models - *state of the art*

The end goal of *in vitro* tissue engineering is development of systems with an *in vivo* like but fully controllable cell environment that enable to manipulate cell-specific measurements from a small number of cells (222). Thus, to create optimal *in vitro* model of the liver, systems with different level of complexity were developed to date by adding into the cell culture system various factors that recreate the physiologic environmental cause of the native liver tissue (Fig. 1.14). Many of this complex organotypic systems successfully capture aspects of microenvironmental stimuli, while the cells cultured in such sophisticated and stabilizing platforms become highly functional (223).

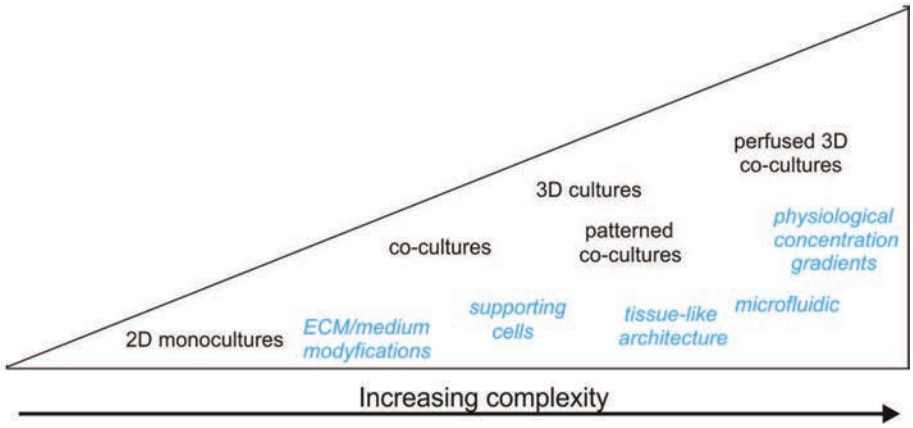

Figure 1.14: Increasing complexity toward liver cell culture models. Example of the systems with increasing level of complexity (black) along with different microenvironmental influences that can be recreated *in vitro* (blue font).

To design a perfused human liver model, several groups have co-cultured hepatocytes as spheroids in perfused system. For instance, Shepers et al. aggregated hepatocytes with 3T3-J2 fibroblasts in pyramidal microwells, encapsulated into small polyethylene glycol (PEG) microtissues and subsequently trapped in a microfluidic device to create perfusable 3D organoids (224). In other approach Rebelo et al. have used dual-step inoculation strategy to form spheroids with an innercore of parenchymal liver tissue with an overlay of stromal cells (Fig. 15 (a)) and subsequently co-cultured the cells in an automated stirred-tank bioreactor environment (224). To more closely mimic the *in vivo* structure of the hepatic cord, Yamada et al. produced cell-incorporating anisotropic hydrogel microfibers, where hepatocytes at the center were closely sandwiched by non-parenchymal cells (225). Such hydrogel fiber-based cultivation enabled heterotypic and homotypic cell-cell interactions but also control the positioning of different cell types with micrometer-scale precision (Fig. 1.15 (b)).
In addition to methods based on cell aggregates that are kept in suspensions, other solutions that allow for advanced co-culture of hepatic cells and incorporate fluid flow across or through the cultured structures are constructs based on microporous membranes and scaffolds. Progress in microtechnology has enabled the development of diverse bioreactors with integrated polymer

scaffolds, where cells self-assemble into an array of 3D microtissue units and were co-cultured under continuous perfusion (226, 227). More recent bioreactor model use modified polyethersulfone (PES) hollow fiber membranes for the creation of a 3D human liver system in static and dynamic conditions (228). Three different cell types were seeded sequentially on hollow fiber membranes (HF) in order to mimic the layers of cells found in vivo (Fig. 1.15 (c)). Cells co-cultured within this membrane system have shown complex cytoarchitecture with the presence of tubelike structure formed by sinusoidal endothelial cells.

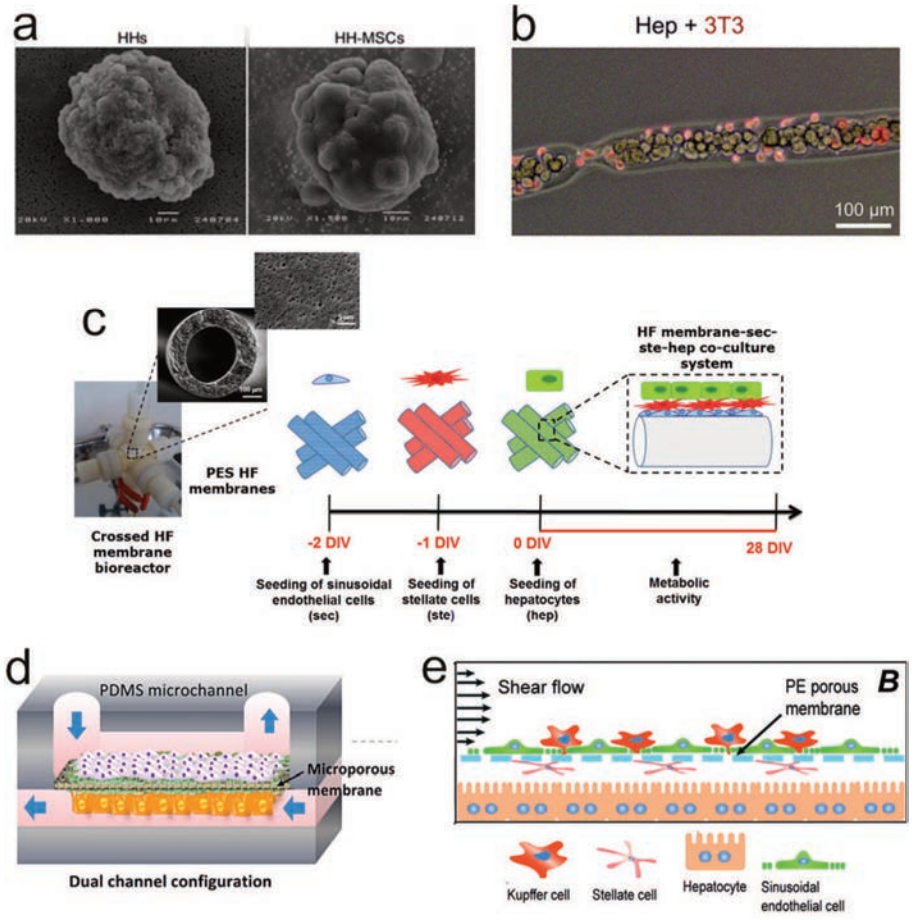

Figure 1.15: Complex liver platforms : (a) primary hepatocytes (HHs) and mesenchymal cells (MSCs) co-cultured as spheroids in bioreactors with perfusion (224), (b) rat hepatocytes encapsulated in microfibers with incorporating nonparenchymal cells (stained with red dye) (225) , (c) bioreactor system with cells co-cultured sequentially on hollow fiber membranes (228), (d) microfluidic platform with dual channel configurations for co-culturing of liver cells in layered configuration (229) and (e) four types of hepatic cells distributed layer-by-layer on two adjacent fluid channels separated by a permeable membrane (230).

Recently, a variety of microfluidic devices with integrated polymer membranes have been reported (231, 232). Application of such microporous membrane enabled co-culturing of parenchymal and non-parenchymal liver cells without direct cell-cell contact. For instance, Salerno et al. explored the capacity to develop a liver tissue construct by indirect co-culturing three different cell types in

a compartmentalized gas permeable membrane bioreactor. Such bioreactor consists of two flat-sheet gas permeable FEP membranes those are separated by a PC microporous membrane. Thus authors established two different compartments, in which cells are co-cultured in adhesion to the membranes within highly perfused and homogeneous microenvironment allowing an adequate O_2/CO_2 mass transfer (231). In another study Li. Et al. demonstrated three layered microfluidic device primarily made of glass with separated flow channels for the sinusoid and the hepatic compartment (232). Using a porous PET membrane vascular channel was separated from the hepatic channel, allowing for communication between channels and in consequence recapitulating the 3D structure of the liver acinus.

To generate complex models with liver's key structures and configurations Kang et al. have designed microfluidically-supported biochip that features a suspended and perfusable membrane (229). Primary hepatocytes and endothelial cells were co-cultured in a dual-channel configuration system with continuous perfusion, in which two microchannels simulate the blood sinusoid and a lower channel for the removal of the secreted factors from hepatocytes (Fig. 1.15 (d)). Lately, Du et al. (230) developed a 3D-configured *in vitro* liver sinusoid chip by integrating the four types of primary murine hepatic cells into two adjacent fluid channels separated by a permeable PE membrane (Fig. 1.15 (e)), while in similar approaches Rennert et al. co-cultured all major liver cell types in a biochip that features perusable PET membrane (233).

Despite remarkable and sustained progress in the development of the liver platforms in recent years, great challenges still remain. One of the biggest inherent drawbacks of available systems is their variability and high production cost (222). Moreover, existing models combine only selected aspects that constitute *in vivo* cellular environment of the liver. More complex systems that recreate different aspects of the hepatic lobule in a single unit are still missing. Thus, the continued evolution of *in vitro* liver platforms and the development of high-throughput production methods are critical for creation of well-defined models with arrayed structures and physicochemically directed cell culture environment that allow for repetitive screens and reliable acquisition of the results (223).

1.5 Account of available cell culture systems and techniques

According to the specific scientific task a family of static cell culture systems as well as microfluidic bioreactor systems for complex cell cultivation has been developed in our group. This section shows some previously established approaches that will be adopted in the different chapters of this thesis.

MatriGrid®

The central elements of our systems are the microstructured polymeric scaffolds that provide support for 3D cell culture. For advanced cultivation of hepatocytes scaffolds termed MatriGrid® were developed. Each MatriGrid® scaffold consists of 187 microcavities that carry the cells and allow for 3D aggregation (Fig. 1.16 (a)). The active seeding area of the MatriGrid® may be in the form of a square with an area of approx. 4.6 x 4.6 mm^2 or in the form of a circle with a diameter of 4.9 mm. To avoid 2D/3D mixed cultures the horizontal surfaces are reduced to a minimum by

hexagonal alignment of the single cavities. The minimal distance between two cavities is lower than 35 µm, while the dimensions of one microcavity are 300 µm in diameter and 270 µm in depth. MatriGrids® were produced in the microthermoforming process from heavy ion beamed PC-foil with a fluence of 10^6 pores per cm^2 and a single pore diameter of 1.3 µm. To avoid pressure loss during the thermoforming process 50 µm thick microporous PC foils were laminated with the 6 µm thick non-porous PC foil. Thus, the pores were temporarily blocked during the microstructuring process. In the microcavities the foils were stretched and the thickness of the foils was reduced, while between the cavities thickness of the foils was almost maintained. To provide optimal perfusion of the cultured cells, the microstructured scaffolds were subsequently etched in NaOH and developed to a pore diameter of 2–4 µm. Moreover, using the appropriate etching time, the selectivly stretched unporous foil was dissolved in the area of convex microcavities, while between the cavities a very thin unporous layer remained undissolved. As a consequence, scaffolds with limited porous regions within the microstructures were produced.

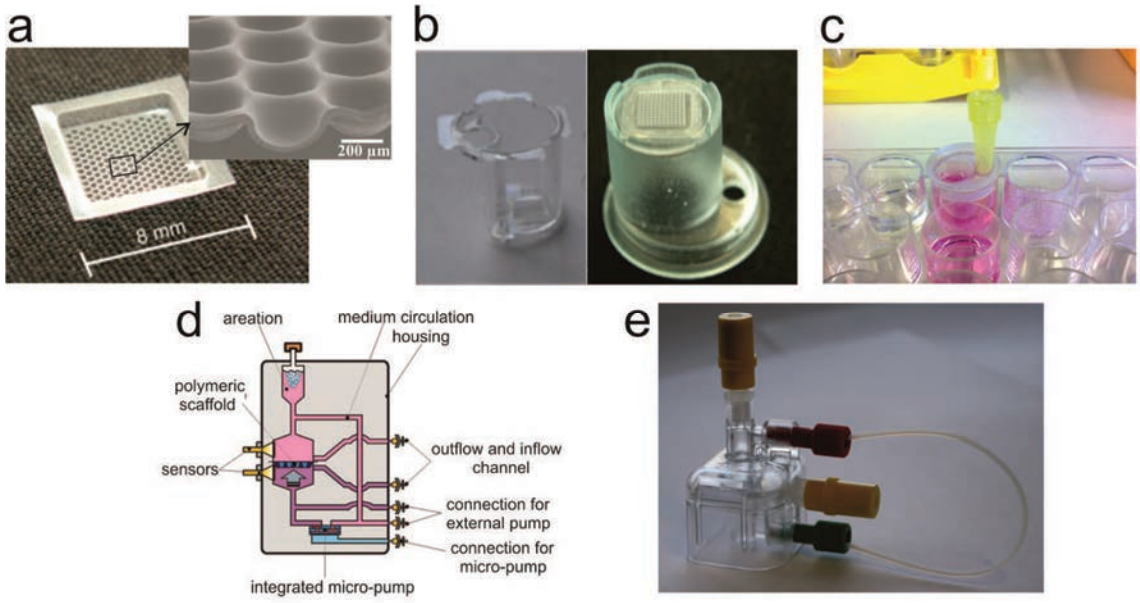

Figure 1.16: Approaches for complex cell culturing developed at the Department of Nanobiosystem Technology in Ilmenau University of Technology: microstructured PC scaffold (MatriGrid) (a), insert system for static 3D cell culture (b), application of insert system inside standard MTP (c), schematic illustration of bioreactor system (d) and an example bioreactor designed for cultivation of hepatocytes (e).

Insert systems

In order to adapt MatriGrid® scaffold for static or partially active cell cultivation in conventional microtiter plates, our group has developed a simple holding system, which we called insert (234). Using this system (Fig. 1.16 (b)), microporous scaffolds such as MatriGrid® can be stabilized and fixed within the wells of the MTP. Scaffolds fixed at the bottom of inserts are positioned to hang in the well. Thus, cultured cells can access media from both sides of the scaffold. The inserts are made of FDA-certified biocompatible PC components that are autoclavable at 120°C and show a

stable behavior to cell culture medium and ethanol. Round opening enables addition and the rapid removal of media using standard pipette tips without moving or shifting of the inserts. As a consequence, medium level can be easy adjusted without damage to the cultured cells. Scaffolds can be stabilized within the system using biocompatible UV adhesive or ultrasonic welding. Insert systems can be used in a wide variety of applications including 3D culturing of single cell type or co-culturing of cells on both sides of the integrated scaffolds or membranes.

Bioreactor

In the context of tissue engineering the term "bioreactor" is used to describe approaches that involves a designed or programmed fluid flow as an integral part of the culture format (219). Many different bioreactor formats have been developed or adapted for liver tissue engineering over the past four decades (235). Our systems are based on a concept published by the Karlsruhe Institute of Technology (236). However, the currently used bioreactor (Fig. 1.16 (e)) is strongly modified and miniaturized. The bioreactor houses the microstructured scaffold such as MatriGrid® and is assembled by two chambers made of FDA-certified PC (Fig.1.16 (e)). Both units are equipped with an in- and out-flow channel to simplify medium exchange and probe extraction (12). Media circulation and cell perfusion is achieved by active pumping in the bioreactor system, which can be operated with an external peristaltic pump connected to the housing.

1.6 Our concept for the complex *in vitro* liver model

In response to the growing demand for complex and well reproducible liver constructs our group has developed a novel concept for a scaffold based multi-layer liver model that include relevant microfluidic for the complex cell culture system. Development of this *in vitro* liver construct is at particular interest with reference to this thesis.

Our model is based on a new concept for replicating 3D liver lobule-like microstructures by microthermoforming of porous polymer foils. According to this concept (237) basic architecture of the liver tissue could be recreated on porous polymer substrate by "feature-transferring-mechanisms"[1] in the microthermoforming process. For this purpose, the structure inspired by basic liver architecture was patterned on a molding tool (Fig. 1.17). The patterned structure comprises abstract hexagonally shaped hepatic lobule, where a central vein is situated at the center. At the outer corners of hepatic lobule is found a Glisson trias. To replicate a larger portion of the liver tissue on one scaffold a seven fold extension of artificial hepatic lobule was patterned on the molding tool in a hexagonal arrangement. Using such molding tool small blood vessels in the form of sinusoids could be replicated on polymer scaffold similar to the *in vivo* counterpart. The master pattern should be replicated from a mold to a polymer sheets during forming process, thereby adapting the microporous polymer foil to the organ morphology.

[1] "feature-transferring-mechanisms": a method for replicating a defined microstructure from a mold to a plastically deformable film. Film is subjected to a temperature and pressure in order to press it into a mold. The mold can comprise formations for pit - like depressions, recesses and/or notches.

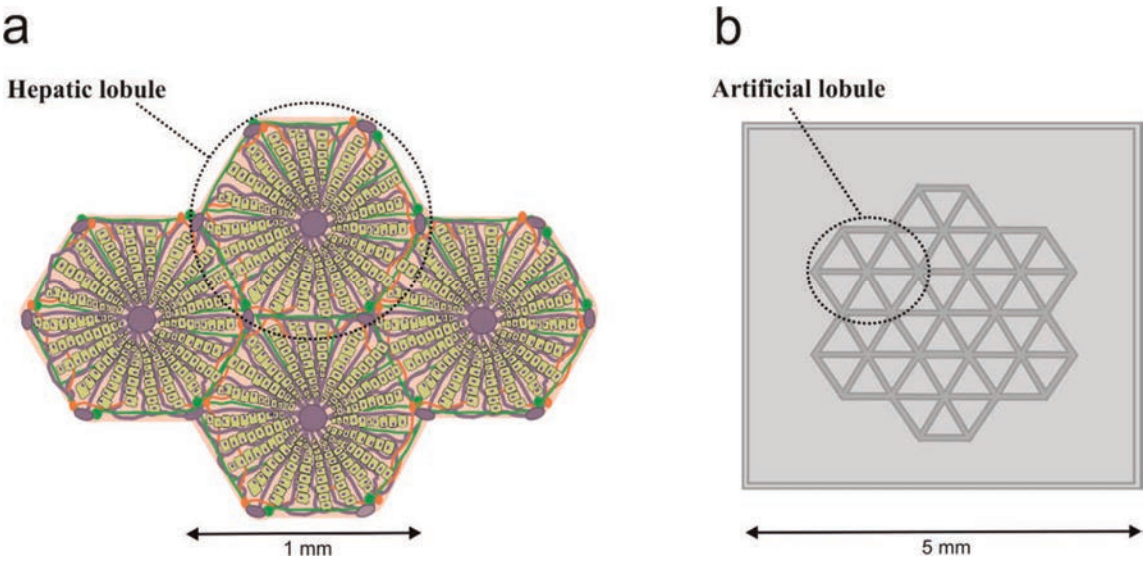

Figure 1.17: Basic structure of a liver lobule (a) and structure patterned on molding tool designed by J. Hampl and F. Weise (b).

With stacking and folding of such patterned scaffolds real three-dimensional constructs can be produced, so a liver tissue can be replicated. To create a stack comprising two layers of the patterned scaffold, two structures with seven artificial hepatic lobules on each should be thermoformed on one polymer sheet and joined together by folding. Pre containing holes at the site location of central vein and Glisson trias can allow the medium flow in the capillaries and back again. Fig. 1.18 shows schematic of such prepared scaffold. The first structure present a sinusoid of the hepatic lobules with the several holes for replicating Glisson trias, while the second structure presents a sinusoid with the holes for replication the central vein. The folding should be done at the folding ridge, which functions here as a film hinge. During folding process the scaffold will be bend at the scaffold hinge by 180°, so that two sides of the scaffold come to lie on each other and form closed sinusoidal channels. In this way, the channels will be brought together at their long sides and form a capillary. The channels will have a shape of a hollow half-cylinder, while the capillary formed should have approximately shape of hollow cylinder.

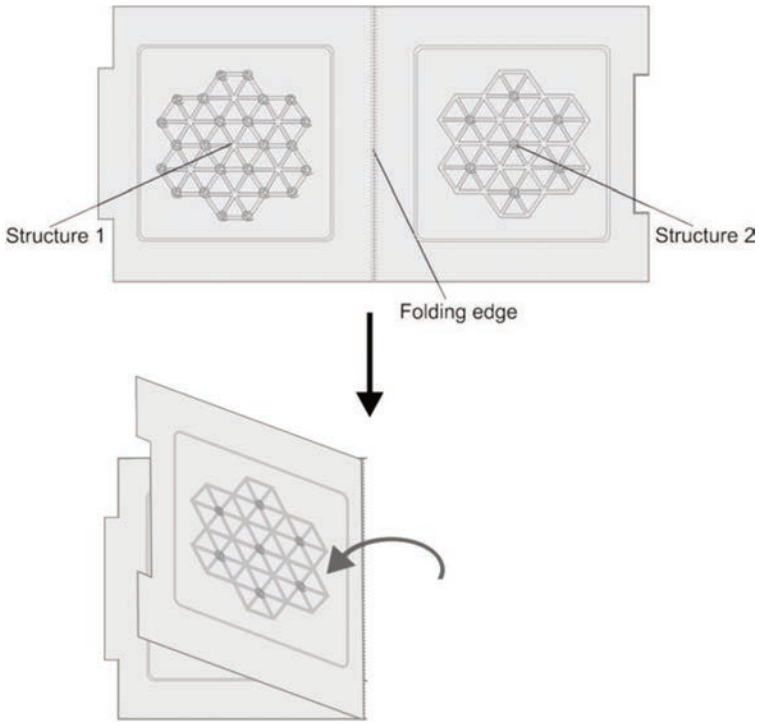

Figure 1.18: Schematic of a micropatterned polymer scaffold with two sinusoidal structures. The structures are joined together by folding at the folding ridge.

Thermoformed scaffolds will form the template for directed co-cultivation of liver cells mimicking microarchitecture of liver tissue. The cells should be arranged on the both sides of the micropatterned scaffold before or after its folding. The endothelial cells should be introduced on the top side of the scaffolds and the cell adhesion should be directed and limited only to the channels (Fig. 19 (a)). Thus, the arrangement of endothelial cells on the microstructured surface should be spatiotemporally controlled. The second type of the cells can be homogeneously distributed onto the bottom side of the scaffold (Fig. 19 (b)). Thus, after folding endothelial cells will colonize inside the capillaries, while hepatocytes will be located on the outer side of the capillaries (Fig. 19 (c)).

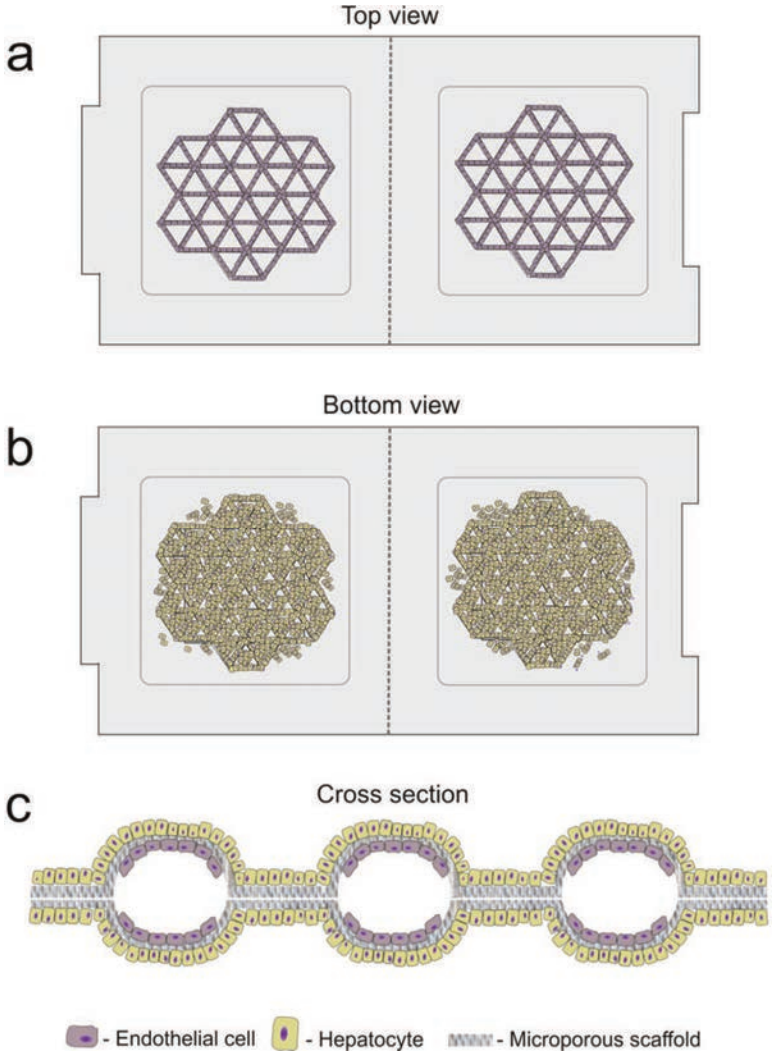

Figure 1.19: Schematic of cell colonization on micropatterned polymer scaffolds. Endothelial cells are cultivated in channels to form hepatic sinusoids (a), while hepatocytes are cultivated on the opposite side to form the hepatic plates (b). After folding two structures with sinusoidal channels are placed face to face forming a capillary (c).

Ideally, the folded scaffolds can be stacked one on top of another and joined together by through holes. Several of the folded scaffolds can be arranged in this way to mimic structured hierarchy of the liver lobules. The opened recesses from each one form should be placed one on top of another, so that they can form a part of the canal, which extends perpendicular to the scaffold. The medium can flow from the canal into the capillaries and back again. Cells would be able to receive medium *via* the capillaries and *via* the canals. Furthermore, biochemical exchange is performed *via* the pores. Such constructs serve for colonization of hepatocytes mimicking liver microarchitecture with capillaries mimicking corresponding vessels, so a liver tissue may be comprehensively replicated.

2. Materials and methods

2.1 Methodology for substrates fabrication

The strategy explained in previous section for fabrication of artificial tissue morphologies on polymer film requires use of various techniques. In the following table we summarize the main devices and techniques used during this research.

Table 2.1: Devices and technics used for scaffold fabrication.

Device	Type	Manufacturer
Spin coater	EMS 5000	Electronic Micro Systems Ltd, Wiltshire
Microthermoforming machine	WLP 1600S	WICKERT Presstech, Landau
Plasma asher	PVA Tepla 200	PVA TePla AG, Wettenberg
Laser ablation apparatus	microSTRUCT C	3D Micromac ,Chemnitz

2.1.1 Fabrication of PLA scaffolds

Polylactic acid (PLA) random stereocopolymer type 4032D Ingeo (P(LLA-co-DLA), 1.40% D-isomer contents, relative solution viscosity 4.00) was purchased from Nature Works LLC (USA). Microporous foils were produced from the PLA granulate according to methods described below.

Salt – leaching method

PLA granulate was first dissolved into a mixture of dioxane (Carl Roth, 4429.1) or chloroform (Carl Roth, 7554.1). The well stirred mixture was warmed up to 60°C to obtain clear solution. Polymer content was varied in the range of 10–20% (w/v). Subsequently ammonium bicarbonate salt particulates (Sigma-Aldrich, A6141) were crashed in mortar, added to the PLA solution and mixed thoroughly with spatula. The weight ratios of PLA and ammonium bicarbonate were 20:10. The solution was poured into a glass plate, uniformly packed, and then dried in a vacuum for 24 h. After the solvent was evaporated, samples were immersed into hot water (90°C) for 5 min and subsequently into cold water (20°C) in the shaker for several days to remove salt. Finally, samples were dried under vacuum for 36 h.

Immersion precipitation

PLA was dissolved into a dioxane (Carl Roth, 4429.1) or chloroform (Carl Roth, 7554.1). Polymer content was varied in the range of 2–10% (w/v). The well stirred mixture was warmed up to 60°C to obtain clear solution. The solution was poured into a glass plate, uniformly packed, and immediately introduced into coagulation bath for 6 h. Different coagulation bath were used: water, ethanol or ethanol-chloroform solutions. Samples were dried under vacuum for 36 h.

Thermally induced phase separation

PLA was dissolved into a mixture of dioxane (Carl Roth, 4429.1) and water. Polymer content was varied in the range of 5–10% (w/v). The volume ratios of dioxane and water were between 86:14 and 90:10. The well stirred mixture was warmed up to 60°C to ensure homogeneity. Subsequently the solution was casted on a polypropylene foil and spin coated at 400 rpm for 30 s. Casted films were quenched by either a liquid nitrogen bath (−196°C), dry ice (−78°C), or freezer (−20°C) and in each case incubated overnight. The solvent was removed by drying in an ice bath under vacuum for 48 h.

Forming of microstructured scaffold from porous PLA foils

The microstructured polymeric scaffolds with 187 microcavities with dimensions of about 300 µm in diameter and 270 µm in depth were created by multilayer microthermoforming the produced PLA-films using a thermoforming mold made from brass. First, PLA microporous foil was inserted into the chamber of the microthermoforming machine. For closing the pores during processing, a 50 µm thick poly-(tetrafluoroethylene-co-hexafluoropropylene) (FEP) foil (DuPont™) was placed underneath PLA film as protection and force transducing layer (Fig.2.1 (b)). Foils were heated to 45°C; the process chamber was completely closed and subsequently evacuated.

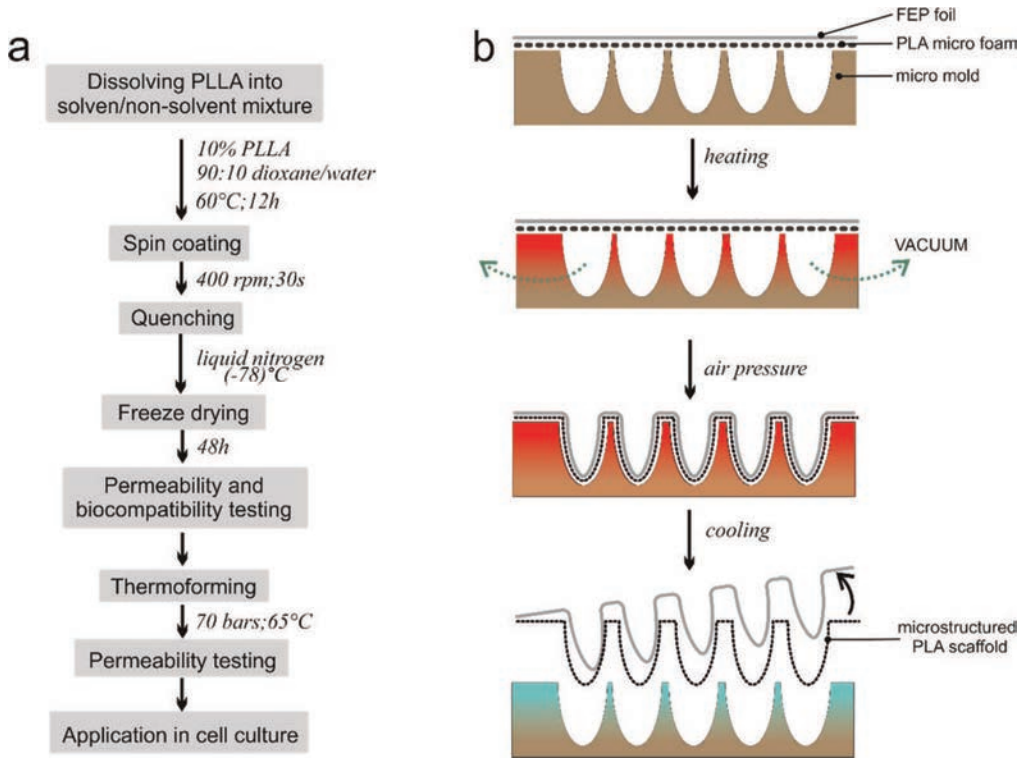

Figure 2.1: Flow diagram for microporous PLA-scaffolds fabrication process (a) and scheme of the thermoforming process of porous foils (b).

Different forming temperatures in the range from 60 to 75°C were tested. The foil was tempered at the selected temperature for 30 s, and a forming pressure in the range from 60 to 75 bar was applied to stretch the foils over the mold. Afterward, the machine was cooled down and vented to atmospheric pressure. FEP foil was removed and the newly formed PLA foil was carefully released from the mold to obtain microstructured PLA scaffold.

2.1.2 Fabrication of PLGA scaffolds

To produce microporous foils applicable for scaffolds fabrication, different PLGA copolymers (Tab. 2.2) were used.

Table 2.2: Properties of different PLGA copolymers used for fabrication of microporous foils.

	PLGA_1	**PLGA_2**	**PLGA_3**
Molecular weight (M_w)	7,000-17,000	24,000-38,000	38,000-54,000
Form	amorphous	amorphous	amorphous
Feed ratio (lactide:glycolide)	50:50	50:50	50:50
Ending of the chain	acid terminated	acid terminated	acid terminated
Degradation time (months)	<3	<3	<3
Transition temperature (°C)	42-46	44-48	46-50
Manufacturer	Sigma-Aldrich, 719897	Sigma-Aldrich, 719870	Sigma-Aldrich, 719900

Foils were produced according to methods described below.

Immersion precipitation

PLGA granulate was first dissolved into a dioxane (Carl Roth, 4429.1) or acetone (Carl Roth, KK40.1). Polymer content was varied in the range of 10-20% (w/v). The well stirred mixture was warmed up to 40°C to obtain clear solution and subsequently casted on a polypropylene foil. Films were spin coated and immediately introduced into coagulation bath for 24 h. Different coagulation bath were used: methanol, ethanol or water. Finally, samples were washed with water and dried under vacuum for 36 h.

Thermally induced phase separation

PLGA was dissolved into a mixture of dioxane (Carl Roth, 4429.1) and water. Polymer content was varied in the range of 10–20% (w/v). The volume ratio of dioxane and water was 90:10. The well stirred mixture was warmed up to 40°C to obtain clear solution. Subsequently the homogeneous solution was casted on a polypropylene foil and spin coated. Casted films were quenched by either a dry ice (−78°C) or freezer (−20°C) and in each case incubated overnight. The solvent was removed by drying in an ice bath under vacuum for 48 h.

Forming of microstructured scaffold from porous PLGA foils

The microporous scaffolds with sinusoidal structures were created by multilayer microthermoforming the produced PLGA-films. A PDMS stamp with features with height of 50 µm and width of 100 µm, mimicking basic structure of liver lobule, was used as a mold for microthermoforming. First, PDMS stamp was placed in contact with the porous PLGA membrane. For closing the pores during processing, a 10 µm thick FEP foil was placed underneath PLGA film. The assembled stack was then inserted into the chamber of the microthermoforming machine and heated to 30°C; the process chamber was completely closed and subsequently evacuated. Different forming temperatures in the range from 36 to 45°C were tested. The foil was tempered at the selected temperature for 30 s, and a forming pressure in the range from 40 to 60 bar to stretch the foils over the mold. Afterward, the machine was cooled down and vented to atmospheric pressure. FEP foil was removed and the newly formed foil was carefully released from the PDMS mold to obtain microstructured PLGA scaffold.

2.1.3 Fabrication of patterned PC scaffolds

2.1.3.1 Fabrication of PC scaffolds with sinusoidal structures

The microstructured polymeric scaffolds with features mimicking basic structure of liver lobule were created by multilayer microthermoforming the microporous PC-films. Foils were thermoformed using silicon mold and 10 µm thick FEP foil as a protection and force transducing layer. The foils were heated to 100°C; the process chamber was completely closed and subsequently evacuated. At 158°C the foil was tempered for 30 s, and a pressure of 40 bar was applied to stretch the PC membrane into the mold. Afterwards, the machine was cooled down and vented to atmospheric pressure. Finally, the newly formed PC membrane was carefully released from the thermoforming mold and FEP layer to obtain microstructured PC scaffold.

2.1.3.2 Fabrication of PDMS stamps

Stamp masters were produced according to standard photolithographic methods (238). Different photomask were used to obtain stamps with features in the shape of lines (with a width ranging from 30 to 400 µm, height from 30 to 75 µm and 400 µm in spacing) as well as stamps with features mimicking basic structure of liver lobule (65 µm in height and 100 µm or 200 µm in widths). PDMS polymer mixture (Sylgard 184, Dow Corning, US, 1:10 ratio of curing agent to prepolymer) was vigorously stirred and degassed in vacuum. To produce PDMS replicas uncured mixture was poured over the whole wafer and subsequently cured on a hot plate (70°C, 30 min). After 24 h at RT, PDMS was peeled off from the master mold, and the required areas were extracted by cutting. The thickness of the stamps was about 2 mm. Finally, the stamps were heat-treated for 1 h at 200°C to outgas the moisture and remaining monomers and reduce shrinkage during the thermoforming process. Stamps were designed in cooperation with J. Hampl, Department of Nanobiosystem Technology, TU Ilmenau.

2.1.3.3 Patterning of the thermoformed scaffolds

2D microcontact printing (2D µCP)

The PDMS stamp was first treated (150 W, 120 s) with oxygen plasma to achieve hydrophilicity. Subsequently, an oxidized stamp was inked with collagen type I (Sigma-Aldrich, C3867). Thus stamp was immersed in collagen solution diluted in distilled water to a concentration of 200 µg/ml. After 1 h stamp was removed from the solution and blow dried with pressurized purified nitrogen gas. The inked stamp was placed in conformal contact with 2D PC foil and pressed to the foil surface, leaving the biomolecules only on the regions defined by the raised structures of the stamp (Fig. 2.2 (a)). After 30 min the stamp was gently peeled off from the substrates followed by washing with distilled water three times.

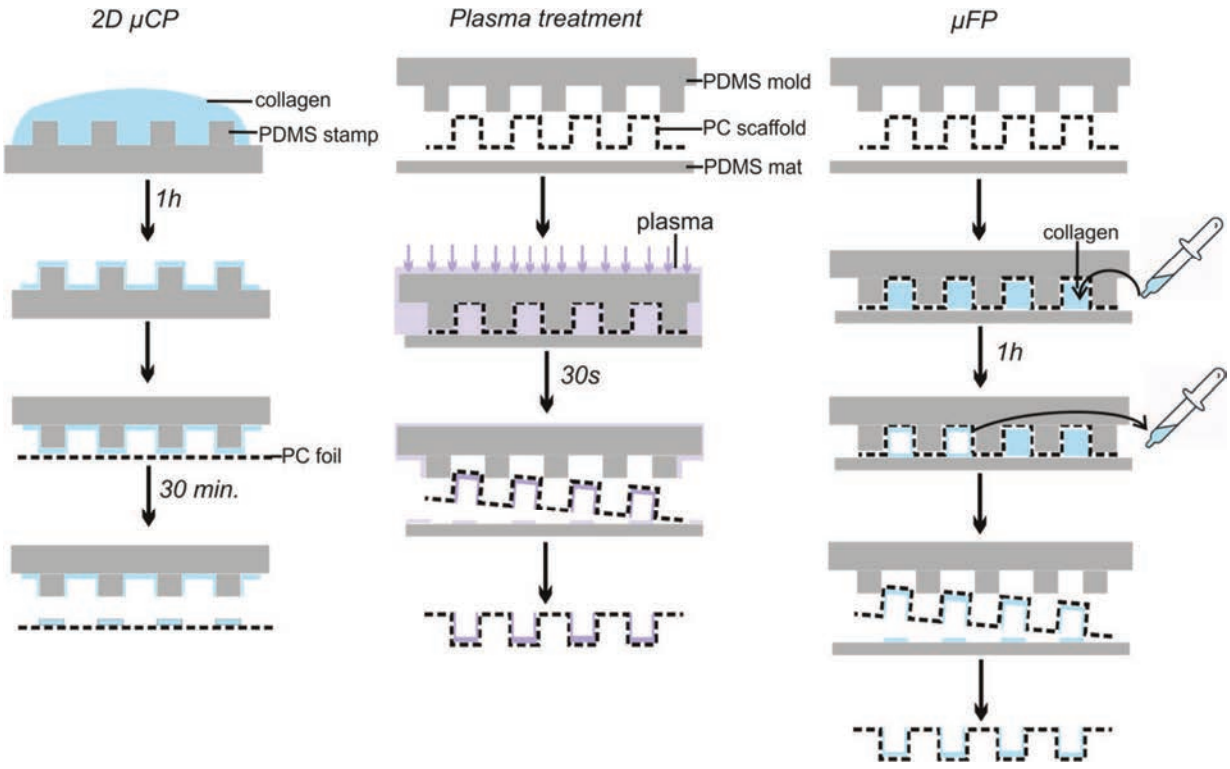

Figure 2.2: Schematic outline of patterning procedures for regional modification of the PC surface that promotes cell adhesion. 2D microcontact printing (2D µCP), plasma treatment and microfluidic printing (µFP) methods were used to promote cell adhesion.

Plasma treatment

Plasma lithography method was used for selective modification of the PC scaffold by shielding the contact of low-temperature plasma with polymer surface using PDMS mold. This selective shielding leaves a chemical pattern, which can guide cell attachment. To achieve micropatterned structures on 2D PC foils a PDMS stamp was turned upside down such that the features were facing down and gently placed onto PC foil. To ensure good contact between the stamp and the PC

surface, the stamp was shortly pressed down using tweezers. The assembly was placed into the plasma chamber. Samples were treated with oxygen plasma under different power and treatment time to achieve hydrophilicity suitable for cell adhering. The plasma modification was studied with contact angle measurements. For patterning of 3D scaffolds, samples were turned upside down and placed onto PDMS mat (Fig. 2.2 (b)). Additionally, PDMS mold with the same microstructure was placed on the top of the scaffold, forming a network of channels. Plasma was introduced to the scaffold surface through the holes cut at the end of each channel.

Microfluidic printing (µFP)

PC scaffolds were turned upside down and gently placed onto PDMS mat. Additionally, PDMS mold with the same microstructure was placed on the top of the scaffold (Fig. 2.2 (c)). The elastomer mold and scaffold made conformal contact with the PDMS mat, forming a network of channels. A collagen solution was gently introduced from one of the open ends of the elastomeric mold to avoid any air gap. Collagen was driven by capillary forces and moved into the microchannels. Scaffold was left for 1 h at room temperature on the PDMS substrate so that the collagen in the fluid was allowed to adsorb onto the surface of the channels. Afterwards collagen solution was removed from the channels using pipette, scaffolds were separated from the PDMS mold and washed with distilled water.

Inverted µCP with Pluronic®

Pluronic® (Sigma-Aldrich, P2443) was first dissolved into PBS. Polymer content was varied in the range of 0.5–10 g/l. Simultaneously PDMS mat was treated (150 W, 120 s) with oxygen plasma to achieve hydrophilicity. Once the Pluronic® was completely dissolved, the plasma-activated PDMS mats were immersed into prepared solution, functionalized for 30 min and subsequently dried with nitrogen gas. For the inverted µCP on 2D surface, PDMS mat was gently placed onto selected area of PC foils. After 30 min of incubation mat was removed and replaced with another PDMS mat prepared in the same way.
For the patterning of PC scaffolds, samples were turned upside down and gently placed onto PDMS mat such that the surface between the channels made conformal contact with the PDMS (Fig. 2.3). After 30 min of incubation scaffolds were removed and placed onto another mat prepared in the same way. To ensure good transfer of Pluronic® from PDMS onto PC surface, µCP process was repeated five times.

Inverted µCP with Agarose

Agarose gel (Carl Roth, 9012-36-6) was first dissolved in distilled water to prepare solution with concentration of 1 g/l. This mixture was heated in the microwave until the agarose was completely dissolved. Subsequently a thin layer of agarose solution was spread on a coverslip. PC scaffolds were turned upside down and gently placed on the coverslip. After a few seconds scaffolds were peeled off and left to dry.

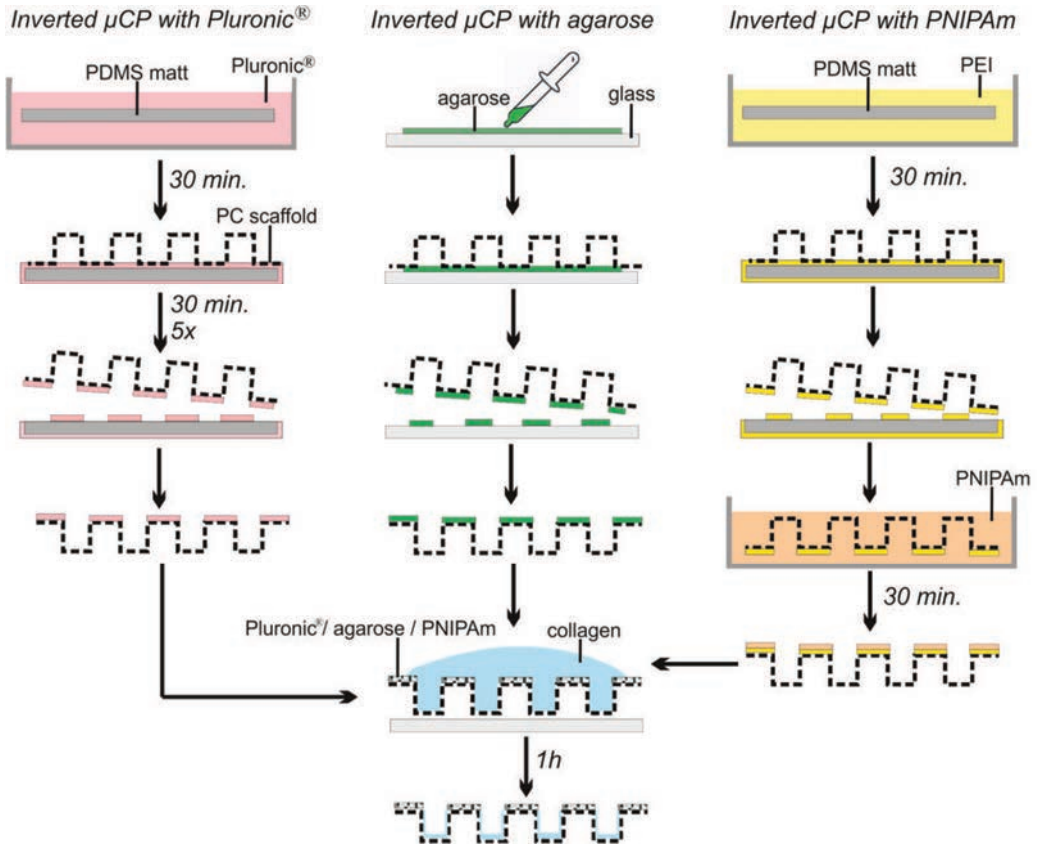

Figure 2.3: Schematic of the inverted µCP methods with three different cell repellent materials. Nonadhesive domains were patterned on the surface to block the adsorption of proteins and cells. Subsequently scaffolds were coated with collagen to promote cell adhesion on the nonprinted regions.

Inverted µCP with PNIPAm

For the directed coupling of a hydrogel onto the PC scaffold, the PC surface was amino-functionalized in a preceding step. This functionalization was carried out using dry chemical method with polyethyleneimine (PEI, Sigma-Aldrich, 408727). First, a PDMS mat was incubated in a PEI solution (1 mg/ml or 10 mg/ml) for at least 30 min and then dried. Thereafter, PC scaffolds were turned upside down and placed on the mat, pressed and incubated for 30 min. Subsequently scaffolds were gently peeled off from the mat and rinsed with distilled water. For coupling of PNIPAm 4 ml of a 1 M solution of N-isopropylacrylamide (Sigma-Aldrich, 731129) was prepared. The solution was purged with nitrogen for 10 min to wash the oxygen from the solution. The amino- functionalized PC scaffolds were immersed into the solution. Subsequently 100 µl of a 0.2 M cerium (IV) ammonium nitrate (J. T. Baker™) solution (dissolved in 1 M sulfuric acid) was added. Scaffolds were incubated into such solution overnight in a sealed container with constant shaking. The next day, samples were rinsed with distilled water and dried. The coupling of the hydrogel was studied with contact angle measurements.

2.1.3.4 3D microcontact printing (3DμCP)

For the selective patterning of ECM molecules, proteins were applied only to the top features of PDMS stamp by inverted μCP. A glass coverslip was covered with collagen type I (Sigma-Aldrich, C3867) diluted to a concentration of 200 μg/ml, laminin (Sigma-Aldrich, L2020) diluted to working concentration of 100 μg/ml or fibronectin (Sigma-Aldrich, F1141) diluted to 50 μg/ml in distilled water. In the meantime, the PDMS stamp was treated (150 W, 120 s) with oxygen plasma to achieve hydrophilicity and to ensure good transfer of proteins from a glass surface to the stamp features. An oxidized stamp was then turned upside down such that the features were facing down and gently placed onto the protein-coated glass. To ensure a good contact of the stamp with the glass surface, the stamp was shortly pressed down using tweezers. After 30 min the stamp was carefully removed and finally used as a mold in the microthermoforming process. Therefore, microstructuring and microcontact printing were performed in one step. First, the patterned face of the PDMS stamp was placed in contact with the PC membrane, while a 50 μm FEP foil was placed underneath the porous foil. The assembled stack was then inserted into the chamber of the microthermoforming machine and heated to 100°C; the process chamber was completely closed and evacuated. At 158°C the foil was tempered for 30 s, and a pressure of 40 bar was applied to stretch the PC membrane over the PDMS mold. Afterward, the machine was cooled down and vented to atmospheric pressure. Finally, the newly formed PC film was carefully released from the PDMS mold and FEP foil to obtain patterned PC scaffold. A flow chart of the patterning procedure is given in figure 2.4.

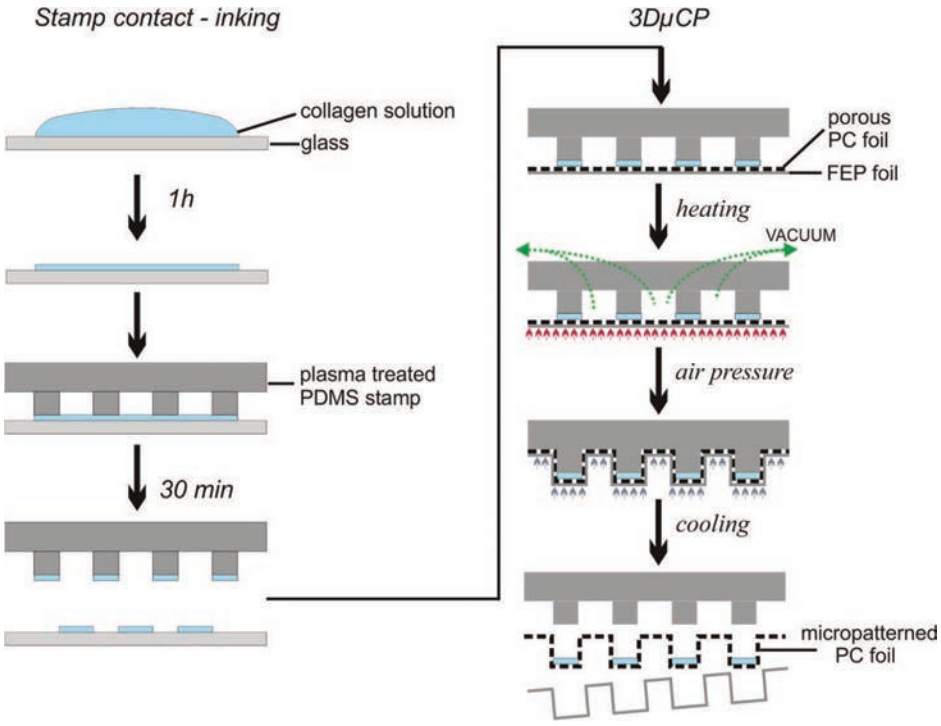

Figure 2.4: Scheme of scaffold fabrication using 3DμCP method.

2.1.3.5 Laser micromachining

The micropatterned scaffolds mimicking the basic structure of liver lobule were fabricated using 3DμCP method described previously. Subsequently, shape of the micropatterned PC scaffolds was adapted to the frame apparatus using a laser micromachining system. Laser micromachining process was prepared and performed by Nam Gutzeit from Department of Electronics Technology at Ilmenau University of Technology. The samples were cut by the picosecond laser ablation apparatus with power of 1 W, pulse length <10 ps and at a wavelength of 355 nm. Due to the short pulse length, a thermal influence on the surface adjacent to the kerf areas of the film was greatly reduced. Additionally, to allow directed medium flow through the sinusoidal structures, small through holes were created by laser cutting in the areas mimicking central vein and portal tracts. Various types of holes such as round holes, spirals or stars were tested for medium flow and cell growth. The shape and size of the holes was designed in cooperation with J. Hampl.

2.2 Characterization of the scaffolds

2.2.1 Optical inspection and measurements of the thermoformed scaffolds

For detailed optical inspection of the fabricated scaffolds scanning electron microscope (SEM) and laser scanning digital microscope (LSM) were utilized. First, samples were sputter-coated with platinum and imaged using SEM (Hitachi S 4800).
To evaluate the patterned microstructures part of the samples was additionally imaged and measured using LSM (Olympus LEXT OLS4100). The LSM images were analyzed to measure the widths and depths of thermoformed structures. All obtained data were expressed as mean ± standard deviation of measurements from three independent samples and at least three channels in each sample.

2.2.2 Mechanical testing

The tensile strength of the samples was measured using a universal testing machine (Instron 33R4467) with a 100 N load cell and crosshead speed of 10 mm/min. For tensile testing of microporous PLA and PC films, rectangular samples (0.05 mm thickness and 10 mm width) of were used. The gauge length was 120 mm. The elastic modulus was calculated from the initial part of the slope from stress–strain curves. For testing of microstructured PLA samples during degradation test, PLA scaffolds with 10 mm width were used. The gauge length was 40 mm. Extension at a break and tensile strength of the samples was evaluated. At least five test samples were tested for each material and the average values are presented. Tests were performed by Robert Albrecht from Faculty of Mechanical Engineering, TU Ilmenau.

2.2.3 Permeability and porosity testing

Permeability was measured by the determination of fluidic resistance in a device which detected pressure difference between two sides of the membrane under air flow. Permeability under medium flow was calculated using Darcy's law. Pore size distribution, total pore volume and surface area of the scaffolds were determined by mercury intrusion porosimetry (Pascal 140 / Pascal 440, Porotec). Permeability was measured by the determination of fluidic resistance Δp between two sides of the microporous sample. All measurements were made in a device that detected the pressure difference under air flow with a flow rate of 25 µl/min. Next, the theoretical permeability under medium flow was calculated using the equations presented below.

As part of the proportionality constant in Darcy's law, permeability can be expressed by the following equation:

$$k = \frac{q\,\eta\,l}{\Delta p\,A} \quad \text{(eq.1)}$$

After transforming equation 1 to:

$$\Delta p = \frac{q\,\eta\,l}{A\,k} \quad \text{(eq.2)}$$

fluidic resistance under air flow Δp_a and under medium flow Δp_m can be expressed by:

$$\Delta p_a = \frac{q_a \eta_a\, l}{A\,k} \quad (\text{eq. 3}) \; ; \qquad \Delta p_m = \frac{q_m \eta_m\, l}{A\,k} \quad (\text{eq. 4}),$$

therefore

$$\Delta p_m = \frac{\Delta p_a q_m \eta_m}{q_a \eta_a} \quad \text{(eq.5).}$$

Nomenclature:

A	*flow-through area of the porous foil (m^2)*
k	*permeability of a porous foil (m^2)*
l	*thickness of the porous foil (m)*
Δp_a	*pressure difference during the air flow (mbar)*
Δp_m	*pressure difference during the medium flow (mbar)*
q_a	*applied superficial air flow velocity through the porous foil (25 ml/min)*
q_m	*applied superficial medium flow velocity through the porous foil (0.025 ml/min)*
μ_a	*dynamic viscosity of the air (0.0181 mPa·s)*
μ_m	*dynamic viscosity of the medium (1 mPa·s).*

The value of the flow rate used for the calculation was 0.025 ml/min and it was compatible with the medium flow occurring in our bioreactor during perfusion of cell cultures.

Porosity, pore size distribution, total pore volume and surface area of the scaffolds were determined by mercury intrusion porosimetry (Pascal 140/Pascal 440, Porotec). Measurements were performed by Dr. Hans Uhlig from Faculty of Chemistry and Mineralogy, Leipzig University.

2.2.4 Wettability measurement

For pressuring the wettability of the PC scaffold surface drop shape analysis method was used. Samples were examined by measuring the water contact angle with the sessile drop method. Drop dispensed onto PC surface was precisely imaged using a drop shape analyzer (DSA10, KRÜSS GmbH, Hamburg) with a uniform LED lighting unit and optical components. The drop shape was automatically evaluated for the contact angle measurement.

2.2.5 Surface roughness

The membrane surface roughness was characterized by a laser scanning digital microscope (Olympus LEXT OLS4100). The surface roughness was estimated with respect to the mean absolute value difference (R_a). The reported roughness values are the average of measurements on four independent samples and five measurements on each sample. To visualize fabricated PC scaffolds, samples were sputter-coated with platinum. PLA specimens were analyzed without any additional treatment.

2.2.6 ATR-FTIR spectra

Attenuated total reflectance Fourier transform infrared spectroscopy (ATR-FTIR) analysis was performed by Dr. Liliana Liverani from the Institute for Biomaterials at University of Erlangen-Nuremberg. ATR-FTIR measurement was carried out to investigate the presence of collagen on the PC substrate and eventual interaction between them by using a spectrometer (Nicolet 6700, Thermo Scientific, Germany) with 32 scans at resolution of 4 cm^{-1} in the wavenumber range between 4000 and 550 cm^{-1}.

2.2.7 Fluorescent staining of ECM molecules

Patterning of ECM molecules was characterized by fluorescent staining using specific antibodies. Samples were fixed for 30 min with 4% paraformaldehyde and subsequently washed with PBS, followed by 15 min of blocking with 5% BSA/PBS and again PBS washing. After this pretreatment, samples patterned with collagen were incubated for 1 h with a conformation dependent anti-collagen I monoclonal mouse antibody (Abcam, ab6306), diluted 1:50 in 1% BSA/ PBS, washed with PBS, and incubated with a purified Alexa Fluor 555 conjugate goat anti-mouse secondary antibody (Thermo Fisher Scientific, A-21422) diluted 1:200 in 1% BSA/PBS for 1 h. Samples printed with fibronectin were stained according to the same protocol using monoclonal anti-fibronectin antibody produced in mouse (Sigma-Aldrich, F0791) followed by staining with Alexa Fluor 405-conjugated goat anti-mouse secondary antibody (Abcam, ab175661). Samples printed with laminin were labeled using anti-laminin antibody produced in rabbit (Sigma-Aldrich, L9393) followed by staining with Alexa Fluor 488-conjugated goat anti-rabbit secondary antibody (Thermo Fisher Scientific, A11034). All samples were then mounted using Mowiol (Sigma-

Aldrich) and examined using a laser scanning microscope FV1000 (Olympus, Hamburg, Germany).

2.2.8 SDS-PAGE and Coomassie Staining

50 µg of collagen, laminin, and fibronectin were thermoformed and subsequently dissolved in 70 µl of Laemmli buffer without (collagen) or with mercaptoethanol (laminin, fibronectin) for 2 h at RT with gentle shaking. The corresponding native ECM molecules were treated in exactly the same way. All samples were heat-denaturated for 5 min at 95°C. 30 µl of the thermoformed and 15 µg of the native ECM molecules in Laemmli buffer were separated on 6% polyacrylamide gels. Gels were stained with Coomassie brilliant blue according to a common protocol. This experiment was designed, performed and analyzed by Dr. Dana Brauer, Department of Nanobiosystem Technology, TU Ilmenau.

2.3 Methodology for cell culture

Primary liver sinusoidal endothelial cells and primary hepatocytes are considered the most suitable cells to create physiologically relevant *in vitro* liver model. However, primary cells can only be passaged for a limited time, while their use generates high financial costs (192). In contrast, immortalized cell lines such as HepG2 have phenotypic stability as well as unrestricted accessibility and from physiological perspective are relevant to primary hepatocytes (239). Therefore they are widely used as substitute for primary cells in liver tissue engineering. Since our characterization studies of microstructured scaffolds have required a large number of cells and many repetitions of experiments, we have decided to use immortalized cell line (Tab. 2.3). Thus, human hepatocyte carcinoma (HepG2) cell line was used as a surrogate to primary human hepatocytes, and an immortal human umbilical vein cell line (EA.hy926) was used as a surrogate to liver endothelial cells. Additionally, to demonstrate biocompatibility of fabricated scaffolds, the mouse fibroblast cell line L929 was used (according to the ISO 10993-5). Cells were cultivated using different cell culture media and components (Tab. 2.4).

Table 2.3: Cell source.

Cell line	Hepatoma cell line (HepG2)	Mouse fibroblast cell line (L929)	Endothelial-like cell line (EA.hy926)
Resource	ATCC, LGC Prochem, Wesel, Germany	ATCC, LGC Prochem, Wesel, Germany	ATCC, Rockville, MD

Table 2.4: Cell culture media and components used for biological experiments.

	Components and concentrations			Manufacturer
Medium	Minimum Essential Medium (MEM)	RPMI 1640 Medium	Dulbecco's Modified Eagle's Medium (DMEM)	Sigma
FCS	10%	10%	10%	Biochrom
Penicillin	100 U/ml	10 U/ml	1%	Sigma-Aldrich
Streptomycin	100 µg/ml	100 µg/ml	-	Sigma-Aldrich
L-glutamine	1%	1%	2%	Sigma-Aldrich
Sodium pyruvate	-	-	1%	Sigma-Aldrich

2.3.1 Cell cultivation on PLA scaffolds

Preparation and sterilization of PLA samples

Before use in the cell culture all PLA samples were fixed in the insert system previously designed in our group (chapter 1.5). Scaffolds were glued into an insert system using Dymax 1120-M-UR UV adhesive. For this, the scaffold was cut into 8 × 8 mm squares. Subsequently, the UV adhesive was applied thinly around the insert system. First, the curing reaction of the UV adhesive was started for 30 s. After a short break, the adhesive was cured for a further 15 minutes under UV light with a wavelength of 365 nm. Subsequently, the insert system with scaffolds were sterilized using 100% ethanol (Roth) and wetted through a graded ethanol series (75%, 50%, 35%, 0%) to avoid air bubbles between pores. Finally, samples were placed into 24 well MTP.

Biocompatibility of solvent casted PLA foils

25 µl of cell suspension containing 5×10^4 L929 cells was seeded per well. For comparison with standard laboratory equipment, empty wells of MTP were used. A positive control was created by wells containing 2% solutions of 2-hydroxyethyl methacrylate (HEMA, Sigma-Aldrich, 128635). Cells were cultivated for a period of 5 days with daily medium exchange. Total cell numbers and vitality of the cells were calculated. All tests were repeated in quadruplicate.

Cell cultivation on PLA scaffolds— 3D PLA versus 2D MTP versus 3D PC

HepG2 cells were used to demonstrate the principal biological applicability of PLA scaffolds. Growth of cells on PLA scaffolds was compared with that on PC scaffolds (MatriGrid®) used previously in our bioreactor systems (section 1.5). The sterilized and washed scaffolds (3D PC, 3D PLA) were placed in 24 well MTP. To provide interaction sites on polymer matrix with cell surface receptors as well as increases the hydrophilic properties of the polymer surface, all PC scaffolds and half of PLA scaffolds were coated with 10 µg/cm^2 type I collagen. As a control material, empty wells of MTP were used. 25 µl of cell suspension containing 2.5×10^5 cells was

seeded per well. Cells were cultivated for a period of 5 days with daily medium exchange. Vital cell numbers, metabolic activity and albumin secretion rate of HepG2 cells were calculated. Tests were repeated in triplicate. All quantitative data were expressed as mean ± standard deviation. A two-tailed paired Student's t-test was used to compare the differences. A difference with $p < 0.05$ was considered to be statistically significant.

Degradation test

The sterilized and washed samples were placed in 24 well MTP. In order to evaluate the degradation rate of PLA scaffolds in phosphate-buffered saline, samples were fully covered with 1 ml pH 7.4 PBS solution and were placed in the incubator at 37°C. The medium was changed once a week. Scaffolds were stored in such conditions from 4 to 24 weeks (Tab. 2.5). Six PLA samples were removed at each follow-up time (three mechanical test samples and three samples for visual examination with SEM). Simultaneously to determine the degradation rate of PLA scaffolds in cell culture, samples were coated with 10 μg/cm^2 type I collagen. Subsequently 25 μl of cell suspension containing 5×10^4 HepG2 cells was seeded per scaffold. Cells were cultured from 1 to 4 weeks. Six PLA samples were removed at each follow-up time and the cell amount and viability were calculated. Subsequently the samples were used for mechanical testing and for visual examination with SEM. Follow-up times for *in vitro* studies are given in Table 2.5.

Table 2.5: Follow-up times for scaffolds during degradation test under PBS and under cell culture.

Follow up	Weeks							
PBS				4	8	12	16	24
Cell culture	1	2	3	4				

2.3.2 Cell cultivation on PLGA scaffolds

Preparation and sterilization of PLGA samples

All PLGA samples were prepared and sterilized using method described in subsection 2.3.1.

Cell cultivation on PLGA scaffolds

Cell cultivation on PLGA scaffolds was tested with the fibroblast cell line L929 and with the hepatoma cell line HepG2. To achieve cell culture on the both sides of the PLGA samples outer side of the scaffolds was first coated with 25 μl of a collagen type I solution (320 μg/ml) and incubated for 1 h at room temperature (Fig. 2.5). Subsequently the drop was carefully aspirated, the insert system with the scaffold was rotated and inner side of the scaffold was coated with collagen. After 1 h, collagen was carefully aspirated and the insert system was gently rotated. 25 μl of cell suspension containing 1×10^4 L929 cells was seeded on the scaffold. After 2 h of incubation, the insert system was carefully rotated again and 25 μl of cell suspension containing 1×10^4 L929 cells was seeded on the inner side of the scaffold, followed by 2 h of incubation.

Finally, 1 ml of medium was added. To cultivate the HepG2 cells on PLGA scaffolds, samples were seeded according to the same protocol; however, to accelerate the degradation rate of the samples, seeding density of the HepG2 cells was increased to 1×10^5 cells per each scaffold side. Cells were cultured from 1 to 4 weeks. Medium was changed every second day. Three samples were removed at the end of each week and the cell amount and viability were calculated. Subsequently, the samples were used for visual examination with SEM. Test was repeated twice.

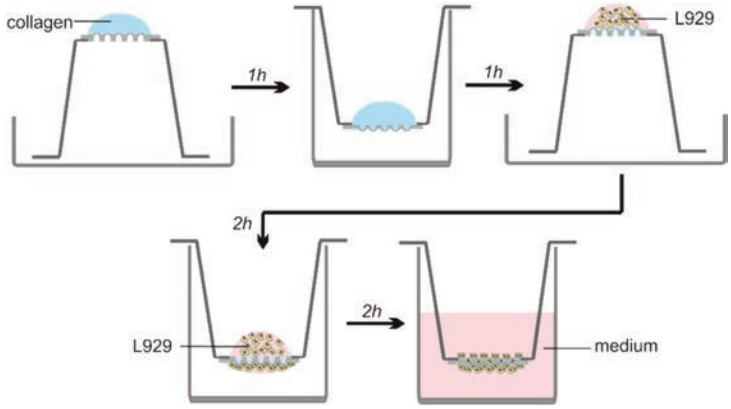

Figure 2.5: Scheme of method used for cell seeding onto both sides of micropatterned scaffold fixed in the insert system.

2.3.3 Cell cultivation on patterned PC substrates

Cell response to the patterned PC surface

All patterned PC scaffolds were placed in 24-well microtiter plates and sterilized with UV treatment in a sterile bench for 15 min. To demonstrate the principal biological applicability of the samples 50 µl of cell suspension containing 1×10^4 EA.hy926 cells, 4×10^4 L929 cells or 2×10^4 HepG2 cells was seeded per substrate. After 2 h, 1 ml of medium was added. The cells were cultured for 24 h. Cell response to the patterned PC surface was observed under the inverted microscope. All tests were repeated in triplicate.

Long-term cell culture on 3DµCP patterned scaffolds

To demonstrate the principal biological applicability of the 3DµCP patterned scaffolds with sinusoidal structures for directed cell adhesion and long-term cell growth, samples were divided into 2 separate parts with one sinusoidal structure on each one and seeded with EA.hy926 cells. 50 µl of cell suspensions containing different number of cells in the range of 0.5×10^4 to 1×10^5 was seeded per substrate. After 2 h, 1 ml of medium was added. The cells were cultured for 10 days. Medium was changed every day. Morphological changes in cells and their migration were monitored daily using SEM and LSM. All tests were repeated in triplicate.

2.3.4 Cells co-culture on micropatterned PC scaffolds with sinusoidal structures

The micropatterned PC scaffolds were placed in a sterile bench and sterilized with UV treatment for 15 min. Subsequently, scaffolds were placed in specially designed frame equipment, which enables precise positioning of the two associated sinusoidal half-structures to each other (Fig. 2.6). Samples were carefully adapted to the shape of the frames by cutting with a laser. Before use the frame equipment was sterilized in 70% ethanol for 15 min.

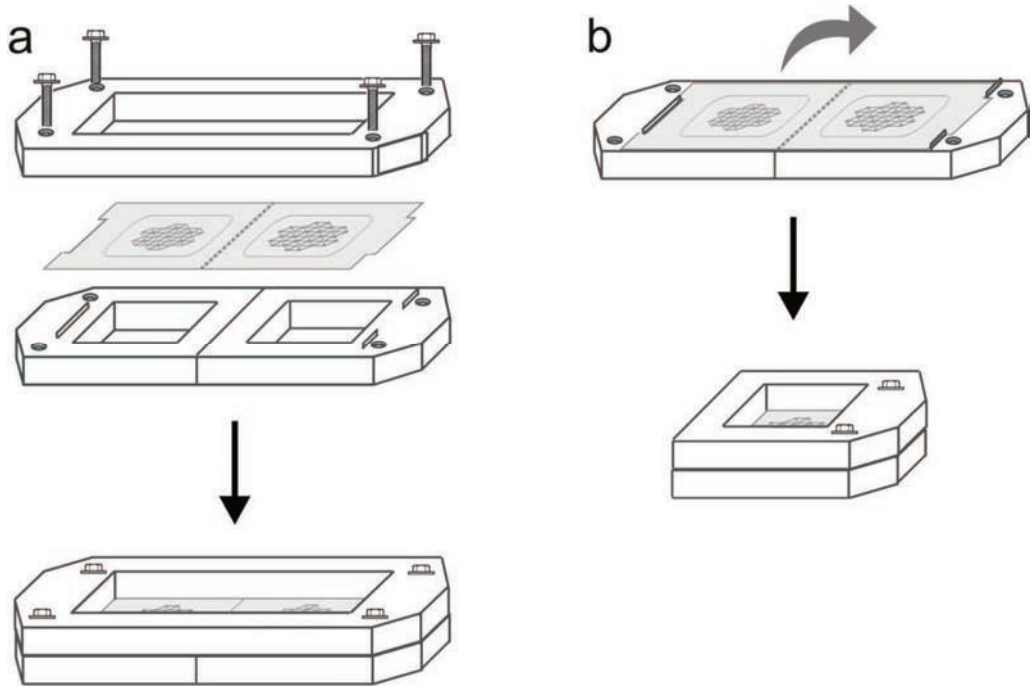

Figure 2.6: Scheme of scaffold stabilization in the frame apparatus. For cell seeding approaches scaffolds were placed in a folding part of the frame apparatus und subsequently fixed from above with the second part of the device (a). For further cell culture experiments the cover of the apparatus was removed and the folding part was folded so that the two associated sinusoidal half-structures were joined together (b).The frame apparatus was designed by J. Hampl from Department of Nanobiosystem Technology at Ilmenau University of Technology (229).

Samples were fixed from above with the second part of the device, placed in a 6-well multiwell plate and colonized with cells using one of the following methods:

Method 1:

25 µL of cell suspension containing 1×10^4 EA.hy926 cells was seeded per inner side of each of the sinusoidal half-structure. The plate was incubated for a 2 h at 37°C and 5% CO_2 to allow the cells to settle into the channels. Subsequently 100 µl of medium was added over the surface of each half-structure. Plates were re-incubated and maintained for further 2 days by medium exchange after 24 h. After 2 days, medium was carefully aspirated and the frame apparatus with scaffolds was gently rotated. The outer side of the scaffolds was coated with 25 µl of a collagen type I solution (320 µg/ml) and incubated for 1 h in the incubator. Subsequently, the residual

solution was carefully aspirated and 50 µl of cell suspension containing 2.5×10^5 HepG2 cells was seeded per each of the half structure, followed by 1 h of incubation. Finally, 5 ml of medium was added from the bottom and above of the scaffolds and plates were placed in an incubator for 24 h.

Method 2:

The outer side of each of the sinusoidal half-structure was first coated with 25 µl of a collagen type I solution (320 µg/ml) and incubated for 1 h at RT. Then the solution was carefully aspirated and the scaffolds were colonized with EA.hy926 cells. For this purpose the frame apparatus with the scaffolds was rotated and 50 µl of cell suspension containing 1×10^4 cells was seeded per inner side of each of the half-structure. After 3 h of incubation, the frame apparatus with scaffolds was carefully rotated again and gently immersed in 3 mL of DMEM so that no air bubbles collect under the scaffold surface. EA.hy926 cells were in contact with medium, while the outer side of the scaffolds stayed dry. Subsequently 50 µl of cell suspension containing 2.5×10^5, 1.5×10^5 or 1×10^5 HepG2 cells was seeded on the outer side of the half structure, followed by 1 h of incubation. Finally, 2 ml of medium was added and cells were co-cultured for 24 h.

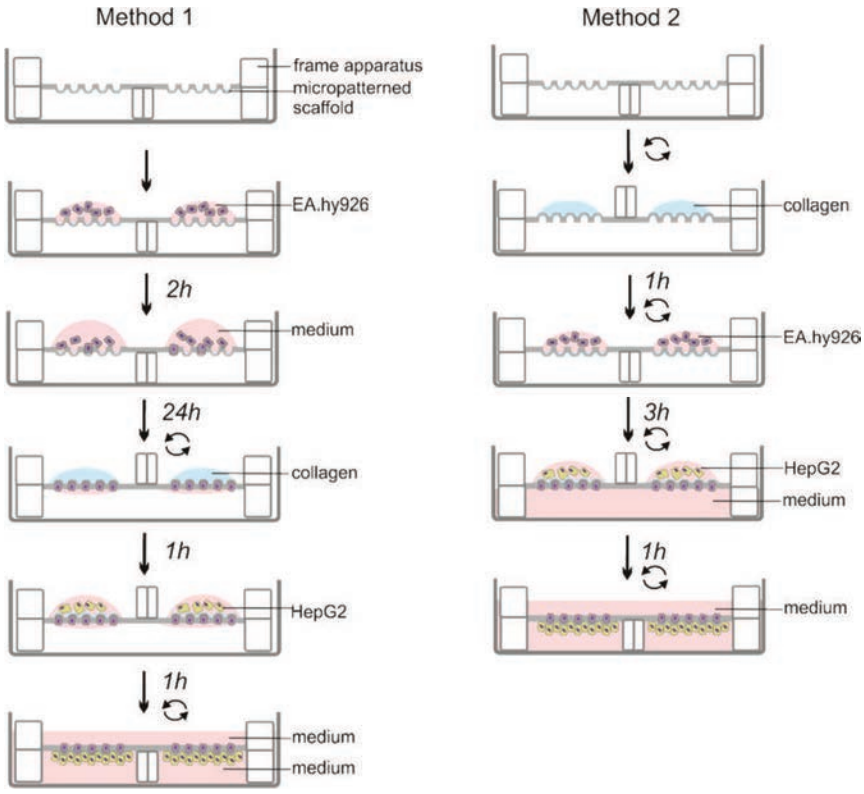

Figure 2.7: Scheme of methods used for directed cell seeding onto micropatterned scaffolds. The scaffold rotation is symbolized by two arrows.

After cell seeding and incubation, the cover of the frame apparatus was taken off and the folding part of the equipment was folded so that the two associated sinusoidal half-structures come to lie

on each other. Folding was always carried out in the same direction; part of the frame apparatus containing sinusoidal structure with perforations mimicking Glisson trias was immobilized using tweezers, while part containing structure with perforation mimicking vena centralis was rotated by 180°, creating an upper layer of the folded scaffold. Structures were placed again in 6 well plate. Subsequently 4 ml of DMEM was added. Samples were stored for 24 h at 37°C in the incubator. Finally, scaffolds were removed from the frame, washed with PBS and investigated using SEM.

2.4 Functional analysis of cell cultures

2.4.1 Total cell numbers and viability

The cells were examined daily under the inverted microscope (Nikon Eclipse TS100; Nikon GmbH) for morphological changes and possible contamination. The total cell numbers [/ml], vital cell numbers [/ml], aggregation and vitality [%] of the cultured cells were determined using the CASY® Cell Counter and Analyzer system (OLS OMNI Life). Cells were trypsinized from the scaffold surface using 400 µl of trypsin. After 5 min 600 µl of cell culture medium was added. Finally, 50 µl of such cell solution was diluted in 10 ml CASY*ton* and measured.

2.4.2 Albumin secretion

For the detection of albumin levels a commercially available Human Albumin ELISA Quantitation Kit (Bethyl Laboratories, Montgomery, TX, USA) was used according to the manufacturer's instructions. The detection range of this kit comprises 6.25-400 ng/ml. Samples were measured in multi-mode microplate reader (SpectraMax M, Molecular Devices, Germany).

2.4.3 Live-dead staining

Cells were incubated with the Live/Dead cellular staining kit II (PromoCell GmbH, Heidelberg, Germany) according to the manufacturer's instructions, repeatedly rinsed in PBS and examined under the inverted microscope (Nikon Eclipse TS100; Nikon GmbH) using epifluorescence method.

2.4.4 Actin Cytoskeleton Labeling

Cells on scaffolds were fixed with 4% paraformaldehyde for 15 min. For fluorescent staining of actin filaments, samples were incubated in 0.25% Triton X-100 for 15 min, blocked with 5% BSA for 30 min, and incubated with 100 nM Alexa Fluor 488 - labeled Phalloidin (Thermo Fisher Scientific) for 30 min at room temperature. Cell nuclei were stained with 4′,6-diamidino-2-phenylindole (DAPI; D8417; Sigma-Aldrich). Cells were two times rinsed with PBS and then mounted with Mowiol. Imaging takes place via a laser scanning microscope FV1000 (Olympus, Hamburg, Germany).

3. Two-step fabrication of scaffolds with controllable topography and microstructure for 3D hepatocyte cultivation

Polymeric scaffolds with high porosity, interconnected pore structures and defined topography are key element for successful 3D cell culture. Diffusion properties and 3D structure of the scaffolds are required for both 3D cell growth and the proper nutrient and oxygen supply. Additionally, reproducible 3D-topography increase the chance of consistent results and facilitates understanding the relevant biological processes, e.g. by simplifying image analyses. Therefore, the ability to fabricate scaffolds with established 3D structure and adjustable porosity is of both methodological and clinical significance and there is a strong demand to develop new and efficient methods to produce such polymer substrates.

As described in chapter 1.5, for defined 3D organotypic hepatocyte cultivation we have previously used scaffolds that were produced from commercially available microporous PC membranes. Biological inertia, high transparency and good form stability make the PC very attractive for cell culture applications; however, it is synthetic and nondegradable polymer. Although PLA is also synthetic material, it is considered as renewable and bio-based plastic because its raw material is synthetized from biomass or renewable resources such as sugars and starch, while their degradation product lactic acid is cellular metabolites (240). Due to high level of biocompatibility, good thermoplastic properties and degradation rate acceptable also for long-term cell culture (241) PLA is one of the most attractive polymers that meet the various physical and chemical demands for both effective polymer processing and safe biological applications. PLA has been commonly used in tissue engineering as a 3D cell scaffold in form of sponges, foams or fibers (242, 243). Although cells cultivated within such PLA substrates have shown 3D configurations and became functional, cellular distribution was limited to a spontaneous manner, depending on the random macro- or micro-porous structure of the scaffolds. In this chapter we explore the possibility to produce complex scaffolds with controllable porosity and topography using bioresorbable PLA polymer.

3.1 Development of the PLA-scaffolds

Despite conventional techniques of scaffold fabrication such as solvent leaching, gas foaming or phase separation are commonly known as simple and effective methods for mass production of porous polymer substrates, the pores are mostly irregular and the possibility to structure them to predetermined regular forms is limited. On the other hand, processing methods like microthermoforming are highly efficient and allow good control of geometry, but they are not suitable for microstructuring of porous and permeable polymer materials. Thus, to overcome these limitations we applied two-step strategy: porous foil formation was followed by multilayer thermoforming.

3.1.1 Fabrication of PLA microporous foils

To create permeable scaffolds with defined topography, first requirement is to produce PLA foils with an open pore network and well-interconnected pores. Thus, different fabrication techniques as well as parameters were tested and the produced foils were evaluated for the pore size and permeability. SEM images of porous PLA foils obtained using different fabrication methods (Tab. 3.1) are given in figure 3.

Table 3.1: Permeability of the PLA foils produced with different methods and parameters.

	Production method	PLA [%]	Solvent/ nonsolvent	Quenching	Permeability [mbar]
1	Salt leaching	10	dioxane	-	-
2	IP	10	dioxane	water	-
3	IP	5	chloroform	ethanol	119,00
4	IP	5	chloroform	ethanol/chloroform (90/10)	194,2
5	IP	10	chloroform	ethanol/chloroform (60/40)	11,14
6	TIPS	10	dioxane/water (87/13)	liquid nitrogen (-196°C)	112,55
7	TIPS	10	dioxane/water (90/10)	liquid nitrogen (-196°C)	18,90
8	TIPS	10	dioxane/water (90/10)	freezer (-20°C)	1,55
9	TIPS	10	dioxane/water (90/10)	dry ice (-78°C)	3,81

Despite using solutions with different polymer content and varying polymer to salt weight ratio, foils with interconnected porous structure were not formed using salt –leaching method (Fig. 3.1 (a)). Moreover, salt was very difficult to remove from the sample and despite repeated immersion into water some salt crystals remained encapsulated in the foils microstructure. Therefore phase separation method was applied. The shape and size of the pores and their interconnectivity was controlled by a balance between several parameters such as polymer concentration, quenching temperature or quenching bad, type of solvent and additives. These parameters altered the early stage of the phase separation, where the initial structure of the scaffolds was formed. When dioxane was used as a solvent and water as a nonsolvent for immersion precipitation method, dense films with irregular and impermeable structures were obtained (Fig. 3.1 (b)). The result suggested that solvent-nonsolvent exchange during phase separation was insufficient. Therefore ethanol was selected as nonsolvent for coagulation bath. Ethanol is less polar than water and thus the solvent-nonsolvent exchange could be faster. Combination of the solvents like dioxane or chloroform with nonsolvent like ethanol has higher compatibility then combination of dioxane with water. This allows for phase separation over the whole extension of the casted foil and resulted in more homogeneous morphology.

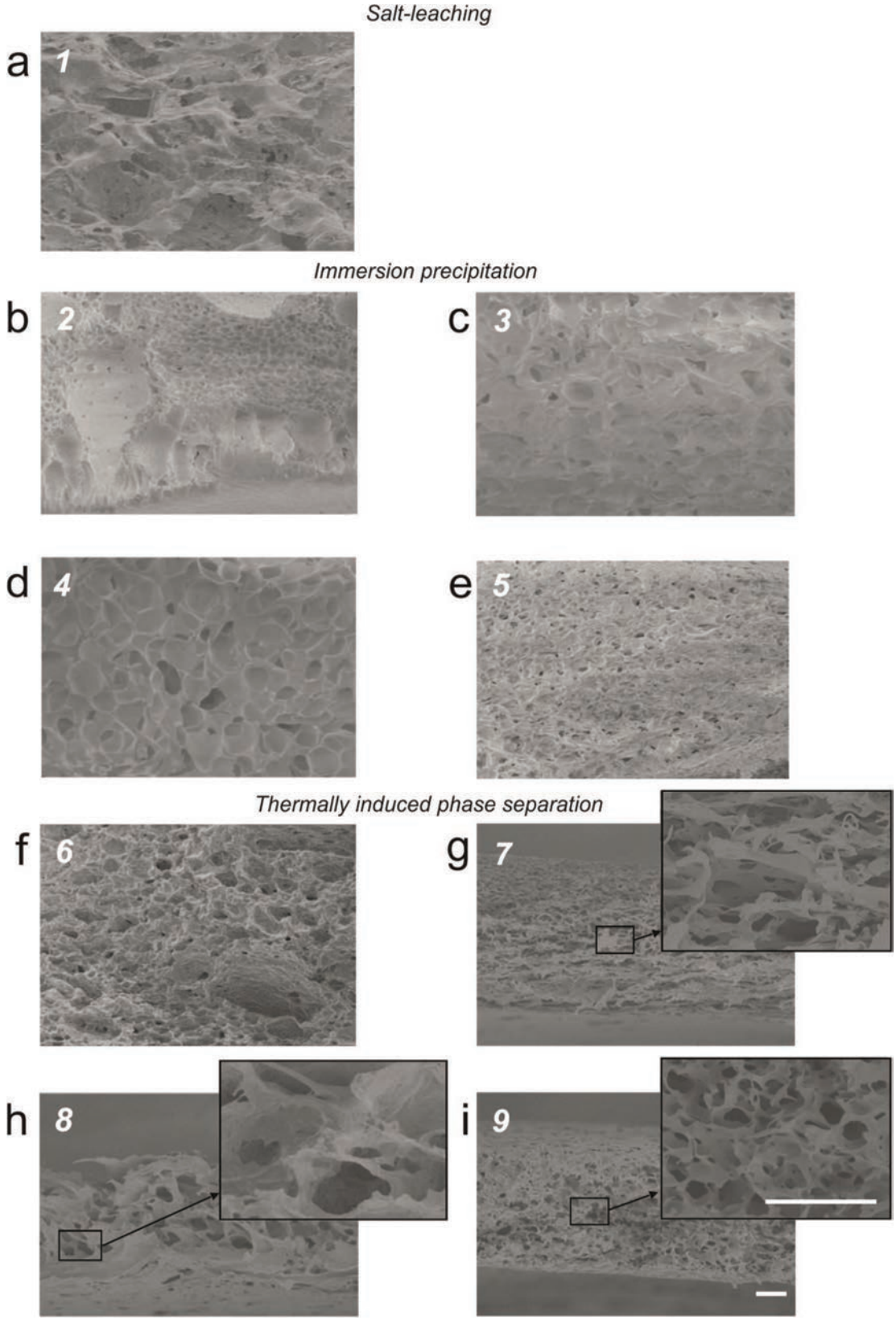

Figure 3.1: SEM images of the cross section of PLA foils obtained using different methods and parameters. Numbers represent production method according to table 3.1. Scale bars indicate 30 µm.

Samples closest to the expectations were obtained using chloroform as a solvent and ethanol-chloroform mixture as a non-solvent bath (Fig. 3.1 (c) – 3.1 (e)). Addition of chloroform to immersion bath caused better penetration of the film by nonsolvent and increased pore size. Foils prepared from more concentrated solutions (10%) needed more chloroform content in immersion bath to form homogeneous structure. For solutions with low PLA concentrations (5%), stable foils were produced as the chloroform content in the immersion bath varied from 0 to 10 wt. %. Higher chloroform content negatively affected mechanical properties of the foils causing brittleness and delicacy of the samples.

Using TIPS method the pore size and the permeability of the PLA foils were controlled by changing the moisture content in the solvent mixture and quenching conditions. To avoid coarsening processes after phase separation (244, 245) and to achieve small and open pores, quenching temperatures were kept below the melting point of dioxane (11.8°C), while foils were quenched directly after spin coating. With increasing quenching temperature the pore size also increased and seemed to have a more closed structure. In contrast, foils quenched in liquid nitrogen had exceedingly small pores. Using higher quenching temperatures, crystallization of dioxane had a low nucleation rate and a high growth rate. As consequence, large solvent crystal formation and large pore sizes was observed within the scaffolds. Simultaneously, composition of the polymer solution was changed. Since addition of the nonsolvent to the polymer solution can induce liquid-liquid phase separation and thus have pronounced effect on the pore size and overall morphology of the scaffold (98), small amount of water were added to the PLA-solvent mixture (Fig. 3.1 (f)-3.1 (i)). The most regular and interconnected porous structure was obtained for 90:10 dioxane:water volume ratio. Further increase in the amount of water generated larger and more irregular pore structures. Desired pore size and morphology allowed perfusion of fluids while retaining the cells. The best samples for our future applications with interconnected pores, homogenous microstructure and the pore size in the range of 5-20 µm were obtained by quenching a 10% PLA solution with 90:10 dioxane:water ratio in dry ice (Fig. 3.1 (i)). Casted and quenched foils were dried under vacuum. However, in the later stage of the phase separation, separated droplets have tendency to come together and proceed to minimizing the interfacial free energy. In consequence, the degree of pore connection could be reduced. To prevent such coarsening phenomenon, foils were dried in vacuum desiccator with dry ice bath.

Table 3.2: Spin coating parameters used to produce foils with different thickness from 10% PLA solution.

Foil thickness (µm)	Speed of rotation (rpm)	Time of rotation (s)
30	600	15
50	400	30
70	250	30

Simultaneously thickness of the microporous foils was conveniently controlled using spin coating procedure. Foils with different dimensions were produced by changing the speed and time of

rotation (Tab. 3.2). Since produced foils should be thin enough to form microcavities but thick enough to withstand mechanical stress during thermoforming, thickness of the tested foils was in the range from 30 to 70 µm. Microporous foils were thermoformed and tested again for permeability. Best results were achieved for the 50 µm thick foil (Fig. 3.2). Thus, such foils were used for the further experiments.

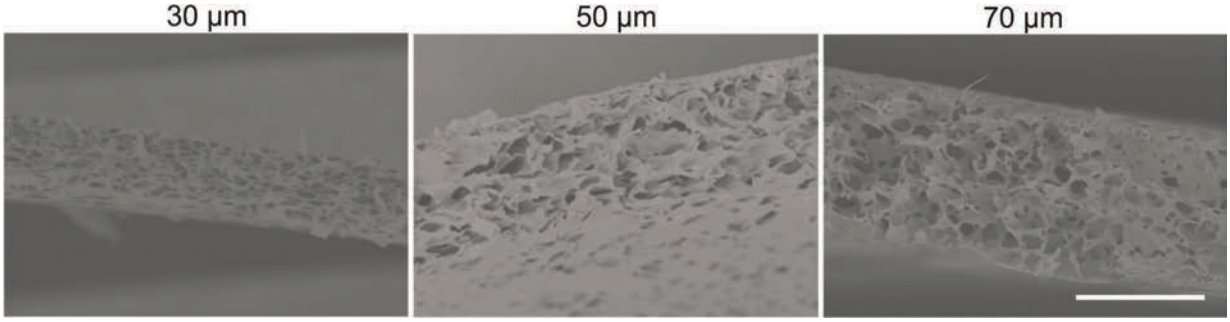

Figure 3.2: PLA microporous foils with different thickness controlled by spin coating. Scale bare indicate 50 µm.

3.1.2 Permeability and mechanical properties

In this study, complex scaffolds were manufactured from porous matrices without disturbing their mechanical and mass transport properties using a novel thermoforming procedure. To produce scaffolds suitable for microfluidic applications, permeability of the samples was measured at various stages of scaffold production. Thus, foils and subsequently scaffolds allowing perfusion of fluids were identified.

Table 3.3: Permeability (P) of the samples as a pressure difference between two sides of a porous foil and theoretical permeability values calculated for the flow of medium. Measurements were made before and after thermoforming under different pressures (p) and temperatures (T).

		Sample								
Step	Sample parameter	1	2	3	4	5	6	7	8	9
1. Pre-process (PLA foils)	Film thickness [µm]	30	30	50	50	50	50	50	70	70
	Permeability [mbar] air	1.3	3.9	4.8	2.3	3.8	3.9	3.4	2.6	4.6
	Permeability [mbar] cell culture medium	0.07	0.21	0.26	0.13	0.21	0.22	0.19	0.14	0.25
2. Thermoforming	Temperature [°C]	65	70	65	70	65	70	70	70	75
	Pressure [bar]	60	65	65	70	70	75	65	65	65
3.Post-process (PLA scaffolds)	Permeability [mbar] air	11.2	26.6	11.6	3.5	21.4	24.2	31.4	3.8	22.0
	Permeability [mbar] cell culture medium	0.60	1.47	0.62	0.19	1.18	1.34	1.73	0.21	1.21

Permeability values under air flow through porous surface of PLA foils and PLA scaffolds and theoretical permeability values calculated for the medium flow are presented in Table 3.3. In the scaffolds suitable for applications in bioreactor system, maximum pressure differences between two sides of a porous sample during air flow testing should not exceed 20 mbar.

Primary mechanical properties of microporous PLA foils were estimated by performing a tensile test. Produced foils were compared with microporous membranes from track-etched polycarbonate (Tab. 3.4). Additionally, to demonstrate the differences resulting from the microstructure of tested material, mechanical properties of unporous polymer films were shown.

Table 3.4: Mechanical properties of polylactic acid (PLA) and polycarbonate (PC). Values measured for the microporous PLA foils and track-etched PC membranes were compared with typical properties of unporous polymer foils from the technical data sheet (NatureWorks® PLA 4032D and MAKROLON®GP).

	Material	Tensile modulus (GPa)	Tensile strength (MPa)	Max strain (%)
Microporous substrate	PC	2.16 ± 0.05	40.61 ± 0.06	37.63 ± 10.90
	PLA	0.32 ± 0.01	5.96 ± 0.30	37.96 ± 6.00
Unporous foils	PC	2.38	65.50	110
	PLA	3.44	103.20	180

Values from the technical data sheet of unporous foils indicate good mechanical strength of PLA substrates and better mechanical properties of PLA in comparison to the PC material. However, values measured for the porous PLA samples are much lower than values noted for unporous PLA foils. Although similar trend can be noticed for PC materials, the difference between porous PC material and unporous foil is not so notable as for PLA. This could be the result of a various pore structure in the tested materials. In contrast to track - etched PC membranes with cylindrical pores, PLA foils have interconnected pores with high surface-to-volume ratio (Fig. 3.3). Thus, higher impact of microporous structure on mechanical properties can be expected for PLA substrates. Nevertheless, microporous PLA foils presented low tensile modulus, maintaining relatively high elongation at break.

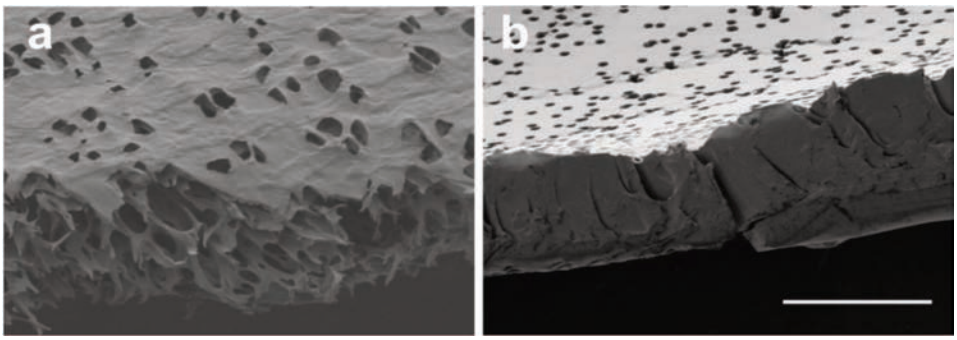

Figure 3.3: Comparison of the surface layer and cross section of PLA scaffold, obtained from microporous polylactic acid foils (a) and PC scaffold, obtained from track-etched polycarbonate membranes (b). Scale bare indicate 50 µm.

3.1.3 Biocompatibility testing

The scaffolds presented in this thesis are meant to be studied for *in vitro* cell culture systems, therefore, a high-degree of biocompatibility of samples is prerequisite and the absence of solvent used for fabrication of the foils must be verified. To assess the biocompatibility of our microporous PLA foils, L929 cells were cultivated on produced samples and compared with cells cultivated on empty MTP as well as with cells containing 2-hydroxyethylmethacrylate (HEMA). HEMA is cytotoxic and genotoxic. This compound induces adverse biological effects, which can lead to DNA damage, apoptosis and cell-cycle delay (246). Therefore, cells containing HEMA were used as positive control, while cells cultivated on MTP were used as negative control.

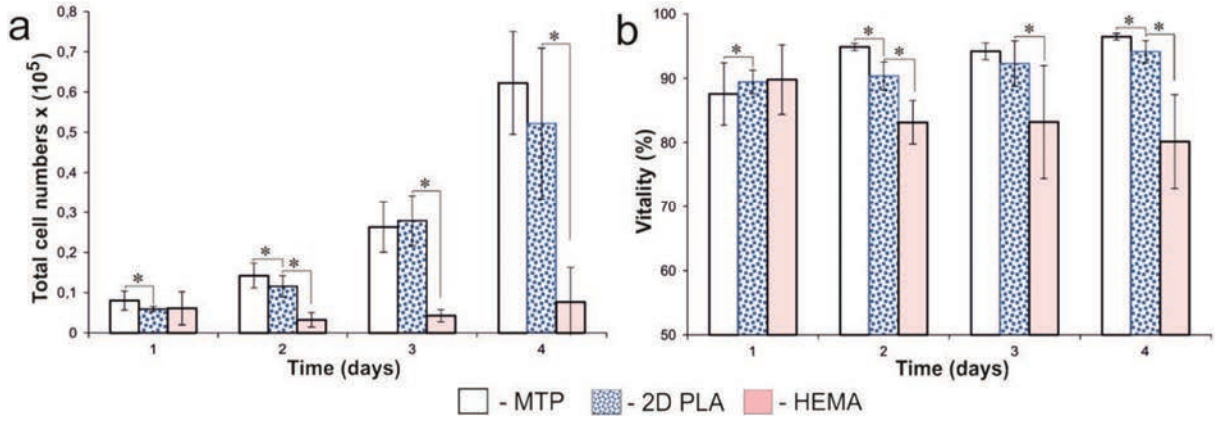

Figure 3.4: Total cell numbers (a) and vitality (b) of L929 cells cultivated on PLA microporous foils (2D PLA), cells cultivated on empty microtiter plate (MTP) and cells containing 2-hydroxyethylmethacrylate (HEMA). Results consist of the average of 4 independent tests. Statistical significance (t-test) relative to positive and negative control is noted (*$p < 0.05$).

The obtained results demonstrated a very high degree of biocompatibility for the produced PLA foils (Fig. 3.4). The total cell number was found to steadily increase with rapid growth, especially during the third and fourth days of cultivation. Vitality of the cells improved considerably with the progress of the experiment and from day 2 onwards was higher than 90%. This data suggest that dioxane was successfully removed from the samples.

3.1.4 Microstructuring process

With the following multilayer microthermoforming, scaffolds with definable permeability and 3D geometry in the shape of microcavities were produced. Recently, it was demonstrated that scaffolds with such topography are suitable for 3D cell cultivation (11, 247). PLA foils were thermoformed using the non-porous and very thin polymer foil as a protection layer. Therefore this process was called multilayer thermoforming. The pores were temporarily blocked, however; after the micromolding step the non-porous protection layer was separated from the scaffold. As

a consequence, it was possible to avoid pressure loss during the thermoforming process and the problem of microstructuring of the porous material was solved. To reduce the impact of the protection layer on the forming fidelity, foil with very good formability and high temperature resistance was required. We used a 10 µm thick FEP foil, which can be efficiently structured in a wide range of thermoforming parameters. Additionally, FEP has a smooth surface of extremely low surface tension and thus can be easily separated from the scaffold after thermoforming. During microstructuring PLA foils should be stretched to a desired shape, while the primary porosity and interconnection between the pores must be preserved. Thus, different thermoforming parameters were tested and the formed scaffolds were evaluated for each parameter setting by analyzing their structure and permeability.

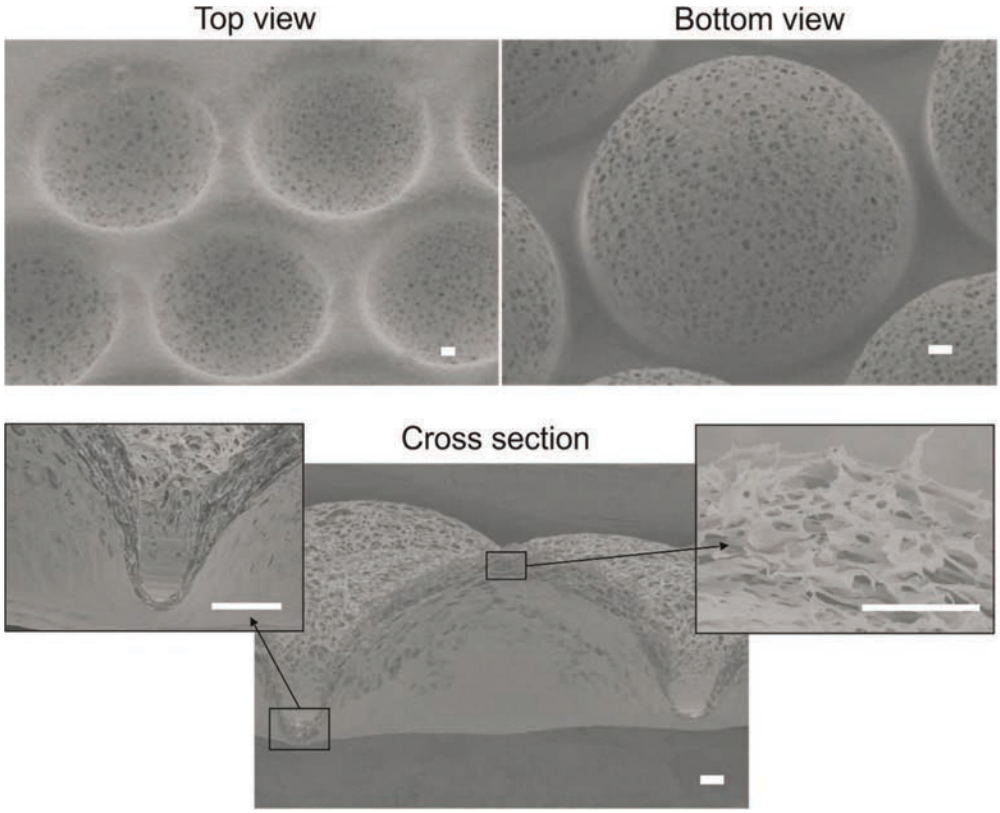

Figure 3.5: Polymeric scaffold with controlled topography and microstructure formed from microporous PLA foil using thermoforming technique. Scale bars indicate 25 µm.

Since thermoforming temperature and working pressure were strictly dependent on each other, both thermoforming parameters were progressively optimized. Starting with temperature close to the glass transition temperature (T_g) of the used PLA (60°C), the minimum pressure causing the formation of microcavities was 60 bar. Parameters were increased progressively until the first signs of deformation were noticed. It was found, that pressure above 75 bar leads to the destruction of the cavities, while temperatures exceeding 75 °C cause irreversible changes in the microporous structure regardless of the pressure applied (data not shown). Scaffolds with desired shape (Fig. 3.5) and permeability were obtained for the foils thermoformed under a pressure of 70 bar and at

65°C (Tab. 3.3). In the microcavities foils were starched and the primary microstructure was preserved, while between the cavities thickness of the scaffolds was significantly reduced and dense surface skin layer was observed. Thus, porous structure was maintained in areas where the permeability was required.

3.1.5 Final pore size distribution and surface roughness

Final pore size evaluation for the PLA scaffolds after thermoforming process was determined by mercury intrusion porosimetry and visual estimation of the SEM images. Average values of porosity, surface area and total pore volume as well as pore size distribution are presented in Fig. 3.6. However, since all values were measured inside whole scaffolds, it should be noted that after thermoforming process PLA scaffolds have heterogeneous microstructure. As described previously, scaffolds are divided into permeable areas, where the porous foil was stretched and regions, where the pores are compressed (Fig. 3.5). For this reason a large dispersion in the size of pores was observed. Thus, the evaluation of the pore size should be performed simultaneously with direct visual estimation of the SEM images.

a

	PLA MatriGrid
Porosity [%]	62.35
Surface area [m^2/g]	2.50
Pore volume [cm^3/g]	1.25

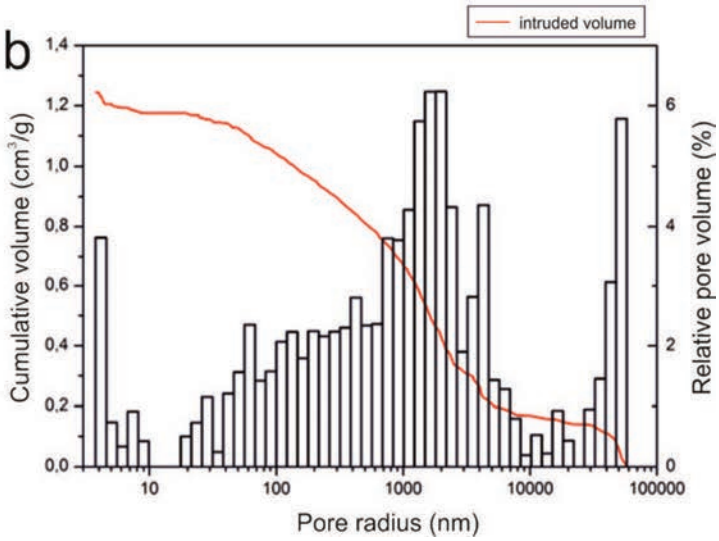

Figure 3.6: Characterization of porous PLA scaffolds (a) and pore size distribution inside PLA scaffolds measured by mercury intrusion porosimetry (b).

Surface roughness was used for expression of the variability of a topographic surface of PC and PLA substrate at nanometer scale. Despite the surface layer of PLA and PC scaffolds observed using SEM have showed similar structure with smooth area and small holes in the range from 2 to 5 μm (Fig. 3.3), surface roughness measured for PLA scaffolds was significantly higher than roughness measured for PC scaffolds (Tab. 3.5). Results obtained indicate that PC samples have highly plane surface and the nanometric scale topography of PLA substrates is significantly different than topography of PC samples.

Table 3.5: Average surface roughnesses of scaffolds obtained from microporous PLA foils and track-etched PC membranes.

Material	R_a (mean ± SD nm)
PC scaffold	12,4 ± 0,72
PLA scaffold	265,6 ± 22,76

3.2 Degradation test

Despite PLA is commonly known as material with long biodegradation time (48), processing and sterilization methods can change polymer parameters such as crystallization rate or T_g and in consequence, complex degradation profile of the polymer may be also altered (248). Since degradation of PLA in an alkaline aqueous medium is influenced by polymer properties such as microstructure, crystallinity and chain mobility, the initial morphology and thermal history of PLA scaffolds are important factors influencing their degradation behavior as well as various mechanical properties. Therefore, to test the applicability of premanufactured porous PLA scaffolds for biological applications, thermoformed samples were first characterized for *in vitro* degradation in cell culture for 4 weeks and additionally for degradation under PBS for 6 months.

Cell culture

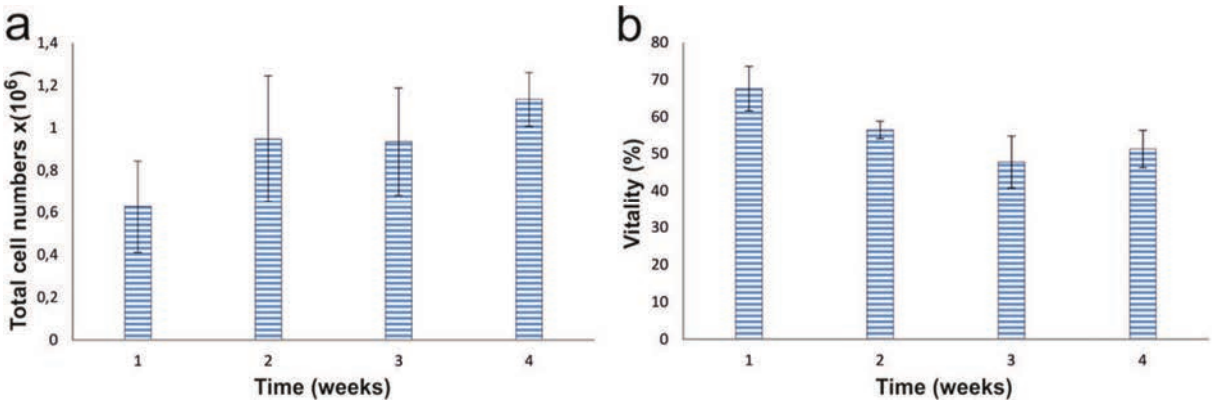

Figure 3.7: Total cell numbers (a) and vitality (b) of HepG2 cells cultivated within 3D PLA microstructured scaffolds for 4 weeks. Results consist of the average of 2 independent tests.

Since the final architecture of the PLA scaffolds was designed for optimal cultivation of hepatocytes, HepG2 cells were used for the degradation test in cell culture. Cell number and vitality of the cells were analyzed weekly (Fig. 3.7). A high increase in the number of cells occurred in the first week, while in the following weeks the number of cells remained at a similar level. Vitality of the cells decrease with the progress of the experiment, but after 4 weeks considerable amount of cells was still viable. Lower viability of the cells long-term cultivated in 3D scaffolds under static conditions could be due to both, a decreasing oxygen supply (221) and a smaller surface area accessible to the cells (12).

Visual examination of the scaffolds

Time-dependent morphological changes during PLA scaffold degradation were evaluated using SEM (Fig. 3.8). During 4 weeks of degradation under cell culture as well as during 24 weeks of degradation under PBS no evidence of phisical disintegration of the scaffolds was noticed. Shrinkage or wrinkling of the scaffolds was not observed. Thermoformed structures remained stable and no changes in the form of the microcavities was observed. After 4 weeks in cell culture as well as after 4 weeks in PBS microporous structure was unchanged. These observations, together with the results of cell culture experiments, indicate that PLA scaffolds have provided a stable environment for cultured cells. First changes in microporous structure were noticed after 24 weeks of degradation under PBS.

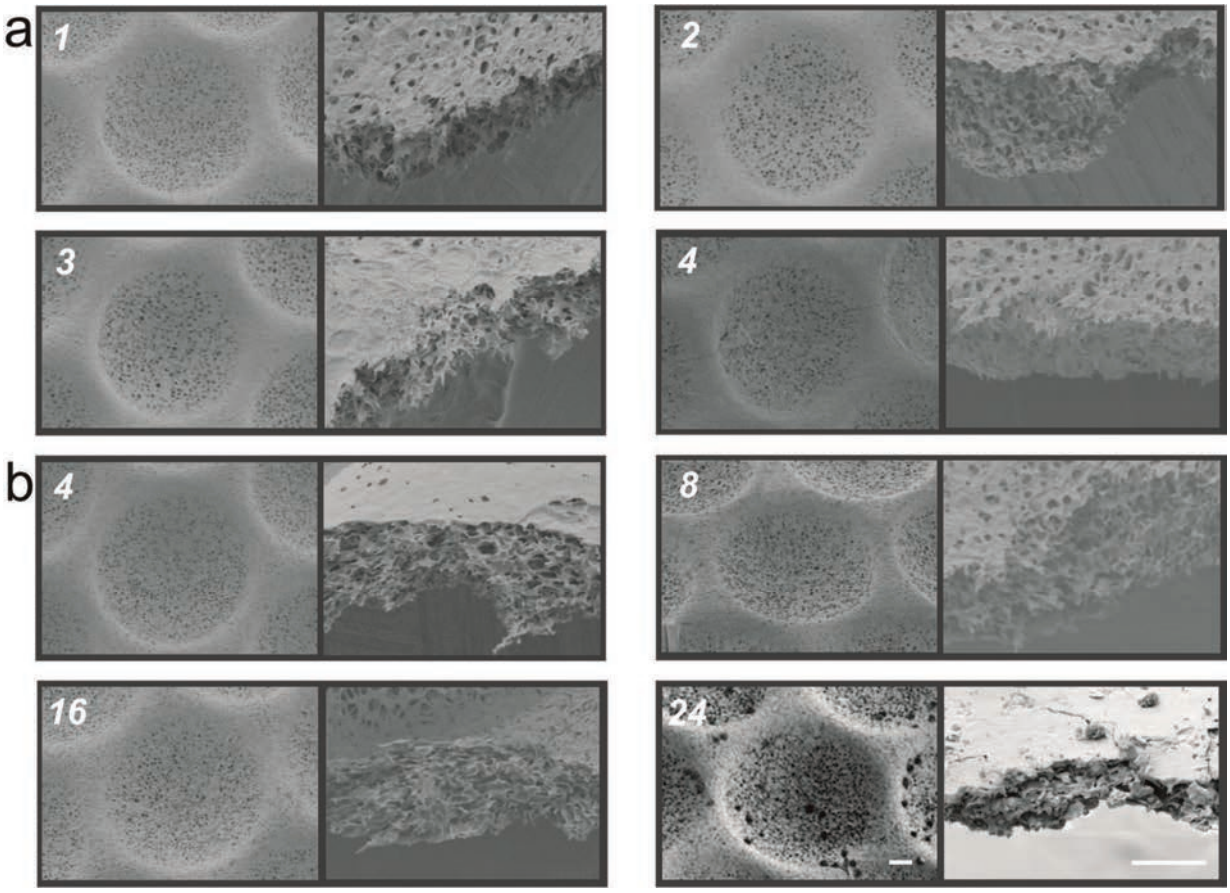

Figure 3.8: Representative SEM images of the microporous PLA scaffolds during 4 weeks under cell culture (a) and during 24 weeks under PBS (b). Numbers represent weeks of degradation. Scale bars represent
50 µm.

Mechanical strength versus time

Primary mechanical properties of the PLA scaffolds during degradation study were estimated by performing a tensile test. Due to complex 3D structure of the thermoformed scaffolds the cross-sectional area of the sample was difficult to calculate. Therefore it was not possible to calculate the

tensile modulus or maximal strain of the samples. However, changes in mechanical properties of the scaffolds throughout degradation period were evaluated by comparison of tensile strength and extension at break (Fig. 3.9). The mechanical strengths of the samples gradually deteriorated with time, with tensile strength reduced by approximately 35% in 4 weeks. Similar trend was observed for samples degraded in cell culture and in PBS. After week four onward a slow decreases in tensile strength of the samples degraded in PBS was noticed. Extension at break significantly decreased within the first two weeks, after which similar values were measured.

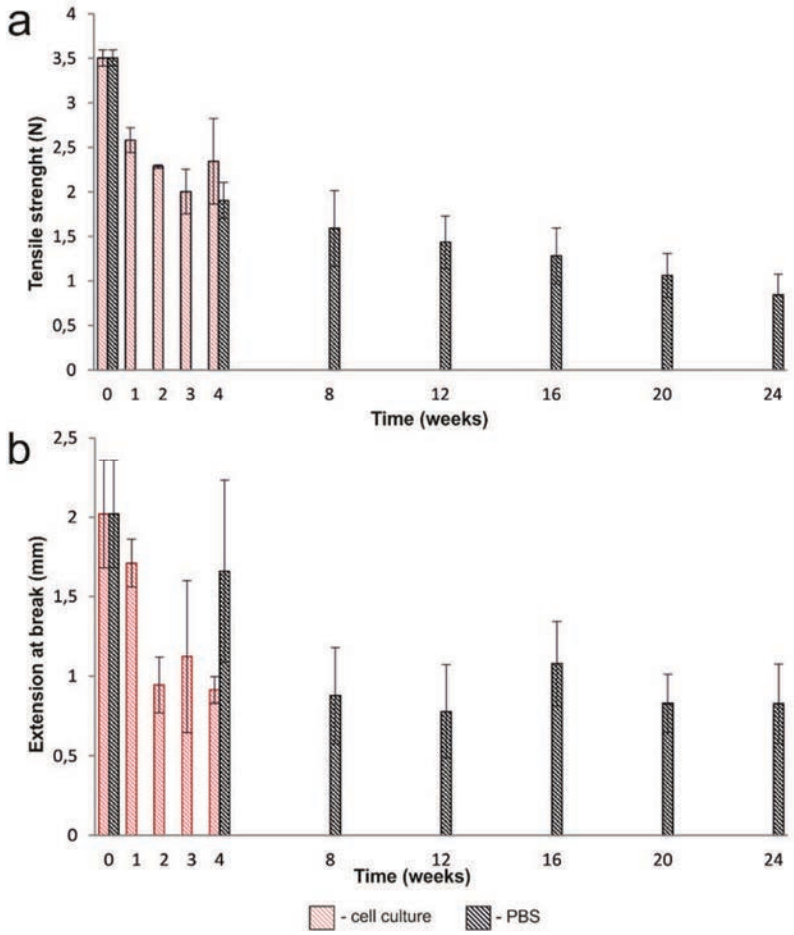

Figure 3.9: Tensile strength and extension at break of the microporous PLA scaffolds during 4 weeks of degradation under cell culture and during 24 weeks of degradation under PBS.

3.3 Biological characterization of the scaffolds

The topography of the scaffolds was designed to minimize cell–polymer contacts and maximize cell–cell interactions in the 3D spheroids. Cell location and -health within the scaffolds was determined using SEM imaging and fluorescence-based live/dead assay (Fig. 3.10). The desired arrangement of the hepatocytes could be detected. HepG2-hepatoma cells were found mostly in the cavities of the scaffold and after 2 days of cultivation cellular agglomeration within the 3D

structures was seen. Good cell vitality within PLA scaffolds (with collagen coating) was detected visually with live-dead staining after 3 days of cultivation (Fig. 3.10 (b)).

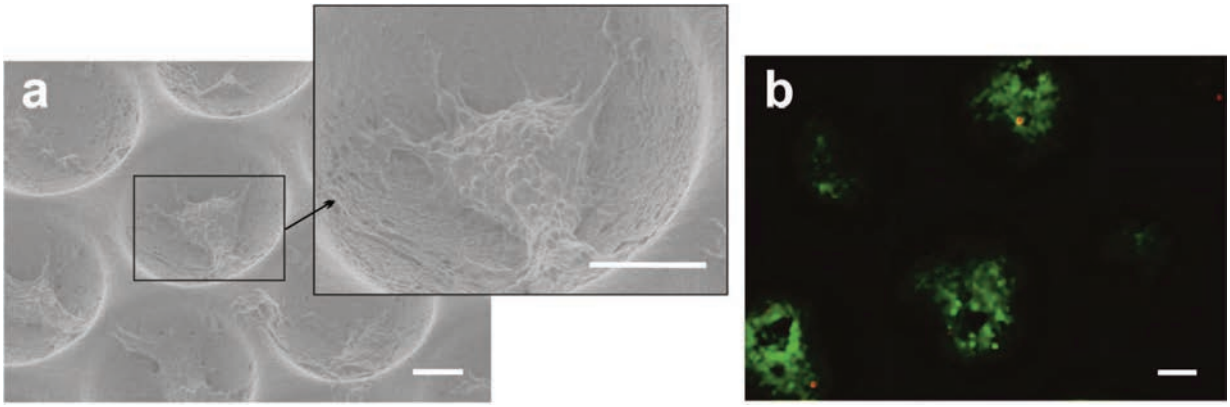

Figure 3.10: The cultivation of HepG2 cells as 3D agglomeration within the structured area of the PLA scaffolds coated with collagen: SEM image after 2 days of cultivation (a) and fluorescence image (vital cells - green, dead cells - red) after 3 days of cultivation (b). Scale bars indicate 100 µm.

Cell growth on PLA scaffolds with and without collagen coating was compared with cell growth in 2D (well) and PC scaffolds. High cell viability was measured for 2D as well as 3D cultured cells (Fig. 3.11 (a)). Nevertheless, quantitative determination of cell numbers showed a decrease of the 3D cultured cells compared to 2D culture (Fig. 3.11 (b)). Lower cell numbers in 3D scaffolds could be due to both, differences in surface area accessible to the cells and a decreasing oxygen supply (12). Active scaffolds surface accessible to the cells within a microcavities is 73.5 mm^2, while surface of MTP well is 193.5 mm^2. As a consequence, the smaller area accessible to the cells may have an impact on the effectiveness of cell division. However, this must be evaluated in further experiments. Furthermore, excessive depletion and waste product accumulation between the daily medium changes could also explain lower cell numbers in the static 3D cell culture (221). The secretion rate of albumin, the key metabolic marker for hepatocyte cultures (249), showed the largest increase for HepG2 cells cultured within 3D substrates, providing a clear advantage of using 3D polymer scaffolds against standard 2D microplates (Fig. 3.11 (c)). In standard 2D experiments albumin levels increased slightly over time in an almost linear manner, while in 3D experiments the measured values were found to be even 2.5 times higher. From day three onwards the advantage of 3D scaffolds was particularly evident. These results are consistent with the data obtained by Zhu et al., where it was described that aggregated hepatoma cells cultivated within PLGA sponges exhibited higher hepatic function but lower proliferation rate than cells cultured in standard MTP (171).

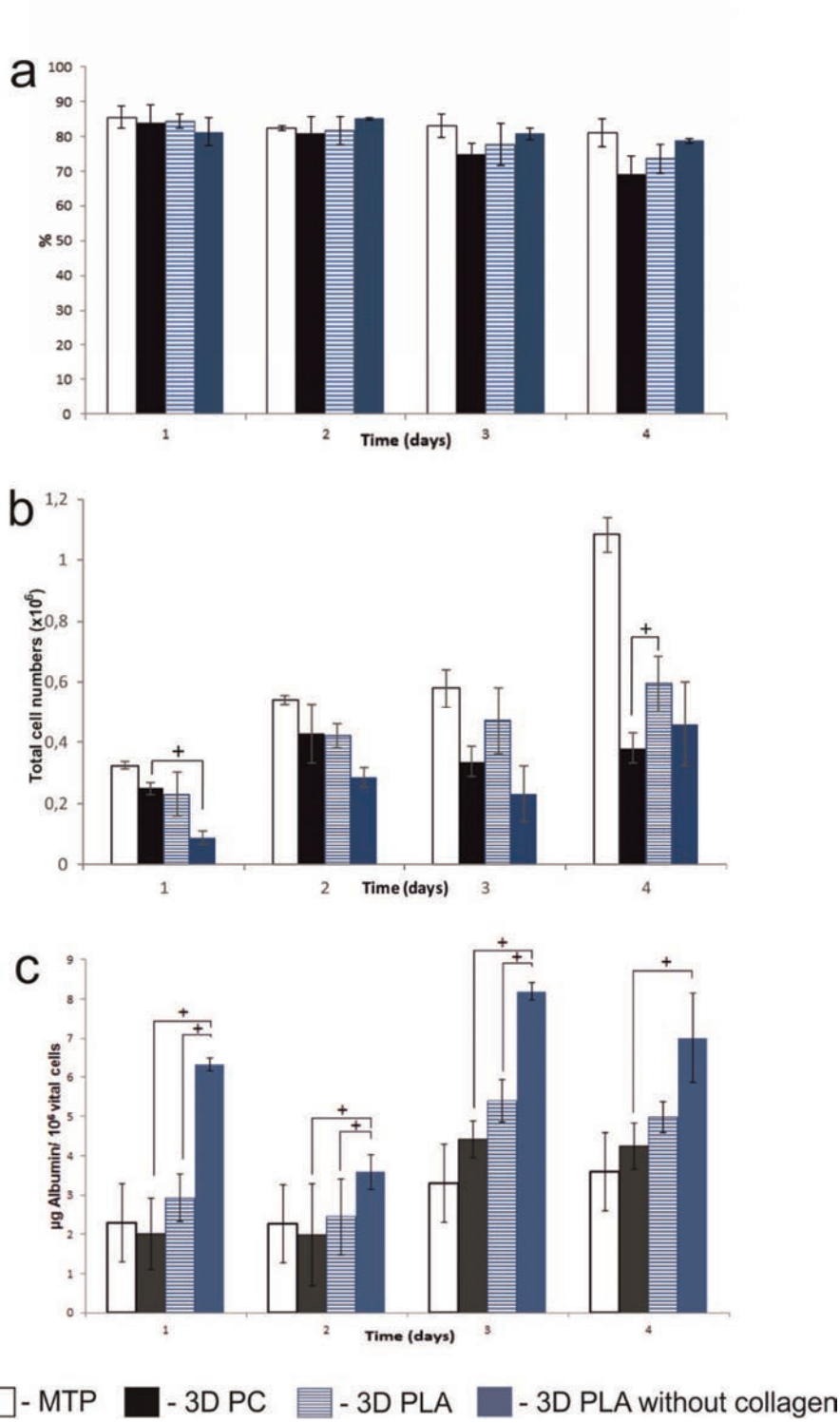

Figure 3.11: Vitality (a), total cell numbers (b) and albumin secretion rate (c) of HepG2 cells cultured on microtiter plate (MTP) coated with collagen, within 3D polycarbonate (3D PC) and polylactide (3D PLA) microstructured scaffolds coated with collagen and within 3D polylactide scaffolds without collagen (3D PLA without collagen). Results are the average of 3 independent tests. Differences between cells were statistically analyzed (t-test). Statistically significant differences between the 3D PLA and 3D PC samples are noted ($^{+}p < 0.05$).

Moreover, there was a the strongest significant increase in albumin production in PLA scaffolds with and without collagen coating in compare to PC scaffolds, suggesting an increase in the hepatocyte functionality of the PLA-scaffold-cultured HepG2 cells. Various factors can cause these results. Initial interaction of polymer matrix with cells can be influenced by the chemical composition, surface energy, topography and roughness of the top polymer layers, those are in direct contact with cell surface (123, 249). However, both PC and PLA are known to have a hydrophobic surface and show no natural recognition sites that promote cell attachment via cell-recognition signal molecules (250). Primary cell attachment on such synthetic materials is generally mediated by the passive adsorption of proteins from the culture (159). Therefore, though the initial attraction between cells and substrates may be similar for PC and PLA substrates, enhanced roughness of PLA scaffolds in comparison to PC substrates (Tab. 3.5) may have considerable effect on cell spreading and adhesion at the nanoscale level. Surface roughness is one of the main properties decisive for colonization of a material with cells and as a consequence, strongly influence cell functions and proliferation (170, 251). A possible reason for this could be enhanced cell spreading on surfaces with greater roughness due to larger contact area. Such heterogeneous surface structure could allow filopodia of the cells to anchor more tightly (252, 253). Thus, surface of non-coated PLA scaffolds may provide environmental stimuli for the cell adhesion directly to the polymer surface, without interaction of collagen. On the other hand, surface roughness could improve the hydrophilicity of the PLA films and therefore enhance the adsorption of collagen during coating (160). PLA scaffolds with heterogeneous surface architecture were previously shown to adsorb four times more proteins than scaffolds with solid surface (253).

Differences in cell adhesion and functionality may also result from mechanical properties of the scaffold that are derived from its composition and architecture. During the tensile test PLA scaffolds with interconnected pores and high surface-to-volume ratio have showed lower elasticity in comparison to PC substrates (Tab. 3.4). In the liver, the physiology and pathology of this organ being strictly correlated to specific modules of elasticity. Healthy liver has a low ECM elasticity, which ensures the polarization and the proper functioning of hepatocytes, while a significant increase of the matrix elasticity indicates the first response of the organ to several injuries (254). Also during *in vitro* tests it was observed that cell properties are strictly depending on mechanical forces exerted by the extracellular environment (255, 256). Tactile sensing of substrate stiffness and elasticity feeds back on cell adhesion and cytoskeleton, as well as on net contractile forces (257). Thus, PLA scaffolds with lower elasticity as compare to PC substrates may provide more attractive environment for liver cell cultivation. However, for a better evaluation of the PLA and PC substrates further examination of the mechanical properties of the scaffolds surface could be considered under the scope of future research.

4. Fast degradable scaffolds with established topography and microstructure for scaffold-less cell sheet engineering

Despite many advantages of using microporous substrates in 3D cell culture described previously, in a cell sheet engineering applications thick and nondegradable microporous scaffolds may act as a barrier for direct heterotypic cell-cell interactions. To overcome this problem, scaffolds with high porosity and fast degradation rate are desired. Such biodegradable and 3D microstructured scaffold may serve as a template to manipulate cell adhesion and growth when cells are seeded and subsequently degrade with time, resulting in the reorganization of the cells into a 3D stacked structure with desired microarchitecture. As the two-step procedure described in previous chapter was successfully used to produce stable scaffolds with controlled properties, in this chapter we explore the possibility of using this method to produce fast degradable substrates with established porosity and topography for scaffold-less cell sheet engineering applications. Among a number of fast biodegradable scaffold material reported so far, PLGA is the most popular synthetic polymer owning to its tunable degradation rates, good mechanical properties and excellent processability into desired configuration. A desirable feature for our application would be synchronization of polymer degradation with the formation of stable cell culture on both sides of the microstructured scaffold.

However, despite *in vitro* degradation of PLGA scaffold in PBS solution was studied in details (71) characterization of PLGA substrates in cell culture and corresponding cell responses as well as cell-material interactions are rather limited. It is still questionable whether PLGA scaffolds will exhibit similar morphologic and dimensional changes during degradation in cell culture as compared to degradation in PBS. In one of the few studies, Lu et al. have shown significantly faster degradation of PLGA 50:50 foams *in vivo* as compared to *in vitro* conditions. Fibrovascular tissue ingrowth into PLGA foams was observed after 1 week of implantation, while by 6 weeks the majority of the space between the polymer was filled with fibrovascular tissue (258). However, those differences were more expected with low diffusion rate of the acidic degradation products and in consequence autocatalysis of the degradation reaction than interaction of cells. In contrast, Kasuya et al. have shown that 2.4 µm thick PLGA membrane was degraded gradually from day 12 preferentially under hepatocyte culture, while the morphology and the porosity of the membrane without the cells remained intact for at least 2 months (259). These results suggested that membrane degradation was significantly promoted by the cells. The increased degradation rate of the membrane for 3D hepatocyte tissue formation in this study was associated with tensional force generated by the cells cultured on opposite sides of the membrane. In addition to the environment in which the scaffolds is placed several other factors can influence the rate of degradation of PLGA material, including the way the material was processed (260). Thus, since interaction of those parameters are complex, the exact degradation dynamics is difficult to predict for new PLGA scaffolds with unique properties and each scaffold must tested individually under the target conditions.

4.1 Scaffolds development

4.1.1 Selection of PLGA foils with suitable microstructure

To enhance cell-cell interactions of the cells cultured on the opposite sides of the scaffolds as well as to fabricate scaffolds applicable for microfluidic applications, PLGA foils with high porosity and well-interconnected pore structure were required. Nam et al. have shown that foils produced from PLGA have different morphology from foils obtained from PLA under the same experimental conditions (96). The differences could be attributed to the molecular rearrangement of the polymer chains that take place during quenching of the foils. It could be expected that amorphous PLGA rearrange more easily and is less stable than semicrystalline PLA. Thus, to produce porous foils from PLGA, fabrication parameters were tested irrespective of the results obtained previously for PLA scaffolds (Tab. 4.1).

Table 4.1: Different methods and parameters used for production of microporous PLGA foils.

	Material	Production method	PLGA [%]	Solvent/nonsolvent	Quenching	Permeability [mbar]
1	PLGA_1	Immersion precipitation	10	dioxane	methanol	-
2	PLGA_1	Immersion precipitation	20	acetone	ethanol	-
3	PLGA_1	Immersion precipitation	10	dioxane	water	136,8
4	PLGA_1	Immersion precipitation	20	dioxane	water	112,3
5	PLGA_1	Immersion precipitation	17	dioxane	water (4°C)	28,69
6	PLGA_1	TIPS	10	dioxane/water (90/10)	dry ice (-78°C)	-
7	PLGA_1	TIPS	20	dioxane/water (90/10)	dry ice (-78°C)	2,03
8	PLGA_2	TIPS	25	dioxane / water (90/10)	freezer (-20°C)	3,26
9	PLGA_2	TIPS	10	dioxane/water (90/10)	dry ice (-78°C)	2,67
10	PLGA_2	TIPS	10	dioxine/water (90/10)	freezer (-20°C)	1,96
11	PLGA_2	TIPS	20	dioxane/water (90/10)	dry ice (-78°C)	1,38
12	PLGA_3	TIPS	10	dioxane/water (90/10)	dry ice (-78°C)	1,26
13	PLGA_3	TIPS	10	dioxane/water (90/10)	freezer (-20°C)	1,11

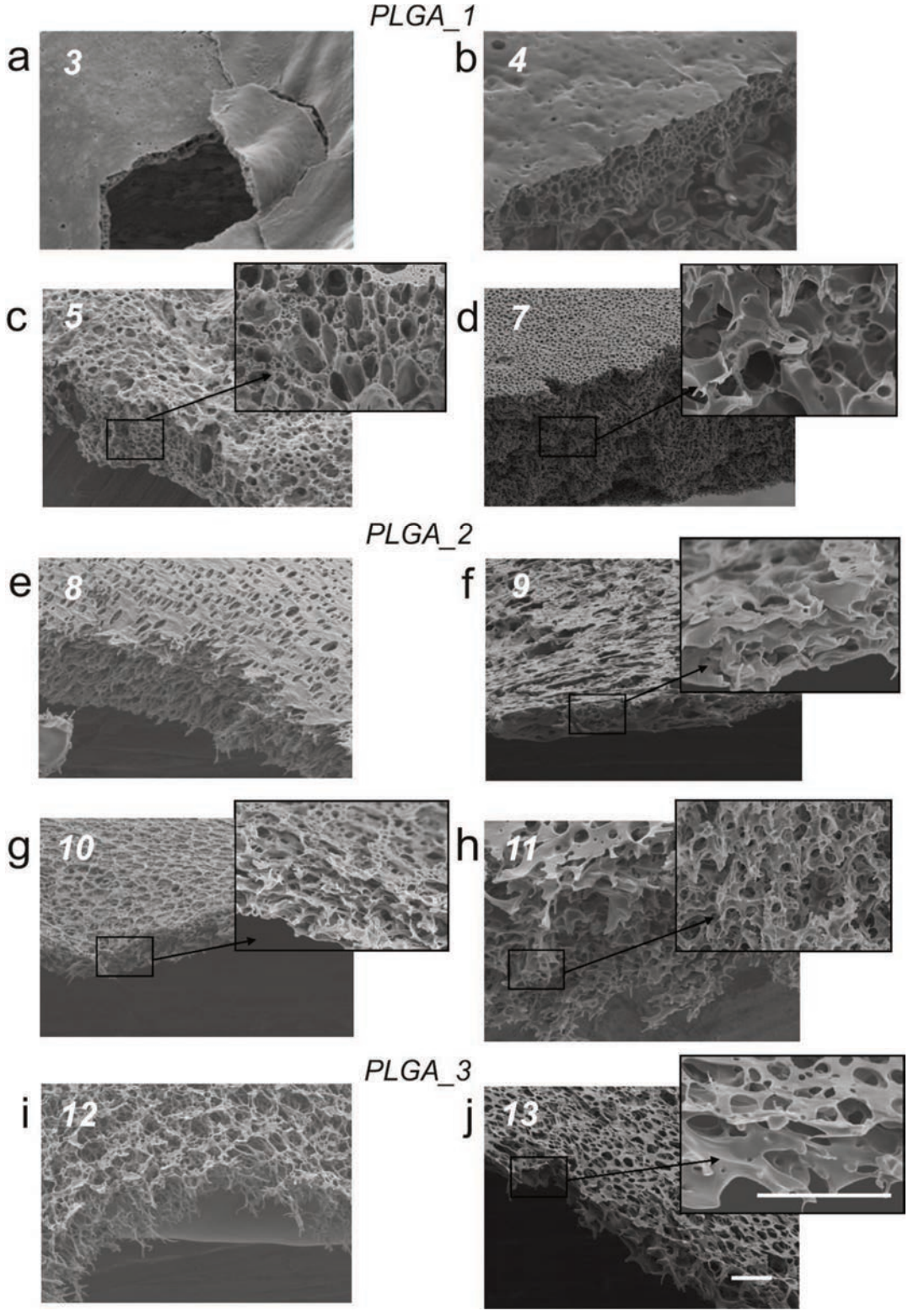

Figure 4.1: Representative SEM images of the cross section and external surface of PLGA foils obtained using different methods and parameters. Numbers represent production method according to table 1. Scale bares represent 20 µm.

Scaffolds morphology was analyzed using SEM and the images obtained are shown in Fig. 4.1. Both the cross section and external surface (skin) of the foils were observed. Since degradation rate of the PLGA copolymers is related to the lactide:glycolide feed ratio and to the molecular weight of the polymer, to create scaffolds with fast degradation rate PLGA_1 copolymer with 50:50 monomers ratio and low molecular weight (M_w) was first used.

Using immersion precipitation method, uniform samples were prepared only by quenching in water. After immersion in methanol or ethanol, samples were shrinking and forming structures with heterogeneous shape (data not shown). Using water as a nonsolvent bath, uniform films were obtained with different microstructures depending on the polymer concentration in casting solution and temperature of the immersion bad. Since membranes immersed in water at room temperature appeared to have an undesirable dense skin layer (Fig. 4.1 (b)), the temperature of the nonsolvent was reduced. Thus, the samples with apparently porous skin were produced (Fig. 4.1 (c)). However, all foils exhibited microcellular morphology with closed cell structures. Pores were not interconnected and thus permeability of the foils was insufficient. In contrast, using TIPS as a production method, foils with open pore network and well-interconnected structure were prepared (Fig. 4.1 (d)). Pores on the surface and in the internal region of the scaffold exhibited high degree of uniformity and a dense surface skin layer was not observed. However, foils produced from PLGA_1 copolymer were very brittle and since the thickness of the foils was below 100 µm, measurement of the permeability was technically not possible due to the fragile nature of the constructs. Thus, for the further experiments, PLGA copolymers with higher M_w were used. Since M_w of the polymer is one of the parameters that affect early stage of the phase separation and can determine the shape and size of the pores and their interconnectivity, all phase separation parameters were tested individually for copolymers with various M_w. The mean pore sizes for different formulations of PLGA foils were approximated by taking measurements of the diameter of pores observed on SEM image. Since our desired pore size and morphology should allow perfusion of fluids while retaining the cells, samples produced from 20% PLGA_2 copolymer quenched in dry ice were used for the further experiments (Fig. 4.1 (h)). The samples have shown interconnected pores with the size ranging from 2 to 4 µm and much less fragility than the samples prepared from PLGA_1 copolymer.

Table 4.2: Spin coating parameters used to produce foils with different thickness. Foils were prepared from 20% PLGA_2 copolymer solution.

Thickness (µm)		Speed of rotation (rpm)	Time of rotation (s)
25	*Step 1*	300	15
	Step 2	600	15
30		500	30
50		300	30

Since casted solutions had different density depending on the type of copolymer used and polymer concentration, speed and time of rotation during spin coating were individually adapted to each solution. Considering the shape and strength of the desired scaffolds, we produced and tested foils with a thickness between 25 µm and 50 µm. Such films were thin enough to form sinusoidal microstructures but thick enough to withstand mechanical stress during thermoforming. Parameters used for the 20% PLGA_2 copolymer solution to produced foils with thickness of 25 µm, 30 µm and 50 µm are presented in Table 4.2. Produced foils were thermoformed and tested again for permeability (Tab. 4.3). The permeability of the foils was determined by the morphology of the porous structure including size, density and distribution of the pores, and the appearance of the skin layer.

Table 4.3: Permeability (P) of the samples as a pressure difference between two sides of a porous foil and theoretical permeability values calculated for the flow of medium. Measurements were made before and after thermoforming under different pressures (p) and temperatures (T).

		Sample								
Step	Sample parameter	1	2	3	4	5	6	7	8	9
1. Pre-process (PLGA foils)	Film thickness [µm]	25	25	25	30	30	30	50	50	50
	Permeability [mbar] air	2.1	1.7	1.1	3.2	1.9	3.1	2.7	3.8	3.3
	Permeability [mbar] cell culture medium	0.12	0.09	0.06	0.18	0.10	0.17	0.15	0.21	0.18
2.Thermoforming	Temperature [°C]	36	40	45	36	40	45	36	40	45
	Pressure [bar]	40	40	60	40	40	60	40	40	60
3.Post-process (PLGA scaffolds)	Permeability [mbar] air	2.9	4.9	3.8	4.9	3.5	9.2	4.7	11.7	8.6
	Permeability [mbar] cell culture medium	0.16	0.27	0.21	0.27	0.51	0.19	0.26	0.65	0.47

4.1.2. Microstructuring process

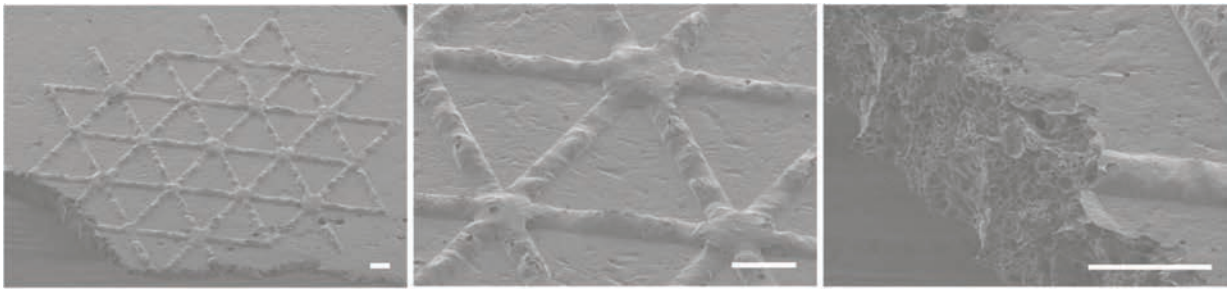

Figure 4.2: Sinusoidal structures formed under 45 °C and 60 bar on foils fabricated from PLGA_1 copolymer. Scale bars indicate 200 µm.

Initially, foils prepared from PLGA_1 copolymer were used for multilayer thermoforming process. However, regardless of the pressure and temperature used, it was not possible to stretch the foils during thermoforming, probably due to high thickness of the foils and fragile nature of the used copolymer (Fig. 4.2). Using foils produced from PLGA_2 copolymer, in a temperature range below the glass transition temperature (T_g) of the PLGA_2 (44-48°C), the minimum pressure causing the formation of microstructures was 40 bar. Starting with these settings, temperature and pressure were gradually increased. To achieve fast degradation rate of the scaffolds and simultaneously provide mechanical support for the cell culture, scaffolds formed from 30 µm thick PLGA_2 foil under 40°C and 40 bar were selected for the further experiments. Selected conditions made it possible to stretch the foils to a desired shape without destroying the primary microstructures and interconnection between the pores (Fig. 4.3). Thus, high permeability of the scaffolds was maintained (Tab. 4.3). The mean widths and depths of the patterned structures were approximated by taking measurements during conventional imaging in the SEM. Sinusoidal channels were formed with depths of 30 µm ± 5 µm and widths of 102 µm ± 2 µm.

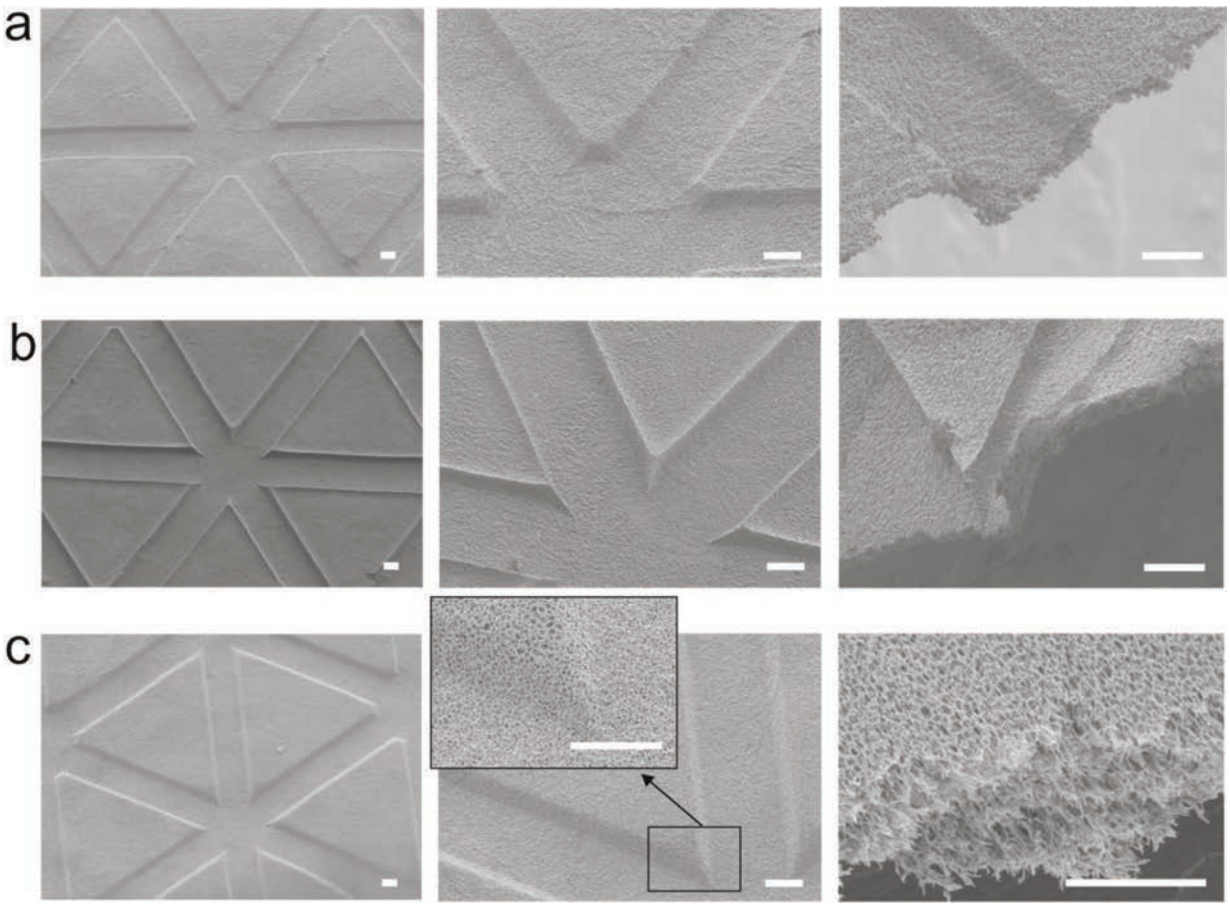

Figure 4.3: Microstructured polymeric scaffolds formed from porous PLGA foils under different parameters: 25 µm thick foil formed under 36°C and 40 bar (a), 30 µm thick foil formed under 40°C and 40 bar (b), and 50 µm thick foil formed under 45°C and 60 bar. Scale bars indicate 25 µm.

4.2 Degradation test

To reveal the relationship between degradation of our microstructured PLGA scaffolds and organization of the cells within the scaffold, viability and morphology of the cultured cells were examined simultaneously with scaffolds morphology. Moreover, to better evaluate the properties and potential of the scaffolds, two different cell types were used.

4.2.1 Cell organization.

Cell attachment and growth were analyzed weekly. The resulting cell number and distribution on the scaffold as well as the cell morphology were evaluated. Fig. 4.4 (a) shows that after 1 week of culture, the surface of the scaffold was covered by thick layer of L929 mouse fibroblast and there existed visible strong cell-cell and cell-scaffold interactions. Similar to the L929, the HepG2 cells stretched and formed confluent monolayers on the surfaces. Homogenous distribution of the cells on the scaffold surface was observed. Growth of both cell types could still be observed on the PLGA scaffolds after a degradation period of 4 weeks, albeit with different cell numbers (Fig. 4.4 (b)).

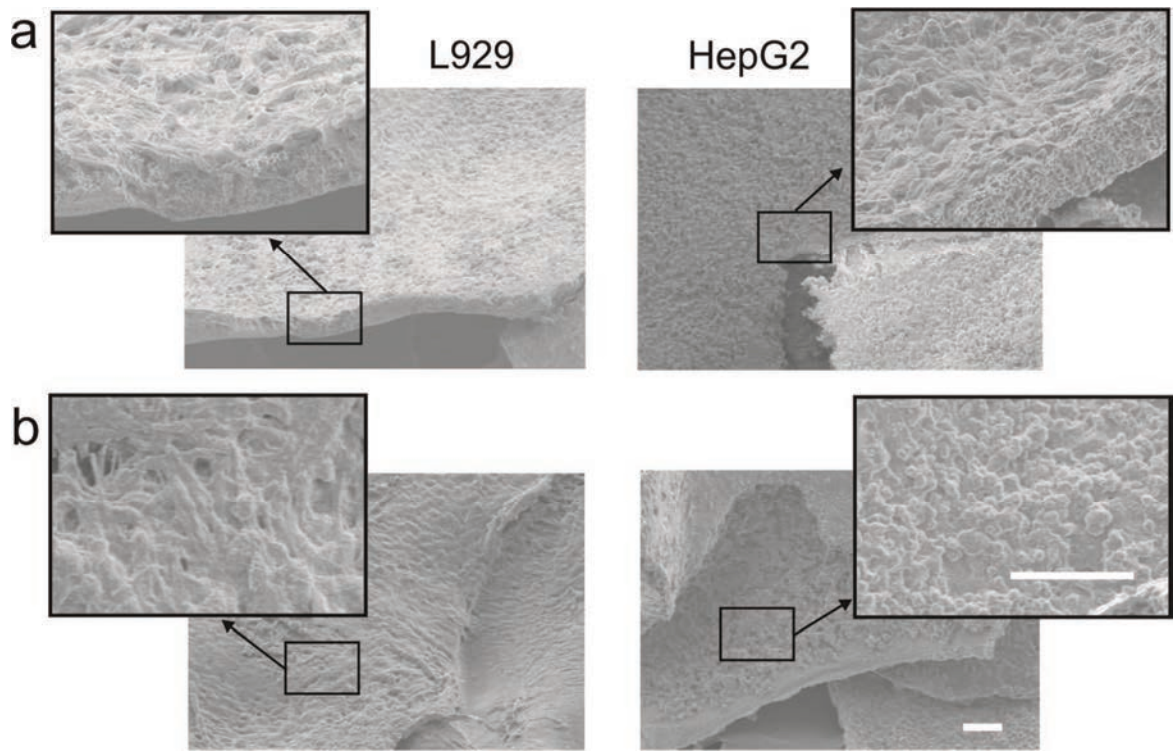

Figure 4.4: SEM images of L929 and HepG2 cells grown for 1 week (a) and for 4 weeks (b) on the microstructured PLGA scaffolds. Scale bars indicate 50 µm.

Starting from a seeding density of 1×10^4 cells per each scaffold side, the total cell number of the L929 cells was found to steadily increase with rapid growth, especially during the first and fourth

weeks of cultivation. Vitality of the cells was usually higher than 90% and improved considerably with the progress of the experiment, thus demonstrating a good biocompatibility of this cell type for the produced scaffolds (Fig. 4.5 (a)). These results also suggested, that degradation products of the scaffolds did not negatively affected the growth of the L929 cells.

Viability of HepG2 cells showed a gradual increase in the first 2 weeks of the experiment but decreased as the cultivation period progressed. In addition, starting from a seeding density of $1x10^5$ cells per each scaffold side, rapid cell growth was observed during first 2 weeks of cultivation. Later on, starting at 3 weeks post-seeding, a significant decrease in cell number was detected (Fig. 4.5 (b)). Since the seeding density of HepG2 cells was higher than the seeding density of L929 cells, this phenomenon could be more attributed to the lack of space for HepG2 cell growth than to the negative effect of scaffold degradation process. Although it was previously shown that viability of the cells cultured in 3D PLGA scaffolds is inversely related to degradation rate, it was dependent on the depth from the upper (seeding) surface to the lower surface. Cells that migrated into the scaffold through the inter-connected porous structure as well as cells on the bottom surface of the scaffold have shown significant decrease in cell viability starting at 2 weeks post - seeding (67). In our system cell growth occurred on the scaffold surface, without penetration of the pores. Moreover, using our insert systems the cells on both sides of the scaffolds were in direct contact with medium. Thus, adhesion of hepatocytes could be more probably inhibited at high concentration in a cell concentration dependent manner. It was observed, that after 3 weeks of culture hepatocytes formed cordlike structures and began to detach from the substrate in large wisps (Fig. 4.4 (b)). Such detachment of cell sheets from the substratum has also been observed in other systems and has been attributed to cell-cell tensions that overcome the cell-substratum tension (249).

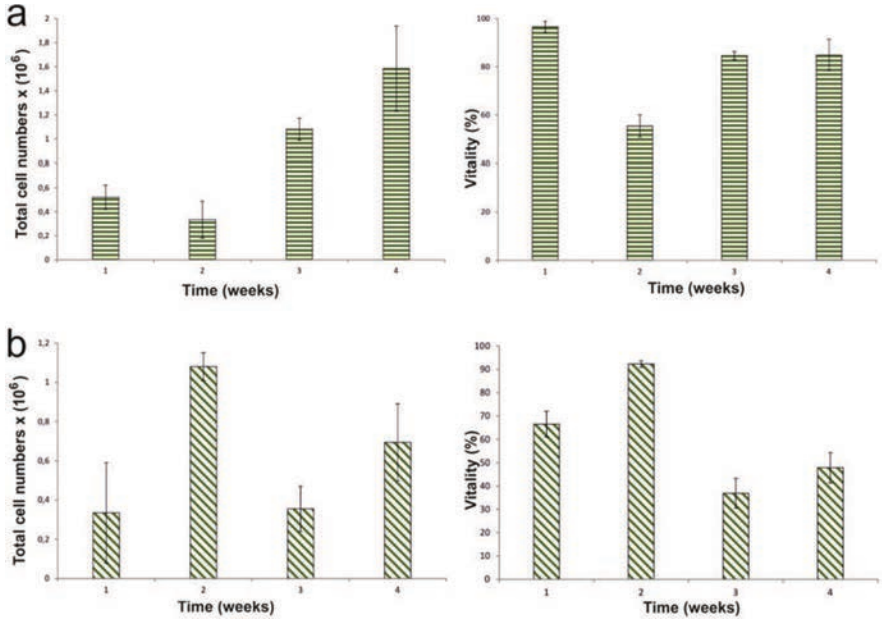

Figure 4.5: Total cell numbers and vitality of L929 (a) and HepG2 (b) cells cultivated on 3D PLGA microstructured scaffolds for 4 weeks. Results are the average of 2 independent tests.

Both cell types were strongly adhered to the scaffold surface and required prolonged treatment with trypsin for adequate cell dispersion. Additionally, to increase cell detachment, aspiration of the cell suspension from the scaffold surface was repeated several times. This could, however, damage the cells and affect lower cell viability. After trypsinization scaffolds were inspected using SEM to ensure whether all cells had been removed from the substrate. However, cell removal was found to be incomplete (Fig. 4.6). L929 cells maintained on the collagen coated PLGA scaffolds were highly spread and flat. The cells showed protrusions on their edges penetrating the pores. HepG2 cells remaining on the surface showed heterogeneous distribution with clusters of cells with high density. The incomplete cell removal from the scaffold surface could also be one of the reasons for the reduced number of HepG2 (Fig. 4.5 (b)), which was observed at 3 weeks post-seeding. One of the possible explanations for this phenomenon can be ingrowth of cells into gradually degraded substrates. Surface micro-scale topography may also play a role. On the scaffold surface pores up to 2 µm in diameter were observed (Fig. 4.8). Moreover, very high pores density was noted. Such micro-scale texture of a scaffold surface can significantly affect behavior of cells and enhance cell adhesion (261).

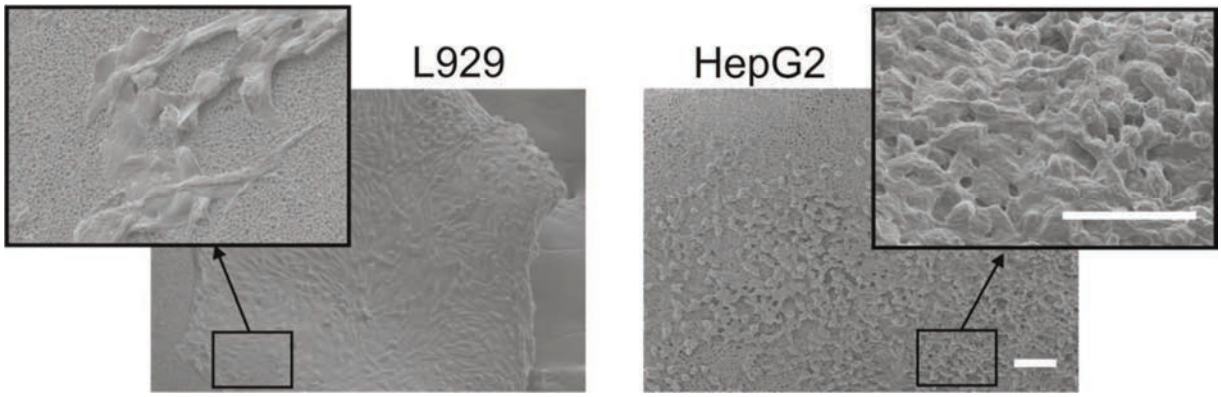

Figure 4.6: Cells remaining adhered to the scaffold surface after trypsinization. Before trypsinization cells were cultured on the scaffold for 1 week. Scale bars indicate 50 µm.

4.2.2 Degradation of the scaffolds

In cell culture medium scaffolds have kept their structural integrity and provided an appropriate supports for cell culture over the entire duration of the experiment, despite high porosity of the scaffolds as well as conditions during cell culture such as “wet” environment, temperature of medium close to T_g of PLGA or ethanol treatment as a sterilization method are known to decrease mechanical properties of this polymer (71). However, if the samples were taken out of the medium after 1 week of experiment, the films became fragile and tended to collapse causing the viscous liquid to escape from inside. At this stage of degradation first changes in the scaffold morphology were also observed (Fig. 4.7). Micropatterned structures were hardly visible. Scaffolds gradually collapsed and have shown first evidence of physical disintegration.

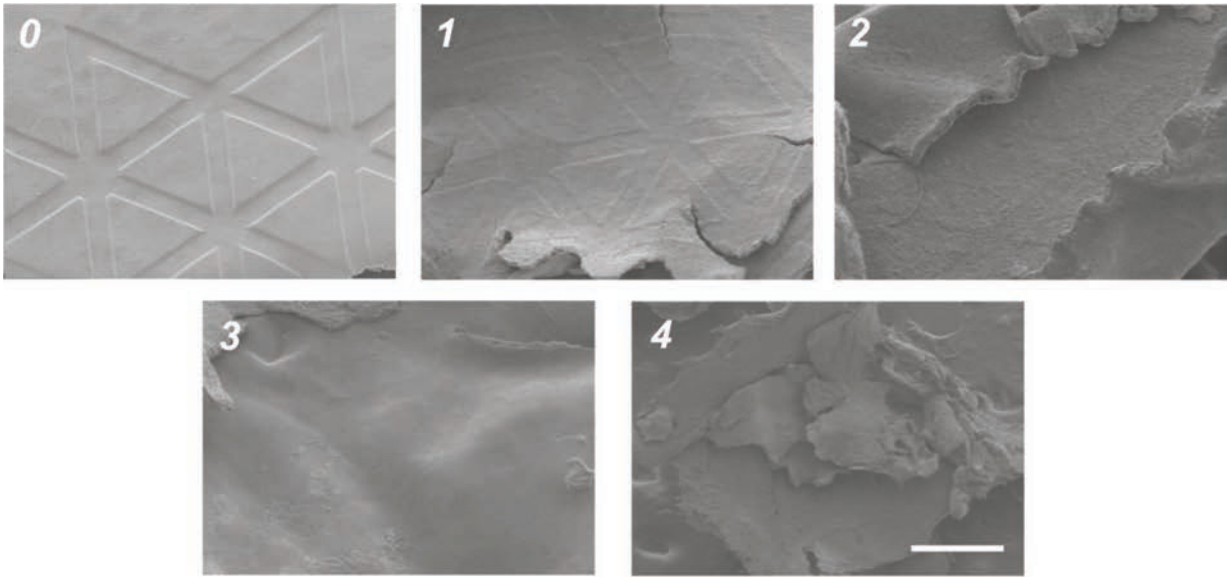

Figure 4.7: Representative SEM mages of the time-dependent morphological changes during PLGA scaffold degradation under cell culture. Numbers represent weeks of incubation. Scale bare indicate 500 µm.

After 2 weeks overall shrinkage and wrinkling was observed. From week 3 onwards sinusoidal pattern disappeared completely. It can be seen that scaffold started to disintegrate after 4 weeks and thickness of the scaffolds was visibly reduced. One of possible explanation can be shrinkage of polymer chains. The PLGA_2 copolymer had a glass transition temperature of 44-48°C. Moreover, it is also possible, that thermoforming process lowered the glass transition temperature of PLGA similar to other processing methods. Thus, thermoformed scaffolds could have glass transition temperature very close to the temperature of cell culture medium during incubation (37°C) and thus the polymer chain mobility increased dramatically after being incubated in medium. Additionally, because of high surface to volume ratio in the microporous surface, the initial water content of the PLGA scaffold was very high. Consequently, under such incubation conditions the relaxation of extended amorphous chains near T_g could cause a large dimensional change in the form of shrinkage (262).

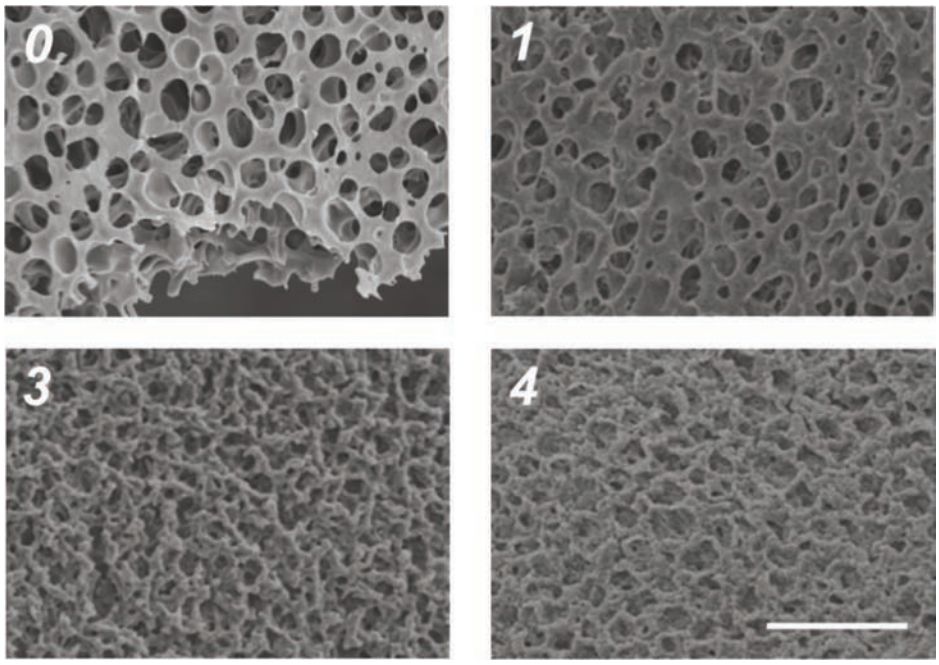

Figure 4.8: Representative SEM images of the surface of the PLGA scaffold during degradation under cell culture at different degradation times. Numbers represent weeks of incubation. Scale bare indicate 10 μm.

Figure 4.8 shows changes in the morphology of the pores as a function of degradation time. Changes in pores morphology were found to be relatively low during first 7 days of degradation. Pores showed oval shape similar to this at the beginning of experiment. However, after 3 weeks in cell culture shape and size of the pores was significantly changed. The microporous structure seemed depleted and ‘‘pitting’’ appearance was noticed. This suggests that large degree of degradation on the scaffold surface had occurred.

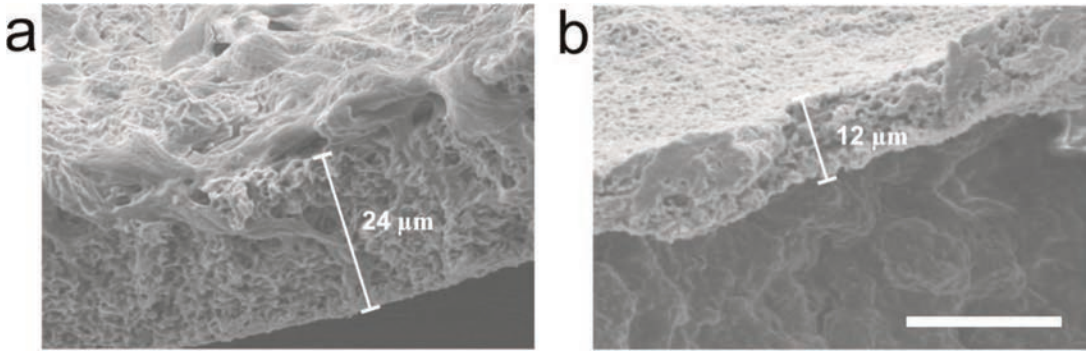

Figure 4.9: Cross-section of the PLGA scaffolds after 1 week (a) and 4 weeks (b) degradation under cell culture. Scale bar indicates 20 μm.

Despite different morphological changes were noted and the thickness of the scaffold was reduced, scaffolds did not completely degraded. The thin microporous polymer substrate was observed between upper and lower cell layer at each follow-up time (Fig. 4.9), blocking the direct physical contact between the cells on the opposite sides of the scaffolds and forming a barrier for direct cell-cell contacts. Such insufficient degradation rate could be at least in part due to relatively high thickness and high porosity of the produced scaffolds. PLGA has been shown to degrade mainly by simple hydrolysis of the ester bond into acidic monomers. Degradation products may serve as catalysts for the reaction of hydrolysis and enhanced autocatalysis in those scaffolds, which are unable to evacuate acidic degradation by-product (263). In scaffolds with higher porosity and permeability the diffusion of degradation products will be facilitated and their rate of degradation will be slower. Most of the carboxyl end groups generated by hydrolytic cleavage may have been able to escape from the matrix along with short soluble chains due to the large surface area. Therefore, it can be also expected that scaffolds placed in bioreactors under flow conditions would have even slower degradation rate compared to those under static conditions (264). Dynamic flow can wash away acidic byproducts and thus reduce the buildup of the acidic local pH in the scaffold.

5. Patterning of microporous polymer scaffolds for directed cell adhesion and growth

In the past decades, many studies have been conducted to develop accurate and experimentally tractable *in vitro* liver model system. Although varieties of 2D or 3D liver models have been designed to date, a perfusable, microscale, biomimetic co-culture system with vascular network is still missing. In response to these demands our group has developed a novel *in vitro* liver model that replicates 3D liver lobule - like microstructures and is integrated within microfluidic platform (chapter 1.6). The key component of our model is a microporous scaffold, which should be able to support directed 3D co-cultivation of liver cells concomitantly allowing microfluidic circulation.

In previous chapter it was shown that microthermoforming technique can be efficiently used for production of microporous scaffolds mimicking basic liver architecture. However, another big challenge in the reconstruction of the microarchitecture of liver lobule *in vitro* is optimal attachment of the liver cells on the microstructured substrate. Especially, directed adhesion and growth of the endothelial cells inside the sinusoidal capillaries is essential in mimicking basic liver structures. Nevertheless, despite micrometer-scale biochemical patterning methods are commonly used to guide the cell attachment and growth on 2D surfaces, the ability to combine chemical patterns with 3D topography of polymer scaffolds into an integrated characteristic still remains a technical challenge. In this chapter various technical solutions for directed patterning of microporous polymer scaffolds are presented and the applicability of the patterned substrates to control 3D arrangement of cells at the microscale level is evaluated.

Developing new patterning techniques demand for the screening of many test parameters and rapid evaluation of the results. Therefore the focus in this study lies on the coating and patterning processes in the context of thermoforming. However, microporous PLA and PLGA foils presented in preceding chapters could not be considered as test materials for optimization purpose because their fabrication and parameter evaluation is intensively time consuming. Therefore, instead of precious self-made material, a commercially available microporous PC substrates were used. PC foils were chosen as our model material for the developing of the new approaches for micropatterning also due to high transparency, good form stability and low material cost as compare to the PLA and PLGA polymers.

5.1 Patterning of the scaffold surface

5.1.1 Nonpatterned scaffolds

Microporous polymer scaffold with sinusoidal structure were successfully produced from microporous PC foils using multilayer microthermoforming process (Fig. 5.1 (a)). Subsequently, L929 cells were seeded on the top side of the scaffolds and examined for preferential adhesion. To mimic basic structure of the liver lobule on the scaffolds cell adhesion should be directed and limited only to the channels. However, since unprinted polycarbonate has low surface free energy and shows relatively low cell attachment (77) the cells seeded on the native PC surface remained

mostly unattached and were removed during medium exchange. In contrast, cells seeded on the PC scaffold homogeneously coated with ECM molecules have shown irregular distribution and were attached mostly on the surface between the channels (Fig. 5.1 (b)). Thus, to achieve directed cell adhesion inside the thermoformed channels, scaffolds were patterned using various physical and chemical methods (Tab. 5.1) allowing controlled transfer of bioactive molecules inside of geometrically restricted sinusoidal channels.

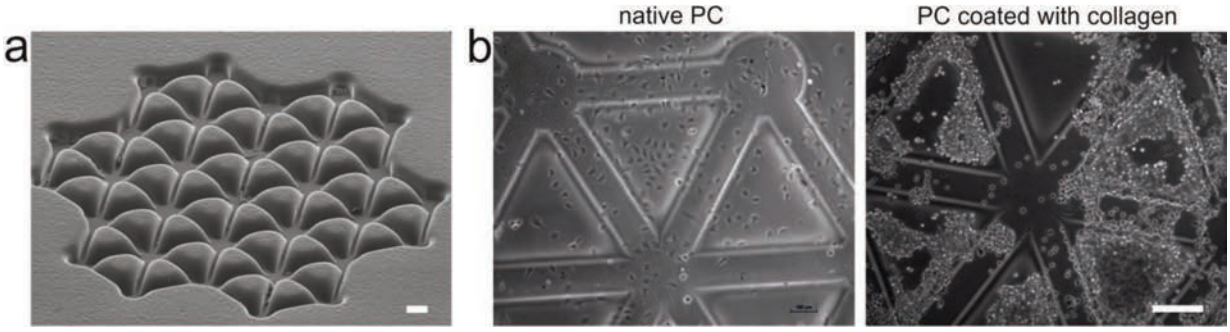

Figure 5.1: SEM image of 3D PC scaffold with sinusoidal structure manufactured by multilayer thermoforming technique (a) and cell adhesion preference to the native surface of the PC scaffold and to the PC scaffold homogeneously coated with collagen (b). Scale bars indicate 100 µm.

5.1.2 Patterning after microstructuring

Different patterning approaches were first applied on 2D PC foils and examined for directed cell adhesion. Subsequently, selected techniques were adapted to 3D surface of polymer scaffolds. Two different strategies were used to localize cells on the PC scaffolds: regional modification of the channels surface that promote cell adhesion or creation of nonadhesive domains on the area between the channels (Tab. 5.1).

Tab. 5.1: Different methods used for patterning of 2D PC foils and/or 3D PC scaffolds. Patterned samples were tested for directed cell adhesion: (+) means directed cell adhesion, (-) means random cell adhesion or no cell attachment on patterned surface and (+ / -) means partially directed cell adhesion.

	Method	Result	
		2D surface	3D scaffold
Patterning of adhesive regions	Plasma treatment	+	-
	µCP of PEI	+	-
	µCP of ECM molecules	+	-
	Microfluidic printing (µFP)	Not tested	-
Patterning of nonadhesive regions	Inverted µCP with Pluronic®	+	+ / -
	Inverted µCP with agarose	Not tested	-
	Inverted µCP with PNIPAM	Not tested	-

On plasma-treated 2D PC foils marked differences in cell adhering ratio were observed between modified and un-modified PC surface. Attachment and growth of L929 cells on plasma treated areas was improved drastically in comparison with untreated PC surface and the cells were spread well (Fig. 5.2 (a)). Since plasma treatment lowers the surface energy of PC, temporarily increasing their wettability, hydrophobic polycarbonate sheet became more hydrophilic and thus more suitable for cells adhering. Wettability of the PC surface after the plasma treatment was determined by water contact angle measurements (Tab. 5.2). The best cell adhesion was achieved on samples with moderate wettability represented by contact angle between 40-45°.

Table 5.2: Wettability of the PC surface determined by water contact angle measurements. Samples were treated with oxygen plasma under different power and exposure time.

Power [W]	0	2	2	5	5	10	10	15	20	40	50	100	150	500
Time [s]	0	10	30	5	30	10	30	30	30	40	120	30	30	30
Contact angle H_2O [deg]	76.2	45.2	46.7	41.5	46.4	40.1	41.6	36.3	33.7	33.8	32.0	25.5	7.0	0.0

Notable differences in cell adhering ratio were also noted on PC surface partially printed with Pluronic®. Contrasting cell attachment was observed between surface area printed with cell repellent and area with attracting collagen coating. Cells adhered well on the surface coated with collagen, while rounded cells on the area modified with Pluronic® were preferentially removed following the medium exchange. The best cell repellent properties were achieved after inverted μCP with 5 g/L solution of Pluronic® (Fig. 5.2 (b)).

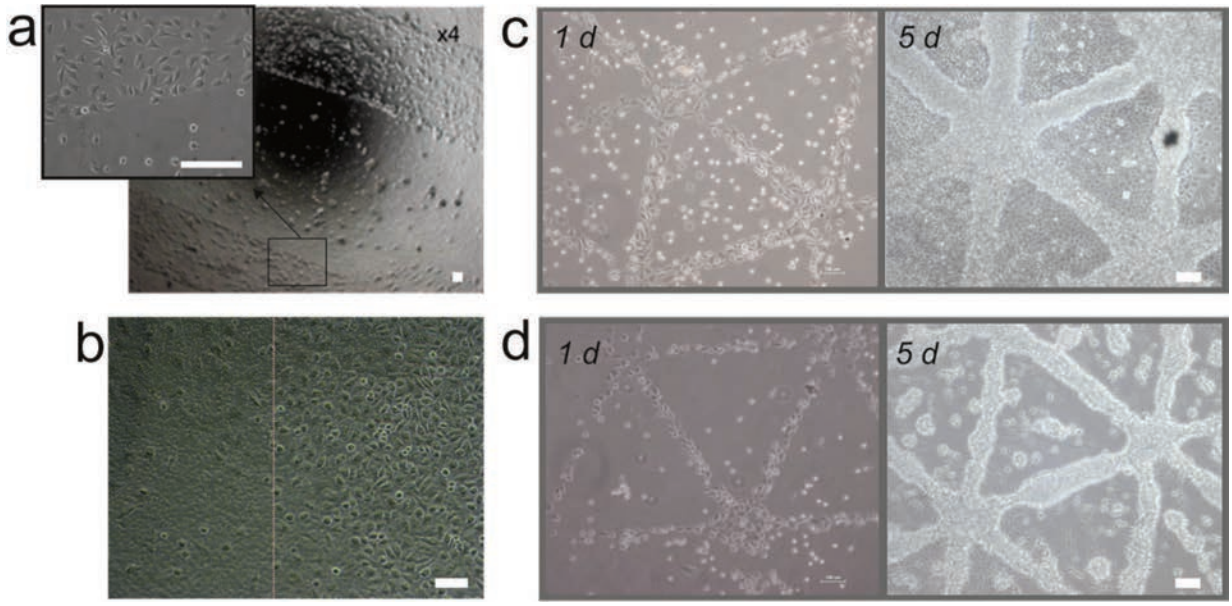

Figure 5.2: Cell adhesion preference. Representative images of L929 cells attached to the patterned regions of the PC foils after 1 day (a,b) and 1 and 5 days (c,d) in cell culture. Foils were patterned using plasma treatment (a), inverted μCP with Pluronic (b), conventional 2D μCP with PEI (c) and 2D μCP with collagen (d). Scale bars indicate 100 μm.

Also conventional μCP was successfully used for the guiding of cell adhesion and outgrowth on the 2D PC foils. Cell attachment was limited to surface that has been patterned with polyethylenimine (PEI) or ECM molecules (Fig. 5.2 (c) – (d)). Despite unpatterned areas were not passivated, cell attachment was confined to the sinusoidal structures even after 5 days and only small amount of cells were observed on unpatterned background.
However, although different patterning approaches were successfully applied on 2D PC surface, those techniques adapted to 3D surface of PC scaffolds were ineffective. On scaffolds treated with plasma no differences in cell attachment was observed. Single rounded cells were randomly distributed on scaffold surface (Fig. 5.3 (a)). These results indicate that despite microporous polymer structure and through - holes at the end of the channels, plasma was not successfully introduced into the channels. Similar results were observed for scaffolds patterned using the MIMIC method. Despite coating solution was successfully driven by capillary forces and moved into the channels, fluid gradually leaked through the microporous structure of the scaffold. Thus, the collagen was not allowed to adsorb onto the surface of the channels. On scaffolds printed using inverted μCP methods partially directed cell adhesion was observed only on samples printed with Pluronic® (Fig. 5.3 (c)). However, due to inhomogeneous topographical structure of the scaffolds, Pluronic® was applied inaccurately on the desired surface. In contrast, on scaffolds patterned with agarose or PNIPAm only rounded and randomly distributed cells were observed (Fig. 5.3 (b)). Cell repellent substrate was probably applied not only on surface between the channels, but also inside the 3D structures. Thus, cell adhesion was inhibited over the entire scaffold surface. Also conventional μCP method was not suitable for patterning of microthermoformed PC scaffolds. Since the 3D sinusoidal structures formed on the PC surface are in micrometer range, appropriate adjustment of the PDMS stamp to the scaffold microstructure and selective μCP of cell adhesive domains inside 3D channels manually was impossible.

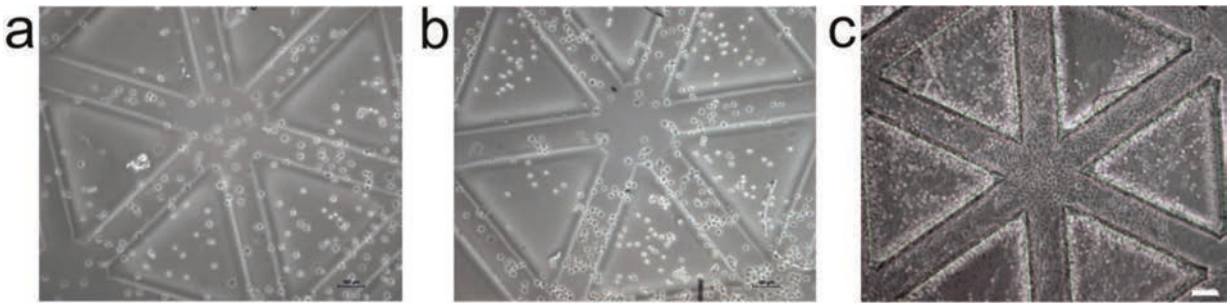

Figure 5.3: Cell adhesion preference. Representative light microscope images of L929 cells attached to the patterned PC scaffold after 24h in cell culture. Scaffolds were patterned using plasma treatment (a), inverted μCP with PNIPAm (b) and inverted μCP with pluronic (c). Scale bars indicate 100 μm.

5.1.3 Simultaneous patterning and microstructuring

Since patterning methods applied after scaffold microstructuring were ineffective, a novel method enabling chemical patterning of polymer surface during thermoforming process was developed. This method is based on the principles of microcontact printing and is intendent for production of patterned 3D polymer substrates, including microporous materials. Thus, we defined it as 3DμCP

technique. The fabrication process for creating scaffolds with chemical and topographical guidance cues using 3DμCP method was shown in Figure 2.4. Appropriate protein concentrations were selected according to protocols of μCP described in the literature (129, 265, 266). However, unlike to conventional microcontact printing, the stamp was not exposed to the protein solution for inking of the entire surface. In order to transfer the ECM proteins exclusively on PDMS stamp features, stamp was placed on the protein-coated glass slice that mediates the transfer of the biomolecules. Thus, using inverted μCP, the proteins were transferred only to the parts where the ink was needed for the subsequent thermoforming process, while the stamp features were not exposed to the capillary forces or swelling (267).

5.1.3.1 Characterization of the surface topography

Thermoforming of PC foil with an elastomeric master turned out to be a reliable method to form up to six micropatterned PC scaffolds during one thermoforming cycle. Since PDMS-based thermoforming mold offers high elasticity, master was simply removed after forming process, preventing damage to the sample or PDMS features. In principle 3DμCP technique was invented for microstructuring scaffolds that mimic basic architecture of liver lobule. However, to better show the potential of this new method, microchannel pattern utilized was first chosen for its illustrative potential. The surface profile of the produced scaffolds was measured and subsequently compared with the designed size and the PDMS master (Tab. 5.3). All samples obtained from this high-throughput production were highly reproducible.

Table 5.3: Pattern size fidelity according to designed size and PDMS master measured using a laser scanning digital microscope.

Designed size		PDMS stamp		PC foil	
Height	Width	Height	Width	Height	Width
30 µm	30 µm	28.39 ± 0.10 µm	28.91 ± 0.10 µm	20.90 ± 0.71 µm	32.05 ± 1.54 µm
50 µm	45 µm	47.18 ± 0.57 µm	43.47 ± 1.15 µm	25.56 ± 4.11 µm	46.32 ± 0.86 µm
50 µm	60 µm	48.62 ± 0.39 µm	61.77 ± 2.66 µm	30.14 ± 0.36 µm	61.24 ± 0.45 µm
75 µm	100 µm	78.76 ± 0.29 µm	105.77 ± 1.28 µm	60.75 ± 1.33 µm	111.06 ± 1.67 µm
75 µm	200 µm	78.88 ± 0.12 µm	206.47 ± 2.86 µm	68.38 ± 0.26 µm	212.51 ± 2.77 µm
75 µm	400 µm	77.46 ± 0.24 µm	405.96 ± 1.57 µm	76.36 ± 2.18 µm	412.34 ± 1.34 µm

The thermoformed foils fully replicated both the height and width of the stamp features with larger dimensions. Measurement of the samples with smaller channels showed less precise reproduction of height of the formed structure, probably due to high foil thickness in relation to master feature height. High shape fidelity was noted for all analyzed scaffolds, indicating no deformation or displacement of the stamp during microstructuring. It was, however, not possible to form features with respect to a ratio (high/width) higher than 2. Exceeding this ratio, the forming pressure

exerted too much stress on the elastomeric structure and caused them to collapse and generate defects in the patterns.

5.1.2.2 Characterization of the patterned ECM molecules

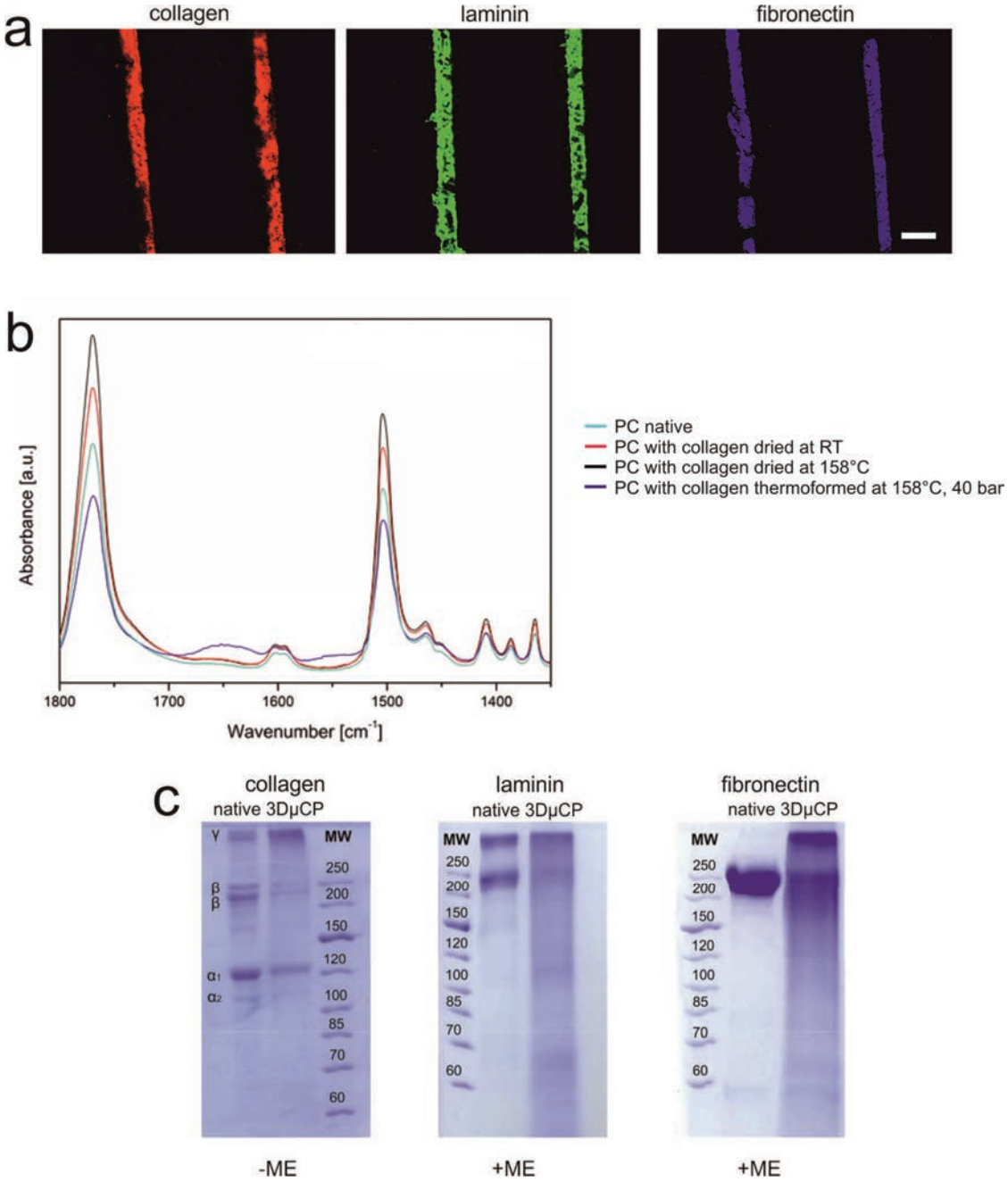

Figure 5.4: Examination of ECM proteins after 3DμCP process: micropatterned PC samples with 45 µm bright channels stained using protein specific antibody (a), ATR-FTIR spectra measured for PC foils coated with collagen under different conditions (b) and SDS gel electrophoresis and Coomassie staining of ECM in native conformation and after thermoforming (c). Collagen was separated under non-reducing conditions (-ME) and laminin and fibronectin under reducing conditions (+ME). ME: ß-mercaptoethanol, MW: molecular weight. Scale bar indicates 100 µm.

Collagen, laminin, and fibronectin were successfully transferred from the PDMS stamp features onto the surface of PC during the thermoforming process. Proteins were selectively patterned on the scaffolds and the localization of printed biomolecules was confirmed by immunofluorescence staining (Fig. 5.4 (a)). Immuno-labeled collagen, laminin and fibronectin were visualized exclusively on the bottom of the thermoformed channels.

The 3DμCP method obviates the use of organic solvents and does not lead to any cytotoxicity, however; high forming temperature was used during microstructuring process. Since in some cases cell attachment to thermally denaturated ECM was previously shown to be as good as or better than to native molecules (268, 269), before biological characterization patterned molecules were additionally characterized.

Although denaturation of native hydrated collagen in physiological conditions occurs at 65°C (± 10°C), in a dry environment the conformational change of the collagen molecules from a triple helix to a random coil was detected first at 220°C (± 10°C). This temperature has been referred as the denaturation temperature of the dehydrated collagen (270). Moreover, collagen fibrils in dry conditions have been shown to maintain their native structure even after 90 min of heating (271). Taking this into account, the conditions used for the microthermoforming, where dry proteins were used, may be considered as mild which do not denature the collagen molecules. Since collagen pattern was immunostained by using a conformation dependent antibody that does not develop with thermally denatured molecules, obtained results indicate that after 3DμCP treatment native collagen structure was present on the thermoformed surface. However, partial denaturation of collagen and small amounts of gelatin, if present, could not be shown using these fluorescence staining. Therefore the presence of intact collagen particles after 3DμCP was additionally shown using SDS-PAGE analyzes (this experiment was designed, performed and analyzed by Dr. Dana Brauer, department of Nanobiosystem Technology, TU Ilmenau). The obtained results confirmed that collagen remained intact after thermoforming. SDS PAGE of patterned collagen of 3DμCP samples revealed the presence of all collagen subunits: α1-, α2-, β-, and γ-chains were still detectable (Fig. 5.4 (c)). The presence of collagen molecules on PC surface after thermoforming process was also examined by the analysis of ATR-FTIR spectra (Fig. 5.4 (b)) in collaboration with the Institute for Biomaterials at University of Erlangen-Nuremberg. In samples with patterned collagen as well as in nonpatterned samples it was possible to notice the prevalence of all the main bands ascribable to PC substrate. The presence of collagen was demonstrated by two weak bands at 1650 and 1555 cm^{-1}, ascribable to amide I and amide II vibrations, respectively.

After 3DμCP with laminin and fibronectin, these patterned molecules could also be recognized by antibodies. However, SDS-PAGE analyses of laminin and fibronectin under reducing conditions showed a partial decomposition of these proteins in a non-dry state. It can be assumed that these conditions do not represent the 3D state of the proteins in a dry and non-reducing environment. These results could be assigned to the application of the reducing agent mercaptoethanol and, as a consequence, to a breakdown of the protein after dissolution of disulfide bridges.

5.2 Biological characterization.

5.2.1 Scaffolds with different geometry.

To evaluate the potential of the patterned surface for guided adhesion of the cells, EA.hy926 cells were seeded on 3DμCP patterned scaffolds with collagen and examined for preferential adhesion and pattern recognition.

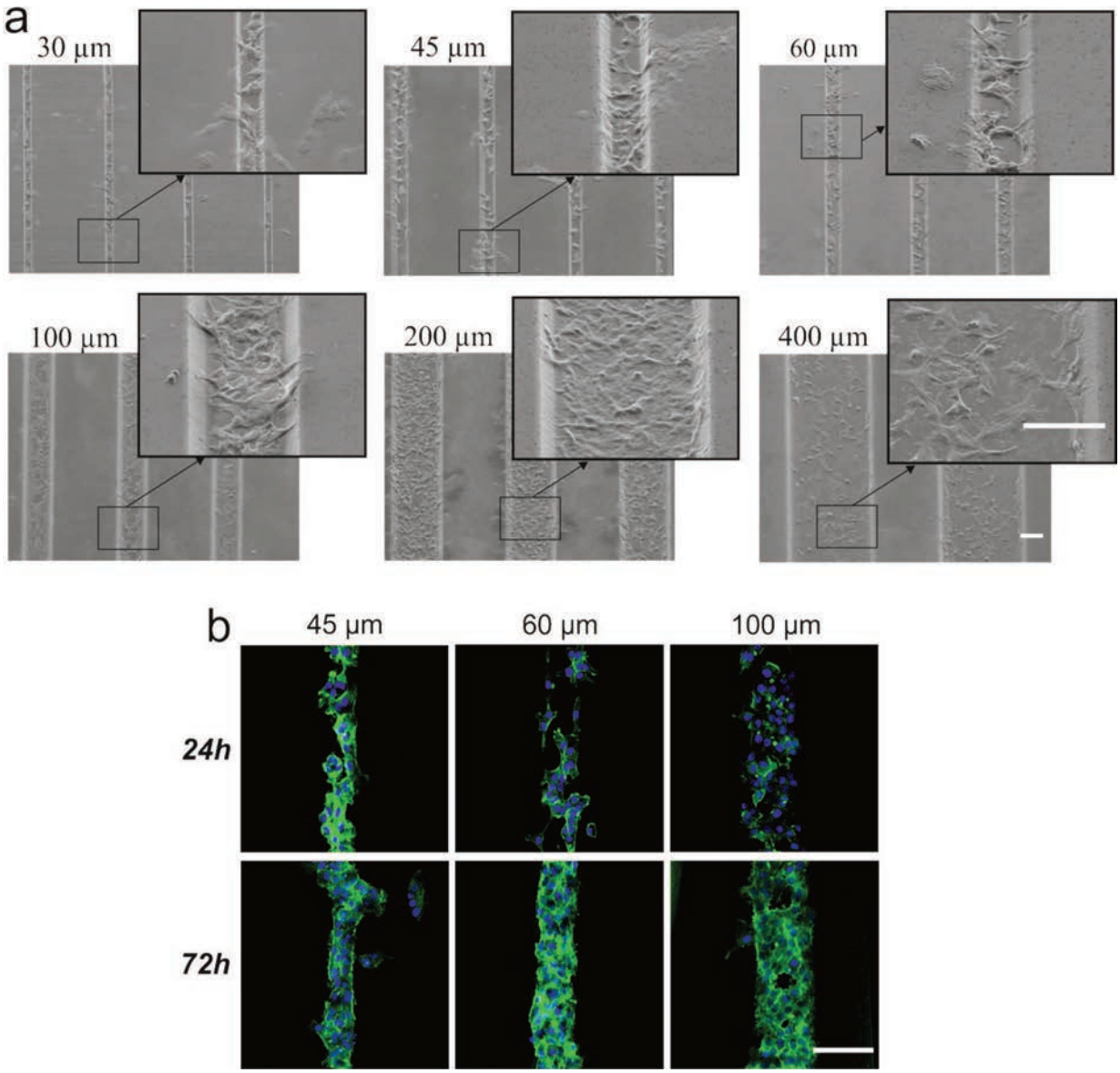

Figure 5.5: Cell adhesion preference to PC scaffolds 3DμCP patterned with collagen: representative phase contrast images of EA.hy926 cells attached to the samples with 30, 45, 60, 100, 200 and 400 μm width channels after 24 h in cell culture (a) and actin cytoskeleton staining of cells cultured on samples with 45, 60 and 100 μm width channels for 24 and 72 h. Samples were stained for actin fibers (green) and nuclei (blue). Scale bar indicates 100 μm.

After 24 h cells were found preferentially attached to patterned regions of the PC surface (Fig. 5.5 (a)). On the scaffolds with wide patterns (200 and 400 μm), cells adhered uniformly within the channels and showed an elongated and frequently flattened morphology. Cell binding was limited to the patterned regions and no cells were found between the channels. Samples with narrow channels (30, 45, and 60 μm) have shown more irregular cell distribution. However, the intervals between the patterned structures were identical for all tested samples. In consequence, surface available for cell adhesion was much smaller for scaffolds with narrow channels. The cells situated outside the channels remained mostly unattached and were removed during medium exchange.

Additionally, EA.hy926 cells adhered on the scaffolds with different dimensions of channels were stained for actin cytoskeleton and subsequently visualized using confocal microscopy (Fig. 5.5 (b)). Thus, cellular organization induced by scaffolds morphology could be better determined. At the beginning of the experiment, cells were individually distributed within the channels. However, after 72 h cells contracted into oligocellular structures and extended chains of cells were observed along the formed channels. 3D form of the patterned scaffolds provides another dimension for external mechanical inputs and thus could generate cell polarization and interaction of the neighboring cells (272). On the 3DμCP patterned scaffolds the surface chemistry provides chemical attraction and repulsion for regulating cell adhesion, while the topography provides additional geometrical limitation for controlling cell arrangement and growth. Additionally, porous structure of the scaffolds could ensure more effective oxygen diffusion and nutrient transfer to the bottom parts of the channels.

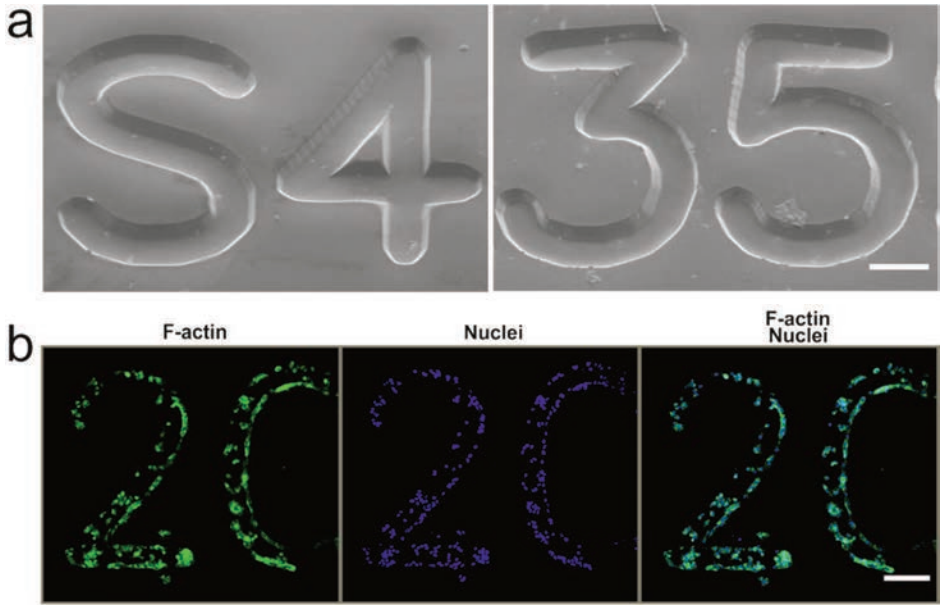

Figure 5.6: PC scaffolds with 3DμCP patterned channels of irregular shape: SEM images of thermoformed surface (a) and DAPI staining, F-actin staining, and merged images of Ea.Hy926 cells cultured into scaffolds for 24 h (b). Scale bars indicate 200 μm.

Apart from channel formation, 3DμCP method allows the generation of more complex free-form geometries. In order to test how the cells attach to the patterned surface with irregular shape, samples with 100 μm width channels with rounded and sharp angles were fabricated. The patterns in the shape of different numbers were chosen for their illustrative potential (Fig. 5.6 (a)). Scaffolds were seeded with cells and examined for cellular adhesion and organization. As shown in Figure 5.6 (b) cell attachment was restricted to the patterned channels. When the shape of the printed structure was changing, the cells were also aligning parallel to the direction of the channel. Mostly they preferred the adhesion to the lateral walls of the channels.

5.2.2 Scaffolds patterned with different ECM molecules.

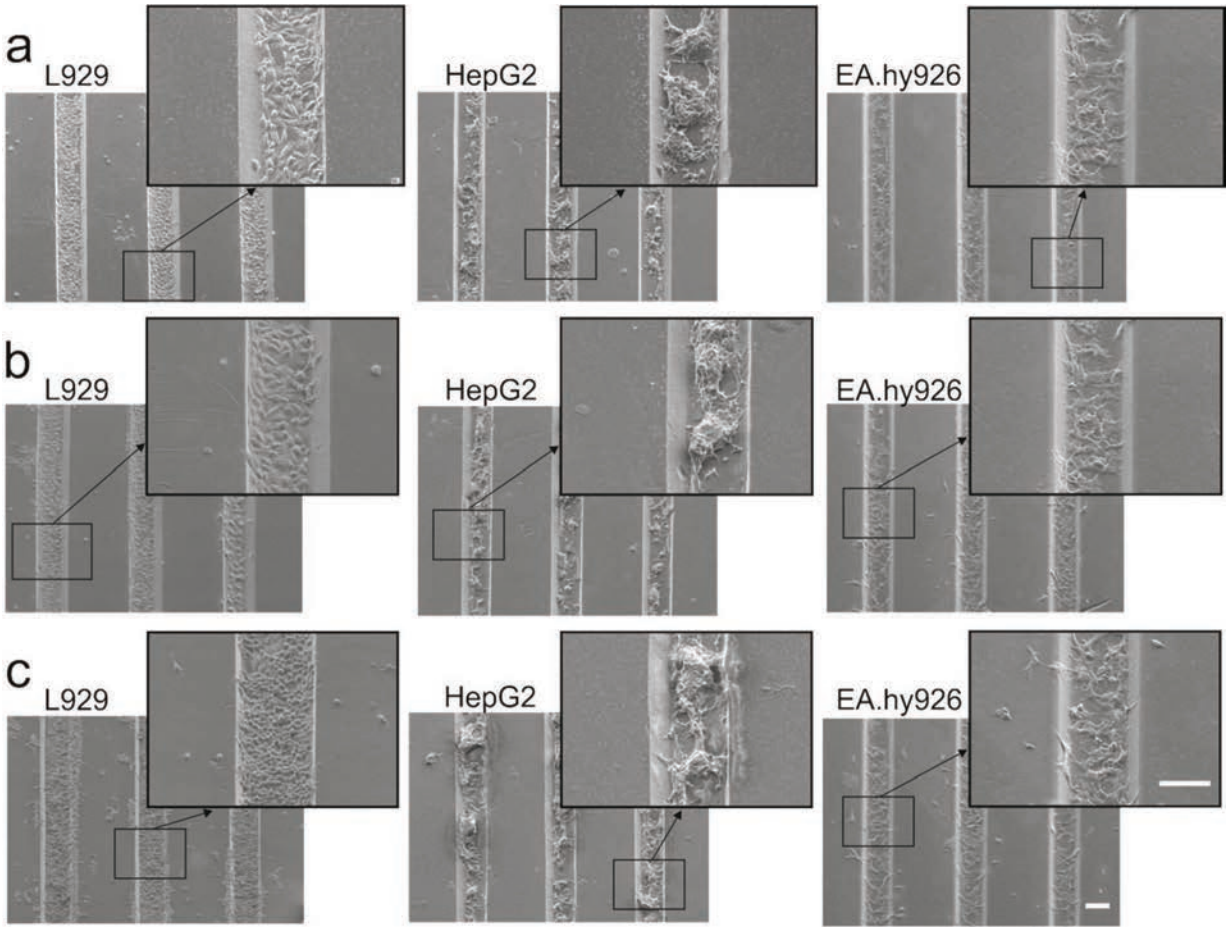

Figure 5.7: Cell adhesion preference to the scaffolds patterned with different ECM molecules. Representative phase contrast images of L929, HepG2, and EA.hy926 cells attached to scaffolds with 100 μm width channels printed with collagen (a), laminin (b) and fibronectin (c) after 24 h in cell culture. Scale bars indicate 100 μm.

To study the adhesion of the cells to PC surface printed with different ECM molecules, cells were seeded on samples 3DμCP patterned with collagen, laminin or fibronectin and examined for pattern recognition. Moreover, to better show the potential of our method for different biological

applications, various cell types were tested. As shown in Figure 5.7, cell attachment occurred preferentially on the patterned regions. For endothelial, fibroblast and hepatoma cells adhesion was restricted to the channels, and only a few cells were observed on nonprinted surfaces. Similar results were obtained for each cell type seeded on the samples patterned with three different ECM molecules.

However, depending on the type of the used cells different cell distribution was observed in the channel. EA.hy926 and L929 cells attached evenly to the printed areas forming a single layer of cells. In contrast, HepG2 cells presented more irregular morphology and some cell aggregates were formed. Despite of those differences, cell adhesion and growth were limited to the patterned channels for all three cell types as well as for the samples patterned with three different ECM molecules. All ECM molecules were recognized by the cells.

These biological results indicate great potential for further use of the 3DμCP method in various fields of modern biotechnology

6. Directed 3-dimensional co-cultivation of hepatic cells on 3DμCP patterned scaffolds.

On scaffolds patterned using 3DμCP method directed cell attachment and growth was observed for different cell types and independently from scaffolds architecture. Additionally, it was shown that more complex geometries could be implemented as well. This opens promising perspectives for biofabrication of 3D polymer scaffolds with native tissue-like morphologies. In the current chapter we use 3DμCP method to produce microporous scaffolds with chemical and topographical guidance cues that replicate key structures of liver sinusoids. We explore the possibility to control well-organized hepatic cell composition by co-culturing the cells on opposite sides of the patterned scaffolds and subsequently to replicate 3D liver microstructure by arranging the patterned substrates in layered configuration.

6.1 Surface Fabrication and Characterization

To establish the radial pattern of liver lobule, PDMS molding tool with features inspired by the morphology of the liver lobule was designed. Thermoforming of PC sheets with such elastomeric master turned out to be a suitable technique to form micropatterned scaffolds with sinusoidal structures and microporous surface (Fig. 6.1). During each thermoforming cycle two PC scaffolds could be formed. By use of the confocal microscope, the surface profile of the thermoformed scaffolds was measured and compared with designed size and the PDMS master (Fig. 6.1 (c)). High shape fidelity was observed for all measured samples, indicating no deformation or displacement of the stamp during thermoforming. For the samples with 200 μm width channels, the foil almost completely replicated both the height and width of the PDMS features (Fig. 6.1 (b)). Samples with 100 μm width channels showed a slight difference in forming accuracy (Fig. 6.1 (a)). In areas where the channels are branched, the structures are wider and therefore these features were better reproduced as compared to the channels, which showed less accurate retention of height (Fig. 6.1 (c)).

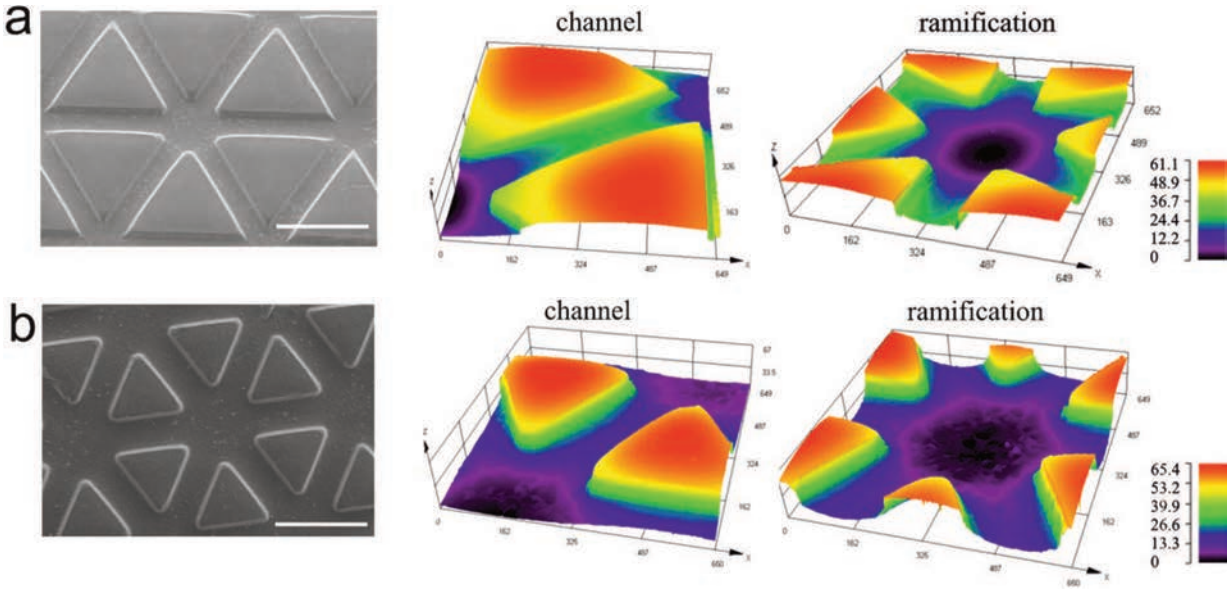

c

		Length [µm]					
		Designed size		PDMS stamp		PC foil	
		High	Width	High	Width	High	Width
Design_1	channel	65	100	63.61 ± 3.11	102.11 ± 2.11	38.61 ± 2.11	108.11 ± 2.11
	ramification	65	200	63.64 ± 3.06	203.08 ± 3.01	58.47 ± 4.77	211.14 ± 3.18
Design_2	channel	65	200	66.82 ± 0.19	205.48 ± 1.92	60.49 ± 4.15	209.92 ± 1.19
	ramification	65	400	66.71 ± 1.16	404.21 ± 2.19	65.22 ± 3.27	408.59 ± 3.12

Figure 6.1: Characterization of scaffolds with sinusoidal structure manufactured by 3DµCP technique: SEM images and surface topography visualization of scaffolds with 100 µm (a) and 200 µm (b) width channels and pattern size fidelity according to designed size and PDMS master (c).

6.2 Cells Adhesion and Long –Term Growth on Surface Patterns.

To mimic the liver microenvironment with a well-organized cell composition, the colonization of the endothelial-like cells was controlled by a cell adhesion molecules, which were selectively printed on the surface using 3DµCP method. To study the potential of the patterned matrixes for guided cell culture, EA.hy926 cells were cultivated on the top side of the scaffolds in serum-containing media over 10 days. After testing different cell seeding densities (data not shown), 10 000 cells per each sinusoidal half-structure was selected for the further applications. Such cell seeding density allowed uniform cell attachment to the patterned channels, leaving enough space to hold seeded cells for a longer time (Fig. 6.2). After 24 h cells were observed preferentially attached to patterned surface and only a few cells were seen on nonprinted area. Single layer of cells was formed on the bottom of the channels, while the endothelial cell-specific cobblestone

shape was preserved. Similar results were seen after 48 h. After 4 days, when the number of cells increased significantly, the surface for cell attachment within the sinusoidal structures was limited. However, cells have not overgrown out of the patterned channels and directed cell growth was still observed. Cells began to interact with other cells inside the channels and proliferate, forming cell bundles and some aggregates. Single cells were migrating onto the unpatterned regions, but generally cells attached on surfaces without collagen pattern had a rounded morphology. Cell aggregation increased over time and as a consequence the cells started to overfill the channels. The maximum aggregation was observed after 8 days in culture. After 10 days directed cell growth was still visible, however, cell bundles formed in the channels were partially detached from the scaffold surface as a continuous chain of cells.

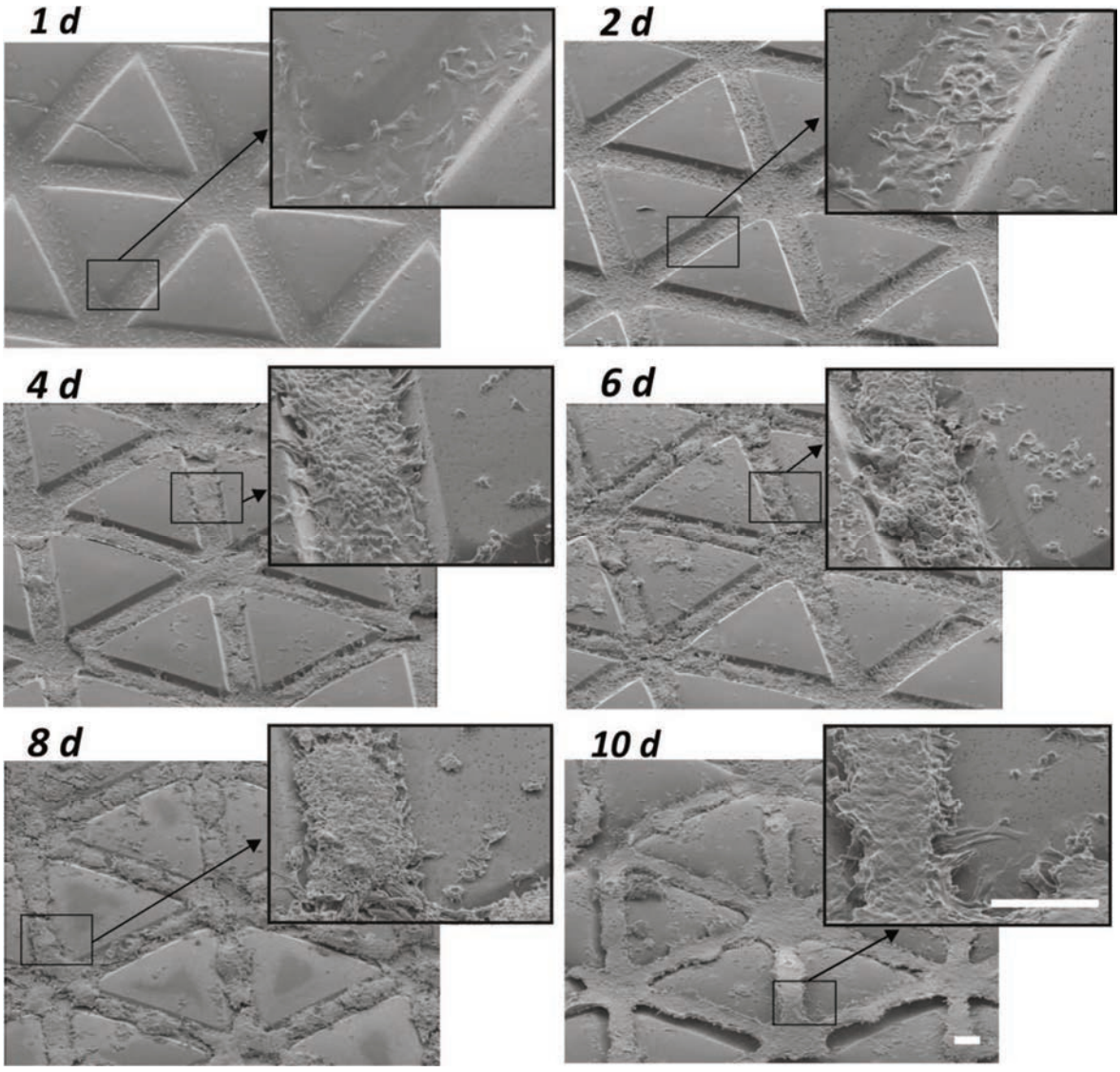

Figure 6.2: Cell adhesion preference. Representative phase contrast images of EA.hy926 cells attached to the patterned regions of the PC scaffolds with sinusoidal channels after 1, 2, 4, 6, 8 and 10 days in cell culture. Cell seeding density was 10,000 cells per well. Scale bar indicates 100 μm.

In order to analyze the cross section of cells structures formed inside the scaffolds, cells were stained for nuclei and imaged using LSM and 3D reconstruction software (XZ and YZ planes), while the viability of the cultured cells was investigated by live-dead staining. The obtained images confirmed directed cell growth and gradual formation of cell bundles. During the 10 days of culture, cells structures changed from flat layer of the cells localized the bottom of the sinusoidal channels to 3D cell bundles overgrowing from the channels (Fig. 6.3 (a)). High cell viability was observed at different time-points (Fig. 6.3 (b)).

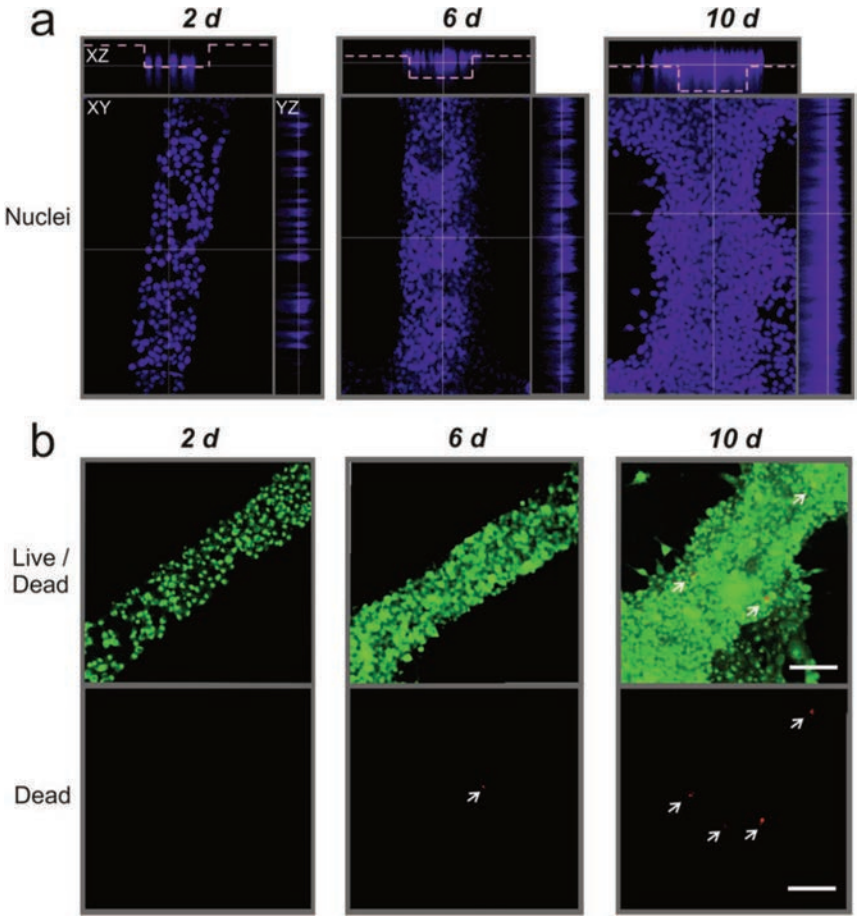

Figure 6.3: LSM images of EA.hy926 cells cultured within 3DμCP patterned scaffolds. (a) Stack LSM images (XZ, XY, and YZ planes) of cell distribution. Samples were stained for nuclei. Pink dashed curves represent the channels that included the cells. (b) Live/dead staining of cells. Green: live cells; red: dead cells. Cells were examined after 2, 6, and 10 days of culture. Scale bars indicate 100 μm.

In actual liver sinusoid, endothelial cells and hepatocytes are organized in layers with the intervening space called the Space of Disse. This morphological structure is filled with the various ECM proteins and proteoglycans and collagen I is one of the dominant components in this matrix. Since the Space of Disse allows the diffusion of molecules from the fenestrated vascular layers to

the hepatocytes, it serves as a ‘‘molecular sieve’’. We adapted this perisinusoidal space in our liver model by applying an endothelial and a hepatic cell layer on the opposite sides of a thin and permeable polymer scaffold coated with collagen. Thus, our scaffold acts as a substrate for both cell types and concomitantly fulfills two additional functions; facilitate the partitioning of cellular microenvironments and mimic the space of Disse. Additionally, microporous structure of the scaffold allows to maintain biochemical and in some cases even physical crosstalk between cells. Culturing cells on opposing sides of a thin scaffold can also bring some other advantages. Cells are supported in a consistent plane that simplifies imaging as well as can be more easily recovered than cells collectively co-cultured within a scaffold, what is an important aspect for analytical readouts (273). At the end of an experiment such co-culture model allows for rapid separation of the cells for biological endpoint assays.

However, to establish co-culture models in which cell populations are spatially confined and able to communicate, an appropriate pore size must be selected. Scaffold should form a barrier for the cells, while allowing free diffusion of factors secreted from the cells for biochemical communication. Using our polymer sheets with 2 µm pores exchange of secreted factors can take place through the porous surface (273), and endothelial cells can contribute to liver-specific functions through paracrine secretion. Simultaneously, such pores are small enough to form a barrier for the cells and prevent cell migration. To better investigate interaction cellular behavior on microporous surface of the scaffold, EA.hy926 were observed by SEM with high magnification (Fig. 6.4). Cells migration through the pores was not noted. Cells were seen to adapt their molecular architecture to patterned surface of the channels by developing protrusive structures (most likely filopodia) out of the cell membrane. These membranous protrusions were seen to anchor the cells to the surface. Moreover, it can also be seen that the part of the protrusive structures penetrated the pores. Thus, despite the direct interaction between hepatocytes and endothelial cells is limited in this configuration due to the presence of the microporous polymer layer, some physical contact between the cells cannot be completely excluded.

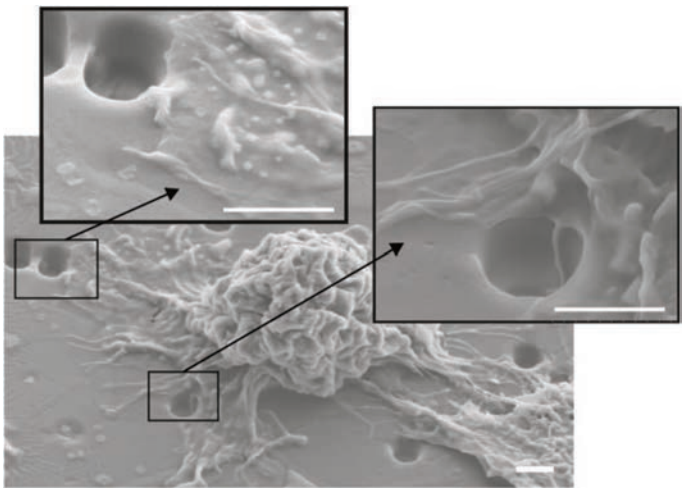

Figure 6.4: Endothelial cells attached to the microporous surface of the sinusoidal channel after 96 h of culture. Cells were observed with high magnification. Scale bars indicate 2 µm.

6.3 Folding of the scaffolds.

To mimic the 3D morphology of the liver lobule, two thermoformed structures with sinusoidal channels were joined together so that the associated channels formed a capillary. However, precise positioning of two structures to each other was hardly possible "by hand" without auxiliary equipment. Thus, scaffolds were placed in specially designed frame equipment (Fig. 2.6). This allowed also for manual handling of scaffolds during cell seeding and finally during cell culture experiments. Furthermore, to facilitate accurate folding of the associated channels, a folding edge was formed between sinusoidal structures during microthermoforming process and subsequently notched using a laser. SEM images have shown that such formed and notched folding edge in combination with frame apparatus enables precise joining of the associated channels so that they form capillary. Using such dual support system folding occurred exactly on the folding edge and the channels were precise adjusted and formed a closed structure (Fig. 6.5).

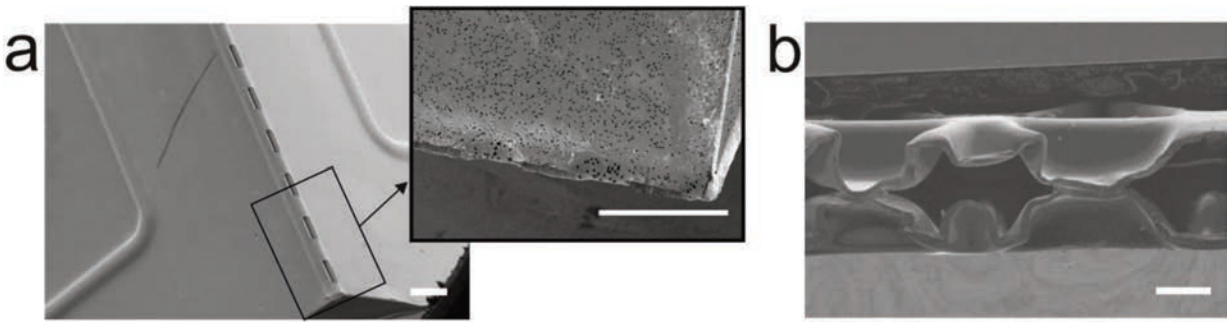

Figure 6.5: Folding accuracy of the micropatterned scaffolds: scaffolds folded along the thermoformed and notched folding edge (a) and cross-section of two channels folded together and forming capillary (b). Scale bares represent 200 µm.

6.4 Guided co-cultivation of liver cells

Next goal of this study was the colonization of the outer side of the scaffolds with a second cell type, while maintaining directed adhesion and growth of endothelial cells in the channels. Different cell seeding strategies were tested and adapted depending on the results obtained. Parameters like cell seeding density, incubation time and seeding order were repeatedly changed and verified.

Initially, to ensure good attachment of the endothelial cells on the top side of the scaffolds and prevent cell lost after scaffold rotation, EA.hy926 cells were seeded on the scaffolds two days prior the seeding of HepG2 cells (Fig. 2.7). Since PC surface has hydrophobic properties and the pores diameter are small, the drop of cell suspension containing EA.hy926 cells remained on the surface during incubation period and medium did not migrate to the other side of the scaffold. However, when scaffolds were rotated and coated with collagen solution so that hepatocytes could adhere to the opposite side of the microporous polymer layer, cohesion forces have caused flow of

the collagen solution to the other side of the scaffold over time. As a consequence PC surface was not properly coated and only a small number of hepatocytes or complete lack of cells was observed on the bottom side of the scaffold, even when the amount of seeded cells increased to 2.5 × 10^5 cells/ml (see Method 1, Fig. 2.7). The number of endothelial cells on the top side of the scaffold was also limited, probably due to prolonged exposure of cells in a small amount of the medium during incubation of collagen and then colonization of HepG2 cells (Fig. 6.6 (a)). Endothelial cells with various morphology from elongated to rounded or irregular in shape were observed on the surface. Few HepG2 cells were observed both individually and in clusters.

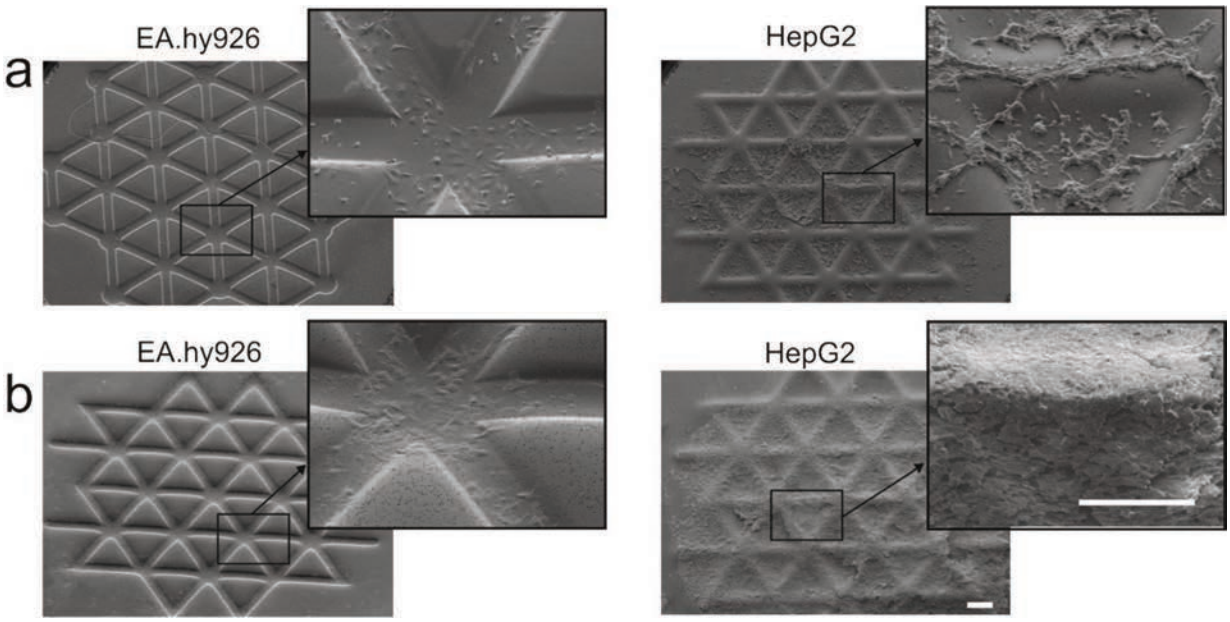

Figure 6.6: Representative images of EA.hy926 and HepG2 cell distribution on two opposite sides of the micropatterned scaffold. Scaffolds were seeded with cells according to Method 1 (a) and Method_2 (b). Scale bars indicate 200 µm.

For this reason seeding strategy was changed. In the final method (see Method 2, Fig. 2.7), the top side of the scaffold was first coated with collagen and then seeded with the hepatocyte cells. Thus, exposure time of endothelial cells in a small amount of the medium was reduced. The drop of collagen solution remained on the scaffold during entire incubation period. Additionally, incubation time of the endothelial cells was reduced and after the scaffolds were rotated medium was added from the bottom of the scaffolds. Therefore, in contrast to the previous method, endothelial cells were in contact with medium also during seeding of hepatocytes. Using this cell seeding strategy, attachment of the both cell types was achieved. Dense layer of hepatocytes was observed on the bottom side of the scaffolds, while on the top side of the scaffolds endothelial cells were observed preferentially attached to patterned channels, preserving endothelial cell-specific cobblestone morphology or elongated shape (Fig. 6.6 (b)). Such directed attachment of endothelial cells suggested the occurrence of chemical pattern even after collagen coating and cell attachment on the opposite side of the scaffold. Thus, despite microporous structure of the polymer

layer, the coating agent has not gone to the other side of the scaffold and both sites were modified individually.

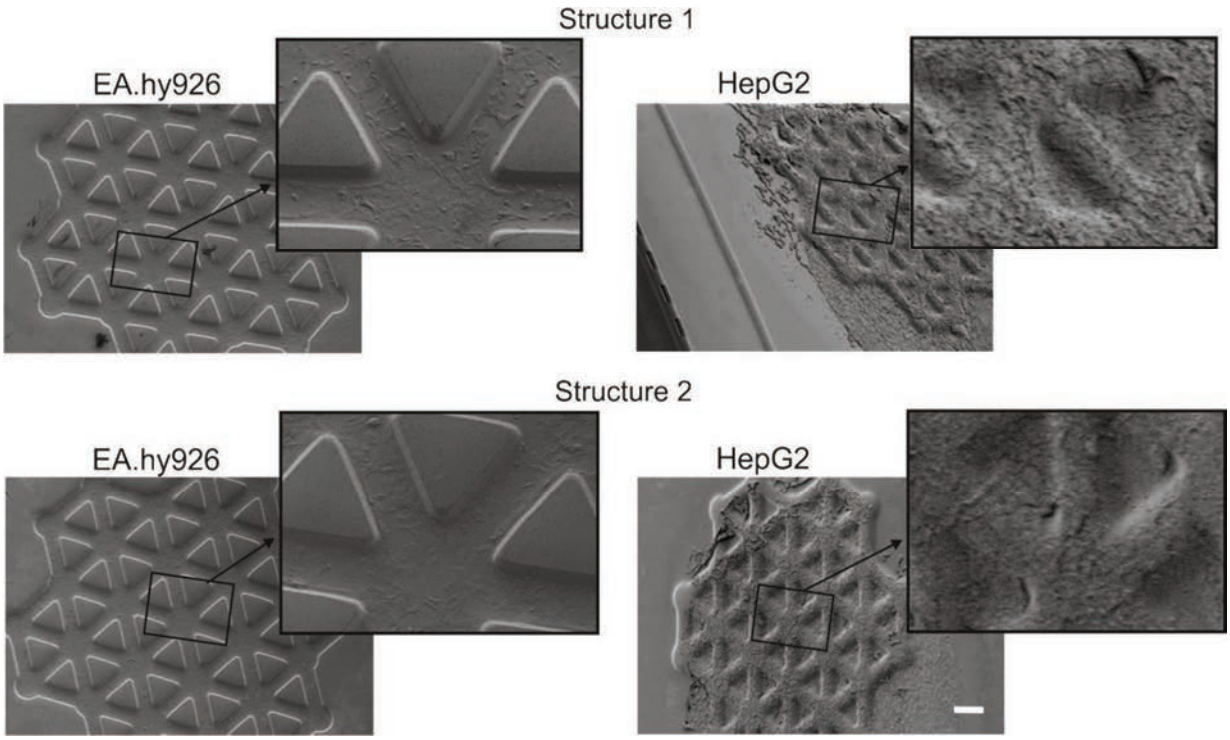

Figure 6.7: Cell distribution on two different sites of the scaffold. Cells were seeded on the scaffold according to Method 2. Structure 1 and structure 2 were folded in the frame apparatus and co-cultured in layered configuration for 24 h. Scale bars indicate 200 µm.

Subsequently, scaffolds were folded in the frame apparatus and cells were co-cultured in layered configuration. As a consequence we achieved a stack comprising two layers of the patterned scaffold and mimicking sinusoidal capillaries with endothelial cells colonized inside the capillaries and hepatocytes surrounding the capillaries from outside. Obtained results shows that endothelial cells cultured on the underside of the capillaries as well as those cultured in the top part of the capillaries, in the reversed direction, remained attached to the 3DµCP patterned surface (Fig. 6.7). Simultaneously the impact of the scaffold rotation and culturing in revised direction on hepatocytes growth was investigated. Dense layer of hepatocytes was observed on both sinusoidal structures. This implies that scaffold folding and cell culturing in revised direction did not have a visible impact on the adhesion and growth of the endothelial cells or hepatocytes.

6.5 Scaffold modification for dynamic culture conditions

Despite single layers of micropatterned PC scaffolds have shown good permeability, two layers of porous PC foils folded together were impermeable for medium flow under pump rates applied in our bioreactor. Impermeability of the folded scaffolds was confirmed by air flow measurements

(Tab. 6.1). Thus, to enable the application of the scaffolds in bioreactor as well as to better mimic the fluidic flow occurring in the actual liver lobule, small through holes were cut in areas mimicking central vein and Glisson trias (Fig. 6.8 (a)).

Table 6.1: Permeability of the scaffolds as a pressure difference between two sides of a porous foil and theoretical permeability values calculated for the flow of cell culture medium.

Sample	Permeability [mbar]					
	Structure 1 *(Glisson's triad)*		Structure 2 *(central vein)*		Structure 1 and 2 folded together	
	air	medium	air	medium	Air	medium
Micropatterned scaffold	7.29 ± 0.81	0.40 ± 0.04	7.67 ± 0,18	0.42 ± 0.01	—	—
Micropatterned scaffold with spirals holes	1.27 ± 0.18	0.07 ± 0.01	2.89 ± 2.01	0.16 ± 0.11	5.47 ± 0.35	0.31 ± 0.02

The holes should enable directed medium flow through the scaffold during cell culture experiments in bioreactor, while preventing medium and cell flow during cell seeding. Thus, micropatterned PC scaffolds with different types of through holes (Fig. 6.8 (a)) were tested for applicability during cell adhesion. On the scaffolds with round holes the whole suspension went through the scaffold after a few seconds from seeding. As a consequence, no cell adhesion was seen on the scaffolds (Fig. 6.8 (b)). On the scaffolds with through holes in the shape of a star cell suspension has remained on the scaffold at the beginning of incubation, but after 3 h no medium was observed on the surface. A small amount of cells were adhered on the surfaces, but mostly in the area of holes.

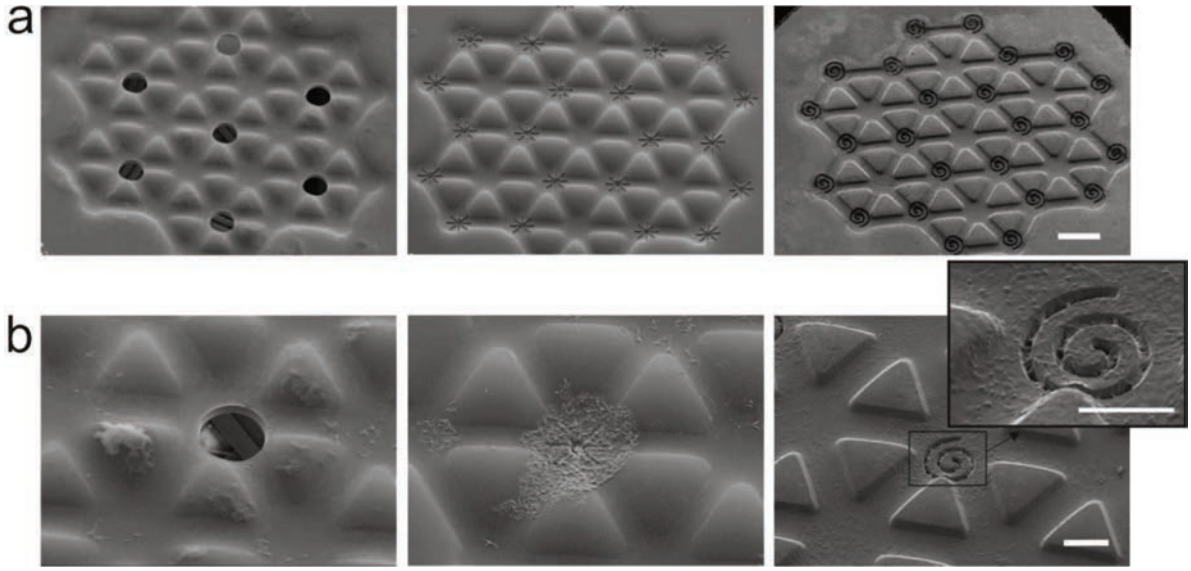

Figure 6.8: Micropatterned scaffolds with through holes with a round shape, in the shape of a star and in the shape of a spiral (a), EA.hy926 cell adhesion to the scaffolds with various types of holes (b). Scale bare

indicates 500 µm (a) and 200 µm (b). The shape and size of the holes was designed in cooperation with J. Hampl.

Best results were observed for the scaffolds with through holes in the shape of a spiral. In this kind of hole the kerf was 20 µm wide, while the diameter of the whole spiral was about 280 µm. Cell suspension has remained on the surface throughout the whole incubation period and the uniform cell adhesion was seen in the channels. In the area of spiral structures cells adhered onto the perforation and only partially migrated into the kerf.
The permeability measured for the folded scaffold with spirals holes was suitable for free medium flow under pump rates applied in the bioreactor (Tab. 6.1). These results indicate that the size of the opening in the spiral holes was adequate to keep the cell suspension on the surface in static conditions, while enabling medium flow in dynamic environment.

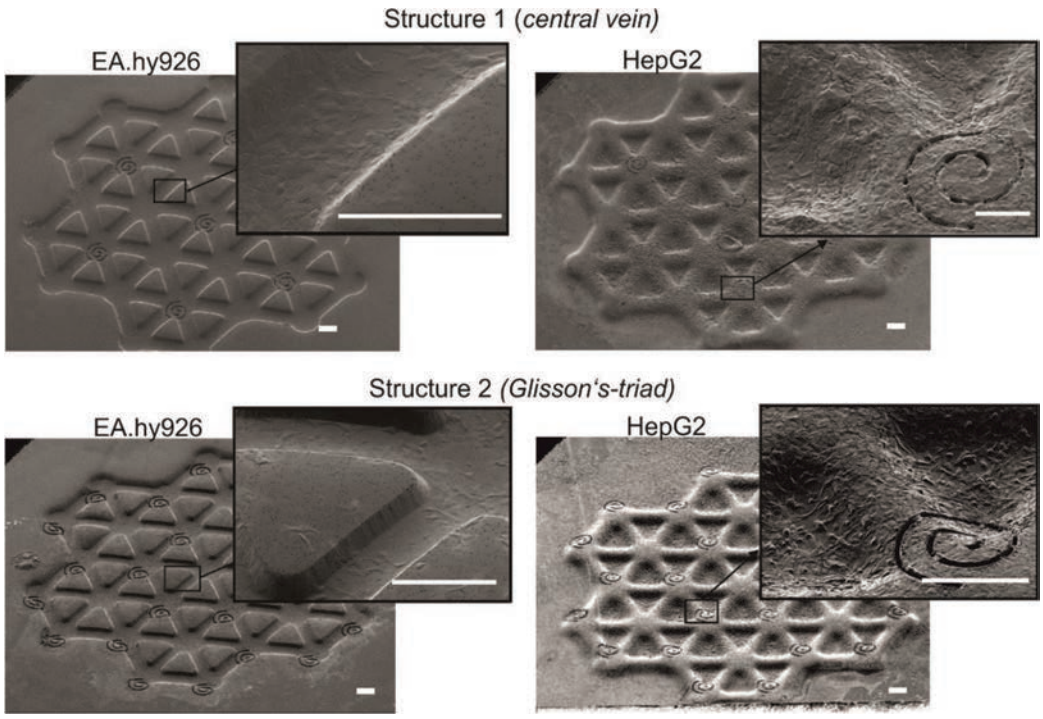

Figure 6.9: Cell distribution on two different sites of the scaffold with spiral through holes. Structure 1 and structure 2 were folded in the frame apparatus and co-cultured in layered configuration for 24 h. Scale bars indicate 200 µm.

Finally, scaffolds with spiral holes were tested for directed cell co-culture. Cell adhesion was observed on both sides of patterned scaffolds. EA.hy926 cells were preferentially attached to patterned area, while bottom site of the scaffold was homogeneously covered with dense layer of hepatocytes (Fig. 6.9). Thus, proper cell distribution was achieved on the both sides of patterned scaffolds. These results indicate a good potential of the scaffolds for the further applications in perfused bioreactor system.

6.6 Evaluation of our system in the context of the currently available methods

The large burden of liver disease and primary liver cancer along with growing need for enhancement of the efficacy of drug development and toxicity testing have led to ever-increasing importance of the *in vitro* hepatic tissue engineering. In the past 10-15 years the development of *in vitro* liver platforms is an extremely active area of research (274, 275). Each year a spectrum of novel human liver models is being developed utilizing engineering tools that provide increasingly better control over the cellular microenvironment and enable integration of cues that modulate cellular responses. Thus, to better evaluate our scaffold based multi-layer liver model presented in this thesis in the context of the currently available methods, we correlated it with relevant systems reported in recent years. In table 6.2 we demonstrated several types of bioengineered liver models of increasing technologic complexities that were developed using various engineering tools, including constructs that are considered the most complex and *in vivo* like liver models currently available. The table is based on our interpretation of structural considerations of the selected models. Additionally, since the new technologies for creating liver models become more complex and utilize more sophisticated engineering tools, practical considerations such as throughput requirements or possibilities of noninvasive imaging and up-scaling were taken into account for the preparation of this table. Finally, we are discussing opportunities and intrinsic challenges that lie ahead each system.

Tab. 6.2: Comparative account of selected liver models from literature with method presented in this thesis (brown front), based on our interpretation of structural and practical considerations.

	Method	Multi-cellularity	Physiological micro-circulation	Lobule-mimetic cell pattern	3D architecture	Up-scaling	Through-put	Imaging	Unique benefits (✓) and potential limitations (✕)
a	Lobule-mimetic DEP cell patterning (131)	•	-	••	-	-	-	••	✓ very well controlled cell–cell interactions ✓ compatible with high-content imaging readouts ✕ require specialized equipment and devices
b	3D hepatic tissues fabricated using cell sheet engineering technology (193, 276)	•	-	•	•	-	-	-	✓ great potential to fabricate unique, functional cell-dense tissue constructs ✕ problems including hypoxia, nutrient insufficiency and waste accumulation may occur ✕ fragile and difficult to handle ✕ complexity of architectures that can be formed as well as maximal thickness of the construct are limited
c	Multi-well scaffold based bioreactor (226, 277)	•	•	-	••	•	••	•	✓ ease of handling, applicable to microplates ✓ ability for *in situ* microscopic examination ✓ scalability of the system by increasing the number of through-channels within the system ✕ spherical morphology of the cultured cells may cause difficulties in oxygen and nutrient diffusion ✕ lack of spatial distribution of co-cultured cells
d	Scaffold-free spheroids in perfused stirred-tank bioreactors (224)	•	•	-	••	-	••	-	✓ reproducible formation of 3D cellular aggregates in a controlled size ✓ spatial segregation of the co-cultured cells ✕ difficulties in high-content imaging for entire spheroid ✕ difficulties in oxygen and nutrient diffusion through large aggregates (spheroids size limitation ~200 µm) ✕ can be difficult to control disorganized cell type interactions over time

Tab. 6.2 *(continued)*

	Method	Multi-cellularity	Physiological micro-circulation	Lobule-mimetic cell pattern	3D architecture	Up-scaling	Through-put	Imaging	Unique benefits (✓) and potential limitations (✕)
e	Liver-on-a-chip platforms based on layer-by-layer cell deposition on microporous membrane (230, 233)	••	•	•	•	-	-	••	✓ easy to control the position of cell layers to mimic the distribution of liver cells ✓ utilize suspended membrane as a cell substrate mimicking the space of Disse ✕ non-specific binding of drugs to chip materials ✕ applicable for small volume of cells ✕ shear stress may cause lower hepatic functions
f	Hollow-fiber bioreactor (228)	••	••	•	•	-	•	•	✓unique fluid flow mimicking of capillary blood-tissue exchange ✓ the fiber shield hepatocytes from the shear stress associated with perfusion ✕ complex system, difficult to establish ✕ binding of drugs to scaffold
g	Bundling-up assembly of cell-laden hydrogel microfibers (225, 278)	•	•	•	•	••	-	-	✓ allow encapsulation of diverse cells in a controlled environment ✓ mimic hepatic cord structures ✓ fiber shape enable good exchange of nutrients and oxygen ✕ complex system, difficult to establish ✕ require specialized equipment and devices
h	Scaffold based multi-layer technique for directed 3D co-cultivation of hepatic cells	•	••	••	•	••	•	•	✓ well-defined microstructure allow for reliable acquisition of the results, cells can be easily harvest from the scaffold ✓ utilize suspended scaffold for mimicking the space of Disse ✓ physiological microcirculation could be replicated *via* the capillaries and *via* the pores ✓ potential for creation of large and vascularized tissue construct ✕ non-specific binding of drugs to scaffold material ✕ lack of direct contact between co-cultured cells ✕ requires the use of a specialized thermoforming machine ✕ downscaling of the features size of the micropatterned structure below 10 µm could be challenging

Tab. 6.2 *(continued)*

	Method	Multi-cellularity	Physiological micro-circulation	Lobule-mimetic cell pattern	3D architecture	Up-scaling	Through-put	Imaging	Unique benefits (✓) and potential limitations (✕)
i	Multicellular hierarchical micromodules fabricated using shape-controllable photolithography (279, 280)	•	•	•	•	••	•	-	✓ micromodules could be spatially organized layer-by-layer to form a 3D construct ✓ enable creation of vessel-like lumen ✕ UV irradiation can influence cells ✕ require specialized equipment and devices
j	Bioprinted liver organoids (281-283)	••	-	••	••	•	-	-	✓ precise control of cell placement ✓ allow creation of diverse architectures as desired ✕ requires complex and expensive equipment ✕ potential heterogeneous nutrient or drug distribution within large and cell-dence bioprinted tissues ✕ vascular network has not been fully developed, with only a few exceptions (282) ✕ high sheer stres to the cells during fabrication
k	Decellularized human liver repopulated with cells (284)	-	-	••	••	••	-	-	✓ extremely well preserved 3D-microanatomy of the liver lobules ✓ expression and distribution of key ECM components of the liver tissue are fully maintained ✕ requires a long decellularization process ✕ highly difficult to uniformly introduce cells or target different types of cells to their correct location ✕ potential xenogenic immune problems

**Double dot (●●) means excellent replication or performance, single dot (●) means partial replication or performance and minus (-) means the absence of the desired characteristics.*

A variety of liver models, each having their own advantages and disadvantages, was presented in table 6.2. It can be observed, that despite much progress has been made towards improving liver-derived *in vitro* models over the last few years and many systems have found utility for addressing focused questions, each has limitations. Although our scaffold based multi-layer co-cultivation technique has its own disadvantages and limitation as well, we were also able to overcome some of the restrictions that were most frequently mentioned for other systems.

In our model cells were cultured on microporous polymer sheets with pre-manufactured properties and stacked in layered configuration. Thus we were able to recreate and control the complex cellular microenvironment, while allowing cell-cell communication via signaling products among the layered scaffold sheets. Culturing cells in layered configuration, so-called "cell sheet engineering" is well known method of fabricating living cellular constructs (Tab. 6.2 (b)). However, this non-scaffold based approach have also structural and practical restrictions. Using microporous scaffolds, we were able to avoid the main limitation of this approach and generate mechanical support for the co-cultured cells. To date many studies presented multilayer tissue construct using polymer scaffolds (285, 286); however, the inner and outer architecture of the scaffold was not controlled simultaneously. Using the multilayer thermoforming technique proposed in the first part of this thesis we were able to overcome limitation described for scaffolds primarily manufactured by conventional methods and produce substrates with "double microstructure" including scaffold microarchitecture and porous structure. In relevant studies B. J. Papenburg et al. have developed PLA sheets with inner-porosity and microarchitecture featuring microchannels. Authors have shown that cells cultured on such porous sheets stacked in multi-layered configuration stay viable and also affect each other (287). Under static conditions nutrient diffusion between the layers was observed through the inner-porosity, while under dynamic culturing the flow of the culture medium into the microchannels was found to improve nutrient supply to the cells. Despite a big step forward, those scaffolds lack of cell adhesion factors that could direct cellular adhesion. Cell organization within these scaffolds was induced only by scaffold microarchitecture. As a consequence, cell attachment and growth was not restricted to the pre designed scaffold microarchitecture. It is well known that for certain tissues, including liver tissue, mimicking *in vivo* organization on cell level prerequisite for proper functionality of the tissue (154, 288). Therefore, proper organization of cells on polymer scaffolds, mimicking cell arrangement in native liver tissue, was one of the main assumptions during design of our scaffolds. Many currently available cell culture models use microporous membranes (Tab. 6.2 (e)) or hollow fiber membranes (Tab. 6.2 (f)) to co-culture liver cells in layered configuration. Although those systems replicate different *in vivo* factors, cultured cells were randomly distributed onto the microporous substrates. Our strategy aimed to create highly biomimetic and bioactive microenvironments on microporous substrates through modulation of the physical (porosity and surface topography) and chemical (micropatterns of the biomolecules) properties of the scaffold. However, the use of common micropatterning techniques is limited to the 2D cell culture substrates (Tab. 6.2 (a)). Therefore we have developed a novel micropatterning method. On 3DμCP patterned scaffolds cells were successfully cultured in pre-designed configuration, while scaffolds architecture and microporous structure were controlled.

To develop a truly functional liver tissue model that enable long-term evaluations, vascularization and dynamic flow within the tissue construct are essential (223). Continuous perfusion of medium support mass transfer as well as exchange of the factors secreted from the different cell types, particularly when the cells are located on the opposite side of the microporous scaffold. Such perfused co-culture systems could not only better mediate in cell–medium interactions but also promote heterotypic cell-cell interactions. Many currently available cell culture models successfully use microporous scaffolds to co-culture liver cells under dynamic conditions (Tab. 6.2 (c)). However, cell viability and optimal function of the construct cannot be sustained through diffusion alone (289). Thus, generation of a functional vasculature remains an important goal of novel liver models. In our system scaffold microarchitecture mimics the liver lobule-like microtissue and compromises corresponding vessels. Additionally, to better mimic physiological microcirculation, small through holes were cut in areas mimicking central vein and Glisson trias. In actual liver multiple types of hepatic cells work together under blood flow *via* well-developed vascular networks and under interstitial flow inside the space of Disse (290). Since our scaffolds mimics sinusoidal blood vessels while maintaining the porous structure**,** during the future applications in perfused bioreactor system physiological microcirculation could be replicated in two ways; *via* the capillaries and *via* the pores, mimicking the capillary and interstitial flow similar to the *in vivo* counterpart in both sinusoids and the Disse space.

As a result, here are four important aspects of liver physiology captured in our model: three dimensional architecture, multiple cell types, design mimicking *in vivo* microenvironment and physiological microcirculation. A big advantage of such tissue model with layered configuration is control of cell distribution throughout the whole construct – cell seeding and adhesion occurs on the particular scaffold layers before stacking. Thus, cells can be arranged evenly throughout the whole tissue construct. Moreover, such layer-by-layer approach allows for analysis per each scaffold layer providing detailed information on local cell behavior, while each cell type can be separated independently for cell-specific readouts.

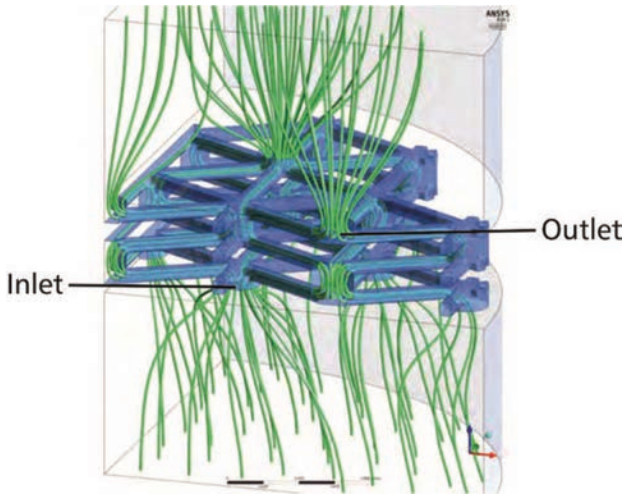

Figure 6.10: Fluidic simulation of medium flow through three layers of folded scaffolds. Designed by F. Weise.

In this thesis first step in the development of a novel liver model was successfully completed. A stack comprising two layers of the patterned scaffold with co-cultured cells was successfully created and subsequently prepared for the further integration in our bioreactor systems. This provide fundamental unit for the further development of our complex liver model. However, to create complete liver microtissue constructs that mimic hierarchical structure of the liver lobules along with physiological microcirculation, various microfluidic and geometrical challenges should be addressed and come under the scope of future research in our group. At least several layers of the folded scaffolds should be arranged one on another and integrated in our bioreactor system (Fig. 6.10).

The work presented in this thesis was considering liver tissue as model for our study, based on which various materials, scaffolds and techniques were explored. However, through variation of the microthermoforming mold, the imprinted scaffold micropattern can easily be tuned for the specific tissue type. Thus, presented methods can be very advantageous for precise and reproducible engineering of other tissue types where specific organization of the cellular microenvironment is required, like muscle or cardiovascular tissue. Moreover, in the first part of this thesis it was shown that scaffolds with “double microstructure”, including controlled porosity and architecture, can be produced from other polymer substrates, including biodegradable materials. This indicate great development potential of our method for other tissue engineering applications.

7. Conclusions and outlook

During the course of this work, different strategies for development of complex scaffolds for advanced cell culture and liver tissue engineering constructs were studied. With the assistance of microthermoforming process we produced microporous polymer matrices that mimic tissue microenvironment in a more excellent manner than standard culture techniques and thus may provide more attractive environment for cell adhesion and growth. We have described a progressional study of creating such microporous scaffolds and confirmed here the basic applicability of the produced constructs. Various important issues concerning scaffold design and production were raised. Figure 7.1 presents individual parameters studied in this thesis regarding the main scaffold design directions.

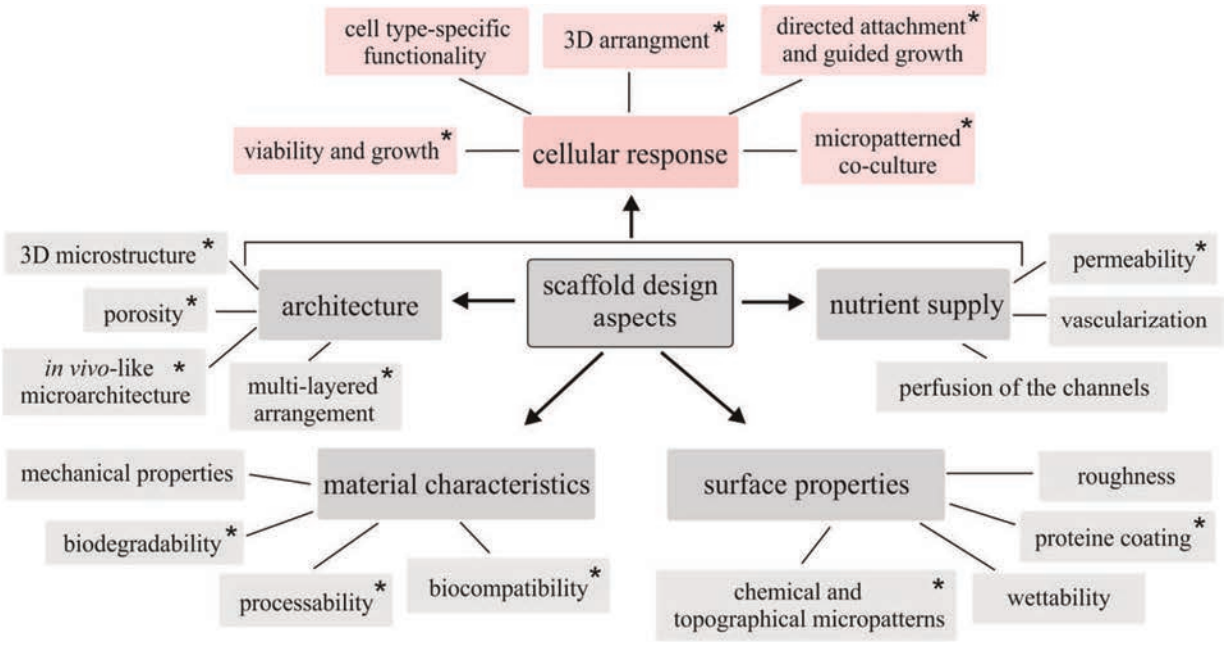

Fig. 7.1: Data tree representing various subcategories in scaffold design and cellular response criteria studied in this thesis. Parameters that were studied in more detail are marked with an asterisk (*).

Certain aspects were studied in more detail, including polymer processing and microstructuring, 3D microstructure and porosity as well as chemical and topographical surface patterning, while some parameters were only briefly included within the main design concept. Cellular response influenced by respective characteristics of the scaffold was evaluated using different criteria.

First, to provide microenvironment for organotypic hepatocyte cultivation, PLA substrates with established 3D structure and controllable porosity were produced using two-step procedure. The shape and size of the pores and their interconnectivity was determined by adjusting compound concentration and quenching parameters during the pre-process step, while the 3D structure was established by varying temperature and pressure during the final microstructuring. Using a modified microthermoforming method we solved the problem of microstructuring of the porous material. Thermoformed PLA scaffolds with the structure of microcavities provided a template for the cell growth and allowed 3D tissue-like aggregation. The resulting pore sizes allowed perfusion of fluids and retaining the cells, while the regular topography enabled modeling of biological processes and analysis of 3D images. Moreover, the cells were easily harvested from the scaffolds. After 4 weeks in cell culture as well as after 24 weeks in PBS solution thermoformed structures remained stable and no evidence of physical disintegration of the scaffolds was noticed. Compared to PC matrixes used previously in our group, enhanced cell growth and a higher secretion rate of albumin within the PLA scaffolds indicate improved suitability of microstructured PLA substrates for 3D cell culture applications. A yet incomplete understanding of the particular interface interactions between polymer-based substrates and biological systems does not allow for a simple interpretation of this outcome. Nonetheless, since either PC or PLA do not provide ligands for cell adhesion, topography variations and mechanical properties may have considerable effect on cell attachment and functions. Greater roughness and lower elasticity of PLA substrates in comparison to PC scaffolds may provide more attractive environment for liver cell cultivation.

Basically, this two-step procedure allows the shaping of any porous thermoplastic material in form of foils or meshes into a wide range of possible 3D structures over a large area. Due to the flexibility of material selection, as well as the ability to easily control scaffold shapes by exchanging of the molding tool, porous substrates for various biomedical applications can be produced using this approach. We have demonstrated that using this method microporous scaffolds with established topography and desired permeability can be produce from fast degradable polymers as well. Scaffolds with sinusoidal structures mimicking the basic structure of liver lobule were produced from bioresorbable PLGA material. Cells cultured on the microstructured PLGA substrates have shown strong adhesion and flattened morphology. During degradation in cell culture thickness of our microstructured scaffolds was visibly reduced and large degree of degradation was observed on the scaffold surface. However, after 4 weeks in cell culture PLGA matrixes were only partially degraded, while micropatterned 3D structure was unstable and disappeared completely after 3 weeks. To achieve scaffolds with higher degradation rate and better form stability, some changes in scaffold parameters should be considered. However, this study presented a new method to produce biodegradable substrates with established 3D structure and controlled porosity that are otherwise not possible to be controled simultaneously and we believe that our results might be stimulating for research and design of degradable substrates for various biological utilizations.

As previously stated, one of the main goals of this work was to integrate multiple scaffolds characteristic within a single scaffold structure in a controlled manner. For directing cell adhesion

onto a microtopographically complex scaffold surface, substrates with 3D microstructure and simultaneously acting chemical or physical stimuli were conceived. We tested different technical solutions of transferring biochemical molecules to the scaffolds microgeometries. Since the surface of the scaffold was highly porous, techniques that require application of liquid components were unsuccessful despite using elastomeric molds as sealing. On the other hand, due to complex topographical structure of the thermoformed substrates methods based on directed patterning of the microstructured surface were technically unfeasible using standard laboratory equipment. For this reason we invented new patterning technique that synchronizes the chemical and topological patterning in one step. 3DμCP method combines the advantages of microcontact printing with microthermoforming, thereby extending the scope of 2D surface patterning to 3D. Thus we were able to form microtopographies on the scaffold surface and precise transfer the ECM molecules into the obtained geometries simultaneously. Samples with microchannels with variety of different dimensions were produced with high shape fidelity, while different ECM proteins were precisely transferred into the bottom of the formed channels. The patterned molecules were successfully visualized by antibody-based immunofluorescence staining and recognized by different cell types. Thus, it can be assumed that essential cell-binding motifs have been preserved after the thermoforming process and a moderate decomposition of the molecules by thermoforming, if present, does not adversely affect cell adhesion. Cells cultivated on the 3DμCP patterned scaffolds gradually contracted into oligocellular structures. Directed cell attachment and growth was observed for different cell types independently from scaffolds architecture as well as after patterning of various ECM molecules. Using 3DμCP technique samples were produced in reproducible and high throughput manner. This method has the potential for creating such combinatorial patterning also on other thermoplastic biopolymers, and more complex geometries could be implemented as well.

We have shown that with the assistance of 3DμCP method, scaffolds with chemical and topographical guidance causes largely emulated complex physiological architecture of organ ultrastructures can be bioengineered from polymer substrates. We used the scaffolds to re-create the stratified structure of the liver *in vivo* and to incorporate the two major cell types found in this organ. Thus, the appropriate patterning of liver parenchymal and NPC cells was combined with 3D cell culture format. It was shown that patterned scaffolds are able to spatiotemporally control cell adhesion and growth in a 3D fashion at a microscale resolution. Two different cell types were successfully integrated on opposite sides of microstructured samples, establishing co-culture model in which cell populations are spatially confined, but able to communicate through microporous structures. After precise scaffold folding our model was able to support co-culture of hepatic cells in a layered configuration. Since we use microporous substrates and additionally adapted our scaffolds for exposure to microcirculation of medium, this micropatterned cell culture construct can be easy adjusted to microfluidic devices. Such perfused co-culture system can be a potentially powerful technique for gaining knowledge about liver function and for subsequent use in toxicological testing, studying disease or the evaluation of novel candidate therapeutics.

Perspectives

Together, current study has shown that microporous templates for the organotypic cell culture can be produced with the assistance of microthermoforming process. However, for further applications of our scaffolds in liver model development studies and toxicological testing, the biological utility of our matrices to enhance hepatocyte function and differentiation should be demonstrated and some technical improvements could be introduced.

The following further steps are proposed:

- To better explain the improved suitability of microstructured PLA substrates for 3D cell culture applications in compare to PC scaffolds further examination of scaffold properties could be considered. Especially, evaluation of mechanical properties of the scaffold surface such as nanoindentantion measurements should come under the scope of future research

- To achieve complete scaffold degradation of the PLGA scaffolds during 4 weeks of cell culture foils with lower thickness can be tested. Other possibility could be longer cell culture period. To prevent cell lost in a cell concentration dependent manner lower cell seeding density should be considered

- To enhance form stability of the microstructured PLGA scaffolds different sterilization method should be considered. Despite it was reported that ethanol have not caused morphologic or chemical damage to polyester scaffolds (291), some surface wrinkling and scaffolds deformation was observed elsewhere (292). Our scaffolds have not shown any significant changes in pore structures after sterilization with ethanol (data not shown), however; some impact on the disappearance of micropatterned 3D structure and scaffold shrunk cannot be excluded

- Depending on desired applications, PLGA scaffolds with deeper channels can be produced. Since the maximum temperature and pressure used for scaffolds formation during thermoforming have not caused any detectable impact on microporous structure, to achieve greater depths of the patterned channels higher thermoforming parameters could be tested

- To create the most physiologically relevant *in vitro* liver model HepG2 and EA.hy926 cell lines should be replicated by primary liver sinusoidal endothelial cells and primary hepatocytes. To more precisely mimic actual liver microenvironment, another hepatic non-parenchymal cells such Stellate cells and Kupffer cells should be included

- To indicate whether co-culture of primary cells in our model will enhance cell specific functionality, liver-specific function such as protein secretion, cytokine production, metabolism and immune response could be explored. Hepatocyte function can be monitored through urea or albumin production, cytochrome P450 enzyme kinetics, oxygen measurements or by immunostaining for bile canaliculi. The activity of endothelial cells could be evaluated as well. To better understand interactions between hepatic cells, one could measure the production of nitric oxide and hydrogen peroxide by endothelial cells Cell viability and functionality should be monitored under long-term co-culture (like 28 days or longer)

- During thermoforming the PC foil was stretched and scaffold thickness was changed, thus actual scaffold thickness in the thermoformed channels should be measured. To enable the physical contact between the co-cultured cells, the thickness of the scaffold could be reduced, thus, microporous PC foils with initial thickness of 45 µm could be replicated by thinner foil (25 µm or even 10 µm thick PC foils could be tested)

- To further confirm the partitioning of cellular microenvironments on the both sides of patterned PC scaffolds, additional investigation of the cell arrangement on the scaffolds should be proceeded. Despite cells should not migrate across the porous surface, some cell migration through spiral holes with 20 µm kerf could be expected. It has been shown that endothelial cells can migrate across membrane with 10 µm width pores (273). Thus, further examinations are needed.

- Finally, to replicate a larger portion of the liver tissue, the folded scaffolds should be stacked one on top of another and joined together by through holes. Several of the folded scaffolds could be arranged in this way.

Bibliography

1. Langer R, Vacanti J. Tissue engineering. Science. 1993;260(5110):920-6.
2. Brown RA. Extreme tissue engineering: concepts and strategies for tissue fabrication: John Wiley & Sons; 2013.
3. Vacanti JP, Vacanti CA. The history and scope of tissue engineering. Principles of tissue engineering. 2000;3:3-6.
4. Nerem RM. The challenge of imitating nature. Principles of tissue engineering. 2000;3:7-14.
5. Zorlutuna P, Vrana NE, Khademhosseini A. The expanding world of tissue engineering: the building blocks and new applications of tissue engineered constructs. IEEE reviews in biomedical engineering. 2012;6:47-62.
6. Matsumura G, Hibino N, Ikada Y, Kurosawa H, Shin'oka T. Successful application of tissue engineered vascular autografts: clinical experience. Biomaterials. 2003;24(13):2303-8.
7. Horch RE, Beier JP, Kneser U, Arkudas A. Successful human long-term application of in situ bone tissue engineering. Journal of cellular and molecular medicine. 2014;18(7):1478-85.
8. Debels H, Hamdi M, Abberton K, Morrison W. Dermal matrices and bioengineered skin substitutes: a critical review of current options. Plastic and reconstructive surgery Global open. 2015;3(1).
9. Atala A. Engineering organs. Current opinion in biotechnology. 2009;20(5):575-92.
10. Macchiarini P, Jungebluth P, Go T, Asnaghi MA, Rees LE, Cogan TA, et al. Clinical transplantation of a tissue-engineered airway. The Lancet. 2008;372(9655):2023-30.
11. Schober A, Augspurger C, Fernekorn U, Weibezahn K-F, Schlingloff G, Gebinoga M, et al. Microfluidics and biosensors as tools for NanoBioSystems research with applications in the "Life Science". Materials Science and Engineering: B. 2010;169(1-3):174-81.
12. Fernekorn U, Hampl J, Weise F, Augspurger C, Hildmann C, Klett M, et al. Microbioreactor design for 3-D cell cultivation to create a pharmacological screening system. Engineering in Life Sciences. 2011;11(2):133-9.
13. Zorlutuna P, Vrana NE, Khademhosseini A. The expanding world of tissue engineering: the building blocks and new applications of tissue engineered constructs. IEEE reviews in biomedical engineering. 2013;6:47-62.
14. Moraes C, Mehta G, Lesher-Perez SC, Takayama S. Organs-on-a-chip: a focus on compartmentalized microdevices. Annals of biomedical engineering. 2012;40(6):1211-27.
15. Fernekorn U, Hampl J, Augspurger C, Hildmann C, Weise F, Klett M, et al. In vitro cultivation of biopsy derived primary hepatocytes leads to a more metabolic genotype in perfused 3D scaffolds than static 3D cell culture. RSC Advances. 2013;3(37):16558-68.
16. Rouwkema J, Gibbs S, Lutolf MP, Martin I, Vunjak-Novakovic G, Malda J. In vitro platforms for tissue engineering: implications for basic research and clinical translation. Journal of tissue engineering and regenerative medicine. 2011;5(8).
17. Breslin S, O'Driscoll L. Three-dimensional cell culture: the missing link in drug discovery. Drug discovery today. 2013;18(5):240-9.
18. Edmondson R, Broglie JJ, Adcock AF, Yang L. Three-dimensional cell culture systems and their applications in drug discovery and cell-based biosensors. Assay and drug development technologies. 2014;12(4):207-18.
19. Bhadriraju K, Chen CS. Engineering cellular microenvironments to improve cell-based drug testing. Drug discovery today. 2002;7(11):612-20.

20. Törnqvist E, Annas A, Granath B, Jalkesten E, Cotgreave I, Öberg M. Strategic focus on 3R principles reveals major reductions in the use of animals in pharmaceutical toxicity testing. PloS one. 2014;9(7).
21. Schober A, Fernekorn U, Lübbers B, Hampl J, Weise F, Schlingloff G, et al. Applied nano bio systems with microfluidics and biosensors for three-dimensional cell culture. Materialwissenschaft und Werkstofftechnik. 2011;42(2):139-46.
22. Fernekorn U, Hampl J, Weise F, Klett M, Läffert A, Friedel K, et al. Microfluidic 3D HepG2 cell culture: reproducing hepatic tumor gene and protein expression in in vitro scaffolds. Engineering in Life Sciences. 2015;15(3):340-50.
23. Ravi M, Ramesh A, Pattabhi A. Contributions of 3D cell cultures for cancer research. Journal of cellular physiology. 2017;232(10):2679-97.
24. Hait WN. Anticancer drug development: the grand challenges. Nature reviews Drug discovery. 2010;9(4):253-4.
25. Harrison RG, Greenman M, Mall FP, Jackson C. Observations of the living developing nerve fiber. The Anatomical Record. 1907;1(5):116-28.
26. Harrison RG. The outgrowth of the nerve fiber as a mode of protoplasmic movement. Journal of Experimental Zoology Part A: Ecological Genetics and Physiology. 1910;9(4):787-846.
27. Taylor MW. A history of cell culture. Viruses and man: a history of interactions: Springer; 2014. p. 41-52.
28. Joseph JS, Malindisa ST, Ntwasa M. Two-dimensional (2D) and three-dimensional (3D) cell culturing in drug discovery. Cell Culture. 2018;2:1-22.
29. Pampaloni F, Reynaud EG, Stelzer EH. The third dimension bridges the gap between cell culture and live tissue. Nature reviews Molecular cell biology. 2007;8(10):839-45.
30. Frantz C, Stewart KM, Weaver VM. The extracellular matrix at a glance. J Cell Sci. 2010;123(24):4195-200.
31. Shin M, Yoshimoto H, Vacanti JP. In vivo bone tissue engineering using mesenchymal stem cells on a novel electrospun nanofibrous scaffold. Tissue engineering. 2004;10(1-2):33-41.
32. Schober A, Fernekorn U, Singh S, Schlingloff G, Gebinoga M, Hampl J, et al. Mimicking the biological world: Methods for the 3 D structuring of artificial cellular environments. Engineering in Life Sciences. 2013;13(4):352-67.
33. Knight E, Przyborski S. Advances in 3D cell culture technologies enabling tissue-like structures to be created in vitro. Journal of anatomy. 2015;227(6):746-56.
34. Zietarska M, Maugard CM, Filali-Mouhim A, Alam-Fahmy M, Tonin PN, Provencher DM, et al. Molecular description of a 3D in vitro model for the study of epithelial ovarian cancer (EOC). Molecular carcinogenesis. 2007;46(10):872-85.
35. Achilli T-M, Meyer J, Morgan JR. Advances in the formation, use and understanding of multi-cellular spheroids. Expert opinion on biological therapy. 2012;12(10):1347-60.
36. Kim B-S, Mooney DJ. Development of biocompatible synthetic extracellular matrices for tissue engineering. Trends in biotechnology. 1998;16(5):224-30.
37. Griffith LG. Emerging design principles in biomaterials and scaffolds for tissue engineering. Annals of the New York Academy of Sciences. 2002;961(1):83-95.
38. Dhandayuthapani B, Yoshida Y, Maekawa T, Kumar DS. Polymeric scaffolds in tissue engineering application: a review. International Journal of Polymer Science. 2011;2011.
39. Williams DF. On the mechanisms of biocompatibility. Biomaterials. 2008;29(20):2941-53.
40. Donaruma LG. Definitions in biomaterials, DF Williams, Ed., Elsevier, Amsterdam, 1987, 72 pp. Wiley Online Library; 1988.
41. Hutmacher DW. Scaffold design and fabrication technologies for engineering tissues—state of the art and future perspectives. Journal of Biomaterials Science, Polymer Edition. 2001;12(1):107-24.

42. Wang M. Materials selection and scaffold fabrication for tissue engineering in orthopaedics. Advanced bioimaging technologies in assessment of quality of bone and scaffold materials Berlin: Springer. 2007:259-88.
43. Hollister SJ, Maddox R, Taboas JM. Optimal design and fabrication of scaffolds to mimic tissue properties and satisfy biological constraints. Biomaterials. 2002;23(20):4095-103.
44. Loh QL, Choong C. Three-dimensional scaffolds for tissue engineering applications: role of porosity and pore size. Tissue Engineering Part B: Reviews. 2013;19(6):485-502.
45. Kim B-S, Nikolovski J, Bonadio J, Smiley E, Mooney DJ. Engineered smooth muscle tissues: regulating cell phenotype with the scaffold. Experimental cell research. 1999;251(2):318-28.
46. Dai Z, Ronholm J, Tian Y, Sethi B, Cao X. Sterilization techniques for biodegradable scaffolds in tissue engineering applications. Journal of tissue engineering. 2016;7:2041731416648810.
47. Allaf RM. Melt-molding technologies for 3D scaffold engineering. Functional 3D Tissue Engineering Scaffolds: Elsevier; 2018. p. 75-100.
48. Rezwan K, Chen Q, Blaker J, Boccaccini AR. Biodegradable and bioactive porous polymer/inorganic composite scaffolds for bone tissue engineering. Biomaterials. 2006;27(18):3413-31.
49. Engel E, Castaño O, Salvagni E, Ginebra MP, Planell JA. Biomaterials for tissue engineering of hard tissues. Strategies in Regenerative Medicine: Springer; 2009. p. 1-42.
50. Rahaman MN, Day DE, Bal BS, Fu Q, Jung SB, Bonewald LF, et al. Bioactive glass in tissue engineering. Acta biomaterialia. 2011;7(6):2355-73.
51. Liu X, Ma PX. Polymeric scaffolds for bone tissue engineering. Annals of biomedical engineering. 2004;32(3):477-86.
52. Ozdil D, Aydin HM. Polymers for medical and tissue engineering applications. Journal of Chemical Technology & Biotechnology. 2014;89(12):1793-810.
53. Richbourg NR, Peppas NA, Sikavitsas VI. Tuning the biomimetic behavior of scaffolds for regenerative medicine through surface modifications. Journal of tissue engineering and regenerative medicine. 2019;13(8):1275-93.
54. Song R, Murphy M, Li C, Ting K, Soo C, Zheng Z. Current development of biodegradable polymeric materials for biomedical applications. Drug design, development and therapy. 2018;12:3117.
55. Gomes M, Azevedo H, Malafaya P, Silva S, Oliveira J, Silva G, et al. Natural polymers in tissue engineering applications. Tissue engineering: Elsevier; 2008. p. 145-92.
56. O'brien FJ. Biomaterials & scaffolds for tissue engineering. Materials today. 2011;14(3):88-95.
57. Malafaya PB, Silva GA, Reis RL. Natural–origin polymers as carriers and scaffolds for biomolecules and cell delivery in tissue engineering applications. Advanced drug delivery reviews. 2007;59(4):207-33.
58. Yang C, Hillas PJ, Baez JA, Nokelainen M, Balan J, Tang J, et al. The application of recombinant human collagen in tissue engineering. BioDrugs. 2004;18(2):103-19.
59. Shoulders MD, Raines RT. Collagen structure and stability. Annual review of biochemistry. 2009;78:929-58.
60. Fratzl P. Collagen: structure and mechanics, an introduction. Collagen: structure and mechanics. 2008:1-13.
61. Glowacki J, Mizuno S. Collagen scaffolds for tissue engineering. Biopolymers. 2008;89(5):338-44.
62. Dupont-Gillain CC. Understanding and controlling type I collagen adsorption and assembly at interfaces, and application to cell engineering. Colloids and Surfaces B: Biointerfaces. 2014;124:87-96.
63. Södergård A, Stolt M. Properties of lactic acid based polymers and their correlation with composition. Progress in polymer science. 2002;27(6):1123-63.
64. Middleton JC, Tipton AJ. Synthetic biodegradable polymers as orthopedic devices. Biomaterials. 2000;21(23):2335-46.
65. Gentile P, Chiono V, Carmagnola I, Hatton PV. An overview of poly (lactic-co-glycolic) acid (PLGA)-based biomaterials for bone tissue engineering. International journal of molecular sciences. 2014;15(3):3640-59.

66. Sato S, Gondo D, Wada T, Kanehashi S, Nagai K. Effects of various liquid organic solvents on solvent-induced crystallization of amorphous poly (lactic acid) film. Journal of Applied Polymer Science. 2013;129(3):1607-17.
67. Sung H-J, Meredith C, Johnson C, Galis ZS. The effect of scaffold degradation rate on three-dimensional cell growth and angiogenesis. Biomaterials. 2004;25(26):5735-42.
68. Yang S, Leong K-F, Du Z, Chua C-K. The design of scaffolds for use in tissue engineering. Part I. Traditional factors. Tissue engineering. 2001;7(6):679-89.
69. Carletti E, Motta A, Migliaresi C. Scaffolds for tissue engineering and 3D cell culture. 3D Cell Culture: Methods and Protocols. 2011:17-39.
70. Lanao RPF, Jonker AM, Wolke JG, Jansen JA, van Hest JC, Leeuwenburgh SC. Physicochemical properties and applications of poly (lactic-co-glycolic acid) for use in bone regeneration. Tissue Engineering Part B: Reviews. 2013;19(4):380-90.
71. Pan Z, Ding J. Poly (lactide-co-glycolide) porous scaffolds for tissue engineering and regenerative medicine. Interface focus. 2012;2(3):366-77.
72. Yoon JJ, Park TG. Degradation behaviors of biodegradable macroporous scaffolds prepared by gas foaming of effervescent salts. Journal of Biomedical Materials Research Part A. 2001;55(3):401-8.
73. Fernekorn U, Hampl J, Weise F, Singh S, Borowiec J, Schober A. Development of Microstructuring Technologies of Polycarbonate for Establishing Advanced Cell Cultivation Systems. Handbook of Polymers for Pharmaceutical Technologies: Processing and Applications, Volume 2. 2015:67-93.
74. Nomiri S, Hoshyar R, Ambrosino C, Tyler CR, Mansouri B. A mini review of bisphenol A (BPA) effects on cancer-related cellular signaling pathways. Environmental Science and Pollution Research. 2019;26(9):8459-67.
75. Hiebl B, Lützow K, Lange M, Jung F, Seifert B, Klein F, et al. Cytocompatibility testing of cell culture modules fabricated from specific candidate biomaterials using injection molding. Journal of biotechnology. 2010;148(1):76-82.
76. Lantos PR. Plastics in medical applications. Journal of biomaterials applications. 1987;2(3):358-71.
77. Lee JH, Lee SJ, Khang G, Lee HB. Interaction of fibroblasts on polycarbonate membrane surfaces with different micropore sizes and hydrophilicity. Journal of Biomaterials Science, Polymer Edition. 1999;10(3):283-94.
78. Booth R, Kim H. Characterization of a microfluidic in vitro model of the blood-brain barrier (μBBB). Lab on a chip. 2012;12(10):1784-92.
79. Liles DT. The Fascinating World of Silicones and Their Im.
80. Owen M. Why silicones behave funny. Chimie nouvelle. 2004(85):27-33.
81. Sollier E, Murray C, Maoddi P, Di Carlo D. Rapid prototyping polymers for microfluidic devices and high pressure injections. Lab on a Chip. 2011;11(22):3752-65.
82. Pedraza E, Brady A-C, Fraker CA, Stabler CL. Synthesis of macroporous poly (dimethylsiloxane) scaffolds for tissue engineering applications. Journal of Biomaterials Science, Polymer Edition. 2013;24(9):1041-56.
83. Mata A, Fleischman AJ, Roy S. Characterization of polydimethylsiloxane (PDMS) properties for biomedical micro/nanosystems. Biomedical microdevices. 2005;7(4):281-93.
84. Johnston I, McCluskey D, Tan C, Tracey M. Mechanical characterization of bulk Sylgard 184 for microfluidics and microengineering. Journal of Micromechanics and Microengineering. 2014;24(3):035017.
85. Mikos AG, Temenoff JS. Formation of highly porous biodegradable scaffolds for tissue engineering. Electronic Journal of Biotechnology. 2000;3(2):23-4.
86. Oh SH, Kang SG, Kim ES, Cho SH, Lee JH. Fabrication and characterization of hydrophilic poly (lactic-co-glycolic acid)/poly (vinyl alcohol) blend cell scaffolds by melt-molding particulate-leaching method. Biomaterials. 2003;24(22):4011-21.

87. Harris LD, Kim B-S, Mooney DJ. Open pore biodegradable matrices formed with gas foaming. 1998.
88. Mooney DJ, Baldwin DF, Suh NP, Vacanti JP, Langer R. Novel approach to fabricate porous sponges of poly (D, L-lactic-co-glycolic acid) without the use of organic solvents. Biomaterials. 1996;17(14):1417-22.
89. Krause B, Diekmann K, Van der Vegt N, Wessling M. Open nanoporous morphologies from polymeric blends by carbon dioxide foaming. Macromolecules. 2002;35(5):1738-45.
90. Pham QP, Sharma U, Mikos AG. Electrospinning of polymeric nanofibers for tissue engineering applications: a review. Tissue engineering. 2006;12(5):1197-211.
91. Hasan A, Memic A, Annabi N, Hossain M, Paul A, Dokmeci MR, et al. Electrospun scaffolds for tissue engineering of vascular grafts. Acta biomaterialia. 2014;10(1):11-25.
92. Jenkins TL, Meehan S, Pourdeyhimi B, Little D. Meltblown polymer fabrics as candidate scaffolds for rotator cuff tendon tissue engineering. Tissue Engineering Part A. 2017;23(17-18):958-67.
93. Hiremath N, Bhat G. Melt blown polymeric nanofibers for medical applications-an overview. Nanoscience & Technology. 2015;2(1):1-9.
94. Tuin S, Pourdeyhimi B, Loboa E. Creating tissues from textiles: scalable nonwoven manufacturing techniques for fabrication of tissue engineering scaffolds. Biomedical Materials. 2016;11(1):015017.
95. Van de Witte P, Dijkstra P, Van den Berg J, Feijen J. Phase separation processes in polymer solutions in relation to membrane formation. Journal of Membrane Science. 1996;117(1-2):1-31.
96. Nam YS, Park TG. Porous biodegradable polymeric scaffolds prepared by thermally induced phase separation. Journal of Biomedical Materials Research: An Official Journal of The Society for Biomaterials, The Japanese Society for Biomaterials, and The Australian Society for Biomaterials and the Korean Society for Biomaterials. 1999;47(1):8-17.
97. Mulder M. Basic principles of membrane technology: Springer Science & Business Media; 2012.
98. Akbarzadeh R, Yousefi AM. Effects of processing parameters in thermally induced phase separation technique on porous architecture of scaffolds for bone tissue engineering. Journal of Biomedical Materials Research Part B: Applied Biomaterials. 2014;102(6):1304-15.
99. Mulder J. Basic principles of membrane technology: Springer Science & Business Media; 2012.
100. Li D. Encyclopedia of microfluidics and nanofluidics: Springer Science & Business Media; 2008.
101. Yao D. Micromolding of polymers. Advances in Polymer Processing: Elsevier; 2009. p. 552-78.
102. Heckele M, Schomburg W. Review on micro molding of thermoplastic polymers. Journal of Micromechanics and Microengineering. 2003;14(3):R1.
103. Zorlutuna P, Annabi N, Camci-Unal G, Nikkhah M, Cha JM, Nichol JW, et al. Microfabricated biomaterials for engineering 3D tissues. Advanced materials. 2012;24(14):1782-804.
104. Lima M, Correlo V, Reis R. Micro/nano replication and 3D assembling techniques for scaffold fabrication. Materials Science and Engineering: C. 2014;42:615-21.
105. Becker H, Heim U. Hot embossing as a method for the fabrication of polymer high aspect ratio structures. Sensors and Actuators A: Physical. 2000;83(1-3):130-5.
106. Gallant ND, Charest JL, King WP, García AJ. Micro-and nano-patterned substrates to manipulate cell adhesion. Journal of nanoscience and nanotechnology. 2007;7(3):803-7.
107. Jeon JS, Chung S, Kamm RD, Charest JL. Hot embossing for fabrication of a microfluidic 3D cell culture platform. Biomedical microdevices. 2011;13(2):325-33.
108. Warby M, Whiteman JR, Jiang W-G, Warwick P, Wright T. Finite element simulation of thermoforming processes for polymer sheets. Mathematics and computers in simulation. 2003;61(3-6):209-18.
109. Truckenmüller R, Giselbrecht S, Rivron N, Gottwald E, Saile V, Van den Berg A, et al. Thermoforming of film-based biomedical microdevices. Advanced materials. 2011;23(11):1311-29.
110. Yeong W-Y, Chua C-K, Leong K-F, Chandrasekaran M. Rapid prototyping in tissue engineering: challenges and potential. TRENDS in Biotechnology. 2004;22(12):643-52.

111. Hollister SJ. Porous scaffold design for tissue engineering. Nature materials. 2005;4(7):518-24.
112. Lee J, Cuddihy MJ, Kotov NA. Three-dimensional cell culture matrices: state of the art. Tissue Engineering Part B: Reviews. 2008;14(1):61-86.
113. Hersel U, Dahmen C, Kessler H. RGD modified polymers: biomaterials for stimulated cell adhesion and beyond. Biomaterials. 2003;24(24):4385-415.
114. Folch A, Toner M. Microengineering of cellular interactions. Annual review of biomedical engineering. 2000;2(1):227-56.
115. Wang S, Cui W, Bei J. Bulk and surface modifications of polylactide. Analytical and bioanalytical chemistry. 2005;381(3):547-56.
116. Katti DS, Vasita R, Shanmugam K. Improved biomaterials for tissue engineering applications: surface modification of polymers. Current topics in medicinal chemistry. 2008;8(4):341-53.
117. Wang Y-X, Robertson JL, Spillman WB, Claus RO. Effects of the chemical structure and the surface properties of polymeric biomaterials on their biocompatibility. Pharmaceutical research. 2004;21(8):1362-73.
118. Chan C-M, Ko T-M, Hiraoka H. Polymer surface modification by plasmas and photons. Surface science reports. 1996;24(1-2):1-54.
119. Dai L, StJohn HA, Bi J, Zientek P, Chatelier RC, Griesser HJ. Biomedical coatings by the covalent immobilization of polysaccharides onto gas-plasma-activated polymer surfaces. Surface and Interface Analysis: An International Journal devoted to the development and application of techniques for the analysis of surfaces, interfaces and thin films. 2000;29(1):46-55.
120. Haddad T, Noel S, Liberelle B, El Ayoubi R, Ajji A, De Crescenzo G. Fabrication and surface modification of poly lactic acid (PLA) scaffolds with epidermal growth factor for neural tissue engineering. Biomatter. 2016;6(1):e1231276.
121. Alvarez-Barreto JF, Shreve MC, Deangelis PL, Sikavitsas VI. Preparation of a functionally flexible, three-dimensional, biomimetic poly (L-lactic acid) scaffold with improved cell adhesion. Tissue engineering. 2007;13(6):1205-17.
122. Singh S, Mai P, Borowiec J, Zhang Y, Lei Y, Schober A. Donor–acceptor Stenhouse adduct-grafted polycarbonate surfaces: selectivity of the reaction for secondary amine on surface. Royal Society open science. 2018;5(7):180207.
123. Miller DC, Thapa A, Haberstroh KM, Webster TJ. Endothelial and vascular smooth muscle cell function on poly (lactic-co-glycolic acid) with nano-structured surface features. Biomaterials. 2004;25(1):53-61.
124. Chung T-W, Liu D-Z, Wang S-Y, Wang S-S. Enhancement of the growth of human endothelial cells by surface roughness at nanometer scale. Biomaterials. 2003;24(25):4655-61.
125. Unadkat HV, Hulsman M, Cornelissen K, Papenburg BJ, Truckenmüller RK, Carpenter AE, et al. An algorithm-based topographical biomaterials library to instruct cell fate. Proceedings of the National Academy of Sciences. 2011;108(40):16565-70.
126. Kaji H, Camci-Unal G, Langer R, Khademhosseini A. Engineering systems for the generation of patterned co-cultures for controlling cell–cell interactions. Biochimica et Biophysica Acta (BBA)-General Subjects. 2011;1810(3):239-50.
127. Carter SB. Haptotactic islands: a method of confining single cells to study individual cell reactions and clone formation. Experimental cell research. 1967;48(1):189-93.
128. Li Y, Huang G, Zhang X, Wang L, Du Y, Lu TJ, et al. Engineering cell alignment in vitro. Biotechnology advances. 2014;32(2):347-65.
129. Théry M, Piel M. Adhesive micropatterns for cells: a microcontact printing protocol. Cold Spring Harbor Protocols. 2009;2009(7):pdb. prot5255.
130. Chiu DT, Jeon NL, Huang S, Kane RS, Wargo CJ, Choi IS, et al. Patterned deposition of cells and proteins onto surfaces by using three-dimensional microfluidic systems. Proceedings of the National Academy of Sciences. 2000;97(6):2408-13.

131. Ho C-T, Lin R-Z, Chen R-J, Chin C-K, Gong S-E, Chang H-Y, et al. Liver-cell patterning lab chip: mimicking the morphology of liver lobule tissue. Lab on a Chip. 2013;13(18):3578-87.
132. Bernard A, Renault JP, Michel B, Bosshard HR, Delamarche E. Microcontact printing of proteins. Advanced Materials. 2000;12(14):1067-70.
133. Zhang K, Xiao X, Wang X, Fan Y, Li X. Topographical patterning: characteristics of current processing techniques, controllable effects on material properties and co-cultured cell fate, updated applications in tissue engineering, and improvement strategies. Journal of Materials Chemistry B. 2019;7(45):7090-109.
134. Liu VA, Jastromb WE, Bhatia SN. Engineering protein and cell adhesivity using PEO-terminated triblock polymers. Journal of biomedical materials research. 2002;60(1):126-34.
135. Falconnet D, Csucs G, Grandin HM, Textor M. Surface engineering approaches to micropattern surfaces for cell-based assays. Biomaterials. 2006;27(16):3044-63.
136. Xia Y, Whitesides GM. Soft lithography. Annual review of materials science. 1998;28(1):153-84.
137. Kaufmann T, Ravoo BJ. Stamps, inks and substrates: polymers in microcontact printing. Polymer Chemistry. 2010;1(4):371-87.
138. Ruiz SA, Chen CS. Microcontact printing: A tool to pattern. Soft Matter. 2007;3(2):168-77.
139. Perl A, Reinhoudt DN, Huskens J. Microcontact printing: limitations and achievements. Advanced Materials. 2009;21(22):2257-68.
140. Kim E, Xia Y, Whitesides GM. Micromolding in capillaries: applications in materials science. Journal of the American Chemical Society. 1996;118(24):5722-31.
141. Dusseiller MR, Schlaepfer D, Koch M, Kroschewski R, Textor M. An inverted microcontact printing method on topographically structured polystyrene chips for arrayed micro-3-D culturing of single cells. Biomaterials. 2005;26(29):5917-25.
142. Gray BL, Lieu DK, Collins SD, Smith RL, Barakat AI. Microchannel platform for the study of endothelial cell shape and function. Biomedical Microdevices. 2002;4(1):9-16.
143. Greene AC, Washburn CM, Bachand GD, James CD. Combined chemical and topographical guidance cues for directing cytoarchitectural polarization in primary neurons. Biomaterials. 2011;32(34):8860-9.
144. Waterkotte B, Bally F, Nikolov PM, Waldbaur A, Rapp BE, Truckenmüller R, et al. Biofunctional micropatterning of thermoformed 3D substrates. Advanced functional materials. 2014;24(4):442-50.
145. Sun Y, Jallerat Q, Szymanski JM, Feinberg AW. Conformal nanopatterning of extracellular matrix proteins onto topographically complex surfaces. Nature methods. 2015;12(2):134-6.
146. Moraes C, Kim BC, Zhu X, Mills KL, Dixon AR, Thouless M, et al. Defined topologically-complex protein matrices to manipulate cell shape via three-dimensional fiber-like patterns. Lab on a Chip. 2014;14(13):2191-201.
147. Bhatia SN, Underhill GH, Zaret KS, Fox IJ. Cell and tissue engineering for liver disease. Science translational medicine. 2014;6(245):245sr2-sr2.
148. Asrani SK, Devarbhavi H, Eaton J, Kamath PS. Burden of liver diseases in the world. Journal of hepatology. 2019;70(1):151-71.
149. Pimpin L, Cortez-Pinto H, Negro F, Corbould E, Lazarus JV, Webber L, et al. Burden of liver disease in Europe: epidemiology and analysis of risk factors to identify prevention policies. Journal of hepatology. 2018;69(3):718-35.
150. Rouiller C. The liver: morphology, biochemistry, physiology: Academic Press; 2013.
151. Arias IM, Wolkoff AW, Boyer JL, Shafritz DA, Fausto N, Alter HJ, et al. The liver: biology and pathobiology: John Wiley & Sons; 2011.
152. Wisse E, De Zanger R, Charels K, Van Der Smissen P, McCuskey R. The liver sieve: considerations concerning the structure and function of endothelial fenestrae, the sinusoidal wall and the space of Disse. Hepatology. 1985;5(4):683-92.

153. Poisson J, Lemoinne S, Boulanger C, Durand F, Moreau R, Valla D, et al. Liver sinusoidal endothelial cells: physiology and role in liver diseases. Journal of Hepatology. 2017;66(1):212-27.
154. Godoy P, Hewitt NJ, Albrecht U, Andersen ME, Ansari N, Bhattacharya S, et al. Recent advances in 2D and 3D in vitro systems using primary hepatocytes, alternative hepatocyte sources and non-parenchymal liver cells and their use in investigating mechanisms of hepatotoxicity, cell signaling and ADME. Archives of toxicology. 2013;87(8):1315-530.
155. Nahmias Y, Berthiaume F, Yarmush ML. Integration of technologies for hepatic tissue engineering. Tissue Engineering II: Springer; 2006. p. 309-29.
156. Dunn J, Yarmush M, Koebe H, Tompkins R. Hepatocyte function and extracellular matrix geometry: long-term culture in a sandwich configuration. The FASEB Journal. 1989;3(2):174-7.
157. LeCluyse EL, Bullock PL, Parkinson A. Strategies for restoration and maintenance of normal hepatic structure and function in long-term cultures of rat hepatocytes. Advanced Drug Delivery Reviews. 1996;22(1-2):133-86.
158. Reid LM, Fiorino AS, Sigal SH, Brill S, Holst PA. Extracellular matrix gradients in the space of Disse: relevance to liver biology. Hepatology. 1992;15(6):1198-203.
159. Carmagnola I, Ranzato E, Chiono V. Scaffold functionalization to support a tissue biocompatibility. Functional 3D Tissue Engineering Scaffolds: Elsevier; 2018. p. 255-77.
160. Yang J, Bei J, Wang S. Enhanced cell affinity of poly (D, L-lactide) by combining plasma treatment with collagen anchorage. Biomaterials. 2002;23(12):2607-14.
161. Hammond JS, Beckingham IJ, Shakesheff KM. Scaffolds for liver tissue engineering. Expert review of medical devices. 2006;3(1):21-7.
162. Wang Y, Kim MH, Shirahama H, Lee JH, Ng SS, Glenn JS, et al. ECM proteins in a microporous scaffold influence hepatocyte morphology, function, and gene expression. Scientific reports. 2016;6:37427.
163. Braiterman LT, Hubbard AL. Hepatocyte surface polarity: its dynamic maintenance and establishment. The Liver: Biology and Pathobiology. 2009:73-105.
164. Zeigerer A, Wuttke A, Marsico G, Seifert S, Kalaidzidis Y, Zerial M. Functional properties of hepatocytes in vitro are correlated with cell polarity maintenance. Experimental cell research. 2017;350(1):242-52.
165. Bell CC, Hendriks DF, Moro SM, Ellis E, Walsh J, Renblom A, et al. Characterization of primary human hepatocyte spheroids as a model system for drug-induced liver injury, liver function and disease. Scientific reports. 2016;6:25187.
166. Tostoes RM, Leite SB, Serra M, Jensen J, Björquist P, Carrondo MJ, et al. Human liver cell spheroids in extended perfusion bioreactor culture for repeated-dose drug testing. Hepatology. 2012;55(4):1227-36.
167. Underhill GH, Khetani SR. Bioengineered liver models for drug testing and cell differentiation studies. Cellular and molecular gastroenterology and hepatology. 2018;5(3):426-39. e1.
168. Tong WH, Fang Y, Yan J, Hong X, Singh NH, Wang SR, et al. Constrained spheroids for prolonged hepatocyte culture. Biomaterials. 2016;80:106-20.
169. Siltanen C, Diakatou M, Lowen J, Haque A, Rahimian A, Stybayeva G, et al. One step fabrication of hydrogel microcapsules with hollow core for assembly and cultivation of hepatocyte spheroids. Acta biomaterialia. 2017;50:428-36.
170. Wang T, Feng Z-Q, Leach MK, Wu J, Jiang Q. Nanoporous fibers of type-I collagen coated poly (L-lactic acid) for enhancing primary hepatocyte growth and function. Journal of Materials Chemistry B. 2013;1(3):339-46.
171. Zhu XH, Lee LY, Jackson JSH, Tong YW, Wang CH. Characterization of porous poly (D, L-lactic-co-glycolic acid) sponges fabricated by supercritical CO2 gas-foaming method as a scaffold for three-dimensional growth of Hep3B cells. Biotechnology and bioengineering. 2008;100(5):998-1009.

172. Tibbitt MW, Anseth KS. Hydrogels as extracellular matrix mimics for 3D cell culture. Biotechnology and bioengineering. 2009;103(4):655-63.
173. Bachmann A, Moll M, Gottwald E, Nies C, Zantl R, Wagner H, et al. 3D cultivation techniques for primary human hepatocytes. Microarrays. 2015;4(1):64-83.
174. Wang B, Jakus AE, Baptista PM, Soker S, Soto-Gutierrez A, Abecassis MM, et al. Functional maturation of induced pluripotent stem cell hepatocytes in extracellular matrix—a comparative analysis of bioartificial liver microenvironments. Stem cells translational medicine. 2016;5(9):1257-67.
175. Glicklis R, Shapiro L, Agbaria R, Merchuk JC, Cohen S. Hepatocyte behavior within three-dimensional porous alginate scaffolds. Biotechnology and bioengineering. 2000;67(3):344-53.
176. Lewis PL, Green RM, Shah RN. 3D-printed gelatin scaffolds of differing pore geometry modulate hepatocyte function and gene expression. Acta biomaterialia. 2018;69:63-70.
177. Chitrangi S, Nair P, Khanna A. Three-dimensional polymer scaffolds for enhanced differentiation of human mesenchymal stem cells to hepatocyte-like cells: a comparative study. Journal of tissue engineering and regenerative medicine. 2017;11(8):2359-72.
178. Kazemnejad S. Hepatic tissue engineering using scaffolds: state of the art. Avicenna journal of medical biotechnology. 2009;1(3):135.
179. Janorkar AV. Polymeric scaffold materials for two-dimensional and three-dimensional in vitro culture of hepatocytes. Biomaterials: ACS Publications; 2010. p. 1-32.
180. Knight E, Murray B, Carnachan R, Przyborski S. Alvetex®: polystyrene scaffold technology for routine three dimensional cell culture. 3D Cell Culture: Springer; 2011. p. 323-40.
181. Xiao Y, Zhou M, Zhang M, Liu W, Zhou Y, Lang M. Hepatocyte culture on 3D porous scaffolds of PCL/PMCL. Colloids and Surfaces B: Biointerfaces. 2019;173:185-93.
182. Török E, Lutgehetmann M, Bierwolf J, Melbeck S, Düllmann J, Nashan B, et al. Primary human hepatocytes on biodegradable poly (l-lactic acid) matrices: A promising model for improving transplantation efficiency with tissue engineering. Liver transplantation. 2011;17(2):104-14.
183. Saavedra YGL, Mateescu MA, Averill-Bates DA, Denizeau F. Polyvinylalcohol three-dimensional matrices for improved long-term dynamic culture of hepatocytes. Journal of Biomedical Materials Research Part A: An Official Journal of The Society for Biomaterials, The Japanese Society for Biomaterials, and The Australian Society for Biomaterials and the Korean Society for Biomaterials. 2003;66(3):562-70.
184. Schutte M, Fox B, Baradez M-O, Devonshire A, Minguez J, Bokhari M, et al. Rat primary hepatocytes show enhanced performance and sensitivity to acetaminophen during three-dimensional culture on a polystyrene scaffold designed for routine use. Assay and drug development technologies. 2011;9(5):475-86.
185. Dash A, Inman W, Hoffmaster K, Sevidal S, Kelly J, Obach RS, et al. Liver tissue engineering in the evaluation of drug safety. Expert opinion on drug metabolism & toxicology. 2009;5(10):1159-74.
186. Malik R, Selden C, Hodgson H, editors. The role of non-parenchymal cells in liver growth. Seminars in cell & developmental biology; 2002: Elsevier.
187. Guguen-Guillouzo C, Clément B, Baffet G, Beaumont C, Morel-Chany E, Glaise D, et al. Maintenance and reversibility of active albumin secretion by adult rat hepatocytes co-cultured with another liver epithelial cell type. Experimental cell research. 1983;143(1):47-54.
188. Bhandari RN, Riccalton LA, Lewis AL, Fry JR, Hammond AH, Tendler SJ, et al. Liver tissue engineering: a role for co-culture systems in modifying hepatocyte function and viability. Tissue engineering. 2001;7(3):345-57.
189. Bhatia S, Balis U, Yarmush M, Toner M. Effect of cell–cell interactions in preservation of cellular phenotype: cocultivation of hepatocytes and nonparenchymal cells. The FASEB journal. 1999;13(14):1883-900.
190. Matsumoto K, Yoshitomi H, Rossant J, Zaret KS. Liver organogenesis promoted by endothelial cells prior to vascular function. Science. 2001;294(5542):559-63.

191. McCuskey RS. Sinusoidal endothelial cells as an early target for hepatic toxicants. Clinical hemorheology and microcirculation. 2006;34(1, 2):5-10.
192. Starokozhko V, Groothuis GM. Challenges on the road to a multicellular bioartificial liver. Journal of tissue engineering and regenerative medicine. 2018;12(1):e227-e36.
193. Kim K, Ohashi K, Utoh R, Kano K, Okano T. Preserved liver-specific functions of hepatocytes in 3D co-culture with endothelial cell sheets. Biomaterials. 2012;33(5):1406-13.
194. Salerno S, Campana C, Morelli S, Drioli E, De Bartolo L. Human hepatocytes and endothelial cells in organotypic membrane systems. Biomaterials. 2011;32(34):8848-59.
195. Harimoto M, Yamato M, Hirose M, Takahashi C, Isoi Y, Kikuchi A, et al. Novel approach for achieving double-layered cell sheets co-culture: overlaying endothelial cell sheets onto monolayer hepatocytes utilizing temperature-responsive culture dishes. Journal of Biomedical Materials Research: An Official Journal of The Society for Biomaterials, The Japanese Society for Biomaterials, and The Australian Society for Biomaterials and the Korean Society for Biomaterials. 2002;62(3):464-70.
196. Morin O, Normand C. Long-term maintenance of hepatocyte functional activity in co-culture: Requirements for sinusoidal endothelial cells and dexamethasone. Journal of cellular physiology. 1986;129(1):103-10.
197. Wang G, Zheng Y, Wang Y, Cai Z, Liao N, Liu J, et al. Co-culture system of hepatocytes and endothelial cells: two in vitro approaches for enhancing liver-specific functions of hepatocytes. Cytotechnology. 2018:1-12.
198. Bale SS, Golberg I, Jindal R, McCarty WJ, Luitje M, Hegde M, et al. Long-term coculture strategies for primary hepatocytes and liver sinusoidal endothelial cells. Tissue Engineering Part C: Methods. 2014;21(4):413-22.
199. Takayama G, Taniguchi A, Okano T. Identification of differentially expressed genes in hepatocyte/endothelial cell co-culture system. Tissue engineering. 2007;13(1):159-66.
200. Kidambi S, Yarmush RS, Novik E, Chao P, Yarmush ML, Nahmias Y. Oxygen-mediated enhancement of primary hepatocyte metabolism, functional polarization, gene expression, and drug clearance. Proceedings of the National Academy of Sciences. 2009;106(37):15714-9.
201. Nahmias Y, Casali M, Barbe L, Berthiaume F, Yarmush ML. Liver endothelial cells promote LDL-R expression and the uptake of HCV-like particles in primary rat and human hepatocytes. Hepatology. 2006;43(2):257-65.
202. Krause P, Markus PM, Schwartz P, Unthan-Fechner K, Pestel S, Fandrey J, et al. Hepatocyte-supported serum-free culture of rat liver sinusoidal endothelial cells∗. Journal of hepatology. 2000;32(5):718-26.
203. March S, Hui EE, Underhill GH, Khetani S, Bhatia SN. Microenvironmental regulation of the sinusoidal endothelial cell phenotype in vitro. Hepatology. 2009;50(3):920-8.
204. Enomoto Y, Enomura M, Takebe T, Mitsuhashi Y, Kimura M, Yoshizawa E, et al., editors. Self-formation of vascularized hepatic tissue from human adult hepatocyte. Transplantation proceedings; 2014: Elsevier.
205. Ware BR, Durham MJ, Monckton CP, Khetani SR. A cell culture platform to maintain long-term phenotype of primary human hepatocytes and endothelial cells. Cellular and molecular gastroenterology and hepatology. 2018;5(3):187-207.
206. Bhatia S, Balis U, Yarmush M, Toner M. Microfabrication of hepatocyte/fibroblast co-cultures: Role of homotypic cell interactions. Biotechnology progress. 1998;14(3):378-87.
207. Bhatia S, Balis U, Yarmush M, Toner M. Probing heterotypic cell interactions: hepatocyte function in microfabricated co-cultures. Journal of Biomaterials Science, Polymer Edition. 1998;9(11):1137-60.
208. Khetani SR, Bhatia SN. Microscale culture of human liver cells for drug development. Nature biotechnology. 2008;26(1):120.

209. March S, Ramanan V, Trehan K, Ng S, Galstian A, Gural N, et al. Micropatterned coculture of primary human hepatocytes and supportive cells for the study of hepatotropic pathogens. Nature protocols. 2015;10(12):2027.
210. Davidson MD, Kukla DA, Khetani SR. Microengineered cultures containing human hepatic stellate cells and hepatocytes for drug development. Integrative Biology. 2017;9(8):662-77.
211. Zarowna-Dabrowska A, McKenna EO, Schutte ME, Glidle A, Chen L, Cuestas-Ayllon C, et al. Generation of primary hepatocyte microarrays by piezoelectric printing. Colloids and Surfaces B: Biointerfaces. 2012;89:126-32.
212. Kidambi S, Sheng L, Yarmush ML, Toner M, Lee I, Chan C. Patterned co-culture of primary hepatocytes and fibroblasts using polyelectrolyte multilayer templates. Macromolecular bioscience. 2007;7(3):344-53.
213. Zinchenko YS, Coger RN. Engineering micropatterned surfaces for the coculture of hepatocytes and Kupffer cells. Journal of Biomedical Materials Research Part A: An Official Journal of The Society for Biomaterials, The Japanese Society for Biomaterials, and The Australian Society for Biomaterials and the Korean Society for Biomaterials. 2005;75(1):242-8.
214. Kang I-K, Kim GJ, Kwon OH, Ito Y. Co-culture of hepatocytes and fibroblasts by micropatterned immobilization of β-galactose derivatives. Biomaterials. 2004;25(18):4225-32.
215. Yamato M, Konno C, Utsumi M, Kikuchi A, Okano T. Thermally responsive polymer-grafted surfaces facilitate patterned cell seeding and co-culture. Biomaterials. 2002;23(2):561-7.
216. Yahya W, Kadri N, Ibrahim F. Cell patterning for liver tissue engineering via dielectrophoretic mechanisms. Sensors. 2014;14(7):11714-34.
217. Ho C-T, Lin R-Z, Chang W-Y, Chang H-Y, Liu C-H. Rapid heterogeneous liver-cell on-chip patterning via the enhanced field-induced dielectrophoresis trap. Lab on a Chip. 2006;6(6):724-34.
218. Busche M, Tomilova O, Schütte J, Werner S, Beer M, Groll N, et al. HepaChip-MP–a twenty-four chamber microplate for a continuously perfused liver coculture model. Lab on a Chip. 2020.
219. Ebrahimkhani MR, Neiman JAS, Raredon MSB, Hughes DJ, Griffith LG. Bioreactor technologies to support liver function in vitro. Advanced drug delivery reviews. 2014;69:132-57.
220. Goral VN, Yuen PK. Microfluidic platforms for hepatocyte cell culture: new technologies and applications. Annals of biomedical engineering. 2012;40(6):1244-54.
221. Weise F, Fernekorn U, Hampl J, Klett M, Schober A. Analysis and comparison of oxygen consumption of HepG2 cells in a monolayer and three-dimensional high density cell culture by use of a matrigrid®. Biotechnology and bioengineering. 2013;110(9):2504-12.
222. Dash A, Blackman BR, Wamhoff BR. Organotypic systems in drug metabolism and toxicity: challenges and opportunities. Expert opinion on drug metabolism & toxicology. 2012;8(8):999-1014.
223. Lee K-H, Lee J, Lee S-H. 3D liver models on a microplatform: well-defined culture, engineering of liver tissue and liver-on-a-chip. Lab on a Chip. 2015;15(19):3822-37.
224. Rebelo SP, Costa R, Silva MM, Marcelino P, Brito C, Alves PM. Three-dimensional co-culture of human hepatocytes and mesenchymal stem cells: improved functionality in long-term bioreactor cultures. Journal of tissue engineering and regenerative medicine. 2017;11(7):2034-45.
225. Yamada M, Utoh R, Ohashi K, Tatsumi K, Yamato M, Okano T, et al. Controlled formation of heterotypic hepatic micro-organoids in anisotropic hydrogel microfibers for long-term preservation of liver-specific functions. Biomaterials. 2012;33(33):8304-15.
226. Domansky K, Inman W, Serdy J, Dash A, Lim MH, Griffith LG. Perfused multiwell plate for 3D liver tissue engineering. Lab on a chip. 2010;10(1):51-8.
227. Wen F, Chang S, Toh Y, Arooz T, Zhuo L, Teoh S, et al. Development of dual-compartment perfusion bioreactor for serial coculture of hepatocytes and stellate cells in poly (lactic-co-glycolic acid)-collagen scaffolds. Journal of Biomedical Materials Research Part B: Applied Biomaterials: An Official Journal of The Society for Biomaterials, The Japanese Society for Biomaterials, and The Australian Society for Biomaterials and the Korean Society for Biomaterials. 2008;87(1):154-62.

228. Ahmed HMM, Salerno S, Morelli S, Giorno L, De Bartolo L. 3D liver membrane system by co-culturing human hepatocytes, sinusoidal endothelial and stellate cells. Biofabrication. 2017;9(2):025022.
229. Kang YB, Sodunke TR, Lamontagne J, Cirillo J, Rajiv C, Bouchard MJ, et al. Liver sinusoid on a chip: Long-term layered co-culture of primary rat hepatocytes and endothelial cells in microfluidic platforms. Biotechnology and bioengineering. 2015;112(12):2571-82.
230. Du Y, Li N, Yang H, Luo C, Gong Y, Tong C, et al. Mimicking liver sinusoidal structures and functions using a 3D-configured microfluidic chip. Lab on a Chip. 2017;17(5):782-94.
231. Salerno S, Curcio E, Bader A, Giorno L, Drioli E, De Bartolo L. Gas permeable membrane bioreactor for the co-culture of human skin derived mesenchymal stem cells with hepatocytes and endothelial cells. Journal of membrane science. 2018;563:694-707.
232. Li X, George SM, Vernetti L, Gough AH, Taylor DL. A glass-based, continuously zonated and vascularized human liver acinus microphysiological system (vLAMPS) designed for experimental modeling of diseases and ADME/TOX. Lab on a Chip. 2018;18(17):2614-31.
233. Rennert K, Steinborn S, Gröger M, Ungerböck B, Jank A-M, Ehgartner J, et al. A microfluidically perfused three dimensional human liver model. Biomaterials. 2015;71:119-31.
234. Schober A, Augspurger C, Weise F, Fernekorn U, Hildmann C, Hampl J. Partially active microfluidic system for 3d cell cultivation and method for perfusion thereof. Google Patents; 2011.
235. Asnaghi MA, Smith T, Martin I, Wendt D. Bioreactors: enabling technologies for research and manufacturing. Tissue Engineering: Elsevier; 2014. p. 393-425.
236. Gottwald E, Giselbrecht S, Augspurger C, Lahni B, Dambrowsky N, Truckenmüller R, et al. A chip-based platform for the in vitro generation of tissues in three-dimensional organization. Lab on a Chip. 2007;7(6):777-85.
237. Schober A, Hampl J, Haefner S, Tobola J, Weise F, Singh S, et al. Moulding for replicating a structure of a biological tissue and method for producing the same. Google Patents; 2017.
238. Tilli M, Paulasto-Krockel M, Motooka T, Lindroos V. Handbook of silicon based MEMS materials and technologies: William Andrew; 2015.
239. LeCluyse EL, Witek RP, Andersen ME, Powers MJ. Organotypic liver culture models: meeting current challenges in toxicity testing. Critical reviews in toxicology. 2012;42(6):501-48.
240. Auras RA, Lim L-T, Selke SE, Tsuji H. Poly (lactic acid): synthesis, structures, properties, processing, and applications: John Wiley & Sons; 2011.
241. Weir N, Buchanan F, Orr J, Dickson G. Degradation of poly-L-lactide. Part 1: in vitro and in vivo physiological temperature degradation. Proceedings of the Institution of Mechanical Engineers, Part H: Journal of Engineering in Medicine. 2004;218(5):307-19.
242. Santoro M, Shah SR, Walker JL, Mikos AG. Poly (lactic acid) nanofibrous scaffolds for tissue engineering. Advanced drug delivery reviews. 2016;107:206-12.
243. Nam YS, Park TG. Porous biodegradable polymeric scaffolds prepared by thermally induced phase separation. Journal of biomedical materials research. 1999;47(1):8-17.
244. Siggia ED. Late stages of spinodal decomposition in binary mixtures. Physical review A. 1979;20(2):595.
245. Gong Y, Ma Z, Gao C, Wang W, Shen J. Specially elaborated thermally induced phase separation to fabricate poly (L-lactic acid) scaffolds with ultra large pores and good interconnectivity. Journal of applied polymer science. 2006;101(5):3336-42.
246. Pawlowska E, Poplawski T, Ksiazek D, Szczepanska J, Blasiak J. Genotoxicity and cytotoxicity of 2-hydroxyethyl methacrylate. Mutation Research/Genetic Toxicology and Environmental Mutagenesis. 2010;696(2):122-9.
247. Altmann B, Giselbrecht S, Weibezahn K, Welle A, Gottwald E. The three-dimensional cultivation of the carcinoma cell line HepG2 in a perfused chip system leads to a more differentiated phenotype of the cells compared to monolayer culture. Biomedical Materials. 2008;3(3):034120.

248. Weir N, Buchanan F, Orr J, Farrar D, Boyd A. Processing, annealing and sterilisation of poly-L-lactide. Biomaterials. 2004;25(18):3939-49.
249. Cima LG, Ingber DE, Vacanti JP, Langer R. Hepatocyte culture on biodegradable polymeric substrates. Biotechnology and bioengineering. 1991;38(2):145-58.
250. Shved I, Kukhareva L, Zorin I, Blinova M, Bilibin A, Pinaev G. Cultured skin cells interaction with polylactide surface coated by different collagen structures. Tsitologiia. 2007;49(1):32-9.
251. Slepička P, Slepičková Kasálková N, Bačáková L, Kolská Z, Švorčík V. Enhancement of polymer cytocompatibility by nanostructuring of polymer surface. Journal of Nanomaterials. 2012;2012.
252. Ng R, Zang R, Yang KK, Liu N, Yang S-T. Three-dimensional fibrous scaffolds with microstructures and nanotextures for tissue engineering. Rsc Advances. 2012;2(27):10110-24.
253. Woo KM, Chen VJ, Ma PX. Nano-fibrous scaffolding architecture selectively enhances protein adsorption contributing to cell attachment. Journal of Biomedical Materials Research Part A: An Official Journal of The Society for Biomaterials, The Japanese Society for Biomaterials, and The Australian Society for Biomaterials and the Korean Society for Biomaterials. 2003;67(2):531-7.
254. Mueller S, Sandrin L. Liver stiffness: a novel parameter for the diagnosis of liver disease. Hepatic medicine: evidence and research. 2010;2:49.
255. Cozzolino AM, Noce V, Battistelli C, Marchetti A, Grassi G, Cicchini C, et al. Modulating the substrate stiffness to manipulate differentiation of resident liver stem cells and to improve the differentiation state of hepatocytes. Stem cells international. 2016;2016.
256. Natarajan V, Berglund EJ, Chen DX, Kidambi S. Substrate stiffness regulates primary hepatocyte functions. RSC Advances. 2015;5(99):80956-66.
257. Discher DE, Janmey P, Wang Y-l. Tissue cells feel and respond to the stiffness of their substrate. Science. 2005;310(5751):1139-43.
258. Lu L, Peter SJ, Lyman MD, Lai H-L, Leite SM, Tamada JA, et al. In vitro and in vivo degradation of porous poly (DL-lactic-co-glycolic acid) foams. Biomaterials. 2000;21(18):1837-45.
259. Kasuya J, Tanishita K. Microporous membrane-based liver tissue engineering for the reconstruction of three-dimensional functional liver tissues in vitro. Biomatter. 2012;2(4):290-5.
260. Vey E, Roger C, Meehan L, Booth J, Claybourn M, Miller AF, et al. Degradation mechanism of poly (lactic-co-glycolic) acid block copolymer cast films in phosphate buffer solution. Polymer Degradation and Stability. 2008;93(10):1869-76.
261. Wan Y, Wang Y, Liu Z, Qu X, Han B, Bei J, et al. Adhesion and proliferation of OCT-1 osteoblast-like cells on micro-and nano-scale topography structured poly (L-lactide). Biomaterials. 2005;26(21):4453-9.
262. Zong X, Ran S, Kim K-S, Fang D, Hsiao BS, Chu B. Structure and morphology changes during in vitro degradation of electrospun poly (glycolide-co-lactide) nanofiber membrane. Biomacromolecules. 2003;4(2):416-23.
263. Athanasiou K, Schmitz J, Agrawal C. The effects of porosity on in vitro degradation of polylactic acid–polyglycolic acid implants used in repair of articular cartilage. Tissue Engineering. 1998;4(1):53-63.
264. Agrawal C, McKinney J, Lanctot D, Athanasiou K. Effects of fluid flow on the in vitro degradation kinetics of biodegradable scaffolds for tissue engineering. Biomaterials. 2000;21(23):2443-52.
265. Sun Y, Jallerat Q, Szymanski JM, Feinberg AW. Conformal nanopatterning of extracellular matrix proteins onto topographically complex surfaces. Nature methods. 2015;12(2):134.
266. Desai RA, Khan MK, Gopal SB, Chen CS. Subcellular spatial segregation of integrin subtypes by patterned multicomponent surfaces. Integrative Biology. 2011;3(5):560-7.
267. Libioulle L, Bietsch A, Schmid H, Michel B, Delamarche E. Contact-inking stamps for microcontact printing of alkanethiols on gold. Langmuir. 1999;15(2):300-4.
268. Hribar KC, Meggs K, Liu J, Zhu W, Qu X, Chen S. Three-dimensional direct cell patterning in collagen hydrogels with near-infrared femtosecond laser. Scientific reports. 2015;5:17203.

269. Abraham LC, Zuena E, Perez-Ramirez B, Kaplan DL. Guide to collagen characterization for biomaterial studies. Journal of Biomedical Materials Research Part B: Applied Biomaterials: An Official Journal of The Society for Biomaterials, The Japanese Society for Biomaterials, and The Australian Society for Biomaterials and the Korean Society for Biomaterials. 2008;87(1):264-85.
270. Bozec L, Odlyha M. Thermal denaturation studies of collagen by microthermal analysis and atomic force microscopy. Biophysical journal. 2011;101(1):228-36.
271. Suwa Y, Nam K, Ozeki K, Kimura T, Kishida A, Masuzawa T. Thermal denaturation behavior of collagen fibrils in wet and dry environment. Journal of Biomedical Materials Research Part B: Applied Biomaterials. 2016;104(3):538-45.
272. Griffith LG, Swartz MA. Capturing complex 3D tissue physiology in vitro. Nature reviews Molecular cell biology. 2006;7(3):211.
273. Chung HH, Mireles M, Kwarta BJ, Gaborski TR. Use of porous membranes in tissue barrier and co-culture models. Lab on a Chip. 2018;18(12):1671-89.
274. Collins SD, Yuen G, Tu T, Budzinska MA, Spring K, Bryant K, et al. In Vitro Models of the Liver: Disease Modeling, Drug Discovery and Clinical Applications. Exon Publications. 2019:47-67.
275. Lin C, Khetani SR. Advances in engineered liver models for investigating drug-induced liver injury. BioMed research international. 2016;2016.
276. Kim K, Utoh R, Ohashi K, Kikuchi T, Okano T. Fabrication of functional 3D hepatic tissues with polarized hepatocytes by stacking endothelial cell sheets in vitro. Journal of tissue engineering and regenerative medicine. 2017;11(7):2071-80.
277. Hwa AJ, Fry RC, Sivaraman A, So PT, Samson LD, Stolz DB, et al. Rat liver sinusoidal endothelial cells survive without exogenous VEGF in 3D perfused co-cultures with hepatocytes. The FASEB journal. 2007;21(10):2564-79.
278. Yajima Y, Lee CN, Yamada M, Utoh R, Seki M. Development of a perfusable 3D liver cell cultivation system via bundling-up assembly of cell-laden microfibers. Journal of bioscience and bioengineering. 2018;126(1):111-8.
279. Cui J, Wang H, Zheng Z, Shi Q, Sun T, Huang Q, et al. Fabrication of perfusable 3D hepatic lobule-like constructs through assembly of multiple cell type laden hydrogel microstructures. Biofabrication. 2018;11(1):015016.
280. Cui J, Wang H, Shi Q, Ferraro P, Sun T, Dario P, et al. Permeable hollow 3D tissue-like constructs engineered by on-chip hydrodynamic-driven assembly of multicellular hierarchical micromodules. Acta Biomaterialia. 2020.
281. Ma X, Qu X, Zhu W, Li Y-S, Yuan S, Zhang H, et al. Deterministically patterned biomimetic human iPSC-derived hepatic model via rapid 3D bioprinting. Proceedings of the National Academy of Sciences. 2016;113(8):2206-11.
282. Zhu W, Qu X, Zhu J, Ma X, Patel S, Liu J, et al. Direct 3D bioprinting of prevascularized tissue constructs with complex microarchitecture. Biomaterials. 2017;124:106-15.
283. Norona LM, Nguyen DG, Gerber DA, Presnell SC, LeCluyse EL. Editor's highlight: modeling compound-induced fibrogenesis in vitro using three-dimensional bioprinted human liver tissues. Toxicological sciences. 2016;154(2):354-67.
284. Mazza G, Rombouts K, Hall AR, Urbani L, Luong TV, Al-Akkad W, et al. Decellularized human liver as a natural 3D-scaffold for liver bioengineering and transplantation. Scientific reports. 2015;5(1):1-15.
285. Bettahalli N, Groen N, Steg H, Unadkat H, de Boer J, van Blitterswijk C, et al. Development of multilayer constructs for tissue engineering. Journal of tissue engineering and regenerative medicine. 2014;8(2):106-19.
286. Mata A, Kim EJ, Boehm CA, Fleischman AJ, Muschler GF, Roy S. A three-dimensional scaffold with precise micro-architecture and surface micro-textures. Biomaterials. 2009;30(27):4610-7.
287. Papenburg BJ, Liu J, Higuera GA, Barradas AM, de Boer J, van Blitterswijk CA, et al. Development and analysis of multi-layer scaffolds for tissue engineering. Biomaterials. 2009;30(31):6228-39.

288. Khademhosseini A, Langer R, Borenstein J, Vacanti JP. Microscale technologies for tissue engineering and biology. Proceedings of the National Academy of Sciences. 2006;103(8):2480-7.
289. Bae H, Puranik AS, Gauvin R, Edalat F, Carrillo-Conde B, Peppas NA, et al. Building vascular networks. Science translational medicine. 2012;4(160):160ps23-ps23.
290. Siggers JH, Leungchavaphongse K, Ho CH, Repetto R. Mathematical model of blood and interstitial flow and lymph production in the liver. Biomechanics and modeling in mechanobiology. 2014;13(2):363-78.
291. Holy CE, Cheng C, Davies JE, Shoichet MS. Optimizing the sterilization of PLGA scaffolds for use in tissue engineering. Biomaterials. 2000;22(1):25-31.
292. Shearer H, Ellis MJ, Perera SP, Chaudhuri JB. Effects of common sterilization methods on the structure and properties of poly (D, L lactic-co-glycolic acid) scaffolds. Tissue engineering. 2006;12(10):2717-27.

Acknowledgment

I would firstly like to thank my advisor Prof. Dr. Andreas Schober for offering me a great opportunity to join his research group and work in the interesting field of biological systems. I would like to express my appreciation for the relaxed as well as open research atmosphere and for allowing me freedom to explore many different directions this research could take.

Particular gratitude is expressed to Dr. Michael Gebinoga, who was a great supervisor during my student internship at the beginning of my stay in Ilmenau and have shown confidence in me and in the obtained results.

Additionally, I would like to extend thanks to Dr. Sukhdeep Singh for giving me great suggestions during writing this work and helping me step back to look at the overall big picture.

This work could not have been possible without the contribution from other members (or alumni) of the nano-biosystem technology group. My appreciation goes to all wonderful people I worked with for their assistance and tips on experimental and theoretical basis, with particular emphasis on:

- Jörg Hampl and Frank Weise for technical support with cell culture equipment, discussion of ideas regarding technical solutions and the introduction to the microstructuring-related aspects
- Dr. Dana Brauer and Dr. Uta Fernekorn, whose biological knowledge was very helpful
- Karin Friedel for the time spent in the SEM room on my behalf
- Patrick Mai and Martin Baca for a great support either at or after work
- Maren Klett for assistance during cell culture experiments
- Dr. Gregor Schlingloff and Lisa Zeußel for a very nice collaboration.

I would also like to thank those from other groups or institutes for the friendly, straightforward cooperation: Dr. Agnieszka Paszuk, Anette Hartung, Dr. Heike Bartsch and Dr. Andrea Knauer.

Special thanks to Maria and Michael Gebinoga, who have been a wonderful friends from the first days when I arrived in Ilmenau. Thank you for a great support!

Last but not the least; I want to thank my family: especially my husband, who supported me a great deal in everything since I have started my PhD journey as well as my mother and my brother for their unwavering love and support. My sincere gratitude to all of you for encouraging!